AEROSPACE
NUCLEAR
SAFETY

RESEARCH REPORT

RE-ENTRY FLIGHT DEMONSTRATION NUMBER ONE (RFD-1):
DESIGN, DEVELOPMENT, AND PERFORMANCE OF
THE RE-ENTRY VEHICLE

Department 7410

SC-RR-64-511
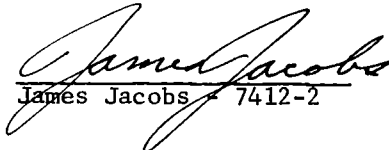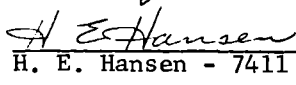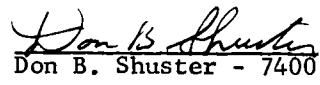TID-4500 (27th Edition)
AEROSPACE SAFETY
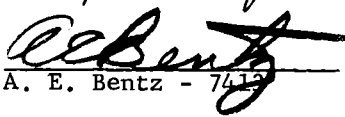
SANDIA CORPORATION

SC-RR-64-511

RE-ENTRY FLIGHT DEMONSTRATION NUMBER ONE (RFD-1):
DESIGN, DEVELOPMENT, AND PERFORMANCE OF THE RE-ENTRY VEHICLE

Prepared By	Reviewed By	Approved By
C. E. Erickson, 7413-1		
H. C. Hardee, 7412-2	James Jacobs / 7412-2	V. E. Blake - 7410
J. I. Hegge, 7412-2		
J. Jacobs, 7412-2	H. E. Hansen - 7411	Don B. Shuster - 7400
S. L. Jeffers, 7412-2		
R. D. Klett, 7412-2		
H. R. Spahr, 7412-2	A. J. Clark, Jr. - 7412	
H. K. Togami, 7412-2		
I. B. White, 7411	A. E. Bentz - 7413	
G. Q. Wilson, 7413-1		

ABSTRACT

This report documents the design, development, and performance of the flight vehicle for Re-entry Flight Demonstration Number One (RFD-1). The RFD-1 re-entry system consisted of the SNAP-10A Simulated Test Reactor (SNAP-10A STR), the external fuel rod experiment, and the re-entry vehicle (RV). The latter included the telemetry package and the vehicle assembly (with recovery system and Scout fourth-stage separation components). The SNAP-10A STR was instrumented to monitor transient temperature response as well as the sequence of reactor disassembly during re-entry heating. The telemetry package transmitted the data obtained with this instrumentation and provided electrical functions for the re-entry vehicle. The re-entry vehicle itself served two purposes: (1) aerodynamically stable support for the SNAP-10A STR, and (2) housing for the telemetry package and the recovery system. The re-entry vehicle was designed to survive re-entry heating and to follow a predetermined trajectory after being carried into outer space on a four-stage NASA Scout vehicle. The exterior fuel rods, which were ejected, contained flare material so that optical information on fuel-rod burnup could be obtained. The performance of the vehicle during the flight is discussed and compared with preflight predictions.

May 1964

ACKNOWLEDGMENT

FOREWORD

Sandia Corporation, a prime nuclear weapon contractor to the AEC, was authorized by the Division of Reactor Development to act as the prime contractor for the independent safety evaluation of aerospace nuclear power systems. The Aerospace Nuclear Safety program at Sandia includes research and development studies, ground testing, flight testing, systems analysis, and independent safety assessment. Re-entry Flight Demonstration Number One is the first re-entry flight test to be conducted since the initiation of this program in March 1962.

The SNAP-10A reactor (Systems for Nuclear Auxiliary Power) was selected for the first re-entry safety flight test. The selection of the SNAP-10A reactor, designed and constructed by Atomics International (AI), was based upon its proposed early use in a nuclear auxiliary power supply for earth satellites.

In the application of nuclear energy to space vehicles, safety features are designed into the power supplies to preclude significant hazards to the earth's population during aborted missions or orbital-decay re-entries.

The Safety Flight Test, called Re-entry Flight Demonstration Number One (RFD-1), employed an inert version of the SNAP-10A reactor to determine the effectiveness of the safety design. The simulated reactor was mounted to a re-entry vehicle (RV), which was placed into the required trajectory by a four-stage NASA Scout booster launched from Wallops Island, Virginia.

Sandia Corporation carried out its assignment in the Aerospace Nuclear Safety Program by performing the following tasks:

1. Design of the flight-test experiment and the configuration of the simulated reactor, in cooperation with Atomics International.

2. Study of the capabilities of the Scout launch vehicle, and recommendation of a trajectory to assure that the desired information would be obtained.

3. Design of the re-entry vehicle and telemetry system; and coordination of interface problems with Atomics International, NASA, and Ling-Temco-Vought Corporation.

4. Theoretical predictions of flight-test results.

5. Preparation of support requirements documents for AMR and the NASA Wallops and Bermuda stations.

6. Provision of complementary downrange instrumentation for collection of telemetry and optical data.

7. Management of flight implementation activities.

8. Data reduction and analysis.

9. Comparison of flight-test results with theoretical calculations.

The following Sandia Corporation reports, together with the present volume, comprise the final documentation of Re-entry Flight Demonstration Number One (RFD-1):

Report No.	Title
SC-RR-64-501	Re-entry Flight Demonstration Number One (RFD-1): Final Flight-Test Plan
SC-RR-64-502	Re-entry Flight Demonstration Number One (RFD-1): Data Book
SC-RR-64-510	Re-entry Flight Demonstration Number One (RFD-1): Comparison of the Preflight and Observed Trajectories
SC-RR-64-515	Re-entry Flight Demonstration Number One (RFD-1): Preflight Disassembly Analysis and Observed Disassembly of the Simulated SNAP-10A Reactor
SC-RR-64-516	Re-entry Flight Demonstration Number One (RFD-1): Optical Data and Fuel Element Experiment
SC-RR-64-517	Re-entry Flight Demonstration Number One (RFD-1): Atmospheric Sciences Support

4

TABLE OF CONTENTS

TABLE OF CONTENTS (cont)

LIST OF ILLUSTRATIONS (cont)

RE-ENTRY FLIGHT DEMONSTRATION NUMBER ONE (RFD-1):
DESIGN, DEVELOPMENT, AND PERFORMANCE OF THE RE-ENTRY VEHICLE

SECTION I -- INTRODUCTION

RFD-1, a re-entry flight test of an inert SNAP-10A reactor, was one of a series of tests conducted to evaluate the safety characteristics of aerospace nuclear power supplies. The SNAP-10A was selected for RFD-1 because it was scheduled to be the first reactor to operate in space.

The SNAP-10A (Figure 1) is a reflector-controlled nuclear reactor providing the heat source for the thermoelectric energy conversion system of the SNAP-10A Auxiliary Power Unit (APU) (Figure 2). The heat transfer medium between the reactor core and the thermoelectric junctions is a eutectic mixture of sodium-potassium (NaK-78). The APU is designed to deliver 500 watts of electrical power for a life of one year.
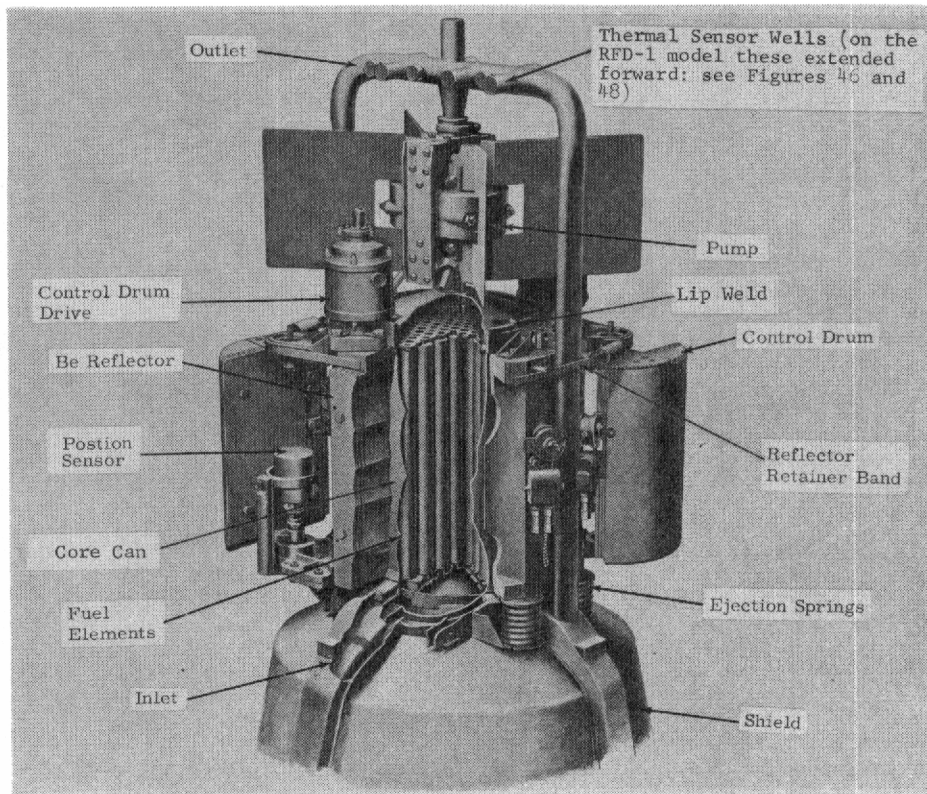
Figure 1. SNAP-10A reactor

DETAIL A ENLARGED
RADIATOR

CONVERTER TUBE
THERMO-ELECTRIC
JUNCTION
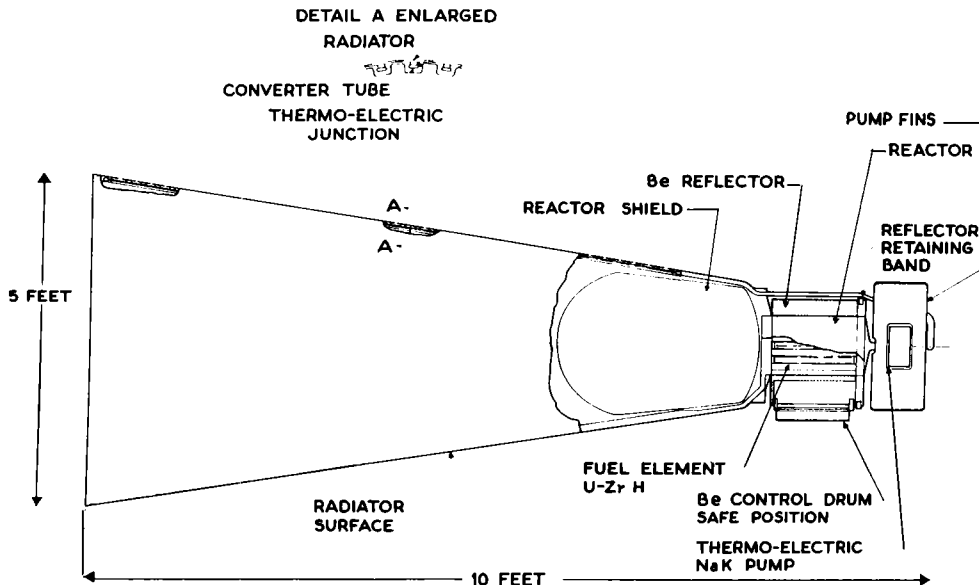
Figure 2. SNAP-10A

After operating at the planned power level for one year, the reactor will have built up a long-lived fission product inventory. In certain orbits, disposal of this inventory will be necessary in order to preclude any significant hazard to the earth's population. The design goal observed by AI is to provide a reactor configuration which will allow disassembly and early dispersion of the core so as to provide the best opportunity for burnup of the core during the aerodynamic heating associated with re-entry into the earth's atmosphere. A detailed description of the mechanical disassembly features included in the reactor design to make possible such early exposure of the reactor core is given in "Re-entry Flight Demonstration Number One (RFD-1): Preflight Disassembly Analysis and Observed Disassembly of the Simulated SNAP-10A Reactor" (Sandia Corporation report SC-RR-64-515).

In an attempt to approximate the aerodynamic heating of the reactor which occurs during orbital decay, the RFD-1 was flown on a re-entry trajectory from Wallops Island, Virginia, to an impact area approximately 200 miles southeast of Bermuda. The NASA Scout booster (Figure 3) was used to place the re-entry system (Figure 4) into the required trajectory. As Figure 5, the flight trajectory, shows, the Scout fourth-stage motor burned out at an altitude of approximately 400,000 feet. This altitude was considered to be the start of re-entry for RFD-1.

The main objective of RFD-1 was to provide experimental data on the sequence of reactor disassembly during re-entry heating, since a comparison between theoretical predictions and experimental heating data measured during the flight would make it possible to determine the validity of present burnup computer programs. To obtain this data, the SNAP-10A Simulated Test Reactor (STR) was instrumented with switches and thermocouples to give the temperature responses of the reactor and to determine at what points in the trajectory the major parts of the reactor disassembled.

12
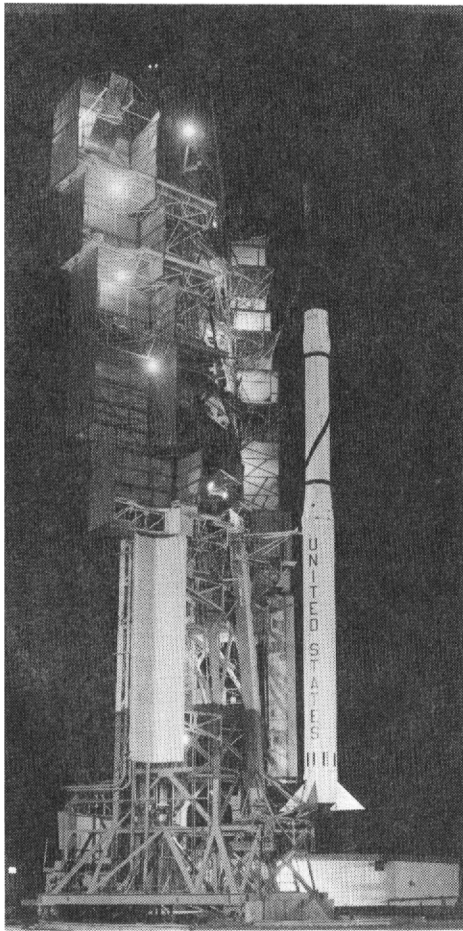
Figure 3.

NASA Scout vehicle

Access Door
C-Band Antenna Window
External Fuel Rods
Disassembly Springs
Simulated Reflector
Fins

TM Antenna Window
Location of Simulated Fuel Rods
Core Can
NaK Tube

Re-entry Vehicle
Reflector Retainer Band
Lipweld
NaK Pump
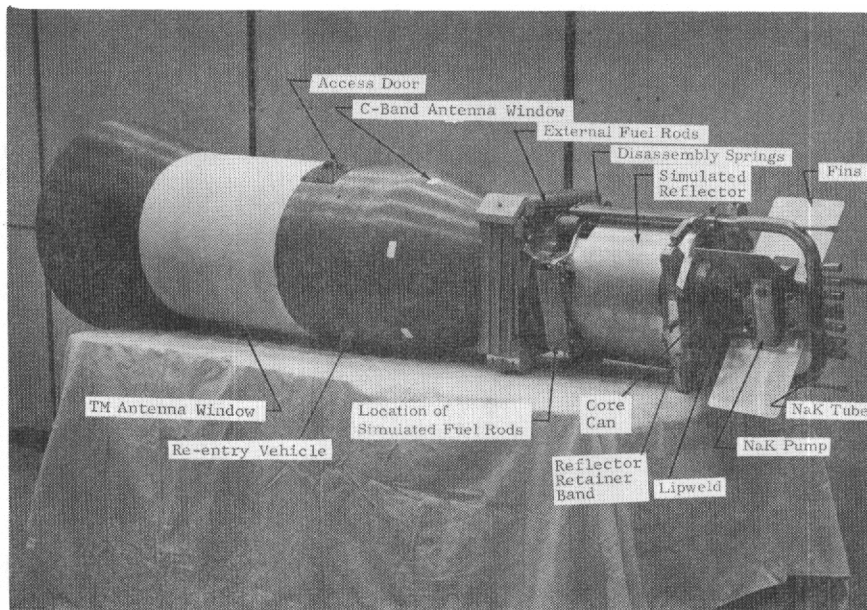
Figure 4.   RFD-1 re-entry system
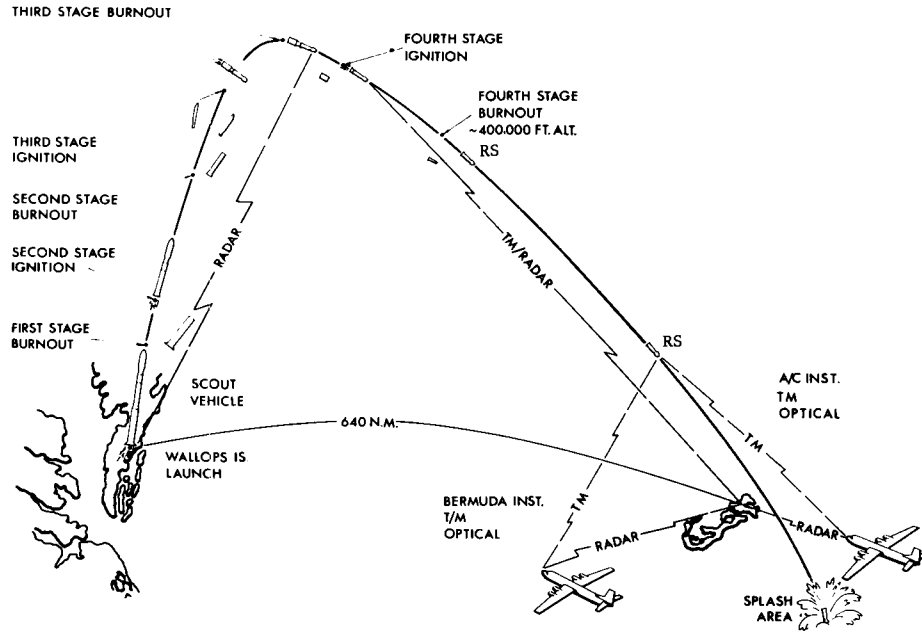
Figure 5. SNAP-10A safety flight-test trajectory

A secondary objective of the flight test was to obtain data on the burnup of full-scale reactor fuel elements. For this purpose, two groups of simulated fuel rods were incorporated into the re-entry system. One group of 12 full-scale simulated SNAP-10A fuel rods filled with tracer material was ejected from the re-entry system before appreciable aerodynamic heating occurred. These rods were specially designed to yield information on burnup rates. A second group of three fuel rods consisting of short cylinders of simulated fuel rod material was embedded in the base of the reactor. These rods, after being subjected to re-entry heating, were to be examined upon recovery of the vehicle. In addition, recovery of the re-entry vehicle (RV) would have yielded useful information for the design of future re-entry systems.

This report, one of a series comprising the final documentation of RFD-1, discusses in detail the design, development, and performance of the re-entry vehicle assembly. In addition, brief discussions of the SNAP-10A simulated test reactor and of the external fuel rod experiment are given. More definitive information on the reactor, external experiments, and the flight test are given in the other reports listed on page 4 of the Foreword to this report.

SECTION II
DESCRIPTION OF THE SNAP-10A SIMULATED TEST REACTOR

The RFD-1 payload was a full-scale SNAP-10A inert reactor mockup fabricated and instrumented by Atomics International (AI). The instrumentation requirements for the reactor-RV interface, and the deviations from an operational SNAP-10A reactor which would be required, were determined by joint agreement between AI and Sandia Corporation. Actual SNAP-10A reactor parts were used wherever possible, with the exception of the following deviations:

1. The beryllium reflectors and control drums were replaced by aluminum components designed to simulate the shape of the beryllium parts and their clearance from the core can. This modification was primarily dictated by the payload weight limitations of the Scout vehicle; however, the substitution of aluminum for beryllium also precluded the possibility of any BeO hazard from burnup or ablation of the beryllium parts. The aluminum reflectors and drums were provided with actual SNAP-10A hinges, ejection springs, and fusible link band.

2. The NaK coolant was omitted from the system to reduce weight, to prevent the large NaK flare from obscuring the tracer material in the external fuel rod experiment, and to prevent extension of the region of RF blackout. (During actual orbital decay, the NaK line will burn off early in re-entry, thereby permitting the NaK to escape.) It was estimated that absence of the NaK would affect heat transfer rates in the range from 0.5 to 6.0 percent, depending on overall conditions.

3. The fuel-rod complement and internal beryllium reflectors were also removed from the core can, since theoretical studies showed that their removal would not appreciably affect heat transfer to the core can. Also, theoretical studies based on measured heat inputs on a full-scale reactor tested in the AEDC 100-inch hot-shot tunnel, and verified by tests of a reactor core can in the Sandia radiant heat facility using the measured heat input, indicated that, for the RFD-1 trajectory, the core can would not have burned up sufficiently to permit fuel-rod separation until an altitude of approximately 120,000 feet. Aerodynamic forces would probably prevent separation of the fuel rods until even lower altitudes. Fuel rods separated at this lower altitude for RFD-1 were not expected to experience enough aerodynamic heating to yield any information on fuel-rod burnup.

These changes were in part necessary to keep the system within the weight specifications of the Scout vehicle. They also made it possible to include the external fuel rod experiment on RFD-1.

The reactor was extensively instrumented with 21 thermocouples to measure temperatures on the fusible link band, the band support, the band weld, the band standoff, the fins, the NaK tube, the base of the NaK pump, the lip weld, the core vessel wall, and the heat meter attached to the reactor base ring. Six switches were mounted to monitor the ejection of the reflector and the disassembly of the core vessel.

In order that the simulated fuel rods might be recovered without the obstacles which a realistic fuel rod assembly would present to the main RFD-1 objective of demonstrating reactor disassembly, three cylindrical pieces of material simulating reactor fuels were attached to the base of the reactor. Two of these simulated fuel rods, consisting of UZrH, were 1-1/4 inches in diameter; a third, consisting of

15

uranium carbide in a graphite matrix, was 1/2 inch in diameter. All three were 1-1/4 inches long. A copper slug heat meter 1-1/4 inches in diameter and 1-1/4 inches long was also fastened to the base of the reactor to register re-entry heat input at this location.

SECTION III -- DESCRIPTION OF THE RE-ENTRY VEHICLE

General

The re-entry vehicle was designed to be (1) a support structure for externally attached test components, (2) a thermal protector for certain components required to survive re-entry heating, and (3) an aerodynamic shape to fly a defined trajectory. The two externally attached components were the SNAP-10A simulated test reactor (STR), mounted forward on the re-entry vehicle, and the components for the fuel rod experiment, attached on the conical nose section aft of the SNAP-10A STR. Supported and thermally protected components included the telemetry package with antenna systems, and the recovery system. In addition, the re-entry vehicle contained an internally mounted separation system, needed to separate the expended fourth-stage Scout motor from the re-entry vehicle. All these components are shown on the re-entry vehicle assembly (Figure 6).

The complete re-entry system is shown together with the Scout 34-inch diameter heat shield (Scout Sta. -25) in Figure 7 (p. 23). For design purposes, the outside configuration of the re-entry vehicle was limited by this 34-inch heat shield between Scout Stations -13 and 94. Its inside configuration, on the other hand, was limited by the Scout fourth-stage motor and by the upper "D" section between Scout 47.78 and 84.65.

Physical characteristics of the RFD-1 re-entry system were as follows:

1.	Weight	482.0 pounds
2.	Weight required for spin balance after mounting the re-entry system on the fourth-stage motor	7.9 pounds
3.	Center of gravity (CG)	Scout Sta. 34.89
4.	Roll moment at CG	6.2 slug ft^2
5.	Pitch moment of inertia at CG	69.6 slug ft^2
	Yaw moment of inertia at CG	69.6 slug ft^2
6.	Length	97.63 inches
7.	Flare Diameter	26.5 inches

Structural Assembly

The support structure of the cone-cylinder-flare re-entry vehicle body used phenolic fiberglass cloth layup both as a supporting member and as insulation. Ablation material, tape-wound in shingled layers on a mold, was machined to dimension and bonded in place over this cloth layup on the flare and nose of the re-entry vehicle body. The tape used was fiberglass impregnated with phenolic resin. The ablation material over the cylindrical section of the vehicle body was teflon. This material was used because it sublimes in ablating, leaving a clean uncharred surface which does not interfere with RF transmission from the cylindrical dipole telemetry antennas inside the vehicle body. Similarly, six teflon windows were used

over the six C-band antennas in the nose for RF transparency. The teflon ablation material over the C-band antennas was bonded in place with high-temperature Epon 931 adhesive.

To provide a thermal expansion joint, a layer of Cohrlastic silicone sponge rubber was bonded between the teflon cylinder and the body with DC 521 silicone adhesive. The ablative nose section was bonded in place with Epon 931 adhesive. Three inches of the fiberglass nose section were made to overlap the leading edge of the teflon to prevent erosion of the latter.

A phenolic fiberglass forward mounting plate was bonded to the nose of the body with Epon 931 adhesive. Three 1/4-inch bolts were then installed to carry the structural load. To this mounting plate the SNAP-10A STR was attached; and in the cavity of the plate, the instrumentation cable connectors were installed. After their installation the fiberglass mounting plate area was thermally protected and sealed with Silastic foam RTV 601 and an ablative coating of Dyna Therm E-300.

Mounting hardware between the body of the re-entry vehicle and the fourth-stage Scout motor included: (1) an aluminum mounting plate, (2) a magnesium ring, (3) a truncated conical magnesium structure, (4) an aluminum ring, (5) an aluminum cylindrical ring, and (6) four centering supports as shown in Figure 6.

The structural portions of the body and the metal alloy mounting hardware were designed to meet the mechanical environmental test levels recommended by the NASA Scout Project Group for design qualification and flight acceptance testing of Scout-launched spacecraft. The structural design criteria used in designing the re-entry system are given in Appendix A. The flight environments and the environmental test levels used in development tests are discussed in Section XII of this report.

The body of the re-entry vehicle was attached to the mounting plate at Scout Station 39.47 with thirteen #10 screws installed radially through the fiberglass body. The holes over the screwheads were covered with ablative material (Dyna Therm E-300) after the re-entry vehicle was assembled.

The body of the re-entry vehicle was simply supported by the fourth-stage motor at Scout Station 84.65 by means of the four centerings supports attached to the motor (these supports were designed to wedge against the re-entry vehicle).

MC-1441
311246-00

SALT WATER SWITCH
2 REQD

N41583-0

N44956-19

SECTION J-J
ROTATED 45° CCW

6 PLCS IN DOOR (N47424-1)

SECTION E-E
ROTATED 15° CCW

SECTION F-F
ROTATED 15° CW

STA
14.33

STA
38.85

STA
47.78

STA
84.65

ROTATED INTO
PLANE

TELEMETRY PACKAGE
N42341

SET N44956-12 BRACKET (SEE
SH 2) SOLID AGAINST ADAPTER
N41482-0, AND SHIM TO TAKE
UP GAP IF NECESSARY, AS
SHOWN.

N41487-0

N47424-1

N44956-16

N44913-0

N41481-1

N41508-0

N41499-0

N41575-9

N44910-2

248 MOTOR

SEE SHEET 2

N   N

N   N

N45068-0

N48679-0

N44964-0

N41486-0

N41482-0

N41530-0

N41578-0
ASSEMBLY
(SHOWN IN
SECTION)

SIMULATED SNAP IOA REACTOR FURNISHED
BY ATOMICS INTERNATIONAL CANOGA PARK,
CALIFORNIA.

B

B

N45068 (REF)

FOAM IN, TO SECURE
BATTERIES
(BATTERIES ROTATED
INTO PLANE)

5.12 ±.06

FLARE CLEARANCE AND ENVELOPE
AVAILABLE FOR RETRO ROCKETS

N41575-8

N41575-7

ROCKET MOTOR
NOT SHOWN

Figure 6.   Re-entry vehicle assembly

YAW AXIS (TOWER SIDE)

SEE DWG NXXXXX FOR INSTALLATION OF FUEL RODS.

YAW AXIS (TOWER SIDE)

F   E

F

E

E   J

J

N41529-0

PITCH AXIS

BATTERIES TWO DEEP HERE

TWO 2% SACKS FLUORESCENT DYE MARKER

N41575-6

N44956-15

SECTION N-N

YAW AXIS (TOWER SIDE)

VIEW A-A
COVER REMOVED

Figure 6 (continued)

ROD EJECTOR ASSEMBLY
(N44964) NOT SHOWN

20

NOTES

1. PURCHASE FROM VOUGHT ASTRONAUTICS BOX 5907, DALLAS 22, TEXAS.

2. MAY BE PURCHASED FROM HI-SHEAR CORP., TORRANCE, CALIF., OR SANDIA APPROVED EQUIVALENT.

3. PC-24 POWER CARTRIDGE TO BE SHIPPED AS A CLASS 'C' EXPLOSIVE AND IS TO BE INSTALLED IN THE FIELD.

4. MAY BE PURCHASED FROM ATLANTIC RESEARCH CORP., ALEXANDRIA, VA., OR SANDIA APPROVED EQUIVALENT.

5. ROCKET MOTOR TO HAVE IGNITER LOCATED AT THE HEAD.

6. MAY BE PURCHASED FROM SIMMONDS PRECISION PRODUCTS INC., TARRYTOWN, N.Y., OR SANDIA APPROVED EQUIVALENT.

7. MAY BE PURCHASED FROM ORDNANCE ASSOCIATES, INC., SOUTH PASADENA, CALIF., OR SANDIA APPROVED EQUIVALENT.

8. ALL WIRES AND CABLES AFT OF PLATE, MTG (N41487-0) TO BE PROTECTED WITH TEFLON SLEEVING .020 WALL MIN.

9. MAY BE PURCHASED FROM RAY-CHEM WIRE CORP., REDWOOD CITY, CALIF., OR SANDIA APPROVED EQUIVALENT.

10. MAY BE PURCHASED FROM ACR ELECTRONICS CORP., 551 W. 22nd ST., NEW YORK 11, N.Y., OR SANDIA APPROVED EQUIVALENT.

11. MAY BE PURCHASED FROM ATLAS CHEMICAL INDUSTRIES, INC., WILMINGTON 99, DELAWARE, OR SANDIA APPROVED EQUIVALENT.

12. MAY BE PURCHASED FROM ENDEVCO CORP., PASADENA, CALIF., OR SANDIA APPROVED EQUIVALENT.

13. BOND WITH EPON 931, PARTS A & B. SANDIA MATERIAL SPEC SG167631. MAY BE PURCHASED FROM SHELL CHEMICAL CO., PITTSBURG, CALIF., OR SANDIA APPROVED EQUIVALENT. REMOVE MOLD FINISH FIRST.

14. FLEXIBLE URETHANE FOAM, FILLER CALCIUM CARBONATE, DENSITY 14.5 ± 0.5 LB/FT³ MAY BE PURCHASED FROM AMERICAN LATEX PRODUCTS CORP., 3341 WEST EL SEGUNDO BLVD., HAWTHORNE, CALIF., MFR'S NO. 292-778-2, OR SANDIA APPROVED EQUIVALENT.

15. SALT-SPRAY CORROSION TEST OF QQ-P-416, & QQ-Z-325 IS HEREBY WAIVED FOR ACCEPTANCE OF MATERIAL.

16. SILASTIC, RTV 601, PRODUCT OF DOW CORNING CORP., MIDLAND, MICHIGAN. INSTALL PER MANUFACTURER'S INSTRUCTIONS.

17. MAY BE PURCHASED FROM WALTER KIDDIE & COMPANY, INC., BELLEVILLE, NEW JERSEY, OR SANDIA APPROVED EQUIVALENT.

18. PRIME SURFACES TO BE BONDED WITH DOW CORNING A1201 PRIMER, AIR DRY MINIMUM OF 30 MINUTES, BOND WITH DOW CORNING 502 RTV PER MANUFACTURER'S INSTRUCTIONS.

19. LOOKING AFT WITH DOOR OPENING ORIENTED ON THE YAW AXIS (TOWER SIDE), RING TO BE LOCATED SO THAT THE PINS ON THE RING ARE TO THE RIGHT AND LIE ON THE PITCH AXIS.

20. BOND WITH RTV 102, PRODUCT OF GENERAL ELECTRIC, SILICONE PRODUCTS DEPT., WATERFORD, NEW YORK. COAT HARD SURFACES WITH S-4004 PRIMER BEFORE BONDING. ALTERNATE: RTV 140, PRODUCT OF DOW CORNING CORP., MIDLAND, MICHIGAN. BOND PER SANDIA MATL SPEC SG127796. COAT HARD SURFACES WITH A-4094 PRIMER BEFORE BONDING.

21. PURCHASE FROM DYNA-THERM CORP., THERMAL SPACE DIVISION, 528 W. AVE. 26, LOS ANGELES, CALIFORNIA. INSTALL PER MANUFACTURER'S INSTRUCTIONS.

22. APPLY BASE COAT OF E-300 (ITEM 156) .200 (APPROXIMATE) THICKNESS. THEN APPLY .040 (APPROXIMATE) THICKNESS OF D-65 (ITEM 155).

23. MAY BE PURCHASED FROM PIONEER PARACHUTE CO., MANCHESTER, CONN., OR SANDIA APPROVED EQUIVALENT.

24. CONSTRUCTED BY NORTON A.F.B., SAN BERNARDINO, CALIFORNIA.

25. MAY BE PURCHASED FROM CUSTOM COMPONENTS SWITCHES INC., 21111 PLUMMER ST., CHATSWORTH, CALIF, OR SANDIA APPROVED EQUIVALENT.

LIST OF PARTS

PART NO.	DESCRIPTION	REMARKS
ITEM 75	DROGUE GUN	8-073-1
76	DC-DC CONVERTER	TYPE 319004 (500V)
77	TRANSMITTER	TYPE 311020 (25W)
78	ACCELEROMETER	MODEL 2235C
79	FLOTATION 9700 CU. IN. SYSTEM	DWG NO. 892449
80	7FT. DIA, SOLID, FLAT, CIRCULAR PARACHUTE	
81	BATTERY (SANDIA STK. #G0083)	MALLORY NO RM-42R
82	FLASHING LIGHT (SWITCH MODIFIED)	MODEL ACR4C
83	FLOATATION BAG	
84	SEPARATION NUT	HIS-SN 2301-2
85	POWER CARTRIDGE	HIS-PC-24
86	ROCKET MOTOR	IKS 40HA-2
87	SWITCH, ABSOLUTE PRESSURE	P/N 8A165
88	AMPLIFIER	MODEL 2646 MI
89		
90	SQUIB SWITCH	DELAY TYPE OM NO. 396
91		
92	RETAINER, BATTERY, AL	SANDIA STK. #G06479
93	RETAINER, BATTERY, AL	SANDIA STK. #G06480
94	WIRE, TYPE R, SIZE #20	
95		
96	NUT, SELF-LKG, HEX. 1/4-28UNF-3B	NAS1022N4
97	NUT, SELF-LKG, HEX. #6-32UNC-3B	NAS1022N06
98		
99	BOLT, MACHINE #10-32UNF-3A x 21/32LG	AN3-5A
100	WASHER, FLAT	AN960-D10L
101	SCREW, MACHINE #6-32UNC-2A x 1/2LG	AN526-632R8
102	SCREW, MACHINE #6-32UNC-2A x 3/8 LG	AN526-632R6
103	CLAMP	AN73504
104		
105		
106	BOLT, MACHINE #10-24UNC-3A x .594LG	MS20074-03-04
107	WASHER-LOCK	AN935-10L
108		
109	WASHER, FLAT	AN960-10L
110	WASHER, LOCK	MS35337-24
111	WASHER, LOCK	MS35337-23
112	BOLT-100° #10-32UNF-2A x .906LG	NAS333-PA7
113		
114	WASHER, LOCK	MS35340-24
115		
116		
117	NUT, SELF-LKG, HEX. #8-32UNC-3B	870123
118		
119	SCREW, CAP, SCH #8-32UNY-3A x 1/2LG	870701
120	SCREW, CAP, SCH #10-32UNF-3A x 5/8 LG	870819
121		
122	PIN, STR, HEADED	MS20392-3-39
123	PIN, COTTER	MS 24665-132
124		
125	SCREW, MACHINE #8-32UNC-2A x 3/8LG	MS35192-40
126	SCREW, MACHINE #10-32UNF-2A x 5/8LG	MS35193-56
127	SCREW, CAP, SCH #8-32UNC-2A x 3/8LG	870541
128		
129	NUT, SELF-LKG, HEX. #10-32UNF-3B	870124
130		
131	SCREW, CAP, SCH #8-32UNC-2A x 3/4LG	
132	WASHER, FLAT	AN960-8L
133		
134	SCREW, MACHINE #2-56UNC-2A x 5/8 LG	MS35208-8
135		
136		
137	SCREW, CAP, SCH #6-32UNC-2A x 1/2 LG	870787
138	NUT, SELF-LKG, HEX. #6-32UNC-2B	NAS1012N06
139		
140	SCREW, CAP, SCH #10-32UNF-2A x 3/8 LG	870713
141	SCREW, CAP, SCH #6-32UNC-2A x 3/8 LG	870597
142	WASHER, LOCK	MS35337-22
143		
144	SCREW, MACHINE #4-40UNC-2A x 7/16 LG	MS35208-15
145		
146		
147		
148	FOAM, SILASTIC, RTV 601	
149		
150	FOAM	
151	BONDING MATERIAL	
152	BONDING MATERIAL	
153	BONDING MATERIAL	
154	LAQUER STAKING	(GLYPTAL 1201) PER SG162073
155	INTUMESCENT PROTECTIVE COATING	DYNA-THERM D-65
156	ABLATIVE COATING	DYNA-THERM E-300

LIST OF PARTS

PART NO.	DESCRIPTION	REMARKS
N41508-0	SHELL SUB-ASSY	
N41481-1	RING, AFT ADAPTER	
N41482-0	ADAPTER	
N41486-0	RING, FWD ADAPTER	
N41487-0	PLATE, MTG	
N41499-0	COVER, PARACHUTE	
N41529-0	SUPPORT, CENTERING	
N41530-0	SHIELD, CLAMP	
N41575-6	SUPPORT, CENTERING	
N41575-7	BRACKET, MOTOR	
N41575-8	RING	
N41575-9	STRAP	
N41583-0	ANTENNA, TE-108	
N42341	TELEMETRY PACKAGE	
N44910-2	STRAP, DROGUE GUN	
N44913-0	SPACER	
N44956-1	CLAMP, SUB-ASSY	
N44956-15	BRACKET	
N44956-12	BRACKET	
N44956-13	PLATE	
N44956-16	GASKET	
N44956-19	HOUSING	
N44964-0	ROD EJECTOR	
N47424-1	DOOR	
N45008-0	RING, WEIGHT	
N48679-0	SHIELD, HEAT	
N44956-17	PLATE	
N44956-18	BRACKET	
311005-00	MC-1192	
311246-00	MC-1441 (MODIFIED)	
320-00023-2	SPRING	
320-00025-3	CABLE	
320-00026-1	PLATE ASSY	
320-00028-1	CLAMP ASSY	
320-00033-1	STUD	
CVC743-4A	SPECIAL WASHER	
CVC754-124-E12	WASHER	

MATCH DRILL CLEARANCE
HOLES IN N41487-0 & N44956-18
AT ASSY

SECTION P-P

N44956-12

109 120 129 MATCH DRILL CLEARANCE
HOLES IN N41487-0 &
N44956-12 AT ASSY

COVER ITEMS 87
COMPLETELY

N44956-17

N44956-18
LOCATE APPROX
AS SHOWN

120 114

COAT FLOATATION BAG
(ITEM 83) AND PULL-OUT
ROPE WITH .040 THICKNESS OF ITEM 185

79

N44956-1

120
129

N44956-13

COVER ITEM 79
COMPLETELY

SECTION B-B
SHEET #1

SECTION M-M

SECTION L-L

YAW AXIS
(TOWER SIDE)

N41481-1 (REF)

.03 MIN GAP

CLAMP GAPS TO BE EQUAL WITHIN .06
AFTER TORQUING.

320-00028-1

TIGHTEN CLAMP NUTS ALTERNATELY
UNTIL A TORQUE OF 35 ± 5 IN-LBS
IS REACHED. TAP CLAMP LIGHTLY
ALONG ITS CIRCUMFERENCE WITH
A MALLET TO SEAT CLAMP UNI-
FORMLY. CHECK NUT TORQUE. RE-
PEAT OPERATION UNTIL CORRECT
NUT TORQUE IS REACHED AND
MAINTAINED.

PITCH AXIS

320-00033-1
CVC 743-4A

LOCATE AND DRILL
ON ASSY

4 REQ'D OF EACH
CVC 754-124-E12
1 WASHER UNDER
EACH NUT

Figure 6 (continued)

21
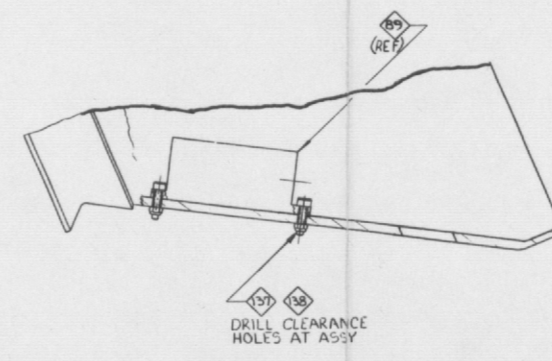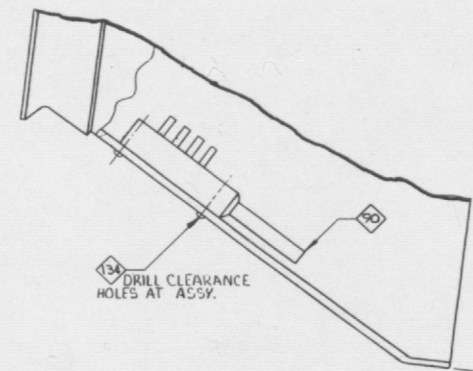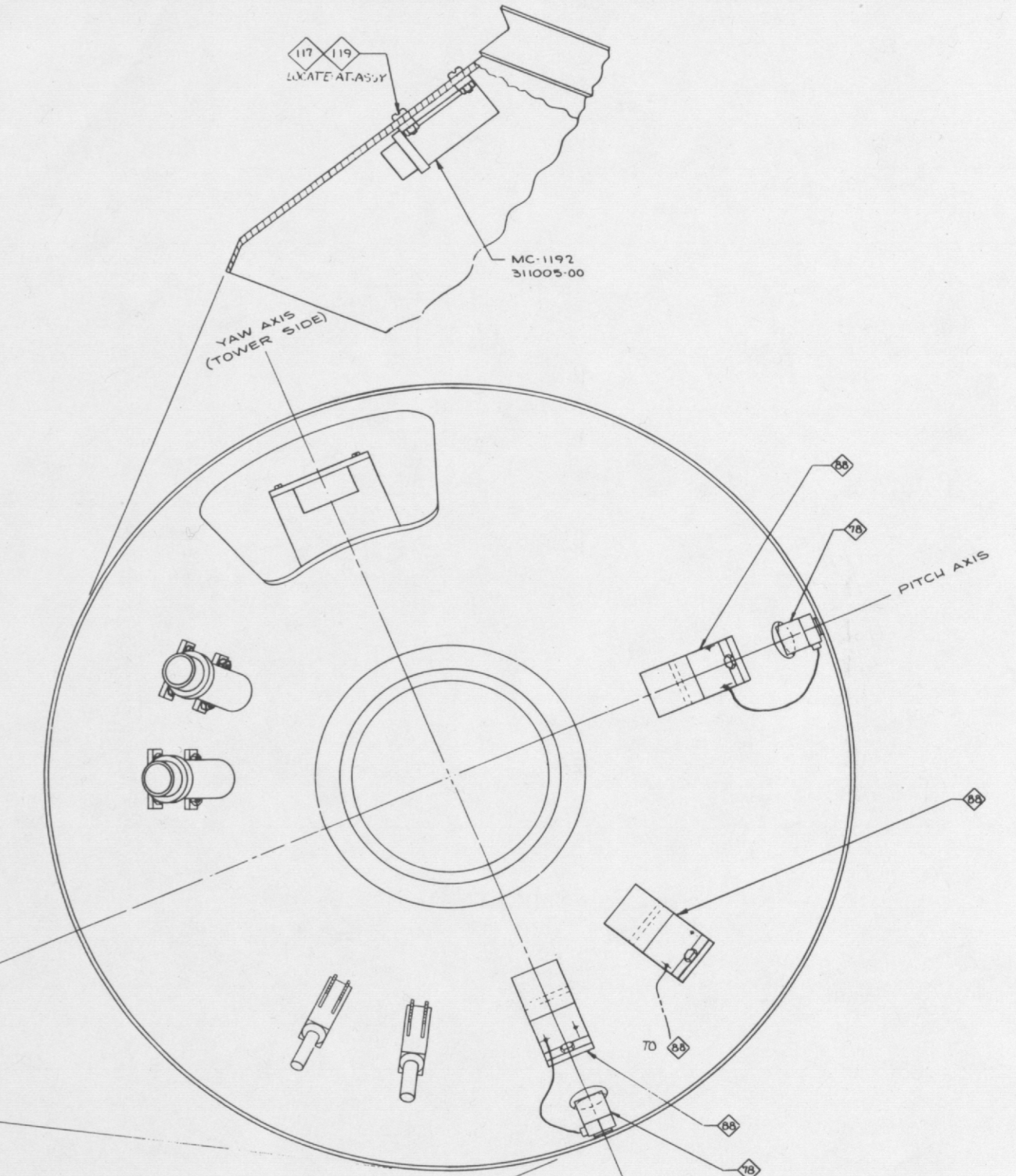
Figure 6 (continued)
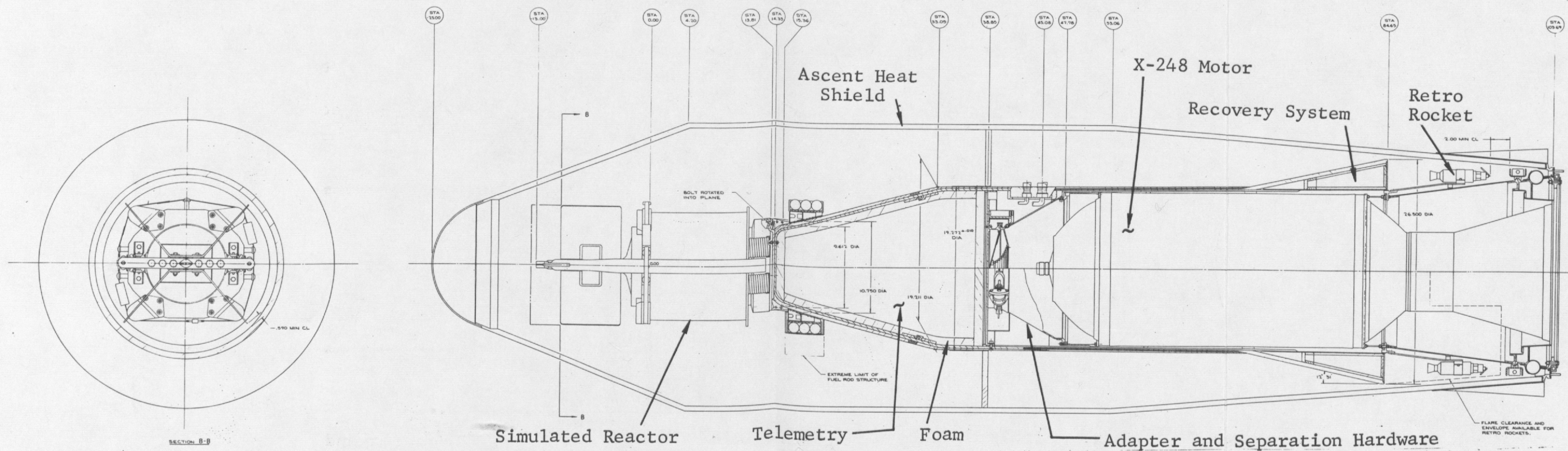
Figure 7. Layout drawing of RFD-1 with fourth stage motor

SECTION IV -- ELECTRICAL SYSTEM

The electrical system in RFD-1 included the telemetry, the C-band beacon, the pyrotechnic circuitry, and a programmer to provide timed signals for the vehicle functions.

Telemetry System

As shown in the block diagram in Figure 8, the telemetry for RFD-1 comprised a standard FM/FM system in which eight subcarriers were transmitted in real time and three were delayed by means of a closed-loop tape recorder. The information stored on the tape during RF blackout was transmitted before impact. The system was designed to supply the following information during flight:

1. Vibration at the head end mounting surface of the X-248 motor

2. Acceleration of the re-entry system

3. Attitude of the re-entry system

4. Temperature at several locations in the reactor, and a reference temperature in the re-entry vehicle

5. Disassembly sequence of the reactor

6. Ablation at two locations on the re-entry vehicle

7. Heating rates at two locations on the re-entry vehicle and one at the base of the reactor

8. Time

9. Pressure at the head end of the X-248 motor.

Each of these categories of information is discussed in detail in the paragraphs which follow.

Vibration -- Three Endevco-type, crystal vibration-measuring systems having a frequency response of from 5 cps to 3 kcps were mounted on the fourth-stage adapter, positioned so as to measure vibration in one longitudinal and two orthogonal lateral axes. To these transducers were allotted the three subcarriers of highest frequency as shown in the block diagram (Figure 8). Since the purpose of this instrumentation was to obtain the magnitude of vibration through fourth-stage burning only, the subcarriers were programmed to turn off after the fourth stage was ejected. Following this, the amplitudes of the remaining subcarrier oscillators were increased to provide maximum deviation of the transmitter. Both turnoff and deviation increase were programmed by the timer-decoder.

The signals of the vibration transducers were brought through the "disconnect" connector at the fourth-stage interface of the re-entry system. This arrangement assured that the three high-frequency channels would receive a signal, when separation occurred, in the form of a loss of subcarrier signal voltage.

MIX AMP.

TRANS-MITTER POWER AMP

RING

70.0 — VIB.

180 VOLTS

250 VOLTS

52.5 — VIB.

40.0 — VIB.

MIX. AMP.

NEGATIVE PEDESTAL TO COMMUTATORS

TAPE RECORDER

PYROTECHNIC CIRCUITRY

TIME DECODER

TIMER

6 CAVITIES

C-BAND BEACON POWER DIVIDER

22.0

HI LEVEL COMM 30 × 5

14.5

WHIP

SARAH

SWITCHES LONG. ACCEL. LAT. ACCEL.

LAT. ACCEL.

SALT-WATER SWITCH ACCEL. SWITCH

TEMPERATURES

30

10.5

LOW LEVEL COMM 30 × 1

7.35

3.9 ROLL 5.4

RELAY CONTROL FUNCTIONS

FROM CONTROL PANEL

3.0 PITCH

CALIBRATOR

2.3 YAW

5 VOLT REG. BATTERY

Figure 8. TM block diagram

Acceleration -- Three resistance-type accelerometers were mounted in the telemetry package to provide information in one longitudinal and two orthogonal lateral axes. For the longitudinal measurement, a range of ±20 g's with frequency response of 50 cps was used, while the other two had ranges of ±3 g and response to 20 cps. The signals from these pickups were fed to the high-level commutator for transmission in real and delayed time.

Attitude -- Since a knowledge of the actual attitude of the re-entry system was considered to be of great importance, a roll-stabilized free gyro system was included in the telemetry package. This was a unit capable of following roll rate up to 180 rpm and of providing indications of yaw magnitudes up to ±85 degrees and pitch magnitudes up to ±360 degrees.

Temperature -- All temperatures, except those at the reference junctions and inside the telemetry package, were measured by means of thermocouples. Eight locations in the reactor used chromel/alumel couples on aluminum materials, and twelve used platinum/platinum-13% rhodium couples on steel materials. Since it was undesirable to run these thermocouple wires from the reactor to the telemetry package,

a reference junction was established at a thermally protected location in the base of the reactor (essentially, between the reactor and the re-entry vehicle). At this location, the thermocouple wires were changed to copper wires to complete the circuit back to the telemetry package inside the re-entry vehicle. To provide a measure of the temperature of this reference junction, two platinum resistors were installed and connected as two arms of two bridge circuits within the telemetry package.

To determine the heat input to the three dummy fuel rods mounted at the base of the reactor, a heat meter using a chromel/alumel thermocouple (measuring range to 2000°F) attached to a copper slug was installed alongside the rods. This thermo-couple was also changed to copper wire at the reference junction.

For the two heat meters installed in the RV nose section, a reference junc-tion for changing the chromel/alumel wires to copper was established in the foam insulation between the telemetry package and the wall of the re-entry vehicle. A nickel resistor was embedded in this volume to perform the same function that the platinum resistors performed in the reactor reference junction volume.

As the block diagram indicates, all temperatures were sampled at the rate of once per second and fed into two low-level oscillators for real time and delayed time transmission. Deviation-limited, these oscillators cannot be deviated more than ±10-1/2 percent by any input voltage up to 1.5 volts. In addition, they can be deviated linearly up to +10 percent to provide a temperature range beyond the calibrated value. Sixteen millivolts, corresponding to +7-1/2 percent deviation, would be the output from the platinum/platinum-13% rhodium thermocouple at the melting point of stainless steel (2550°F), although temperatures to over 2900°F would be accommodated by the oscillator at +10 percent deviation.

A voltage divider was inserted in each of the chromel/alumel circuits to pro-vide approximately full-scale (+7-1/2%) deviation at the melting point of aluminum (1200°F). Again, higher temperatures, corresponding to approximately 49 millivolts (2200°F), would be accommodated by the oscillator.

The thermocouples and their copper lead wires were exposed to a strong RF field from the telemetry antenna. To prevent anomalous deviation of the low-level oscillators by RF voltage picked up and rectified within their low-level circuits, it was necessary to place a filter in their signal inputs. Filtering the signals as they entered the telemetry package was not satisfactory because the effects of RF leakage within the telemetry package and of pickup on external control and power leads still remained. All RF effects were successfully eliminated, however, by placing a filter at the input connectors of the two oscillators. Each filter con-sisted of one National Radio R45-254 ferrite choke in each of the two low-level signal leads with a 4700 μμf capacitor shunted between them on the oscillator side of the chokes. As an added precaution, all cables entering the telemetry package were shielded.

Reactor Disassembly Sequence -- Eight switches were installed in the reactor to provide indications of the disassembly events as they occurred. Until reactor dissassembly during re-entry, all eight switches were in the closed position.

Ablation -- Ablation information was obtained by means of two Sandia-designed switches which would constitute an open circuit until a certain depth of ablation was reached, at which depth the conductive products of the phenolic fiberglass would complete the circuit between two conductive leads. Each of the two ablation sensors was designed to indicate three different levels of ablation depth (Figure 9).

Time -- The purpose of the on-board timer was twofold: to supply a time reference to the tape recorder during blackout, and to activate the time decoder at the proper times for the various programmed functions. The time generator (or timer) supplied time information in the form of ten, parallel, binary-coded out-puts. These outputs were multiplexed onto five commutator segments for transmis-sion and recording.

DEPTHS BELOW SURFACE OF PROBES

PROBES	FORWARD CONE	AFT CONE
A	.105	.077
B	.210	.155
C	.105	.077
D	.310	.232
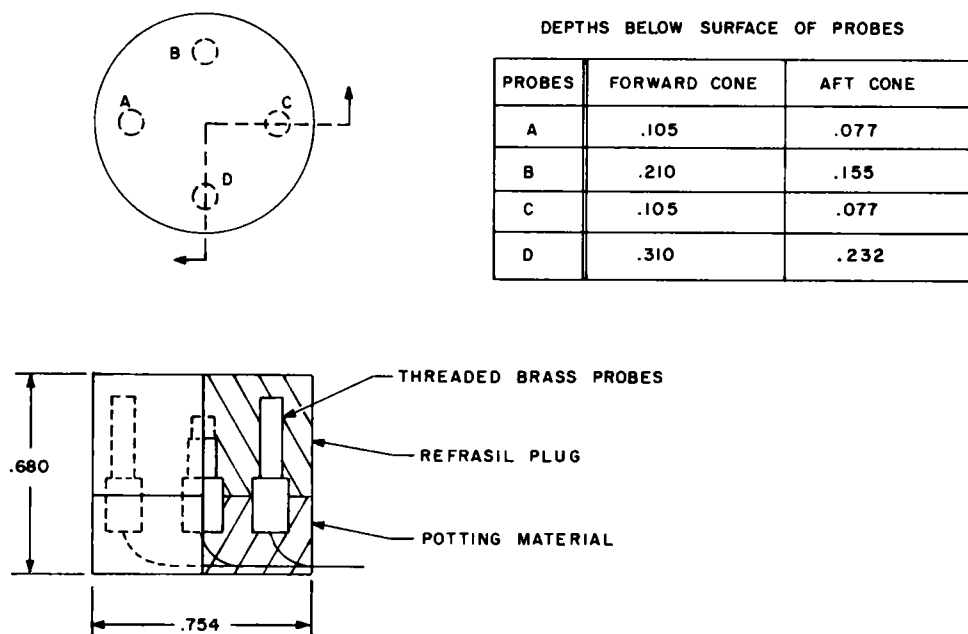
Figure 9. Ablation sensors

Pressure -- The output of a pressure gage supplied by NASA was fed to the high-level commutator and sampled ten times per second.

From a study of the preflight trajectories and from past experience with re-entry tests of other vehicles, it was estimated that RF blackout would begin at about 300,000 feet and end at from 50,000 to 75,000 feet. To cover the time period corresponding to these altitudes, a magnetic tape recorder having a 100-second time delay was used. This recorder, based on a previous Sandia-CEC (Consolidated Electrodynamic Corporation) design, obtained the delay by means of a continuous tape loop driven at a constant speed. In previous Sandia flight tests involving shorter time delays, it had been proved reliable and able to operate during the environments expected in RFD-1.

A three-step calibrator was included in the telemetry package to provide three known voltage levels to the continuous channel oscillators. Calibration for the commutated channels was provided by zero and full-scale volts applied to two contacts on the commutator.

The 5-volt regulator supplied the calibrator and the resistance-type transducers with a stable and known source of voltage. A negative 5 volts, provided by the 180-volt supply, was divided down to the values required for pedestal voltages for the commutated channels. (The pedestal aids in postflight automatic decommutation.)

The RF amplifier provided an output of 10 watts when driven by the 2 watts from the RF transmitter. Both amplifier and transmitter were standard models used and proved by Sandia Corporation in previous missile flight tests. Figures 10 through 13 show the telemetry package.
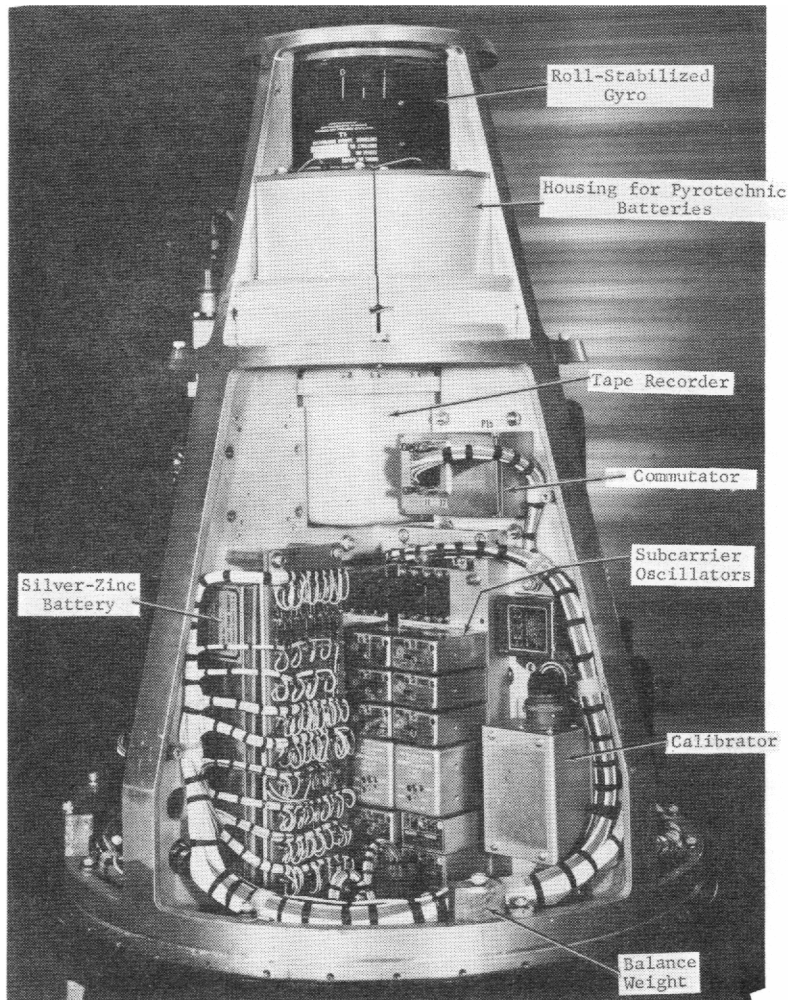
Figure 10. TM package
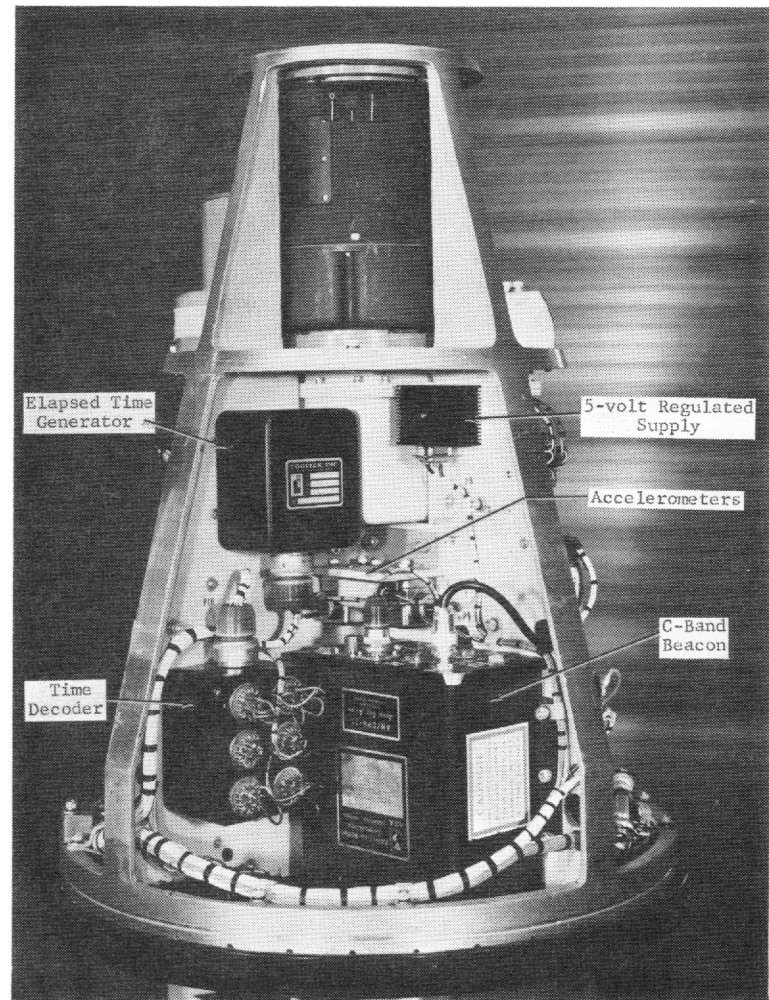
Figure 11. TM package
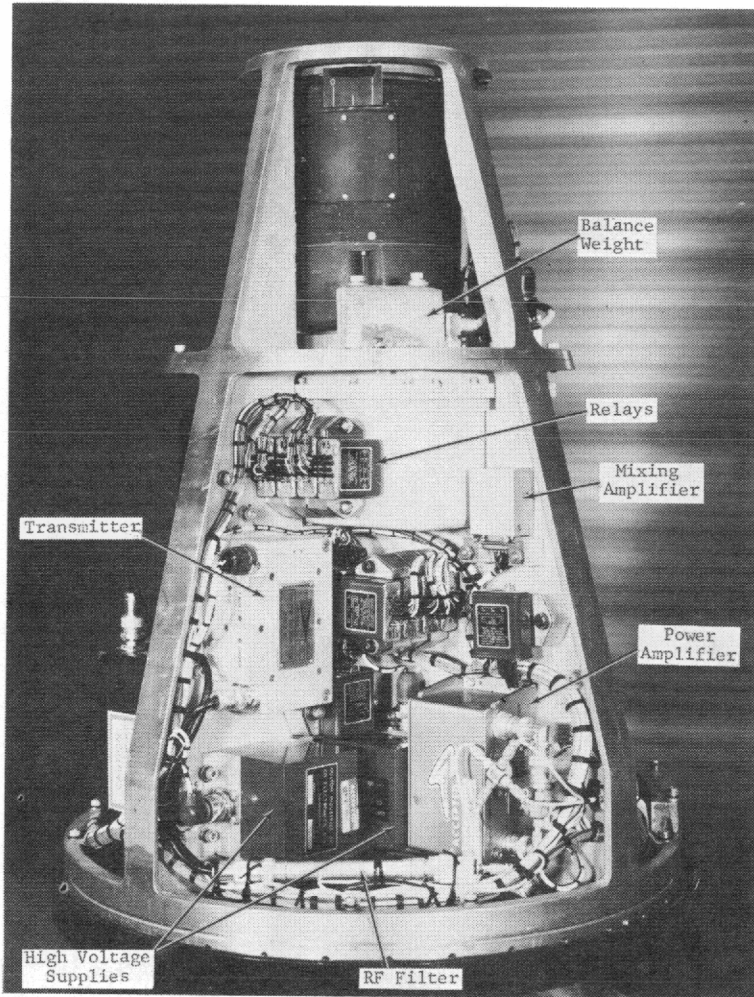
Figure 12. TM package
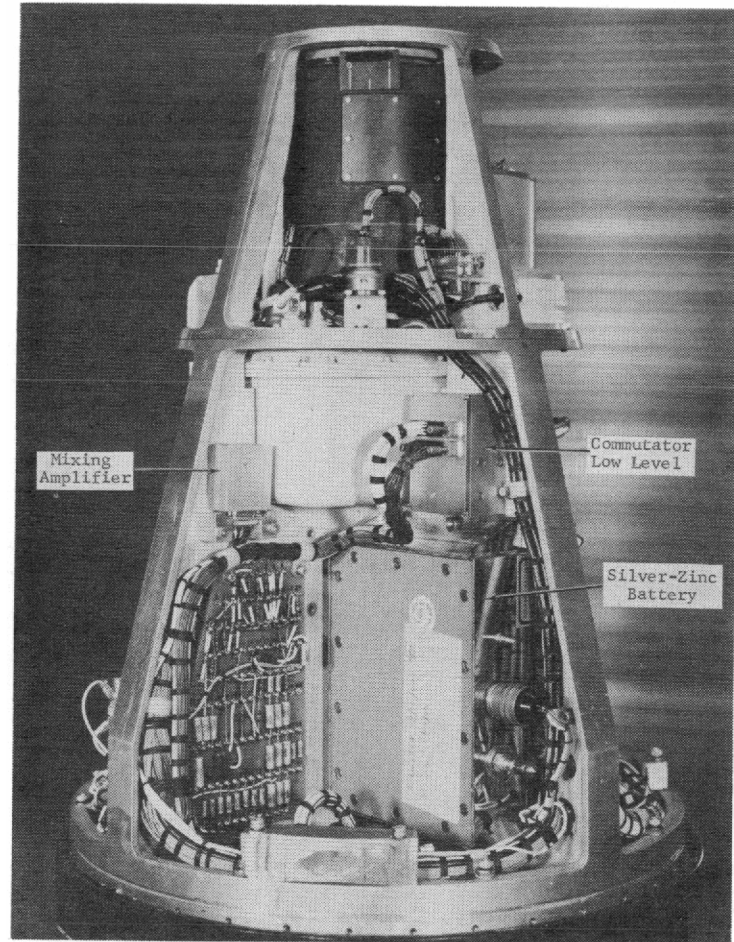
Figure 13. TM package

Antenna System

A "fat" dipole antenna was designed to radiate the RF power from the amplifier. This antenna consisted of two cylindrical shells, each about 11 inches long, electrically separated by 0.4 inch. The antenna is driven across this gap like a standard wire dipole, but because of the large surface area of the cylinders, RF currents are not confined to particular flow paths. Considerable cross-polarization and undesirable patterns result, and voltage breakdown is possible, unless the antenna is driven at more than one point. A complete test for radiation pattern and high altitude breakdown under full power indicated that three equally spaced feed points would provide the characteristics required, and this configuration was accordingly used for RFD-1. Because of space limitations, miniature cable and miniature connectors were used between the RF power amplifier and the antenna.

C-Band Beacon

The beacon, or transponder, selected was the AGA Model 505, which has a peak power output of 400 watts and a sensitivity of about -60 dbm. To prevent the telemetry transmitter from causing faulty operation, the beacon was connected to a power-dividing network through a high pass filter. The power divider matched the 50-ohms output of the beacon to the six cavity antennas mounted in the nose cone portion of the re-entry vehicle. These cavities were canted forward at an angle of 60 degrees from the longitudinal axis to ensure early acquisition by the FPS-16 radar at Bermuda. Again because of space limitations, miniature cable and connectors were also used between the beacon and the cavities.

Pyrotechnic Circuitry

The block diagram for the pyrotechnic circuitry is given in Figure 14. The time decoder shown in the Telemetry Block Diagram (Figure 8, p. 26) was the source of the signals controlling the "fire" relays in the squib circuitry. This decoder was programmed to supply the signals at the correct time and to hold the relays closed for 1 second. With this arrangement, any squib which did not open after firing would not drain the squib batteries. The arming/safing function was controlled and monitored from the blockhouse. Finally, an umbilical connector was provided on the re-entry vehicle for checking the pyrotechnic circuitry after assembly.

Two MC1192 thermal batteries and two time-delay relays to fire the retrorockets were wired in series and mounted on the fourth-stage adapter. The relays were then connected by teflon-insulated wire to the rockets at the rear of the fourth stage. The fire signal for the thermal batteries was brought through the "disconnect" connector at the interface of the fourth stage of the re-entry system.

Thermal Instrumentation

The fuel rod heat meter consisted of a copper slug in an aluminum-oxide ceramic cylinder. The ceramic cylinder was mounted in the base of the reactor near two uranium-zirconium-hydride (UZrH) fuel samples; its dimensions were the same as those of the UZrH fuel samples, so that it would experience the same heating they received. A smaller uranium-carbide fuel sample was also mounted at the same station.

A chromel/alumel thermocouple was mounted in the base of the copper slug in the heat meter for a temperature reading proportional to the total incident heat. Differentiation of this heating curve yielded a heating rate which could be correlated to the rate for the UZrH and uranium-carbide fuel samples.

The re-entry vehicle heat meters consisted of two copper slugs mounted in the skin of the nose. The copper slugs were instrumented with chromel/alumel thermocouples and were designed to operate in the same manner as the fuel rod meter described above.
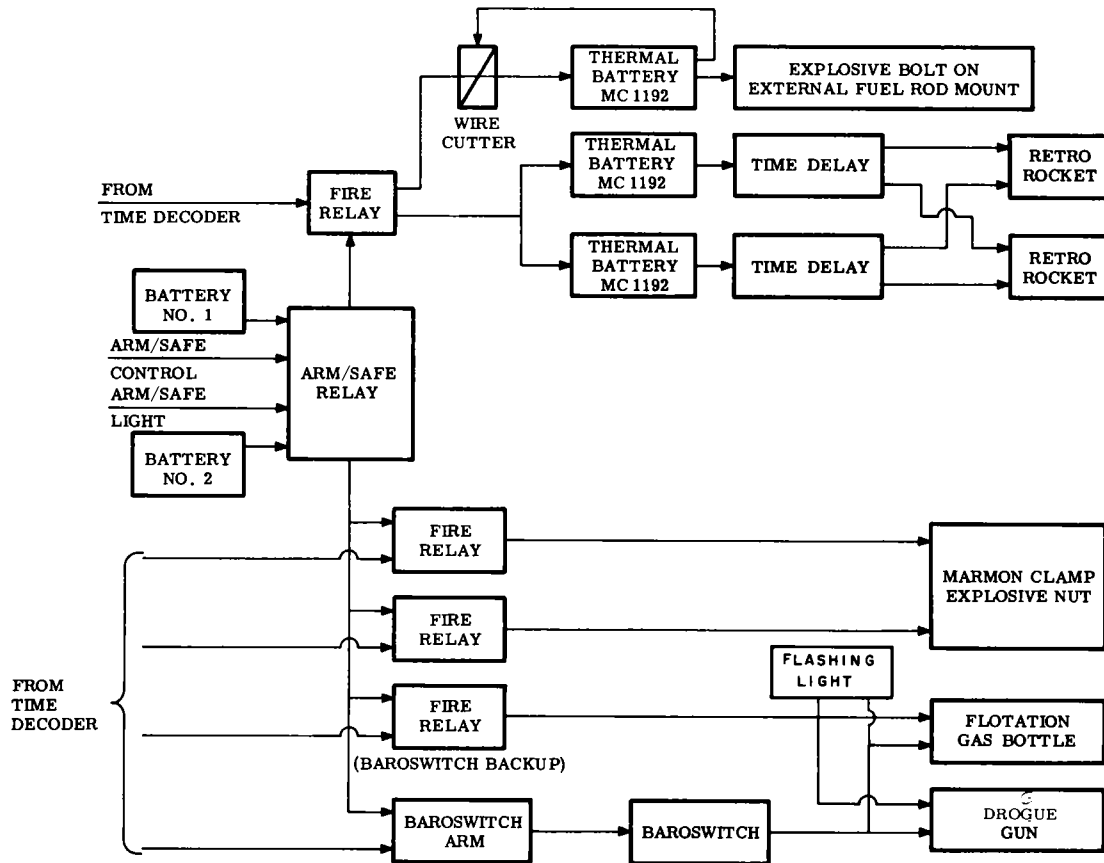
Figure 14. Block diagram of pyrotechnic circuitry

(This type of heat meter was tested in the Sandia plasma jet and radiant heat facilities (see Figure 15). One plasma jet test was run in order to check for erosion and for thermal expansion problems. Numerous radiant heat tests were run over a period of several months in order not only to check response times and heat loss at various heat fluxes but also to compare the Sandia copper slug meters with heat meters of commercial design.)

During the actual RFD-1 flight, the fuel rod heat meter yielded the data shown in Figure 16. The end of the usable data obtained via telemetry before RF blackout occurred, came at a point representing approximately 15 percent of the total integrated heat.

One of the re-entry vehicle heat meters yielded no significant data during the flight. Unlike the fuel rod heat meter, the RV heat meters had been designed to operate throughout the heat pulse. However, at the end of the telemetered data, one of the meters was at about 200°F and the signal-to-noise ratio was so low that the data were useless. (The fuel rod heat meter, on the other hand, was at 800°F at the end of telemetered data, so that the signal-to-noise ratio was high enough to make their data useful.)
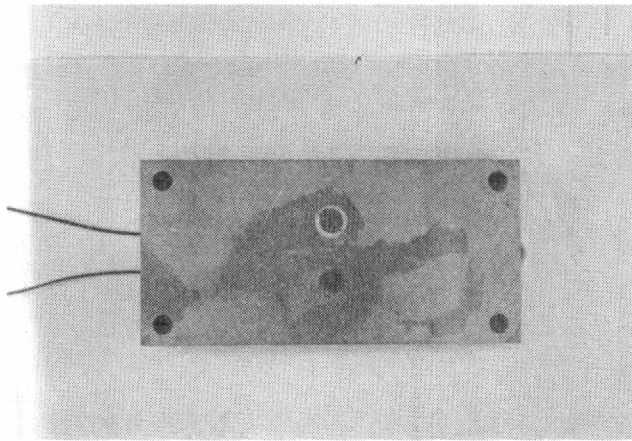
a. Before test
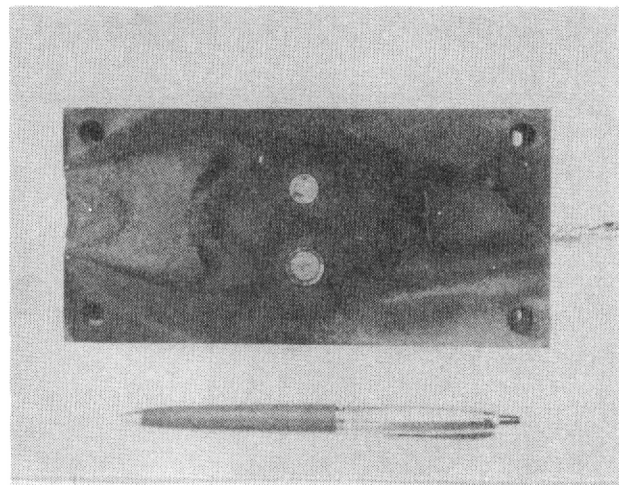
b. After test
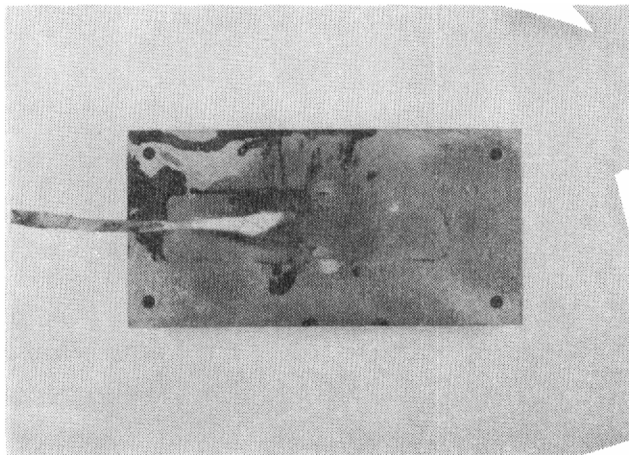
c. Back side of sample
   after test

Figure 15.   Heat meter tested in
             plasma jet facility
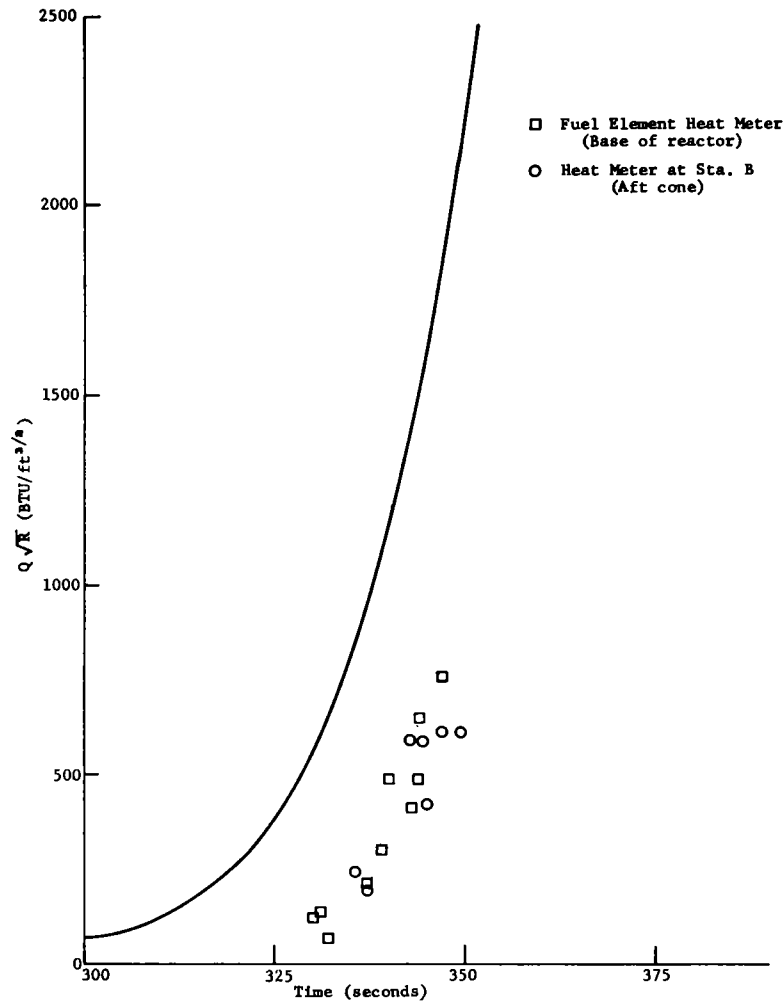
Figure 16. Heat meter results on RFD-1
integrated heating

Ablation Depth Sensors

Two ablation depth sensors capable of measuring three distinct ablation depths were mounted in the nose of the re-entry vehicle, each next to a re-entry vehicle heat meter. These sensors consisted of brass probes threaded into a phenolic refrasil plug at various depths below the surface. The external dimensions and ablation depths of the sensors are shown in Figure 9, p. 28. As ablation proceeded during testing, the reaction zone reached each of the various probes in turn, causing the electrical resistance between adjacent probes to drop from several megohms to about 5 ohms in approximately 1 second, apparently as a result of breakdown of the phenolic into carbon.

The ablation depth sensors tested in the plasma jet facility (Figure 17) yielded the data for change in electrical resistance shown in Figure 18.

No signals from the ablation depth sensors were recorded during flight; the first sensor was designed to trigger in the neighborhood of peak heating, but the end of the telemetered data came about one-quarter of the way to peak heating.

34
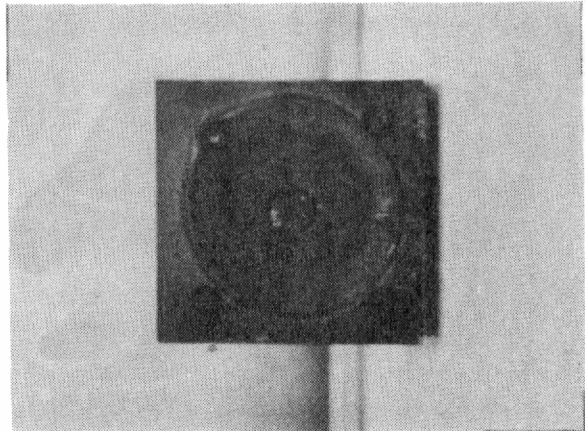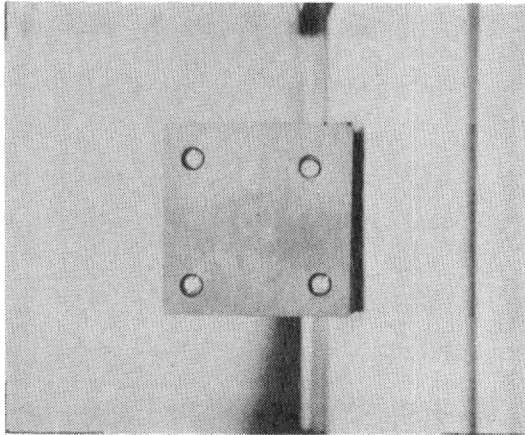
a. Before test   b. After test

Figure 17. Ablation depth sensors tested in plasma jet facility
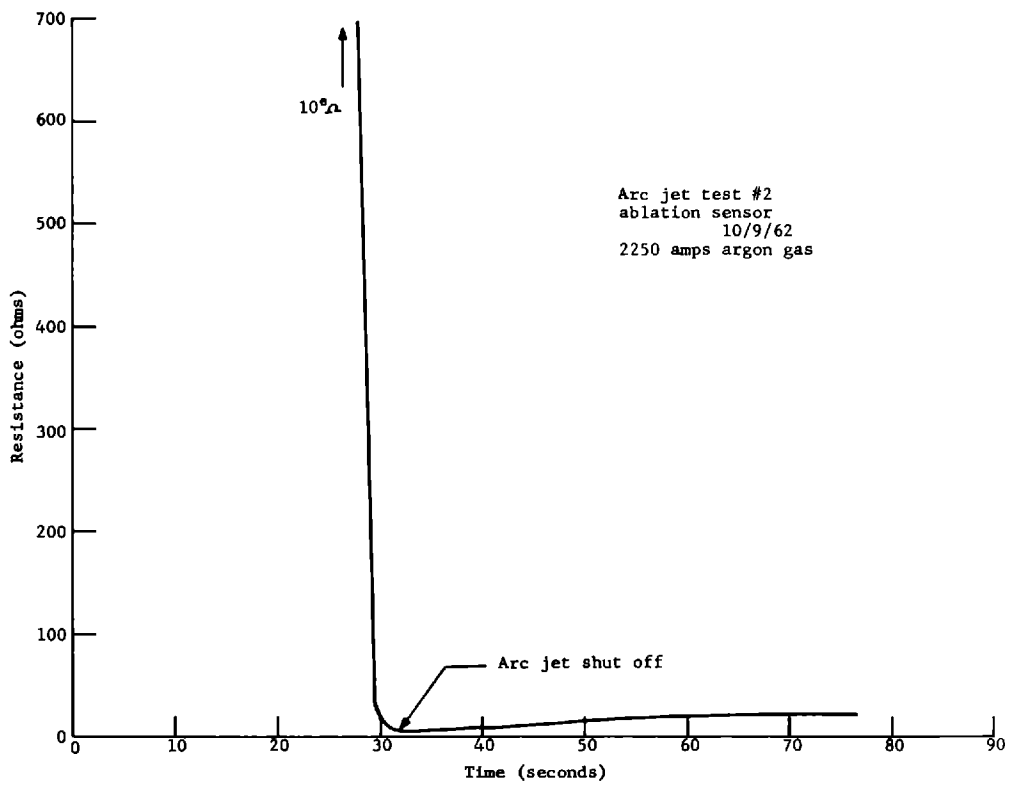
Figure 18. Results of arc-jet test of ablation depth sensors
(change in electrical resistance)

SECTION V -- FOURTH-STAGE-MOTOR SEPARATION SYSTEM

In the interests of establishing a center of gravity to render the re-entry vehicle aerodynamically stable, the Scout fourth stage had to be separated as soon as possible after motor burnout. The separation system was designed to accomplish this separation reliably and also to serve as the structural link between the fourth-stage motor and the re-entry system. The components making up the separation system are individually described below and are shown in Figure 6, p. 19.

Structural Members

The structural members included an adapter and a forward adapter ring, defined, respectively, by Sandia drawings N41482 and N41486. Both were machined from AZ-31A-H24 magnesium so that their weight would be at a minimum.

Separation Spring

The separation spring used was a nonlinear, helical-wound compression spring designed to be compressed between the two structural members. Its physical characteristics were as follows:

Free length	7.75 inches (maximum)
Working height	1.50 inches
Compression load	215 to 236.5 pounds
Minimum spring energy	35 foot-pounds

Purchased from Chance Vought Corporation (CVC), this spring is defined by CVC drawing 320-00023.

Marmon Clamp and Explosively Actuated Nuts

The structural members were held together with a marmon clamp and two separation nuts. The marmon clamp, purchased from Chance Vought Corporation, is defined by CVC drawing 320-00028. The explosively actuated separation nuts, purchased from Hi-Shear Corporation, are defined by Hi-Shear drawing numbers HIS-SN 2301-2 (separation nut) and HIS-PC-24 (power cartridge).

Retro-rockets

Because outgassing of the fourth-stage motor produces an appreciable residual thrust (Figure 19) the energy derived from the spring was not sufficient to permanently separate the fourth-stage motor from the re-entry vehicle. (The curve of separation distance versus time given in Figure 20 shows that the fourth-stage motor would overtake the vehicle in approximately 7 seconds if the energy of the spring alone were used for separation.) Two 1-KS-40 Atlantic Research Corporation retro-rockets were therefore attached to the Scout fourth-stage motor. Their characteristics are tabulated below:

Thrust	46 pounds
Burning time	1.09 seconds
Total impulse	53 pound-seconds

To decrease the possibility that the exhaust from the retro-rockets would interfere with the stability of the re-entry vehicle, it was necessary to provide for the maximum possible separation distance between the fourth-stage motor and the re-entry vehicle before igniting the retro-rockets. Ignition was therefore delayed (Figure 8, p. 26) for about 3 seconds after the separation of the marmon clamp. As Figure 20 shows, 3 seconds corresponds to a separation distance of about 6 feet.
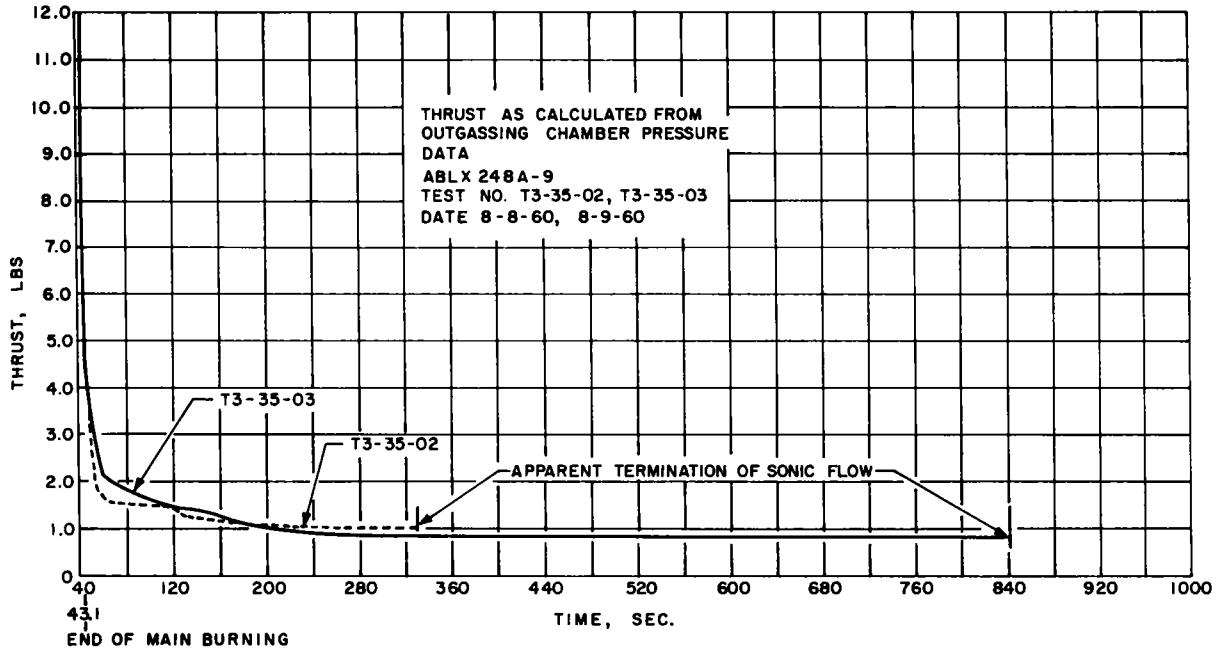
Figure 19. Fourth-stage motor thrust as calculated from outgassing chamber pressure data

THREE POUNDS RESIDUAL THRUST IN 4TH STAGE MOTOR
NO RETRO-ROCKETS FIRED
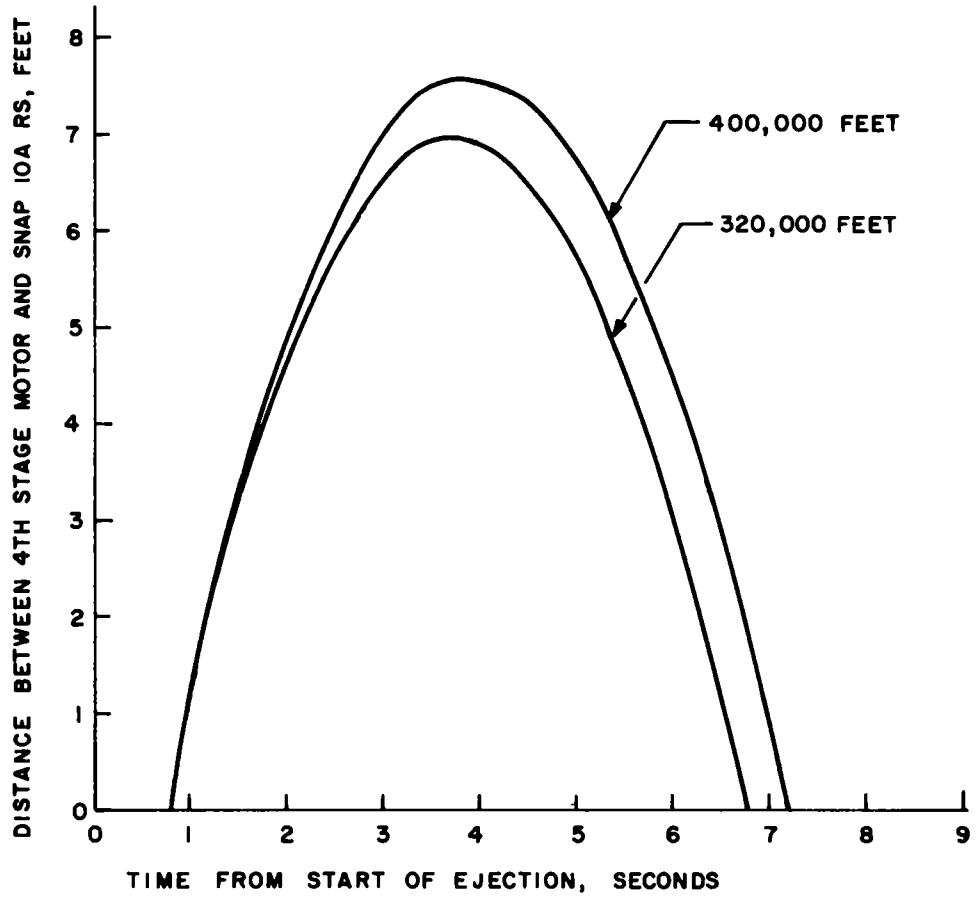
Figure 20. Fourth-stage-motor separation
distance versus time

38

SECTION VI -- RECOVERY SYSTEM

General

After the preliminary design of the re-entry vehicle was complete, it was decided that the re-entry vehicle should be recovered, in order to: (1) determine what portion of the reactor remained after re-entry heating, (2) determine the extent to which the attached fuel rods had ablated, and (3) evaluate the design of the vehicle.

The recovery system was divided into three parts to satisfy three requirements:

1.	Recovery	Parachute
		Flotation bag
2.	Long-range acquisition	SARAH beacon
		Radar tracking
3.	Short-range acquisition	Dye marker
		Flashing light

It was believed that in order for recovery to be highly probable, (1) the parachute and flotation bag would have to function as designed, and (2) any combination of two of the four acquisition aids would have to function properly.

However, even if the parachute were to stream, resulting in a higher than normal water entry velocity, a finite probability existed that the vehicle could still be recovered. A water entry velocity of 102 ft/sec was calculated for normal chute operation, as compared with a maximum velocity of 495 ft/sec for a streamed chute (a C_dS of zero was assumed in estimating the upper limit of the impact velocity). Calculations had indicated that if the parachute streamed, the vehicle would decelerate to zero velocity at a water depth of approximately 45 feet. Theoretically, the flotation bag would survive this environment if it had not been damaged at water entry. Figure 21 shows a vehicle used in a drop test in which the parachute streamed. After recovery from this test, the flotation bag remained inflated for approximately 3 hours. All of the acquisition aids used in this test were inoperable after recovery.

Design

The decision to incorporate a recovery system was not made until the preliminary design of the re-entry vehicle was nearly complete. Since the external shape of the vehicle was limited to some extent by the Scout heat shield configuration, it was desirable if not mandatory to package the recovery aids in existing unused volume. As shown in Figures 22 and 23, the flotation bag and gas bottles were mounted on the mounting plate, and the remaining recovery aids were installed in the flare compartment of the vehicle. (The flotation bag was designed to be pulled into position by a line connected to the shroud lines of the parachute.)

Since RFD-1 was a night test, it was established as a minimum requirement that the flotation bag should remain inflated and that the SARAH beacon should remain in operation for 24 hours. In addition, the recovery system was designed to survive the environmental conditions outlined in Section VII.

The various components of the recovery system are described in detail below.
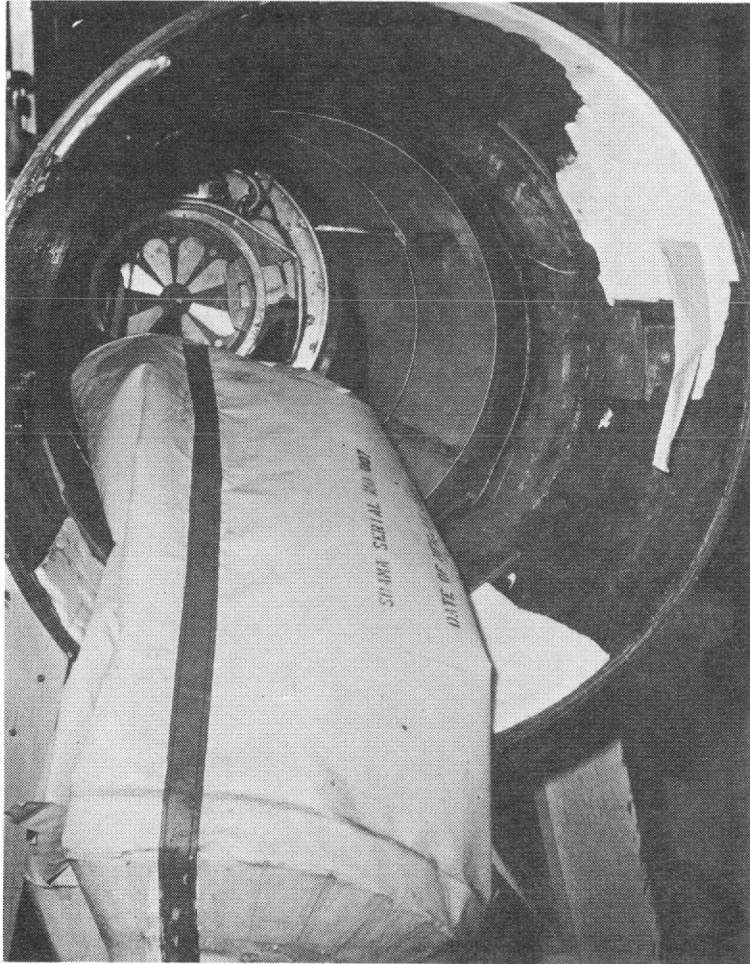
Figure 21. Re-entry vehicle after drop test
in which parachute streamed
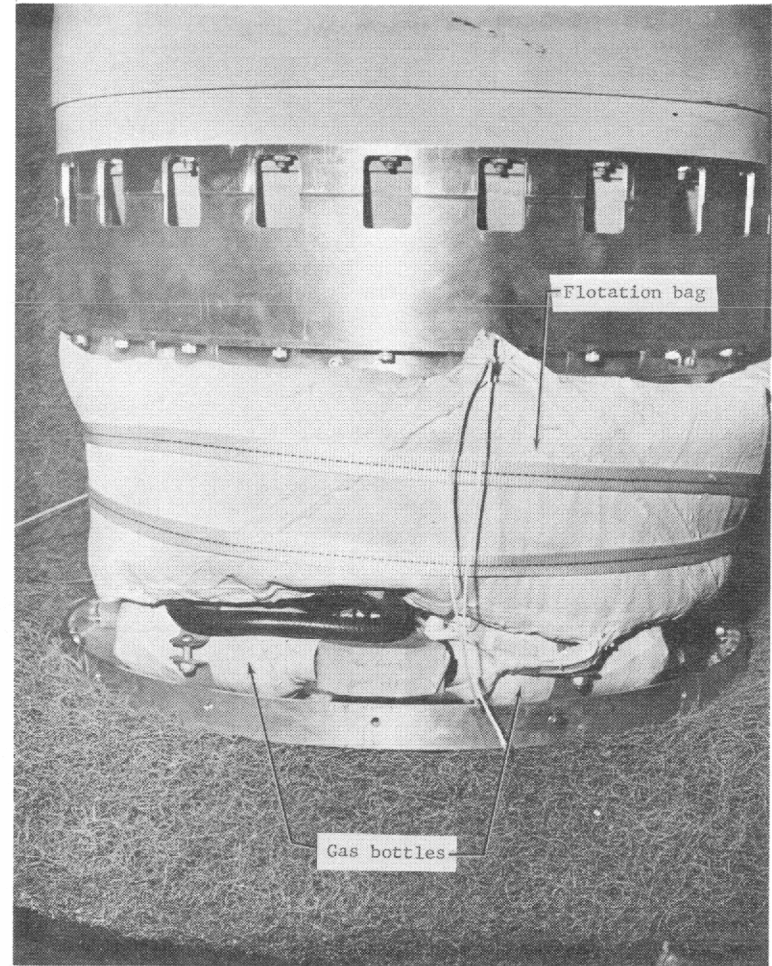
Figure 22. Mounting of recovery aids (flotation
bag and gas bottles)
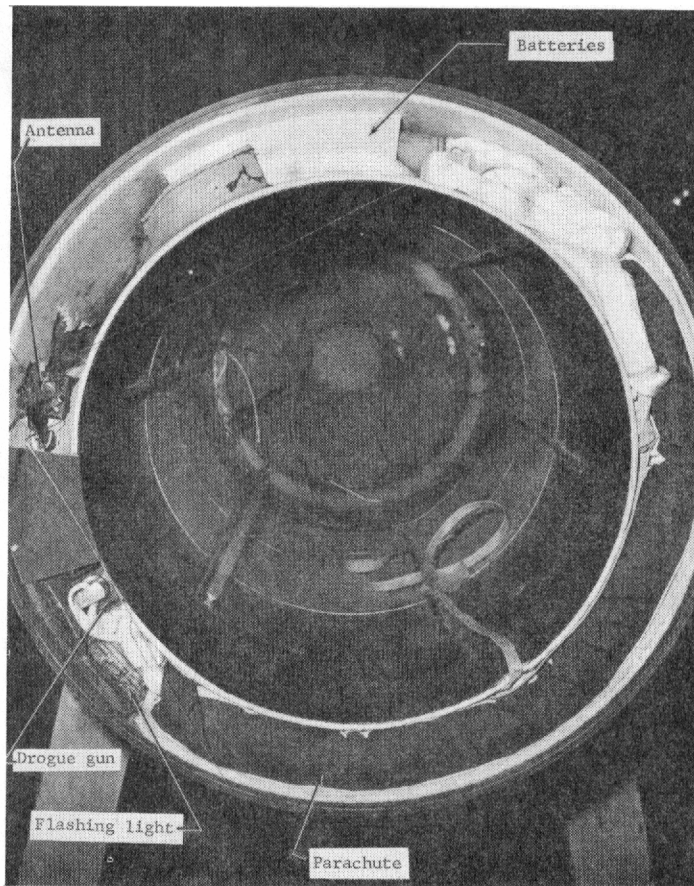
Figure 23. Mounting of recovery aids
(flashing light, batteries,
antenna, drogue gun, and
parachute)

Dye Marker

Six ounces of dye marker were installed in the flare of the vehicle. The dye marker used was the standard Navy rescue marker (used in Mae West life jackets) defined by MIL S-19335.A. - Sea Marker: dye, fluorescein.

Flashing Light

The flashing light installed in the flare of the vehicle was an ACR Electronics Corporation 4C Personnel Distress Light. This light can be seen both at night and in daylight. Depending upon visibility conditions and altitude, acquisition ranges between 10 and 20 nautical miles may be expected.

Specifications for this light are as follows:

Size	5-1/2 x 2-7/8 x 1 inches
Weight	16 ounces, including batteries

Light output	1/2 million peak lumens per flash
Flash rate	60 per minute
Duration	Continuous flash for 16 hours at specified flash rate
Temperature range	-32° to 140°F

In addition, the unit is completely waterproof and extremely rugged (completely encapsulated).

Salt-Water Switch

A schematic of the Sandia-designed salt-water-switch circuit is given in Figure 24. This circuit consists of a 2N886 silicon-controlled switch, a resistor, two probes, and an MC824 squib switch. It was so designed that the two probes would be exposed and surrounded by salt water upon water entry. After impact, the probes would become part of a voltage divider to bias the silicon-controlled switch. When the silicon-controlled switch became biased to the proper level, it would be triggered and would activate the MC824 switch. The normally open section of the MC824 squib switch, upon closing, would apply power to the SARAH beacon.
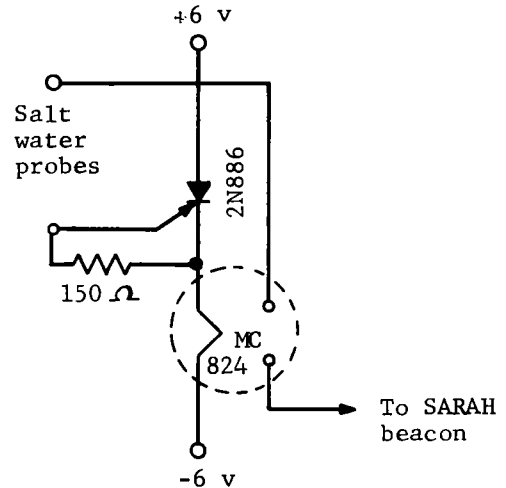
Figure 24. Block diagram of salt-water switch

SARAH Beacon System

The SARAH (Search and Rescue and Homing) system, manufactured by Simmonds Precision Products, Inc., is described in the following section. A block diagram of the system is given in Figure 25.

1. Type 311020 Transmitter Module

   Size   1-1/2 x 1-3/8 x 3-5/8 inches

   Weight   2 ounces (unpotted)

   Input power requirements   6.2 v at 200 ma or 500 v at 1.5 ma

   Operating characteristics

Transmitter frequency	235 mc/sec
Power output	25 watts
Pulse repetition frequency	200 cps

   Acquisition range   100-200 nautical miles (depending on altitude of aircraft)

2. Type 319004 Converter Module

   Size   2-5/8 x 2-7/8 x 1-1/4 inches

   Weight   4 ounces

Input voltage requirements   6.2 v DC

Output voltage   500 v DC

3. Antenna - The Sandia-designed antenna was a quarter-wave vertical
   whip with four folding flexible radials (defined by
   Sandia Corporation drawing N41583, "TE-108 Antenna").

4. Salt-Water Switch

5. Batteries - The beacon system was powered by five RM-42 Mallory
   Mercury cells having an output voltage of 6.75 volts
   and operating time of 26 hours. These cells were
   encapsulated in Silastic RTV-601 as shown in Figure
   23, p. 41.
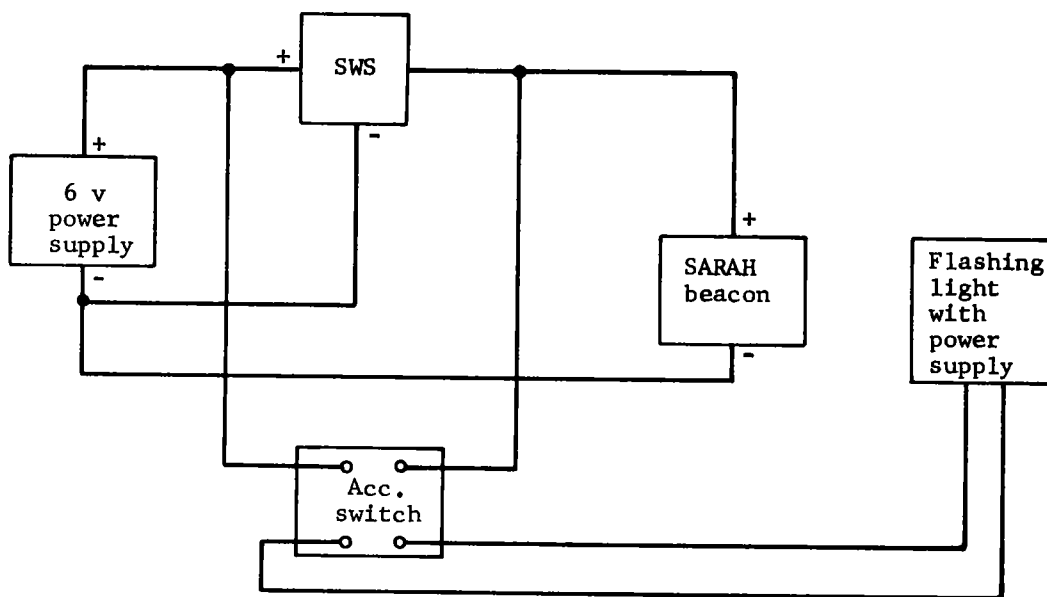
Figure 25. Block diagram of SARAH beacon system

Flotation Bag and Gas Bottles

The flotation bag, fabricated from fiberglass cloth impregnated with silicone rubber, was approximately 34 inches long and 19 inches in diameter (approximately 5.7 ft^3), and weighed approximately 7 pounds including insulation.

Filling the void vacated by the Scout fourth-stage motor, the bag was inflated to approximately 1 psig (at standard conditions) using carbon dioxide contained in the two gas bottles shown in Figure 22, p. 40. A squib-actuated valve was used in the line between bottles and bag. The bottles and valve are defined by Drawing 892449 of the Walter Kidde Company. Additional information on the development of the flotation bag and parachute is given in Reference 1.

Parachute

The parachute used in this system was 7 feet in diameter ($C_dS = 27.0$) and had a solid canopy. It was reefed to a diameter of approximately 0.65 foot ($C_dS = 8.6$),

and was so designed that 10 seconds after line stretch of the chute, the reefing line would be cut by three mechanically actuated Holex cutters. The parachute was deployed by a drogue gun firing a 1-pound slug at a muzzle velocity of 250 ft/sec; a swivel was used between the bridle and the parachute shroud lines to prevent twisting during deployment.

Development

The heat pulse associated with re-entry heating caused problems in the design of the recovery system. Since the fourth stage was to be ejected at an altitude of approximately 350,000 feet (before the heat pulse), the flotation bag and gas bottles, and the inside surfaces of the vehicle from Station 38.85 to Station 84.65, would be exposed to re-entry heating. Since the vapor pressure of CO_2 rises with temperature, the gas bottles had to be thermally protected to prevent the diaphragm from rupturing and allowing the bag to fill prematurely. In the final design, the bottles were coated with 0.2 inch of Dyna-Therm E-300 and 0.040 inch of Dyna-Therm D-65, to keep their temperature within an acceptable range. Since the material used in the flotation bag is limited to 500°F, the outer protective bag that contained the flotation bag was fabricated from fiberglass cloth impregnated with silicone rubber, and then coated with 0.040 of Dyna-Therm D-65.

The drogue gun used to deploy the parachute caused some structural problems. Various attempts were made, during the preliminary design of the vehicle, to estimate the reaction load associated with firing the gun; the manufacturer was also queried. Eventually, the estimated figure for reaction load was set at 8000 pounds maximum. However, during the first two sled tests conducted on preliminary test hardware, the drogue gun mounting block failed, despite having been designed to a safety factor of 2. These failures made the estimated reaction load questionable.

Several tests were therefore conducted to measure the actual reaction force. In the first of these tests, the drogue gun was mounted on a load cell and the output was displayed on an oscilloscope. For a 250 ft/sec squib and a 1-pound slug, the peak force was 27,000 pounds as shown in Figure 26. Since this load would place severe structural requirements on the fiberglass case of the re-entry vehicle, a study of lower energy squibs (175 and 125 ft/sec) was undertaken, and design effort to strengthen the structure was begun. The drogue gun slug was attached to the parachute deployment line in the reaction load tests conducted on the low energy squibs. The reaction forces obtained, respectively, with the 175 and 125 ft/sec squibs is also shown in Figure 26. The amplitude of the force associated with these squibs was acceptable, but the energy they supplied was not large enough to deploy the parachute properly. Note that the force curves for the two low energy squibs are about equal in magnitude. Although their similarity made the data somewhat questionable, the short time scales of the SNAP program would not allow time for further study. There was no alternative but to add the weight required to strengthen the structure, although this made worse an already adverse center of gravity.

Both solid canopy and ribbon parachutes were tested during the development period. Most of the early development work was spent on the solid canopy type; but during the early sled and aircraft drop tests, it was observed that this type of chute was very unstable. Coning angles as large as 45 degrees were observed during some of the drop tests, and these resulted in impact angles that caused actuation failures in the impact switches (mounted parallel to longitudinal axis of vehicle) used to turn on the SARAH beacon system. (In order for these switches to work, the degree to which parachute instability might be allowed to influence the water-entry angle was limited to 30 degrees from the vertical.)

Accordingly, ribbon chutes were investigated, because these are theoretically more stable than solid canopy chutes. Ribbon chutes with the same C_dS as the solid canopy chute previously used (that is, about 27 ft²) were successfully tested on the sled track at the maximum expected dynamic pressure (330 psf). Later, a ribbon chute was incorporated into the fuzing and firing drop test at Wallops Island. The parachute deployed properly (at a dynamic pressure of about 100 psf), but it failed to open completely after line stretch.
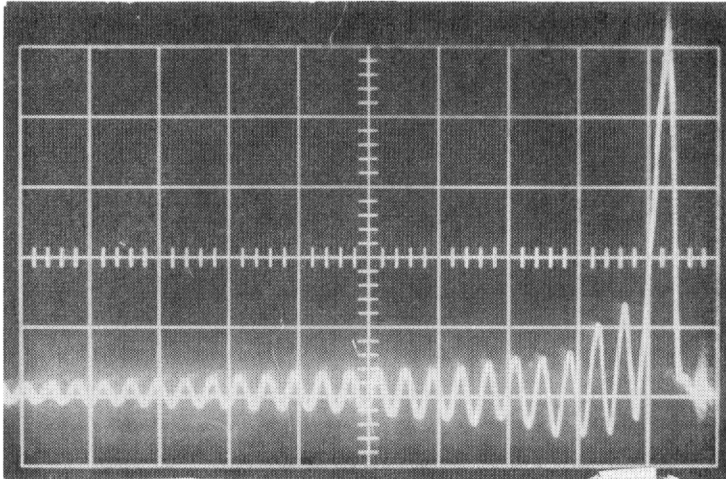
a. 250 ft/sec squib
    1.0 millisec/cm,
    5000 lb/cm
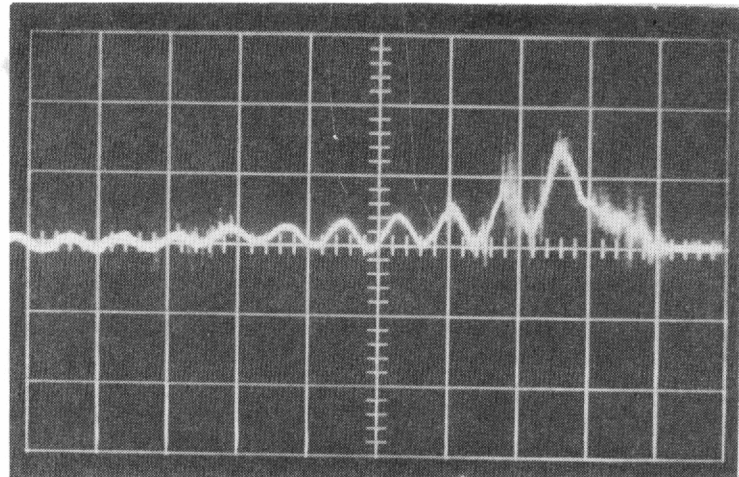
b. 175 ft/sec squib
    0.5 millisec/cm,
    5000 lb/cm
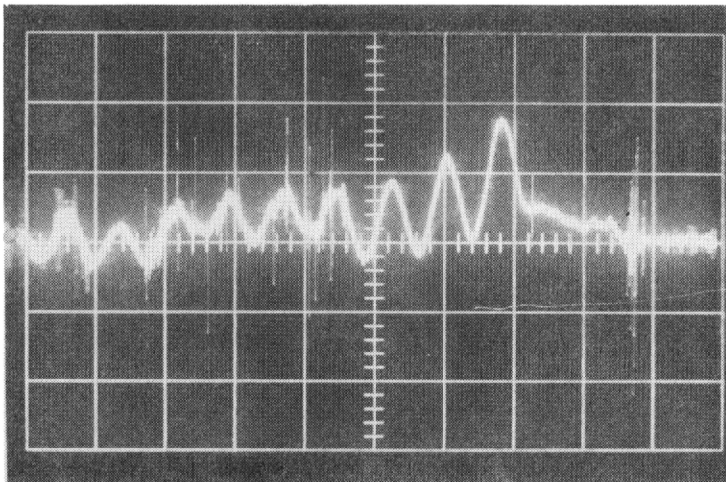
c. 125 ft/sec squib
    0.5 millisec/cm,
    5000 lb/cm

Figure 26. Oscilloscope records of tests of the reaction load associated
            with firing the drogue gun used to deploy the parachute
            (vertical axis = force, horizontal axis = time)

At this point, it was decided to abandon the ribbon chute system since there was not enough time to develop it properly. The impact-angle problem associated with the solid canopy chute was solved by employing the previously described salt-water switch for primary initiation of the SARAH beacon (the salt-water switch is not affected by angle of water impact).

Further details of the tests conducted in developing the recovery system are given in Reference 1 and in Chapter VII of this report.

SECTION VII -- AERODYNAMIC DESIGN OF THE RE-ENTRY VEHICLE*

Selection of Shape

The purpose of the re-entry vehicle was twofold: (1) to house and protect the instrumentation, the telemetry, and the recovery system, and (2) to ensure that the reactor payload would re-enter aligned with the flight path and with fins forward.

Major limitations on the shape of the re-entry vehicle were the following:

1. Scout Heat Shield -- The re-entry system had to fit inside the 34-inch diameter Scout heat shield extending forward to Scout Sta. -25.0 (Figure 7, p. 23). (This was the largest heat shield available for the Scout vehicle.) A clearance of 0.5 inch was required between the re-entry system and the heat shield. The most forward part of the re-entry system could not extend past Scout Sta. -13.0.

2. Scout Fourth-Stage Motor -- The re-entry vehicle had to be built around the fourth-stage motor as shown in Figure 7, p. 23, in order to achieve a shape that would be aerodynamically stable with the reactor attached. A clearance of 0.150 inch had to be provided, between the fourth-stage motor at Scout Sta. 67 and the inside of the re-entry vehicle, to permit expansion of the motor during its burning. In addition, since the motor had to be ejected from the re-entry system in order for the center of gravity to be established in a location desirable from the standpoint of aerodynamic stability, space had to be provided in front of the fourth-stage motor to accommodate the separation mechanism of the ejection system.

3. SNAP-10A Reactor Mockup -- The nose of the re-entry vehicle could not extend forward of Scout Sta. 14.33 once the full-scale reactor shape was laid out in the heat shield. Since the reactor was mounted on the front of the re-entry vehicle, the size of the base of the reactor determined the flat diameter of the nose of the re-entry vehicle.

4. Telemetry System -- Internal volume had to be provided to house and protect the telemetry system.

5. Ablation System and Structure -- Enough ablation material to survive re-entry heating had to be added to the basic structure of the vehicle. As a result, although the inner dimensions of the re-entry vehicle were fixed, the thickness and structure of the ablation material affected its outside shape.

6. Aerodynamic Heating -- The total weight and aerodynamic drag of the re-entry system had to be minimized in order to obtain the maximum possible velocity and aerodynamic heating. By maximizing velocity and aerodynamic heating, orbital decay could be simulated as close as possible using a Scout launch vehicle and a -6 degree re-entry angle.

---

*As a part of an overall report covering other subjects, this section can only summarize the extensive theoretical and experimental aerodynamic studies that were performed to determine the aerodynamic characteristics of the RFD-1 re-entry system. For additional information, the reader is referred to References 2 through 6. More detailed definitions of the symbols used are also available in Reference 2.

The need to provide packaging volume for the recovery system was not included among the factors affecting shape, since the requirement for recovery was not established until after the shape of the re-entry vehicle had been decided upon. As was explained earlier in this report, the recovery system was later accommodated in unused volume in the re-entry vehicle.

To select the shape, various shapes for the re-entry vehicle without the reactor in front of it were compared for aerodynamic stability. The best of these was selected, and then the aerodynamic stability coefficients were computed for the re-entry vehicle/reactor combination for several stages of reactor disassembly.

In selecting the best shape, the theoretical values of the static and dynamic stability coefficients were computed using modified Newtonian flow theory for 17 different re-entry vehicle shapes. The shapes investigated included truncated cone-cylinder-conical flare shapes, truncated cone-cylinder-biconic flare shapes, and a truncated cone shape. Of these, those that did not have the desired static stability and low drag characteristics, or which did not meet all the shape criteria presented earlier, were eliminated. From the remaining choices, the re-entry vehicle shape shown in Figure 27 was selected as the best compromise of static and dynamic stability characteristics within the design restraints used for the preliminary design. As more information became available during the early part of the development phase of the program, the re-entry vehicle shape shown in Figure 28 was defined for the wind tunnel tests and the theoretical aerodynamic analyses. As more information became available during the development of the re-entry system, minor modifications to the re-entry vehicle were made. The final re-entry vehicle shape flown on the RFD-1 flight is presented in Figure 29.

Theoretical Aerodynamic Coefficients

After the shape for the re-entry vehicle had been selected, the aerodynamic coefficients of the re-entry system were computed for several stages of reactor disassembly. The major configurations analyzed and/or tested are shown in Figure 30, p. 50.
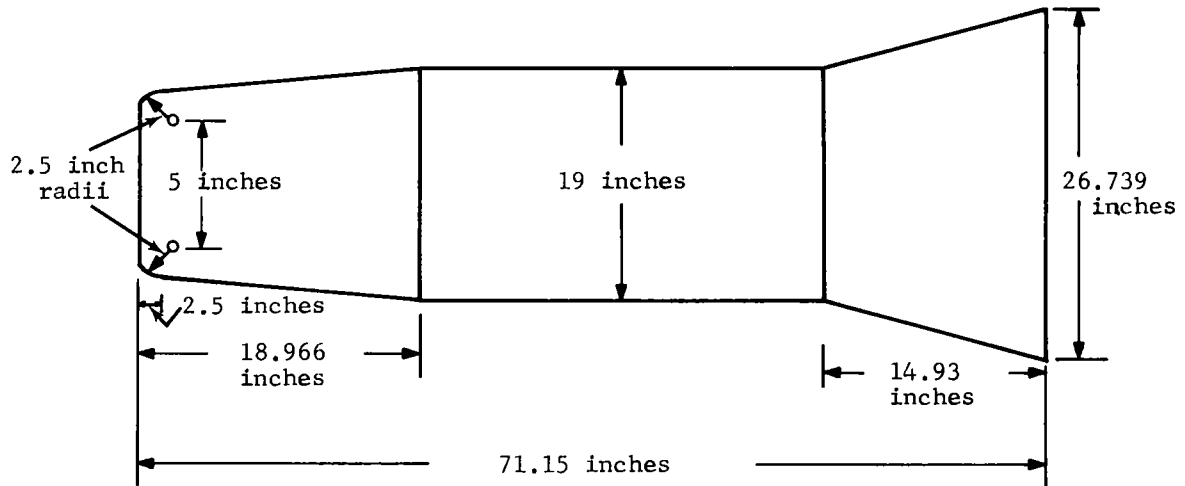
Figure 27. Preliminary design of the external
shape of the re-entry vehicle

48
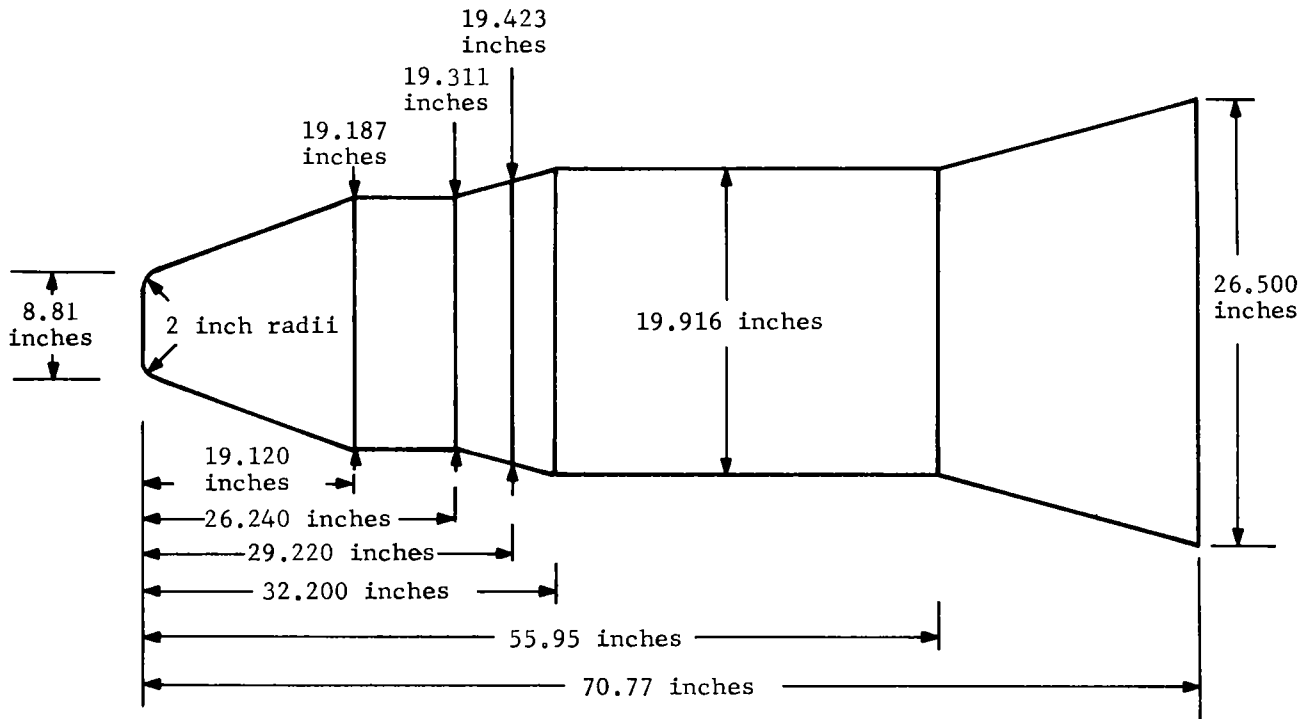
Figure 28. External shape of the re-entry vehicle used for
wind-tunnel-test models and for theoretical analysis
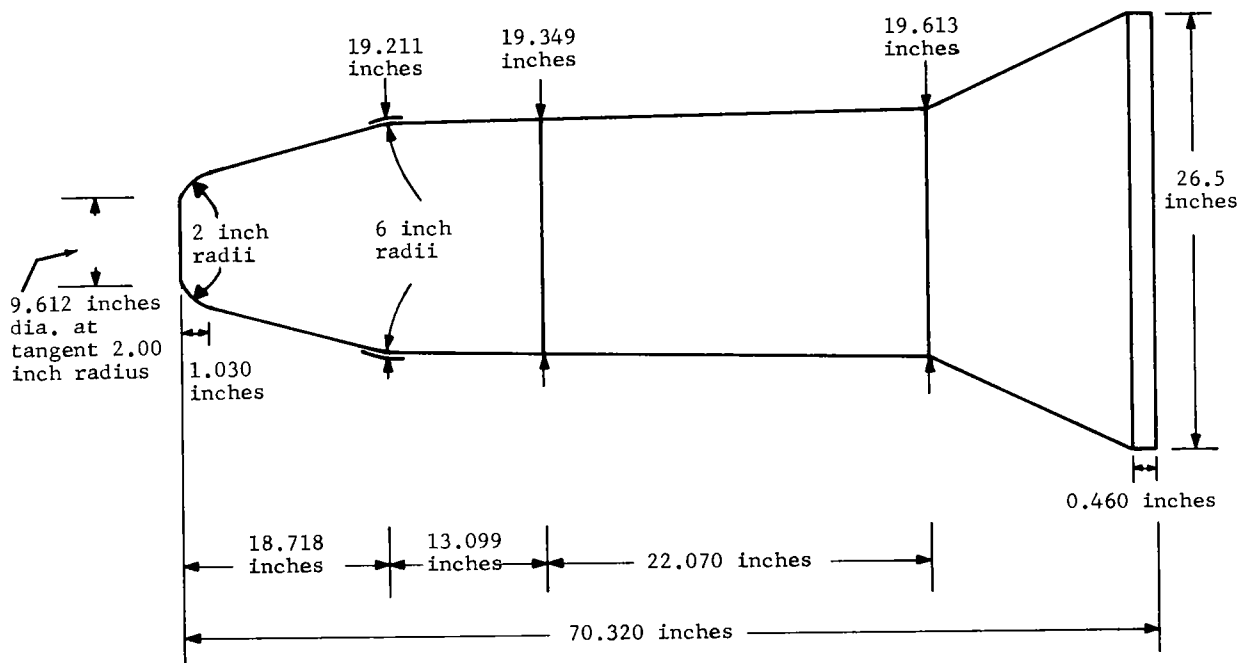
Figure 29. Final external shape of the re-entry vehicle

49

Configuration 1   Configuration 2   Configuration 3   Configuration 4   Configuration 5   Configuration 6
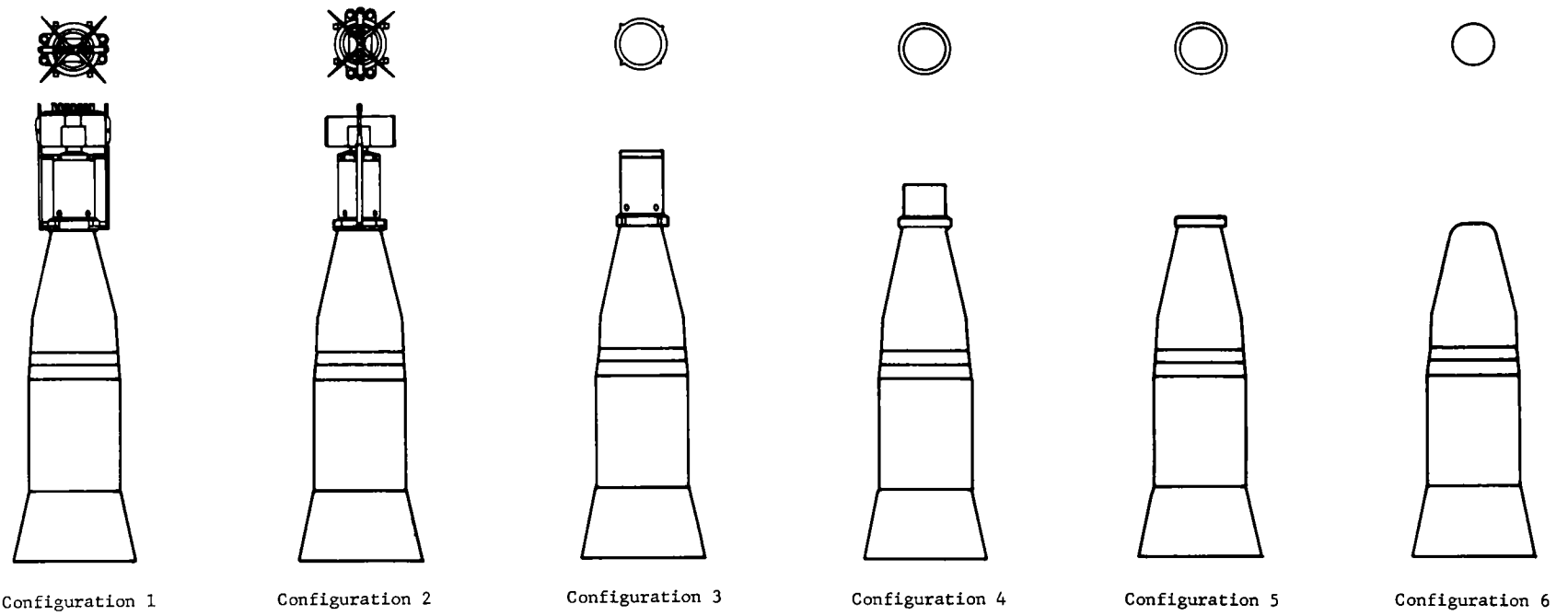
Figure 30. Wind tunnel tested re-entry system configurations

First, theoretical drag and static stability coefficients were computed for Configurations 1 and 6 (Figure 30), since these presented the extremes in shape during re-entry. Modified Newtonian flow theory, corrected for blast wave effects[2] was used to compute these coefficients in the range of hypersonic Mach numbers. Conical flow theory was used to compute the same coefficients in the range of supersonic Mach numbers. Information from aerodynamic tests of similar shapes was used in combination with theoretical calculations to predict these coefficients for the transonic and subsonic Mach number ranges.

Next, using modified Newtonian flow theory, the dynamic stability coefficients were calculated, for Configuration 6, for the range of hypersonic Mach numbers. (Only Configuration 6 was considered, since the increasing dynamic pressure in the early part of the re-entry trajectory, when Configurations 1 through 5 would exist, would contribute more to damping than the dynamic stability coefficients would; and in addition, the magnitude of the damping forces in the early part of the re-entry would be slight.) The dynamic stability coefficients for Configuration 6 were predicted for the supersonic, transonic, and subsonic Mach numbers, using data from aerodynamic tests of similar shapes.

Experimentally Measured Aerodynamic Coefficients

Wind-tunnel tests were conducted in order to verify the theoretically computed coefficients and to investigate certain effects, such as viscous interaction effects, which are not readily treated theoretically. The conditions of these wind-tunnel tests are described briefly below.

1. Sandia Corporation 12-Inch Trisonic Wind Tunnel -- Static force tests of one-sixteenth scale models of all the re-entry system configurations, $0.5 \leq M \leq 3$, Reynolds numbers (based on re-entry vehicle length) of from 1.1×10^6 to 4.55×10^6, angles of attack of from -6 to +10 degrees.[3]

2. Sandia Corporation 18-Inch Hypersonic Wind Tunnel -- Static force tests of one-tenth scale models of all the re-entry system configurations, $M = 7.5$, Reynolds number (based on re-entry vehicle length) of 0.3×10^6 and 0.6×10^6, angles of attack of from -6 to +9 degrees.[4]

3. Cornell Aeronautical Laboratory 48-Inch Shock Tunnel -- Static force tests of one-tenth scale models of all the re-entry system configurations except Number 2, $12.8 \leq M \leq 22.3$, with the viscous interaction parameter, i.e., the Mach number divided by the square root of the Reynolds number (based on re-entry vehicle length), varying from approximately 0.015 to 0.25, angles of attack of from -6 to +20 degrees.[5]

4. Cornell Aeronautical Laboratory 8-Foot Transonic Wind Tunnel -- Dynamic stability test of a one-third scale model of re-entry system Configuration 5, $0.7 \leq M \leq 1.25$, Reynolds number (based on re-entry vehicle length) of 4.4×10^6 to 6.51×10^6 (Ref. 6).

Conditions for the first three of these tests were based on the re-entry phase of a preliminary Scout launch vehicle trajectory arrived at by the use of theoretically calculated aerodynamic coefficients. The coefficients obtained from these three tests were in turn used in a trajectory to obtain test conditions for the fourth test. (See next section.) In the third test, the viscous interaction parameter was simulated within the limitations of the facility. In the other three tests, the Reynolds number was simulated as closely as the limitations of the facilities permitted. Figure 31 presents typical photographs of the flow field around scale models of two of the re-entry system configurations during wind-tunnel tests.
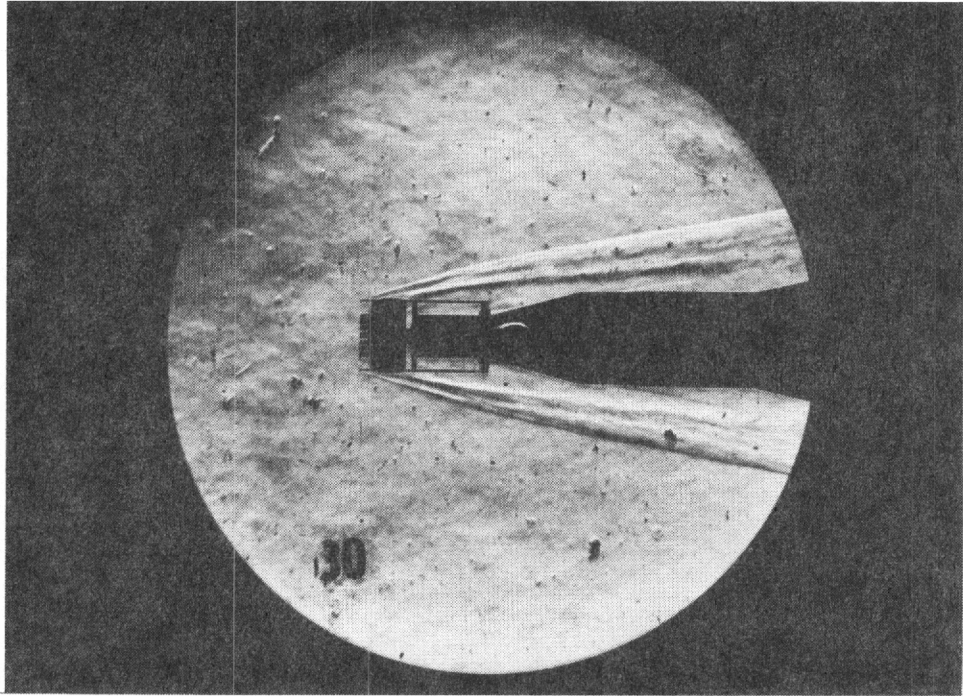
a. Schlieren photograph, M = 12.8
   Cornell 48-inch shock tunnel (Bust. 51)
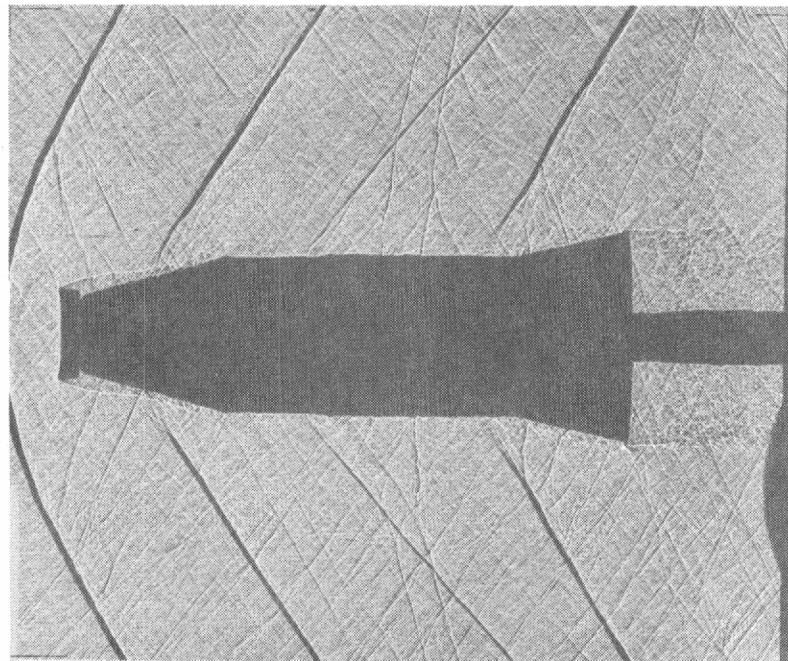
b. Shadograph photograph, M = 1.3
   Sandia Corporation 12-inch transonic
   wind tunnel (Bust. 43)

Figure 31.   Representative photographs of the flow field
             around scale models of re-entry system
             Configurations 1 and 2.

Re-Entry System Trajectory

The trajectory of the re-entry system is a product of complex relationships among:

1. The aerodynamic coefficients of the vehicle (a function of configuration, Mach number, and Reynolds number)

2. The changes in configuration of the re-entry system during re-entry (a function of the aerodynamic heating of the re-entry system)

3. The weight of the re-entry system (a function of disassembly of the reactor and ablation of the re-entry vehicle shell, both of which are determined by the aerodynamic heating of the re-entry system).

The above interactions were solved iteratively, using the Sandia Corporation 3-degree-of-freedom point mass trajectory program in conjunction with passive analog computer calculations of the temperature versus time response of the re-entry system.[6] (Use of the 3-degree-of-freedom point mass trajectory program with zero degree angle of attack drag coefficients yielded accurate results, since stability studies had shown that the angle of attack of the re-entry system should be small.)

Early calculations of the trajectory used estimates of the variation of re-entry system configuration with altitude, theoretical computations of re-entry drag coefficients as a function of Mach number, and estimates of the variation of re-entry system weight with altitude. As additional information became available from aerodynamic force and heating tests, it was incorporated in later iteration of the same relationships.

The final preflight nominal trajectory for the re-entry system was arrived at using experimentally measured force and heating coefficients and actual measured values for re-entry system weight, center of gravity, and moments of inertia. Initial conditions at burnout of the Scout fourth-stage motor had been computed by Chance Vought Corporation, using the final figures (at launch) for the weight, center of gravity, and moments of inertia of the re-entry system. The results obtained from this computation are summarized in Figure 32, presenting pertinent parameters as a function of altitude. (Additional information on the trajectory is available in Sandia Corporation report SC-RR-64-510.) The final predictions for variations of weight, moments of inertia, and center of gravity with altitude based on the final nominal re-entry system trajectory, are presented in Figures 33 and 34.

Re-Entry System Aerodynamic Coefficients

The wind-tunnel data were used together with theoretical calculations to define the aerodynamic coefficients for the re-entry system during the re-entry trajectory. Since the re-entry system undergoes considerable variation in configuration and weight and experiences a wide range of Mach numbers and Reynolds numbers during the re-entry trajectory, the variation in aerodynamic coefficients is quite pronounced. Figure 35, in which wind-tunnel and theoretical estimates for C_{n_α} are plotted as a function of Mach number, shows the change of configuration during the re-entry flight. The effects of changes in configuration, Mach number, and viscous interaction at hypersonic Mach numbers are apparent. Obviously, the task of relating aerodynamic coefficients to flight Mach number becomes harder at hypersonic speeds for shapes which experience appreciable changes in configuration.

The following procedure, used previously in re-entry trajectory calculations to define variation in re-entry system drag coefficient as a function of Mach number, was used to define a curve for each of the stability parameters (C_{m_α}, C_{n_α}, and center of pressure) which would include effects of changes in shape, viscous interaction, and Mach number during re-entry.
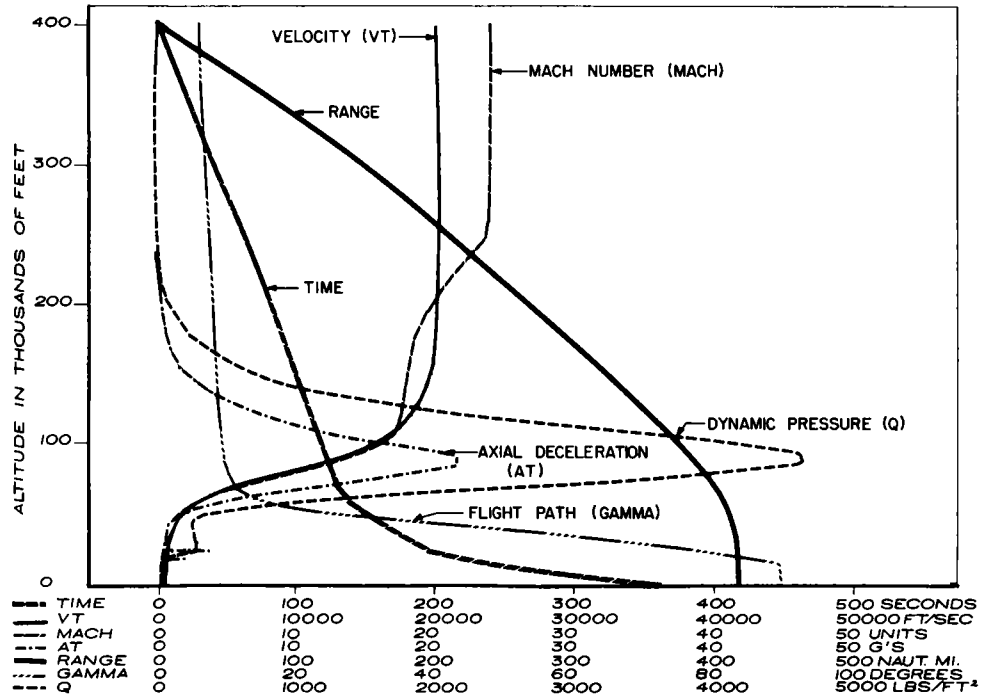
Figure 32. Final nominal preflight re-entry system trajectory for RFD-1
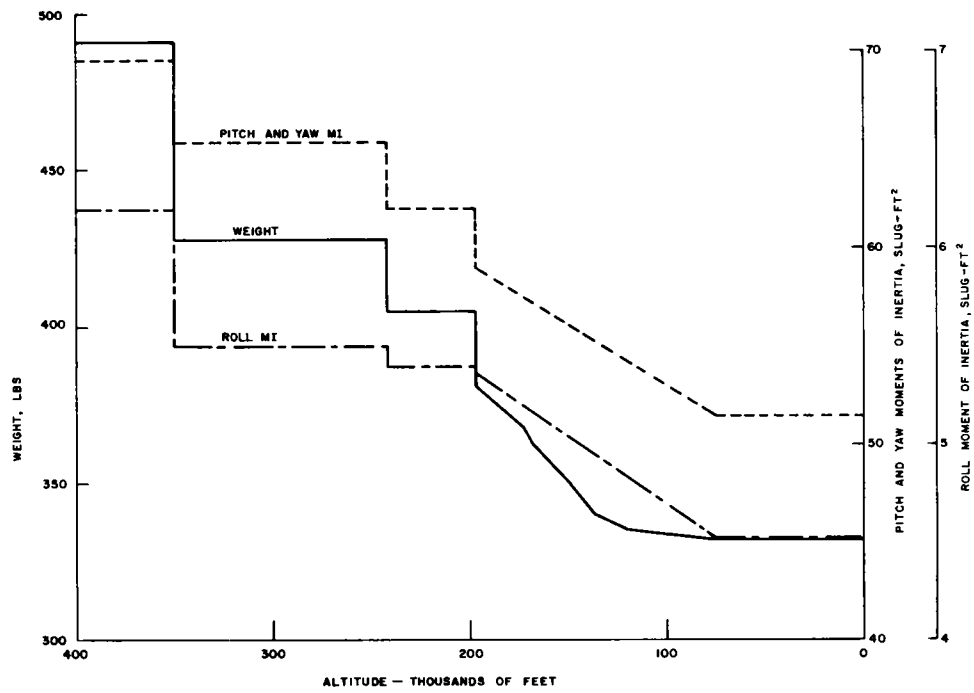
Figure 33. Variations of re-entry system weight and
moments of inertia during re-entry (not
including fourth-stage motor)

54
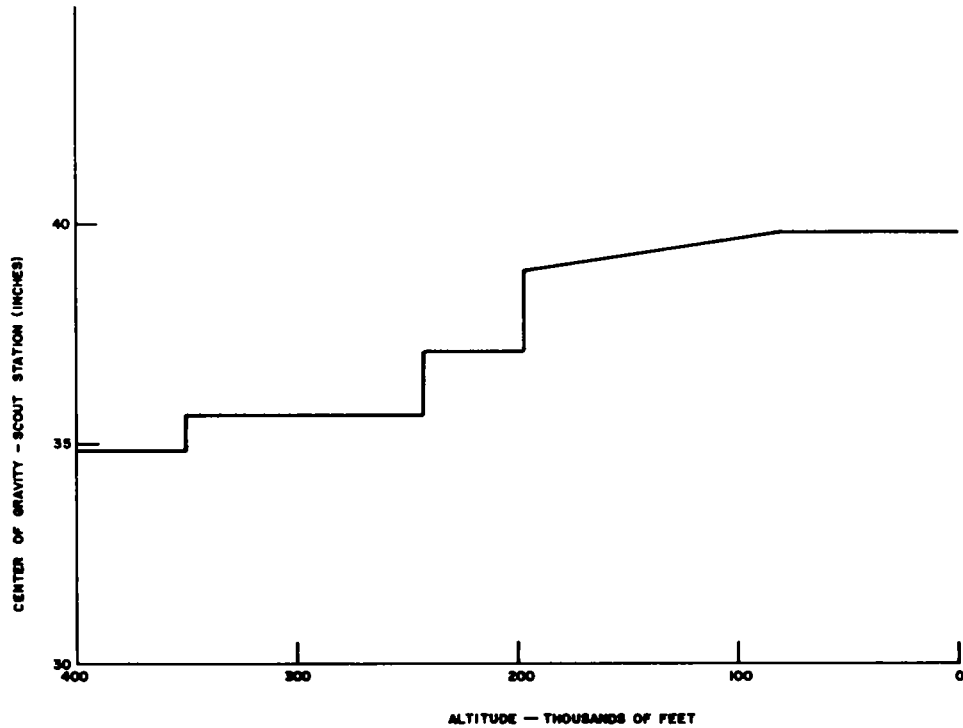
Figure 34. Variations of re-entry system center of gravity
during re-entry (not including fourth-stage motor)

○ Sandia Scarf VI hypersonic tunnel
▽ △ ○ □ Cornell "48" shock tunnel
────── Sandia Scarf III trisonic tunnel
── ── ── Modified Newtonian theory corrected for
             blast wave effect
──·── Conical theory
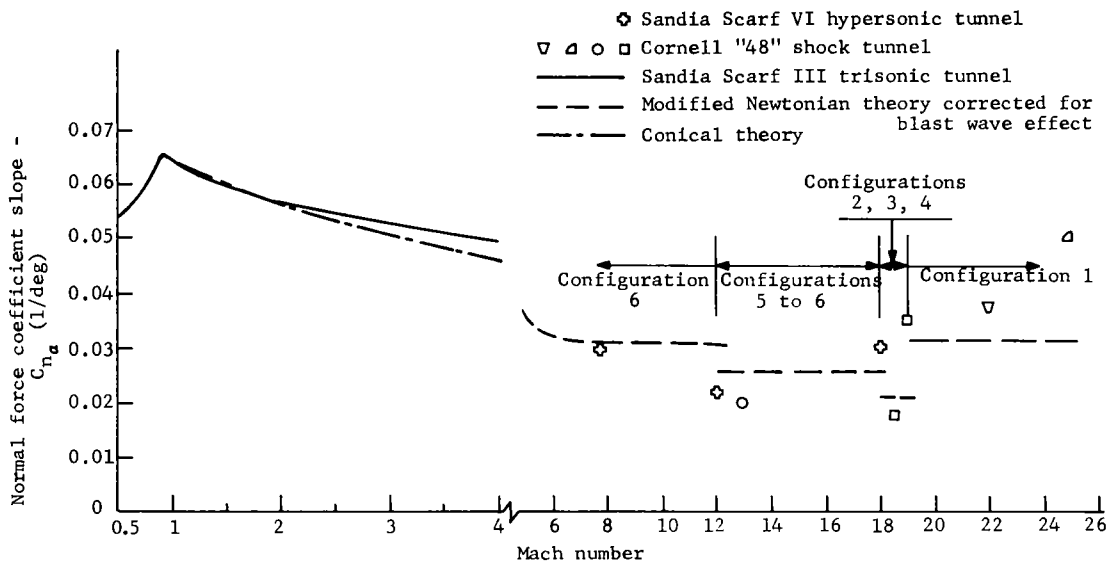
Figure 35. Experimental and theoretical normal force coefficient
derivatives for the re-entry system during re-entry

First, three curves were plotted. Curve 1 was a plot of altitude versus viscous interaction parameter. On this, the altitudes at which the re-entry system changed configurations were superimposed. Curve 2 was a plot of the coefficient being determined (based on wind-tunnel tests and theoretical calculations) as a function of the viscous interaction parameter. Curve 3 was a plot of Mach number as a function of altitude. Using these plots, the interaction parameter was obtained as a function of altitude (Curve 1) at the altitude of interest. This interaction parameter was then used to obtain the coefficient for the configuration at the altitude selected (Curve 2). Finally, before the coefficient could be expressed as a function of Mach number, Curve 3 had to be used to obtain the proper Mach number.

The aerodynamic characteristics of the re-entry system during re-entry are summarized in Figures 36 through 42 and will be discussed below.
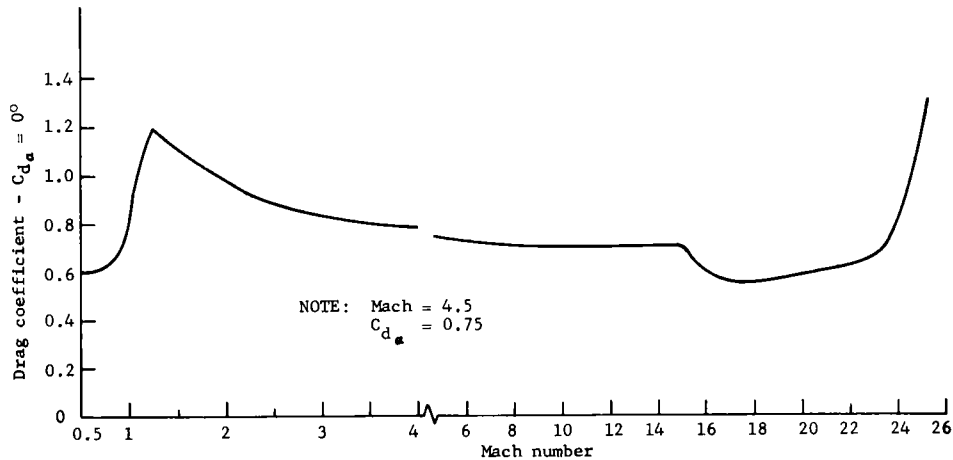
Figure 36. Drag coefficient for the re-entry system during re-entry (including the effects of changes in configuration and viscous interaction effects)
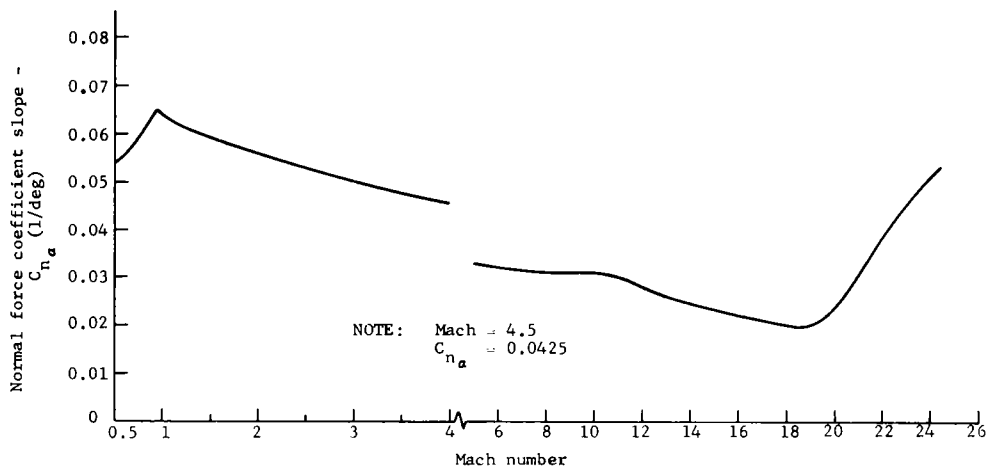
Figure 37. Normal force coefficient derivatives for the re-entry system during re-entry (including the effects of changes in configuration and viscous interaction effects)

56
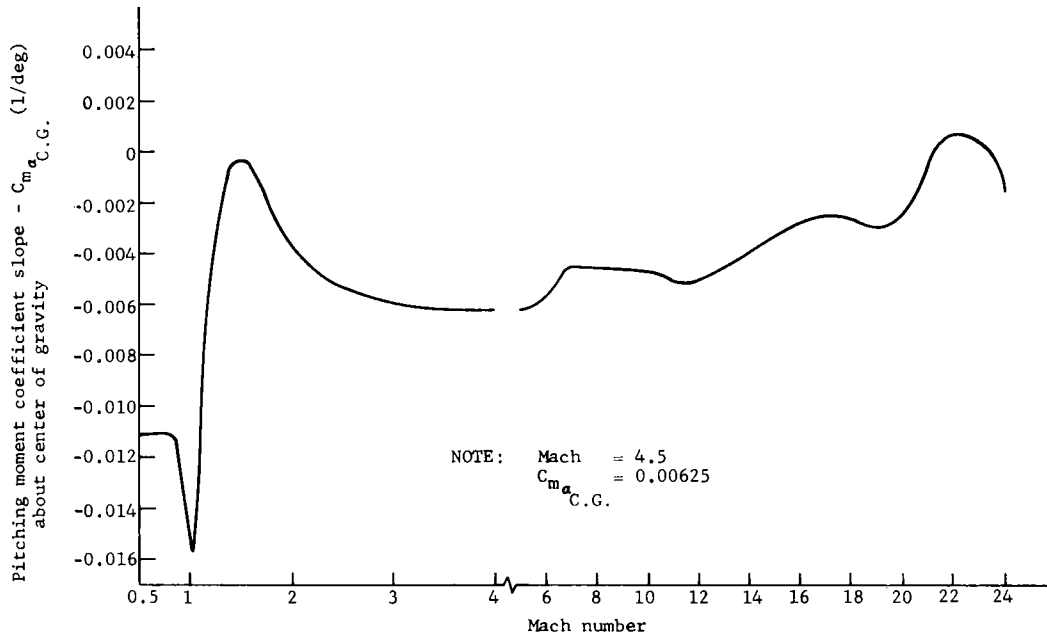
Figure 38. Pitching moment coefficient derivative, about the center
of gravity, for the re-entry system during re-entry
(including the changes in configuration and viscous
interaction effects)
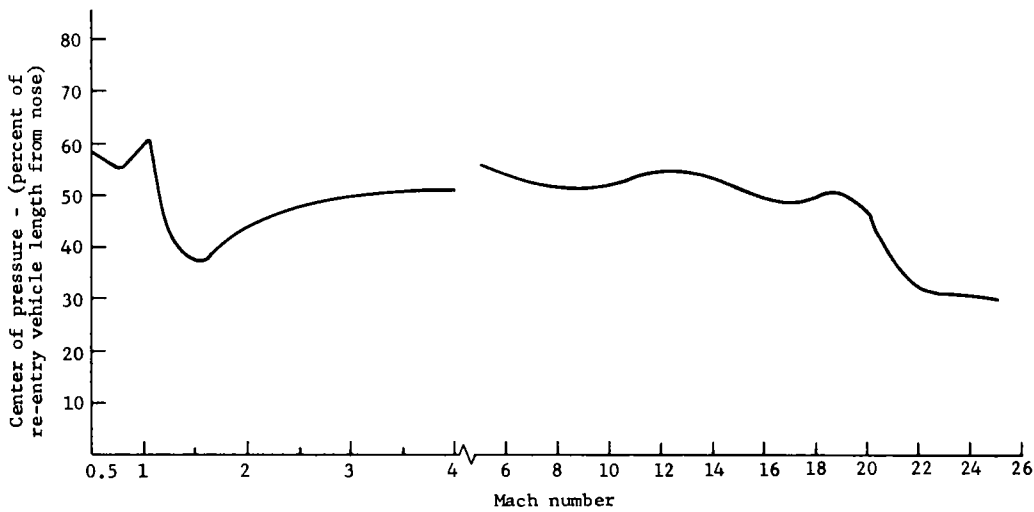
Figure 39. Center of pressure for the re-entry system during
re-entry (including the effects of changes in
configuration and viscous interaction effects)
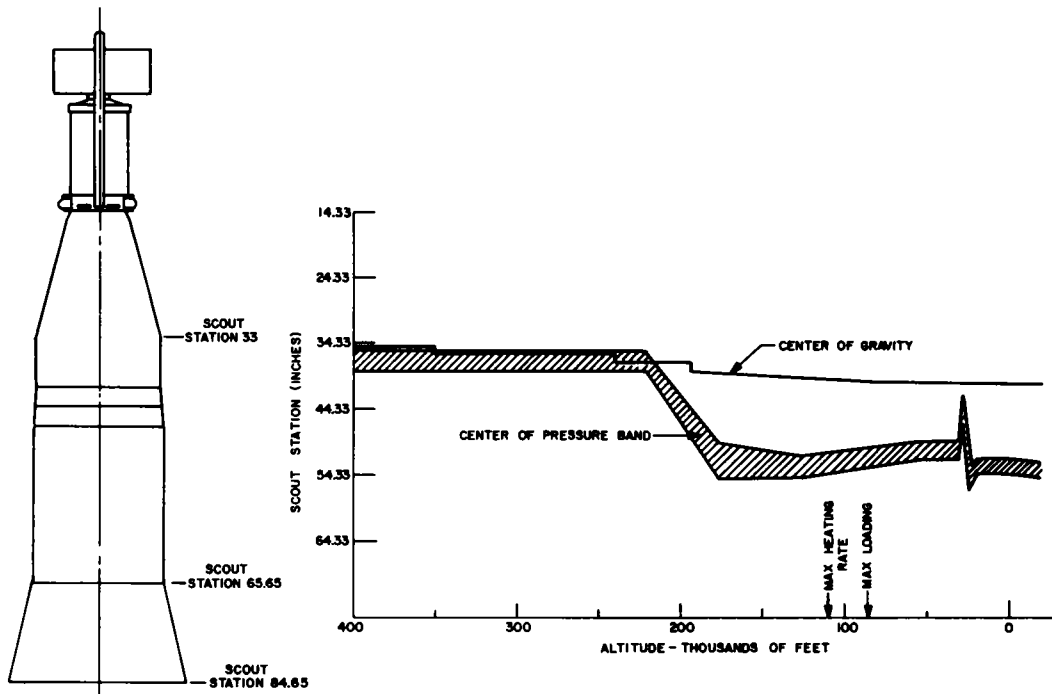
Figure 40. Center of gravity and center of pressure for the re-entry
system during re-entry (including the effects of changes
in configuration and viscous interaction effects)
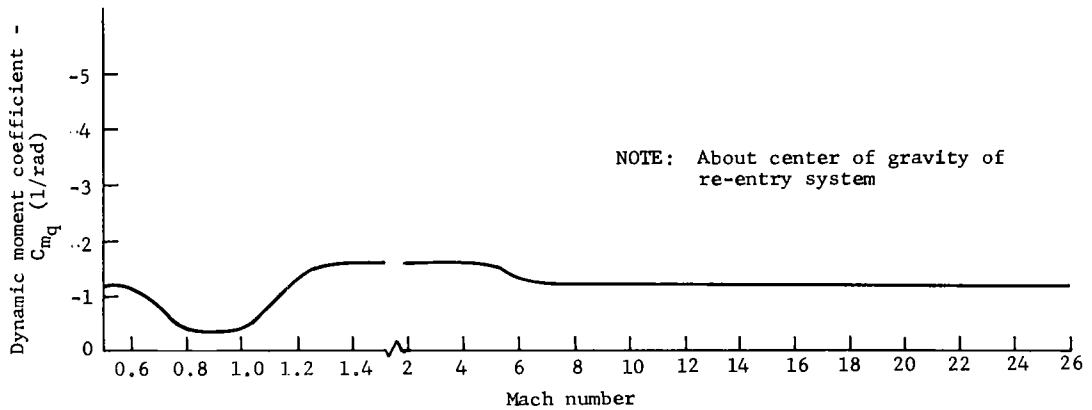
Figure 41. Dynamic stability derivative for re-entry system
Configuration 6 during re-entry

58
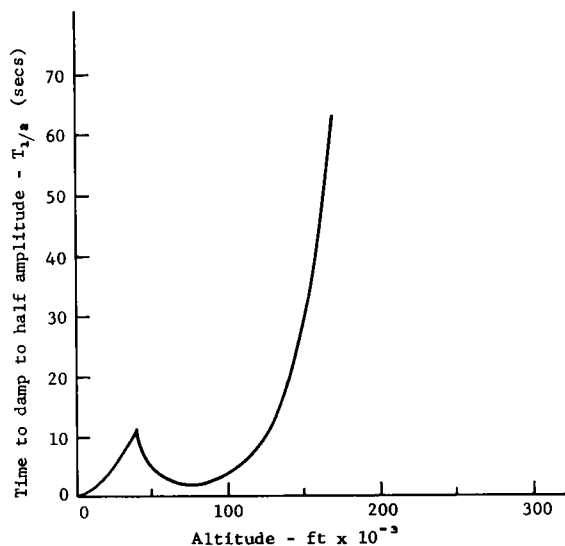
Figure 42.

Time to damp to one-half
the original oscillation
amplitude for the re-entry
system during re-entry

Static Stability -- The re-entry system must be statically stable so that it will oscillate rather than tumble if a disturbing force acts on it. Also, since dynamic pressure increases rapidly during the early portion of re-entry, static stability actually contributes more aerodynamic damping to the re-entry system than the dynamic stability derivative does, until the altitude of maximum dynamic pressure is approached.

The static stability characterisitcs of the re-entry system are summarized in Figures 38, 39, and 40. Figure 38 shows the re-entry system pitching moment coefficient during re-entry. Figure 40 presents the centers of gravity and pressure for the re-entry system during its re-entry. These figures make it clear that the re-entry system has very little static stability down to an altitude of about 225,000 feet. Since the aerodynamic forces would be small at altitudes higher than this, the gyroscopic stability of the re-entry system, spinning at approximately 130 rpm, would be adequate to keep the re-entry system stable until aerodynamic forces became appreciable. By the time aerodynamic forces were appreciable, the fins would be burning off the reactor, and the static stability would be adequate.

Dynamic Stability -- Dynamic stability is most important during the latter portions of re-entry, when it is the major source of damping. The dynamic stability characteristics of the RFD-1 re-entry system are shown in Figures 41 and 42. Figure 41 shows the dynamic stability derivative for the re-entry system during re-entry. Figure 42 shows the time to damp to one-half the original oscillation amplitude for the re-entry system during re-entry. (In this second figure, the time to damp to one-half amplitude is computed for the re-entry system flying at constant altitude at that velocity which it would have during re-entry when passing through the altitude for the calculation. Not included are the effects of static stability and increasing dynamic pressure during the early portion of re-entry, which would make for more rapid damping during that portion than this figure reflects.)

From Figures 41 and 42, it is apparent that the re-entry system has adequate dynamic stability throughout re-entry. Any oscillation caused by the later stage of generator disassembly should therefore damp rapidly to small angles.

Pitch-Roll Coupling Analysis -- The fourth stage of the Scout launch vehicle was spin-stabilized. Since the re-entry system was not despun, it would be spinning during re-entry. Dynamic coupling of its pitch rate and spin rate when the two were equal during re-entry was theoretically possible, and if it occurred, would nullify

59

the aerodynamic stability of the re-entry system. Any initial angle of attack might be amplified to large angles of attack, resulting in large loads and subsequent failure of the structure of the re-entry vehicle.

When pitch frequency during re-entry was calculated for the re-entry system and compared with the spin rate during re-entry, it appeared that pitch-roll coupling problems could occur at altitudes of approximately 94,000 and 74,000 feet. A simplified theory[2] was used to determine how much the magnitude of the initial angle of attack would be amplified as the result of such coupling. These calculations showed that in view of the dynamic stability possessed by the re-entry system, amplification would be very slight.

To verify the results obtained with the simplified theory, 6-degree-of-freedom re-entry trajectories were computed using a computer program obtained from NASA. The results of these trajectories verified the results predicted by the simplified theory.

Selection of Times for Ejection of the Fourth-Stage Motor and for Ignition of the Retro-Rockets

It was explained earlier in this report that the fourth-stage motor had to be ejected from the re-entry system in order to achieve a center of gravity that would give adequate aerodynamic stability. In selecting the best time for ejection, an optimum compromise between the following conflicting requirements had to be achieved:

1. The fourth-stage motor had to be ejected as soon as possible after burnout in order to ensure that the re-entry system would start damping as soon as appreciable aerodynamic pressure was involved.

2. The fourth-stage motor had to be retained as long as possible in order to allow motor residual thrust to decay (to minimize the chance that the re-entry system could be struck by the motor).

Theoretical calculations using an assumed constant residual thrust value of 3 pounds, which was greater than that expected for the X-248 fourth-stage motor at the times considered, showed that:

1. Provided both retro-rockets on the fourth-stage motor fired, the re-entry system could not be hit by the ejected motor at any altitude of motor ejection.

2. Provided only one retro-rocket on the motor fired, the re-entry system could not be hit by the ejected motor at altitudes of motor ejection of 350,000 feet or less.

3. Because the motor could catch up with the re-entry system only if it remained aligned axially, the probability of impact at any altitude would be small if at least one retro-rocket fired.

Calculations using experimentally measured motor ejection velocities showed that the retro-rockets on the fourth-stage motor should be fired about 3 seconds after the explosive bolts on the marmon clamp were blown, starting the motor ejection sequence. With such timing, the retro-rockets would be fired just before the assumed 3-pound residual thrust caused the motor to decelerate to zero velocity (relative to the re-entry system) at approximately 6 feet behind the re-entry system.

An altitude of 350,000 feet was selected as the nominal altitude for ejecting the motor because it appeared to provide the best compromise between the two requirements. Corresponding to this altitude, the time of 283 seconds from launch was selected for the timer signal for blowing the explosive bolts on the marmon clamp. A 4-second delay timer to be initiated by a timer signal at 282 seconds after launch would fire the retro-rockets on the fourth-stage motor at 286 seconds after launch.

Selection of Parachute Deployment Time

The drogue gun was fired and the parachute deployed by a signal from the decoder in the telemetry package. (The timer was started just before launch.) Two considerations affected the time selected for parachute deployment: (1) the need to deploy the parachute as high as possible, to ensure enough time to transmit all the post-blackout data, and (2) the need to deploy the parachute at an altitude low enough to ensure that the Mach number and dynamic pressure would not cause chute failure. An additional complication was the possibility of variation in the Scout launch vehicle trajectory and thus in the re-entry system trajectory.

An analysis of the effects of variations in Scout trajectory on conditions at parachute deployment indicated 455 seconds from launch as a good time for parachute deployment. Nominal and 2-sigma tolerances on the conditions at parachute deployment are tabulated below:

Altitude (feet)	Dynamic Pressure (lb/ft²)	Mach Number
$21,000 \pm 11,000$	$292 \; {}^{+9}_{-32}$	$0.67 \; {}^{+0.12}_{-0.11}$

A barometric switch was connected in parallel with the timer signal, as a backup method for initiating the drogue gun. The barometric switch was armed 340 seconds after launch, at a nominal altitude of 200,000 feet, by the timer signal, and was set to operate at a pressure corresponding to an altitude of about 21,000 feet. (This pressure setting was corrected to include base pressure effects as calculated with measured base pressure coefficients obtained in wind-tunnel tests.)

61

SECTION VIII -- THERMAL DESIGN

Design Parameters

The RFD-1 re-entry system (RS) was designed with a full-scale, simulated SNAP-10A reactor mounted on the nose of a cone-cylinder-flare re-entry vehicle (RV); the simulated reactor was aligned with the NaK pump forward as shown in Figure 1, p. 11. The RV acted as a stabilized platform for the reactor experiment and housed the telemetry, TM antenna, C-band tracking antenna, and recovery gear. The factors relating to thermal protection of the RV were as follows:

1. Possible temperature extremes and temperature shock during shipping handling, storage, and on the launch pad had to be prevented from causing excessive thermal stresses in the vehicle.

2. No special thermal protection was required for the nose of the RV since it was protected during the entire flight by the base of the reactor, which in turn was potted with an ablative epoxy. A detailed description of the reactor base can be found in Sandia Corporation report SC-RR-64-515.

3. Since the phenolic-fiberglass reactor mount, which was partially covered by a tungsten nose weight, had to be kept below 500°F, the temperature of the tungsten contacting the mount could not exceed 500°F.

4. In order to ensure that sufficient strength would be retained, and to prevent pyrolization from shorting the antennas where they contacted the structure, the inner 0.040 inch of the phenolic fiberglass RV structure could not exceed 500°F. An additional requirement of the thermal protection for the portion of the outer shell over the C-band and TM antennas was that it be transparent to RF transmission: that is, that it must be an electrical insulator and must not be a lossy material. This precluded the use of a charring ablater in these areas.

5. The telemetry package in the nose of the RV could not exceed 165°F.

6. Since the C-band and TM antennas mounted inside the structure could withstand the same temperature as the phenolic-fiberglass case, heat from the outer surface presented no additional problems in these areas. However, the inner surface of the TM antenna, which was exposed to aerodynamic heating after the fourth-stage motor was ejected, needed additional thermal protection.

7. Because an RV of the size of the RFD-1 vehicle approached the weight and volume limitations of the Scout launch vehicle, the primary criterion used in selecting thermal protection systems was high specific thermal efficiency (amount of heat absorbed, or blocked, per unit weight of material).

8. The outer surface of the vehicle had to be strong enough during the heating pulse to withstand both the impact of debris from the disassembling reactor at the nose of the RV and aerodynamic shear and pressure forces.

Stagnation Point Heating

In order to simulate orbital decay heating on the SNAP-10A experiment as closely as possible, the RFD-1 RS was flown with as high a re-entry velocity and as low a re-entry angle as was possible, given a Scout vehicle and the restraints of re-entering within a given distance of Bermuda. Flight parameters used for the design trajectory were:

Re-entry velocity	20,176 ft/sec
Re-entry angle	-6°
Re-entry system weight	482 lb
Vehicle impact weight	332 lb

The ballistic coefficient (W/C_DA) varied from 134 to 329 lb/ft^2 due to Mach number effects and to the changes in drag coefficient (C_D) and weight with disassembly of the reactor and ablation of the RV. The method of calculating the trajectory is described in Sandia Corporation report SC-RR-64-510. Altitude and velocity as functions of time from 404,066 feet are shown in Figure 43.
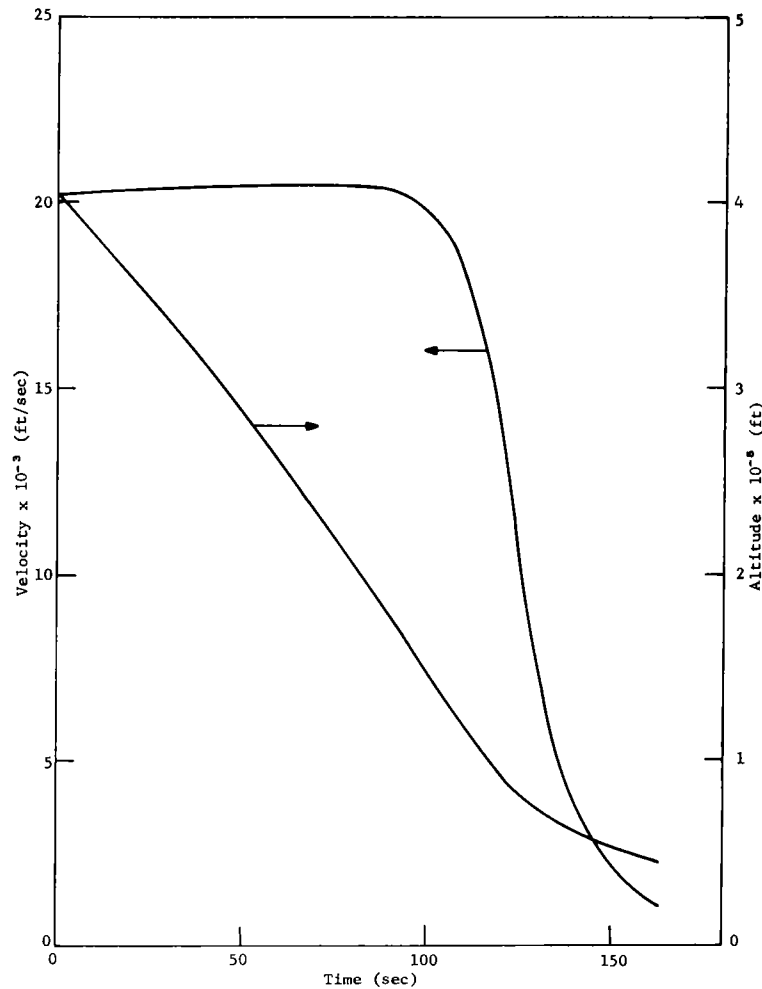
Figure 43. RFD-1 trajectory (altitude and velocity versus time)

Stagnation heating of a 1-foot radius sphere using data from the above trajectory was calculated on the CDC 1604 computer by a method described in References 7 and 8. (Reference 9 describes the computer program used for both trajectory and stagnation point heating computations.) Basic heating equations used in this computer program for convection and radiation, including the effects of dissociation and ionization, were:

Convective heat rate

$$\dot{q}_c = \frac{17,600}{\sqrt{R}} \left(\frac{\rho_\infty}{\rho_s}\right)^{.5} \left(\frac{V_\infty}{V_c}\right)^{3.15} , \quad BTU/ft^2 \ sec$$

where

R = nose radius (ft)

$\dfrac{\rho_\infty}{\rho_s}$ = ratio of local free-stream density to density at sea level

V_∞ = free stream velocity (ft/sec)

V_c = the circular orbital velocity

Radiation heat rate

$$\dot{q}_r = AR\left(\frac{\rho_\infty}{\rho_s}\right)^{1.78} \left(\frac{V_\infty}{10^4}\right)^{B} , \quad BTU/ft^2 \ sec$$

where

A = 0	B = 0	when	V_∞ < 25,000
A = 6.8	B = 12.5	when	25,000 ≤ V_∞ < 30,000
A ⇒ 0.003	B = 19.5	when	30,000 ≤ V_∞ < 35,000
A = 20.4	B = 12.5	when	35,000 ≤ V_∞

Since velocities for the RFD-1 flight never exceeded 25,000 ft/sec, only convective heat transfer to the RV was considered. Predicted stagnation heating rates $\left[\dot{q}_{ss} \ \sqrt{R} \ (BTU/ft^{3/2} \ sec)\right]$ and integrated stagnation heating $\left[Q_{ss} \ \sqrt{R} \ (BTU/ft^{3/2})\right]$ are shown in Figure 44.

Local Heating Rates

The ratio of local-to-stagnation heating $\left(\dot{q}_L/\dot{q}_{ss} \ \sqrt{R}\right)$ could not be calculated because of the complex shape of the RS. This ratio was determined experimentally at Arnold Engineering Development Center, Tullahoma, Tennessee. The test facility used was the 100-inch hot-shot tunnel shown in Figure 45.
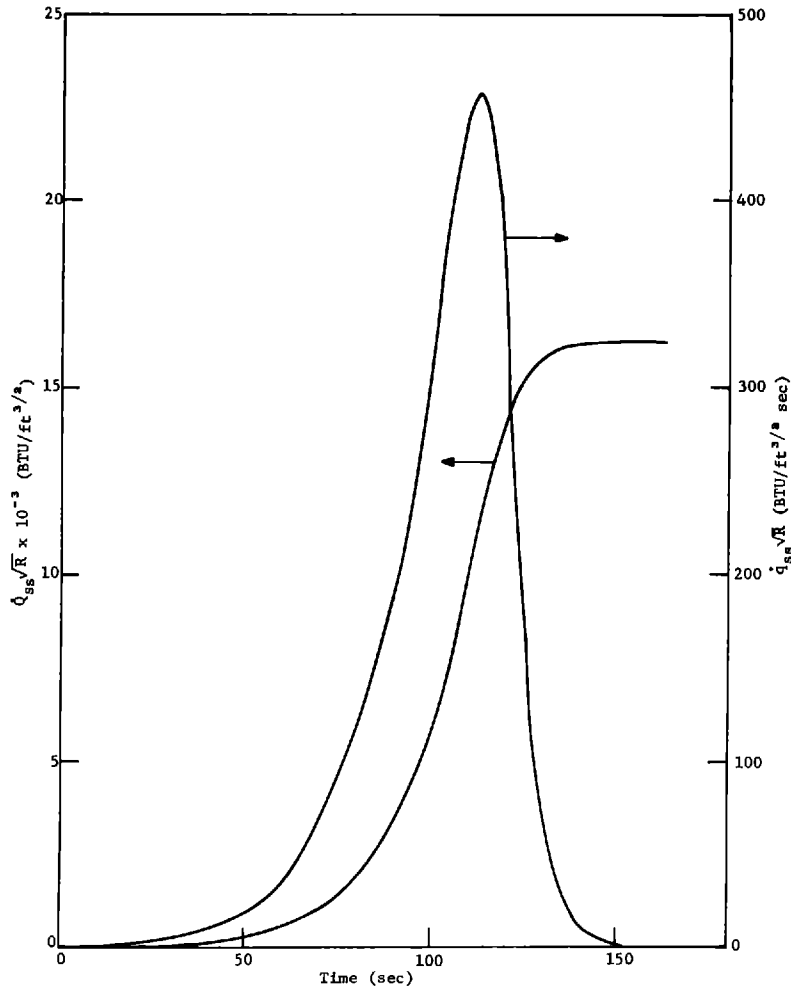
Figure 44.

RFD-1 trajectory (pre-
dicted stagnation heating
rates and integrated
stagnation heating)
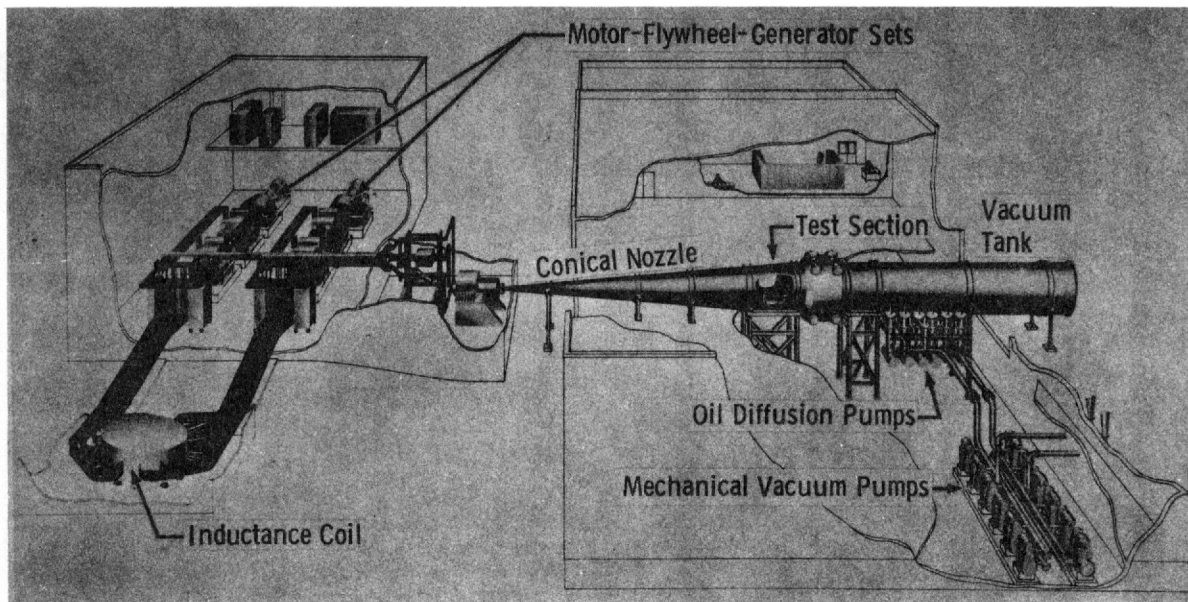
Figure 45. Arnold Engineering Development Center 100-inch
hypervelocity wind tunnel (Tunnel F)

The three models used for these tests are shown in Figures 46, 47, and 48. Configuration 1 was a full-scale model of the forward part of the cone section of the RV and the reactor, less the reflectors. Configuration 2 is the same as 1, but the NaK pump and tubes have been removed to represent a later stage of disassembly. Configuration 3 was a quarter-scale model of the entire RS. All three models were run at 0- and 4-degree angles of attack and were instrumented with thermocouple-type heat gages which measured heating rates by the slope of the temperature rise of a thin disc heat meter at the surface of the model. Heat gage locations for Configurations 1 and 2 are shown in Figure 49 and for Configuration 3 in Figure 50. Heating rates were referenced to stagnation heating rates on 1-inch diameter hemisphere-cylinder calibration probes located on either side of the models. With heating rates on the model and the calibration probes, it was possible to calculate $\dot{q}_L/\dot{q}_{ss} \sqrt{R}$.
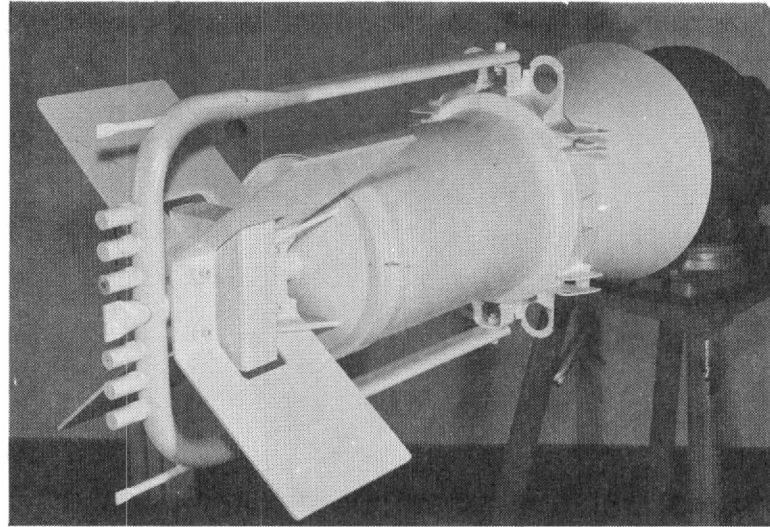
Figure 46.   Model used in 100-inch hot-shot
tunnel test (Configuration 1)
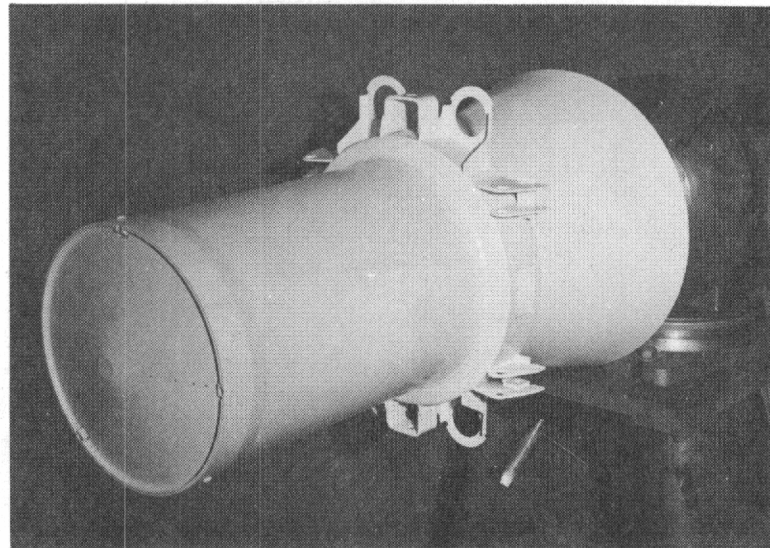
Figure 47.   Model used in 100-inch hot-shot
tunnel test (Configuration 2)
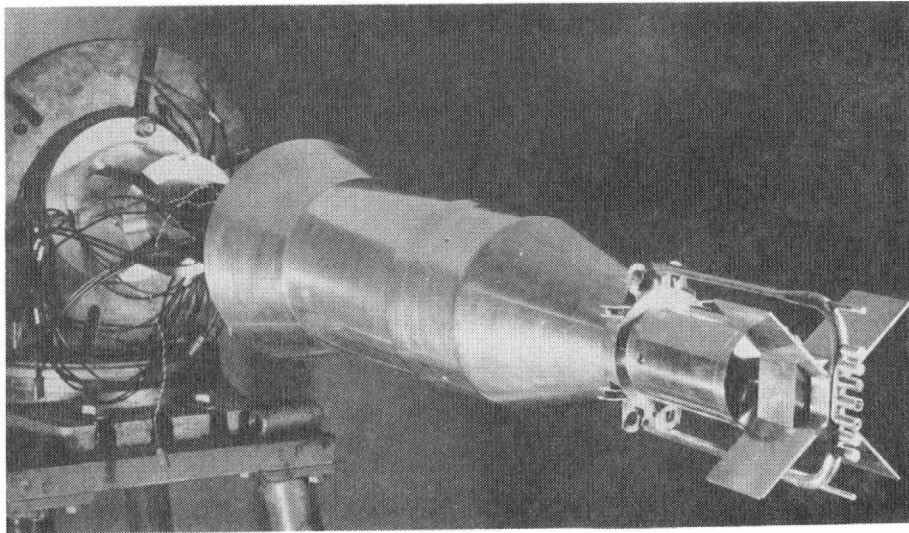
Figure 48. Model used in 100-inch hot-shot
tunnel test (Configuration 3)

CONFIGURATION I

NOTES:
  1. Heat transducer locations designated H
  2. Configuration 2 obtained by removal of
      radiative heat fins, tubing, and pump
      from Configuration 1
  3. All dimensions are in inches
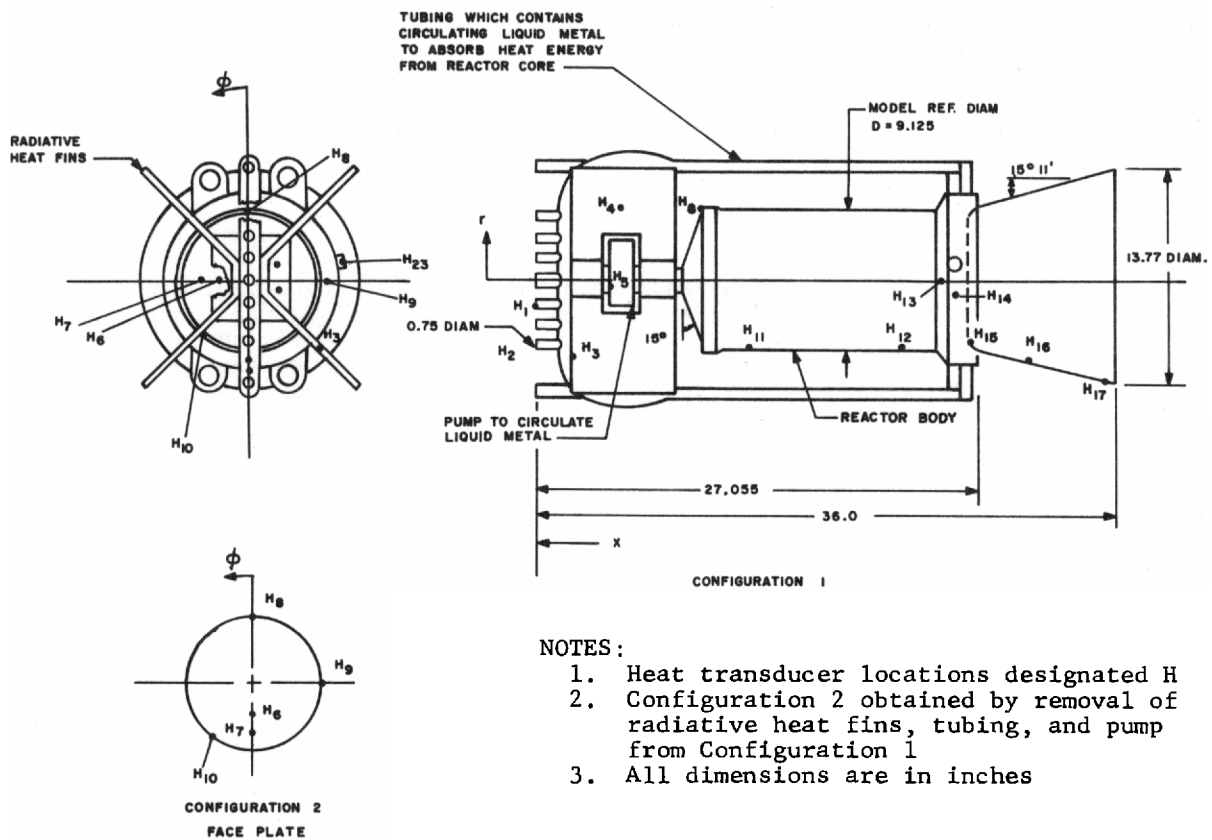
Figure 49. SNAP-10A Configurations 1 and 2
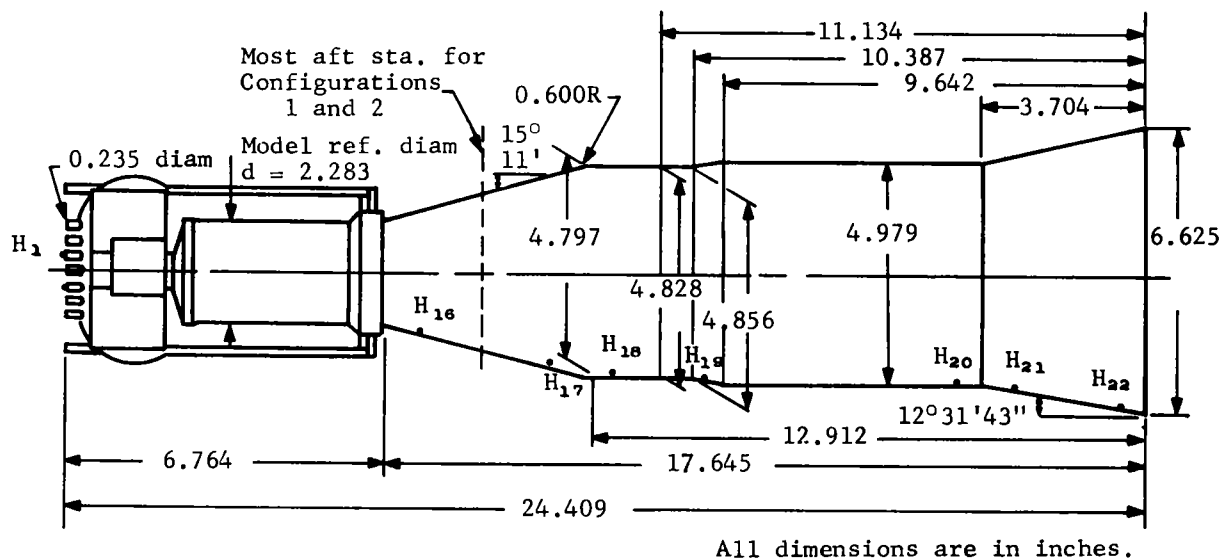
Figure 50. SNAP-10A Configuration 3

The test series was run at Mach numbers ranging from 17.3 to 20.6 and free-stream Reynolds numbers (N_{Re}) ranging from 6113 to 48,283 per inch. Although the maximum flight Reynolds numbers as shown in Figure 51 were not obtained in these tests, particularly on the quarter-scale model, they were high enough to obtain fully developed turbulent flow. While other flight conditions were matched during this series, tunnel enthalpy was approximately one-fourth that of the flight.

The $\dot{q}_L/\dot{q}_{ss} \sqrt{R}$ was found to be a function of N_{Re} in all areas except stagnation regions. In separated flow regions, this ratio decreased exponentially with increasing N_{Re} over the entire test range which is in agreement with theory and other experimental data.[10] In attached flow regions, the heating ratios were found increased by as much as a factor of 5 on the RV, from Reynolds numbers of 5×10^5 to Reynolds numbers of 3×10^6 based on scaled vehicle length. This increase, found on all three configurations, was probably due to transition from laminar to turbulent flow. Whereas transition does not usually take place at N_{Re} values as low as this, Schlieren photographs show that the irregular shape of the reactor breaks up the laminar boundary layer and causes turbulent flow at a lower N_{Re}. With the boundary layer trip at the front of the vehicle, transition takes place over the entire RV at the same time. Figure 52 shows the N_{Re} effect on heating ratios for location H_{16}, which is typical of the same effect on all attached flow areas (H_{16} through H_{22}). The range of heating ratios found from this test series for laminar and turbulent flow was used in the design of the RFD-1 RV. This range is shown in Figure 53. The AEDC final report[11] gives tunnel conditions in greater detail as well as pressure distributions along the vehicle.

Structure and Materials

Exterior Surfaces -- Figure 54 shows the overall exterior thermal system for the re-entry vehicle, including the support structure, primary ablation system, antenna windows, reactor mount, and nose weight. The cone-cylinder-flare support structure which also acts as insulation is made of CTL 91-LD phenolic on 181 glass cloth. A flat layup was used to minimize thermal conductivity in the radial direction and to give maximum strength. The thickness of this structure varied over the vehicle surface depending on the ablation and reaction zone temperature of the outer ablation material and on the local heating rates. Areas with lower heating rates required less ablation material but more insulation and a larger heat sink.
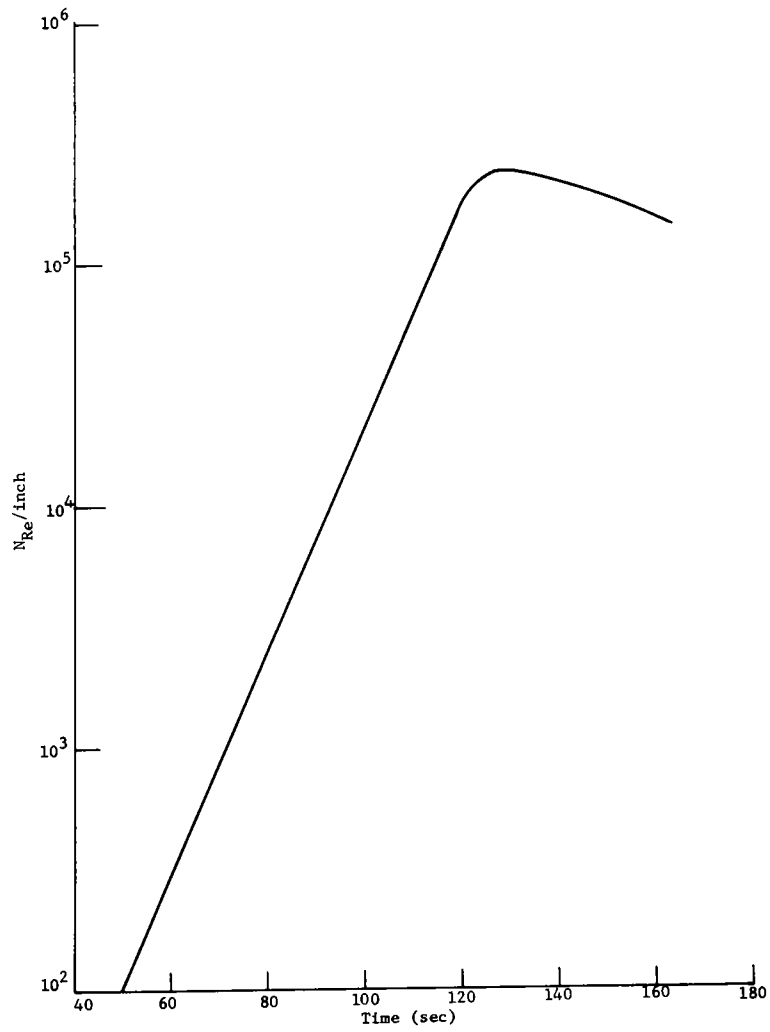
Figure 51. RFD-1 trajectory (maximum flight Reynolds numbers)
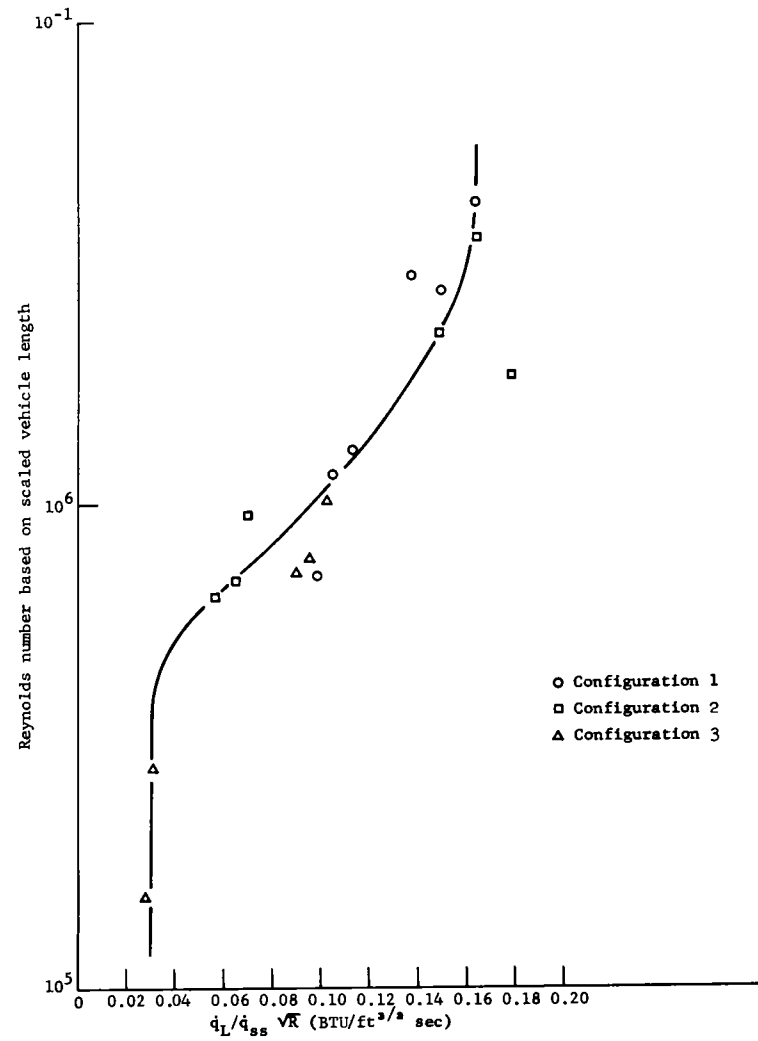
Figure 52. N_{Re} effect on heating ratios for location H_{16}
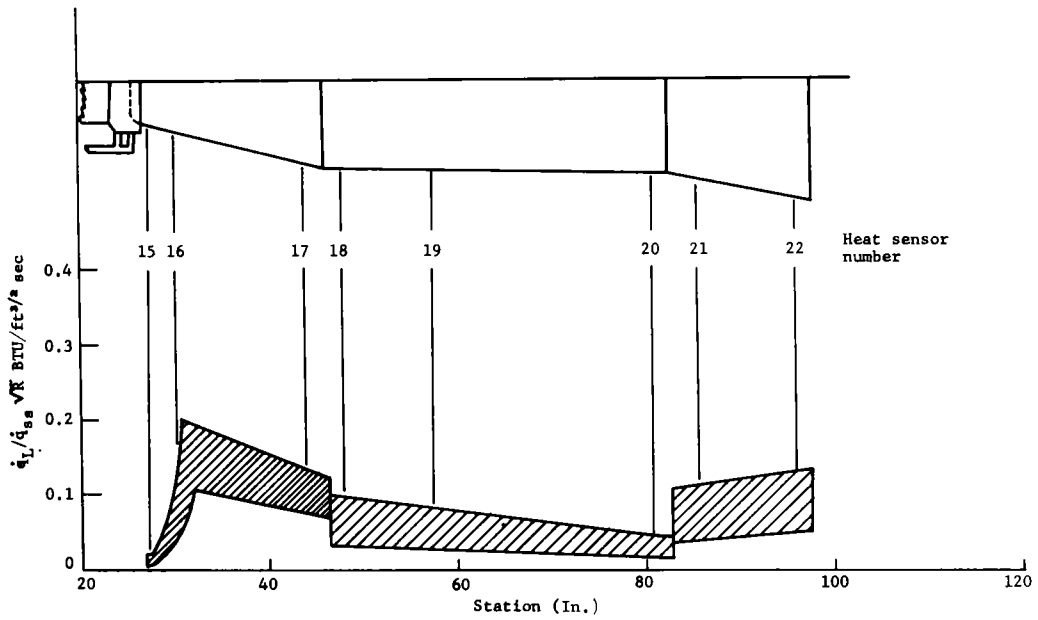
Figure 53. Range of heating ratios for laminar and turbulent flow

	Material thickness (inches)									
Station	A	B	C	D	E	F	G	H	I	J
Outer phenolic-fiberglass	0.41	0.28	0.19	0.13	0.13	0.05	-	-	-	-
Bond	0.01	0.01	0.01	0.01	0.01	0.01	-	-	-	-
Inner phenolic-fiberglass	0.24	0.26	0.25	0.25	0.12	0.12	0.12	0.12	0.46	0.46
Teflon	-	-	-	-	0.05	0.12	0.18	0.12	-	-
Cohrlastic and bond	-	-	-	-	0.08	0.08	0.08	0.08	-	-
Total	0.66	0.55	0.45	0.39	0.39	0.38	0.38	0.32	0.46	0.46
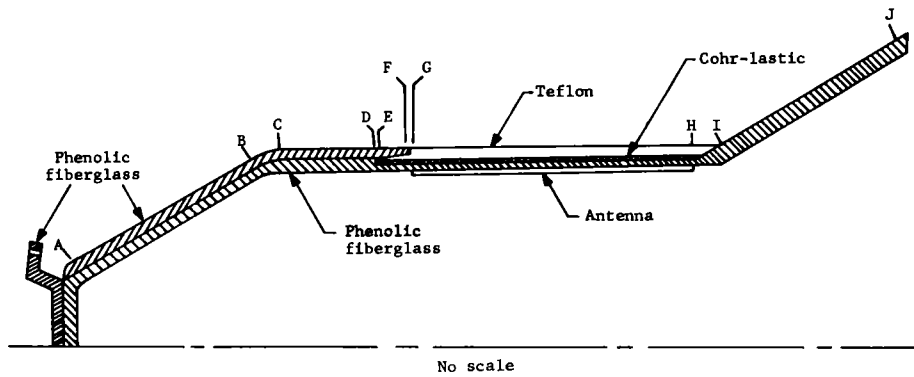
Figure 54. Overall exterior thermal system for the re-entry vehicle

70

Since the structure would reach 500°F during re-entry, the prospect of thermal expansion required the ablation material and structure to have similar coefficients of thermal expansion. The long heating pulse experienced during a -6 degree re-entry also dictated that the ablation material have a low conductivity and reaction temperature. A primary ablation system consisting of two 20-degree shingle wrapped, tape-wound shells made of CTL 91-LD phenolic on 181 glass cloth was chosen to fulfill these requirements. The forward shell covered the cone and the forward portion of the cylinder extending over the leading 3 inches of the TM antenna window. The aft shell covered the flare of the vehicle. Both ablative sections were bonded to the structure with Epon 931 adhesive. Counterbored bolt holes through the ablation system were filled with Dyna-Therm E-300.

The six C-band antennas, equally spaced radially around the conical section of the vehicle, were protected by windows made of teflon. Teflon is a subliming ablater which leaves a clean, uncharred surface which is transparent to RF. The windows, 1.69 inch wide by 0.7 inch long, were of the same thickness as the surrounding phenolic fiberglass ablation material. When exposed to the same heat flux, teflon ablates faster than phenolic fiberglass. However, as soon as the teflon window recedes below the surface of the material surrounding it, the heat flux to the window is reduced as a consequence of separated flow. Calculated separated flow heating rates, using the method described in Reference 10, were verified by heating sample RV sections in a plasma jet. These tests are described in Section XIII of this report. The C-band antenna windows were bonded with Epon 931 into dove-tailed slots in the surrounding ablation material to securely hold them in position during re-entry.

The TM antenna window was also made of teflon so that it, too, would remain transparent to RF. The coefficient of thermal expansion of teflon is 10 times that of the phenolic fiberglass structure. To allow relative expansion of the large window, it was necessary to provide an expansion joint between the teflon and case. This joint consisted of a 0.060-inch thick layer of Cohrlastic silicone sponge rubber, bonded between the cylindrical window and case with DC 521 silicone adhesive. The phenolic fiberglass nose section overlapped the leading edge of the TM antenna, preventing radial expansion. With the leading edge held down in this manner, the teflon could not be peeled back by aerodynamic forces. Since it was held rigidly in the front, all longitudinal expansion of the window took place in the aft direction, so that it would ride up the base of the flare during re-entry. Where the door bisected the overlapping nose, the teflon was held down by the beveled trailing edge of the door.

The reactor mount, which was bolted and bonded to the nose of the RV, was made of 0.25-inch phenolic fiberglass. The forward surface of the mount was protected by the reactor base. A Heavymet nose weight was attached directly behind the reactor mount to protect that surface from aero heating. The gap between the nose weight and the mount was filled with RTV-601 silicone rubber to protect the mount and the ten No. 10 reactor mounting bolts from aero heating. The outer periphery of the nose weight and reactor mount were coated with 0.20 inch of Dyna-Therm E-300 to reduce aero-heating inputs.

Parachute Door -- The thermal protection for the parachute door consisted of 0.100 inch of T-500 ablative coating, 0.250 inch of phenolic fiberglass, and 0.19 inch of urethane foam. Since the back surface of the foam was in contact with the parachute, its temperature needed to be kept below 200°F up to the time of parachute deployment. Figure 55 shows the results of a radiant heat test on this parachute-door structure, for an expected heat pulse of 50 BTU/ft² sec peak heating.

Flare Liner -- The flare liner was the portion of the structure between the parachute chamber and the cavity. The thermal protection provided for this liner was similar to that used for the parachute door, except that the thickness of the T-500 and the fiberglass was less because lower heating was expected. It was again necessary to keep the back surface of the foam below 200°F. Figure 56 shows radiant heat-test results for the expected heating pulse of 18 BTU/ft² sec and for a higher pulse of 27 BTU/ft² sec peak.
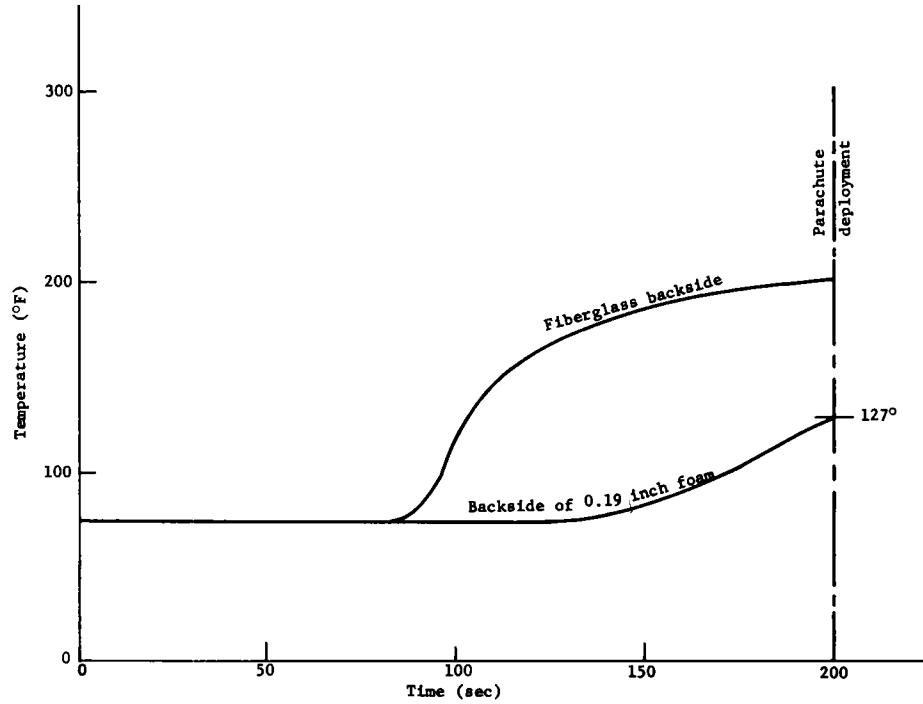
Figure 55. Results of radiant heat test of
parachute door structure
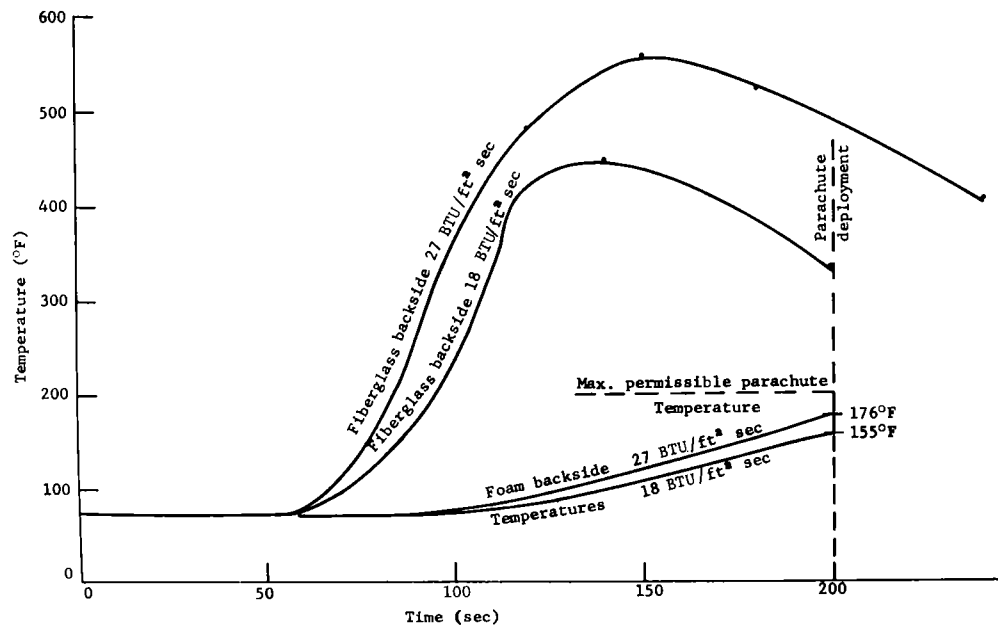
Figure 56. Results of radiant-heat test of
flare liner

Dipole Antenna -- The surface of the dipole antenna which was exposed in the cavity was supplied with thermal protection in the form of a 0.040-inch coating of D-65 intumescent coating. Figure 57 shows temperature results for a section of the antenna exposed to an expected peak heating pulse of 18 BTU/ft^2 sec in the Radiant Heat Facility.
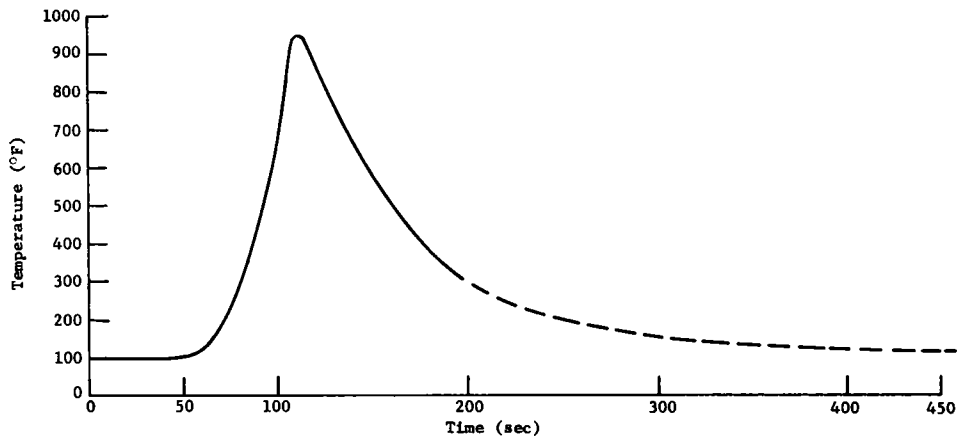
Figure 57. Results of radiant-heat test of dipole antenna

CO_2 Bottles -- The purpose of the CO_2 bottles was to inflate the flotation bag in the recovery system. The squib controlling the valve on the bottles had to be protected against temperatures higher than 250°F in order to prevent premature inflation of the flotation bag. In addition, the bottles themselves had to be kept below 300°F.

The first design of the thermal protection system provided for a 0.15-inch layer of E-300 ablative coating on the bottles. With only this coating, however, the temperature of the front side of the bottles exceeded 300°F in a radiant heat test (see Figure 58). A 0.040-inch layer of D-65 intumescent coating was then added on top of the E-300 coating, with the result that the temperature of the bottles for an expected peak heat pulse of 9 BTU/ft^2 sec stayed below 250°F and the squib temperature at the valve never exceeded 100°F (see Figure 59).

Flotation Bag Cover -- The flotation bag cover needed to be a thin, light-weight, flexible material able to withstand an expected peak heating pulse of 9 BTU/ft^2 sec. Various materials such as fiberglass cloth, nylon, impregnated fiberglass cloth, and assorted ablative coatings were tested for this purpose in the Radiant Heat Facility. The most satisfactory solution found was a layer of heavy refrasil cloth coated with 0.040-inch of D-65 intumescent coating, and bonded to an inner layer of silicon-rubber-impregnated fiberglass cloth. (This inner layer had to be kept below 500°F in order to protect the flotation bag.) The results for a radiant heat test of this cover are shown in Figure 60.

Baroswitches -- The thermal protection system used on the baroswitches was identical to that used on the CO_2 bottles. The baroswitches were subjected to a peak heating pulse of 18 BTU/ft^2 sec (twice the expected value) in the Radiant Heat Facility. Temperatures and switch function were monitored during the test. The switch operated satisfactorily, and the temperature recorded on the switch, as shown in Figure 61, was within acceptable limits.
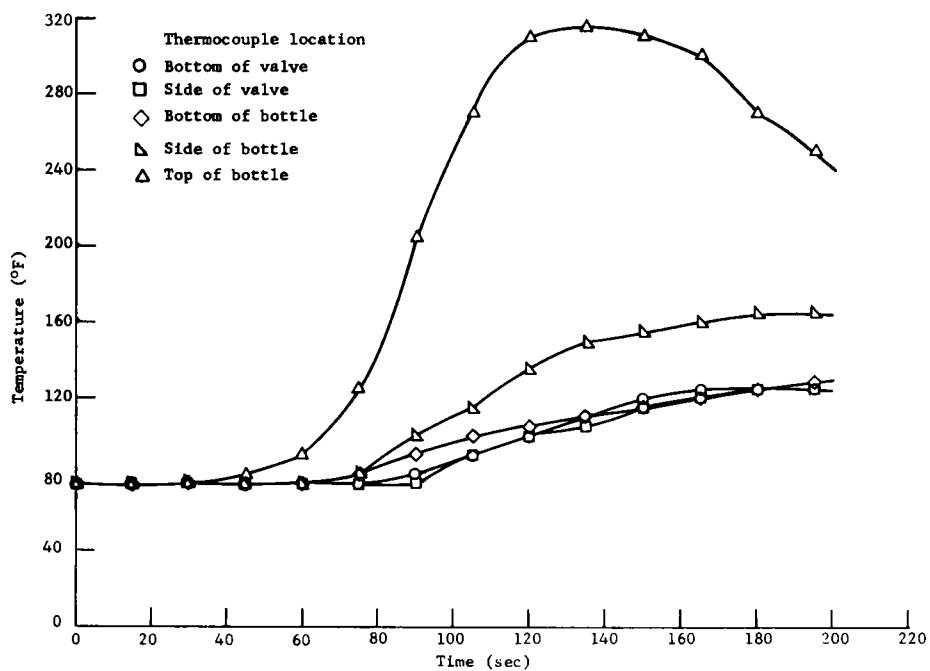
Figure 58.   Results of radiant-heat test
of CO_2 bottle (uncoated)
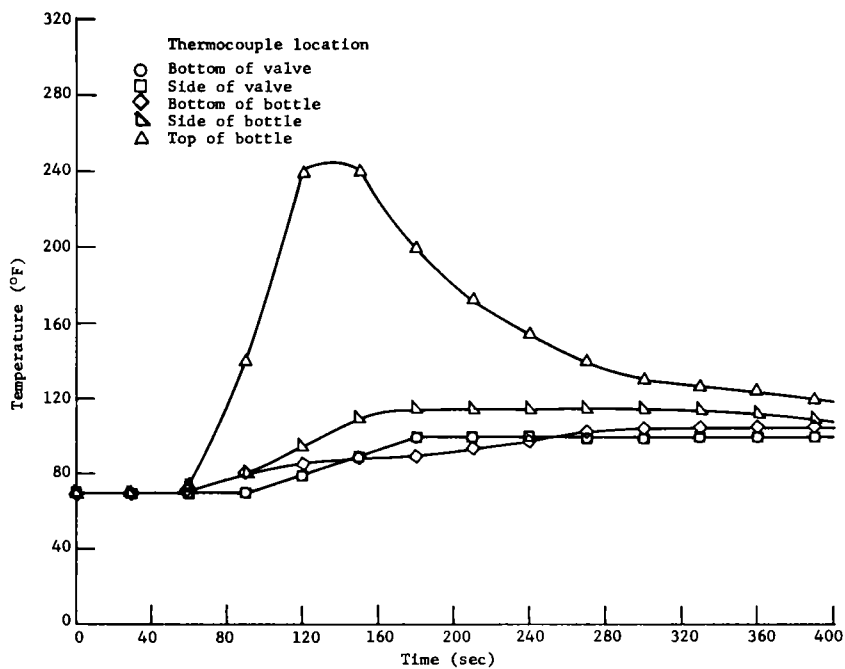
Figure 59.   Results of radiant-heat test
on CO_2 bottle (coated)
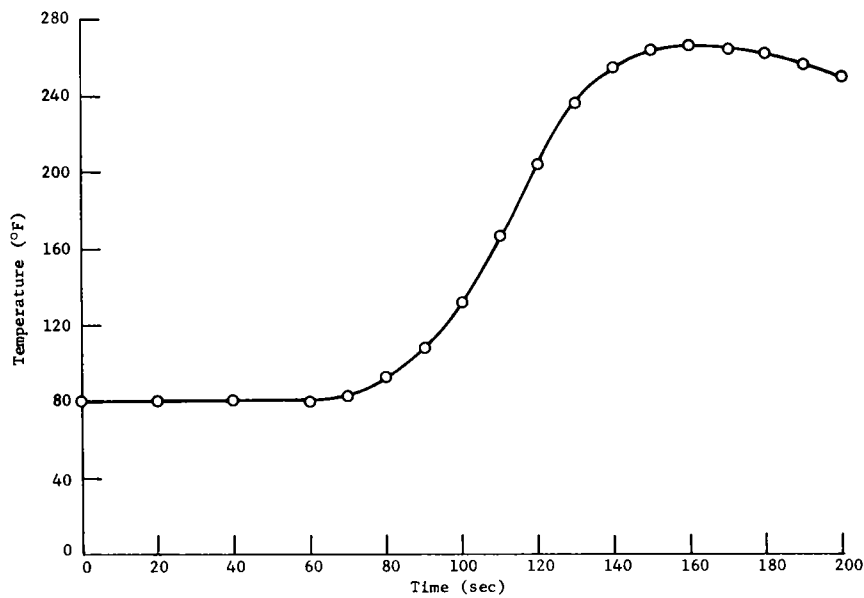
Figure 60. Results of radiant-heat test
of flotation bag cover
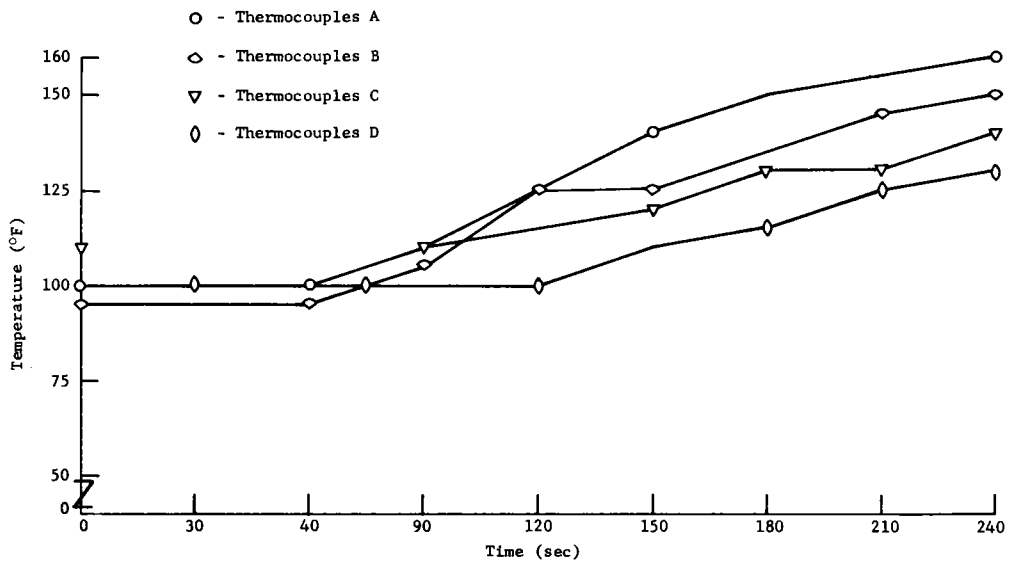
Figure 61. Results of radiant-heat test
of baroswitches

Parachute Cord -- The parachute cord which connected the recovery chute to the re-entry vehicle consisted of a flat, woven, 1-inch wide fiberglass cord coated with a 0.040-inch layer of D-65 intumescent coating. When this cord was subjected to an expected peak heating pulse of 9 BTU/ft² sec in the Radiant Heat Facility, the maximum temperature experienced by the fiberglass under the layer of D-65 coating was 435°F (see Figure 62). The cord was subsequently tensile-tested in a 425°F oven. It failed at 700 pounds in the oven test, as against its strength of 980 pounds at ambient temperature. However, the 700-pound strength was adequate for service with the recovery parachute.
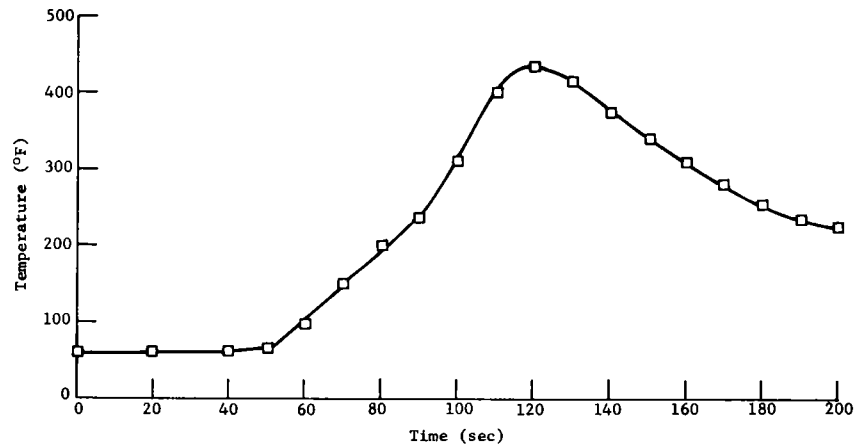
Figure 62. Radiant-heat test of the parachute cord

Connectors and Wires Exposed in the Cavity -- Several radiant heat tests were run on the wiring and connectors exposed in the cavity. Figure 63 shows a set of connectors after they had been tested at the expected heating pulse. It was found that they did not need any additional thermal protection. The wiring, however, did need extra thermal protection, and this was provided in the form of a 0.020-inch wall of teflon tubing. After this tubing had been slipped over the electrical cables, the cable insulation remained below its maximum operating temperature when exposed in the Radiant Heat Facility to the expected heating pulse.

Ablation Computer Program

Ablation studies were conducted with the aid of the Sandia Thermalog, which utilizes a one-dimensional passive electric analog representation of heat conduction and radiation with a given heat input. The phase change processes are represented electrically by biased Zener diodes with current integrators. The heat of vaporization and heat blockage terms in Q* or heat of ablation equations, and the resultant mass removal, is accomplished in discrete steps or nodes. The radiation term in Q* was handled separately at the time varying surface temperature. The one dimensional conduction network is constructed utilizing the procedures as outlined in Reference 12. Properties of materials used in this analysis are as follows:

Material	Density (lb/ft³)	Thermal Conductivity (BTU/hr ft °F)	Specific Heat (BTU/lb °F)	Ablation Temp. (°F)	Q* (BTU/lb)
Cohrlastic	20	0.032	0.35	-	-
Phenolic fiberglass	117	0.125	0.23	3600	2700
Teflon	137	0.142	0.25	1000	1000

Inner and outer temperatures of the vehicle are shown as functions of time in
Figures 64 through 71. (Refer to Figure 54, p. 70, for vehicle structure, stations,
and material thicknesses.) Times given are from 400,000 feet during re-entry, for
Trajectory Number 394.
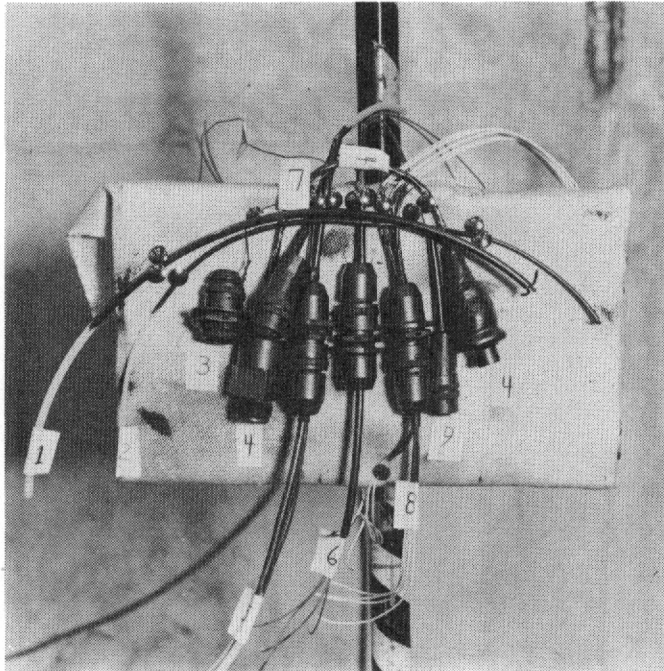
Figure 63.

Results of radiant-heat
test on connectors
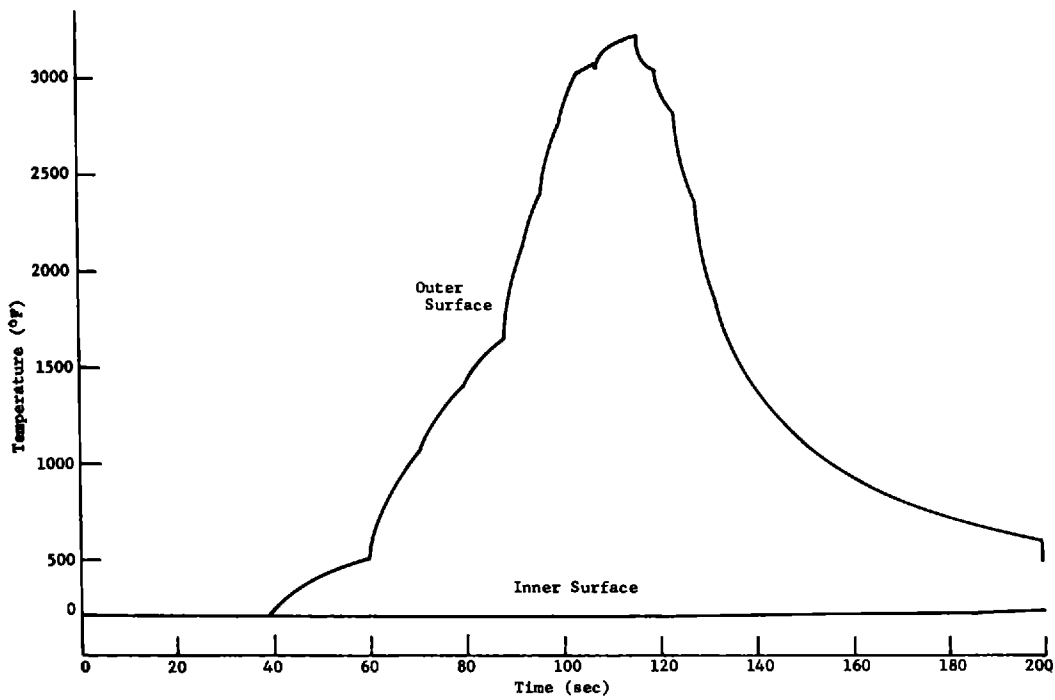
Figure 64. Temperature response of fiberglass at Station A
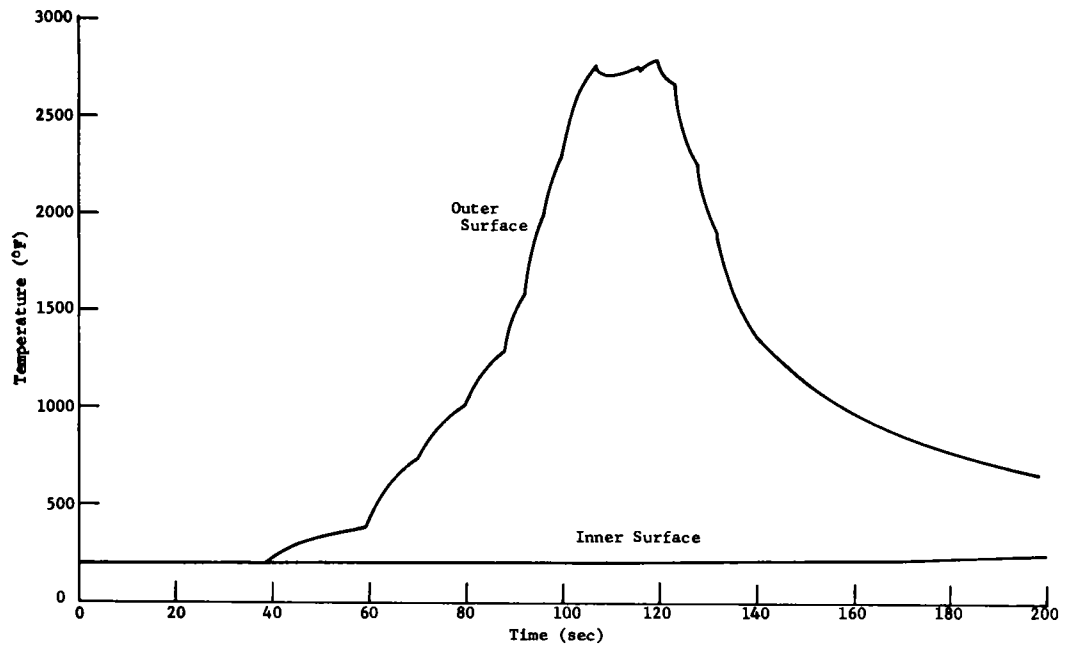
Figure 65. Temperature response of fiberglass at Station B
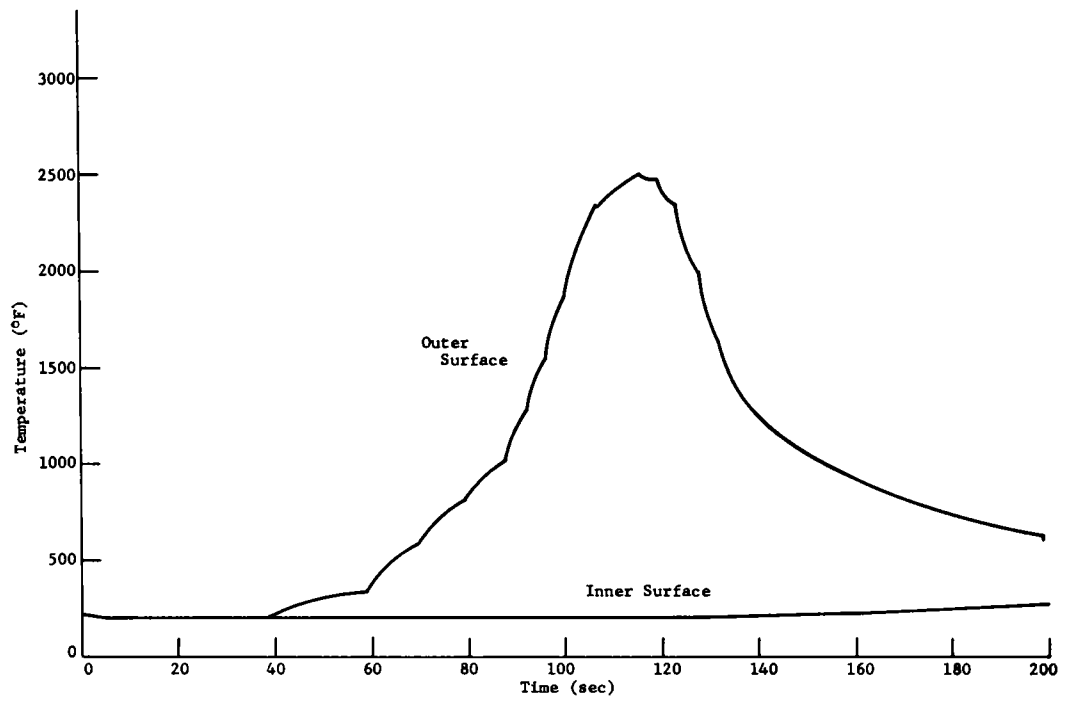
Figure 66. Temperature response of fiberglass at Station C

78
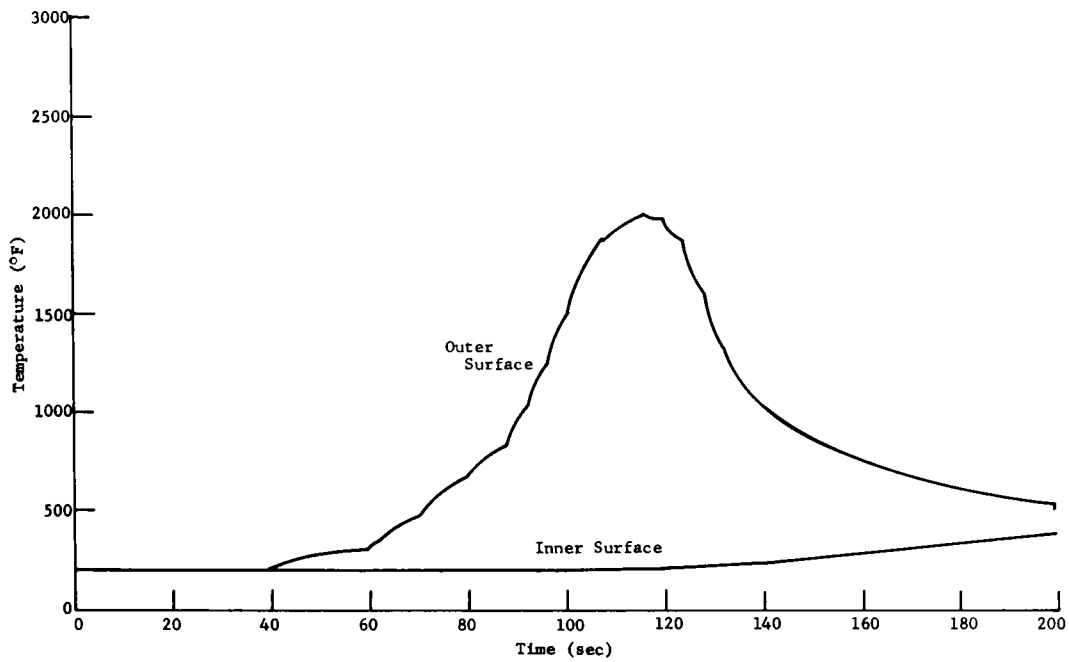
Figure 67. Temperature response of fiberglass at Station D
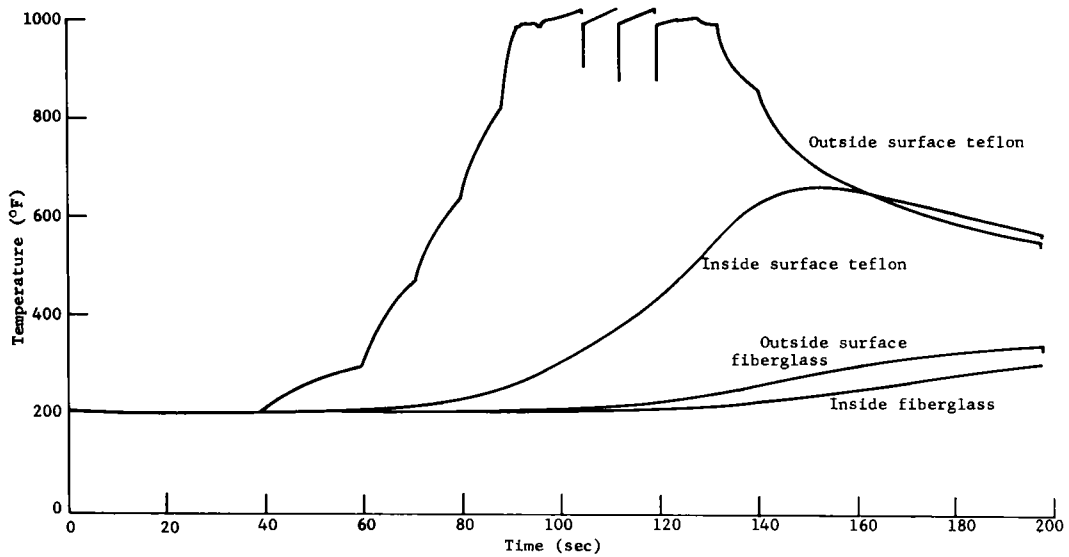
Figure 68. Temperature response of fiberglass at Station G
(0.070 inch teflon ablated)
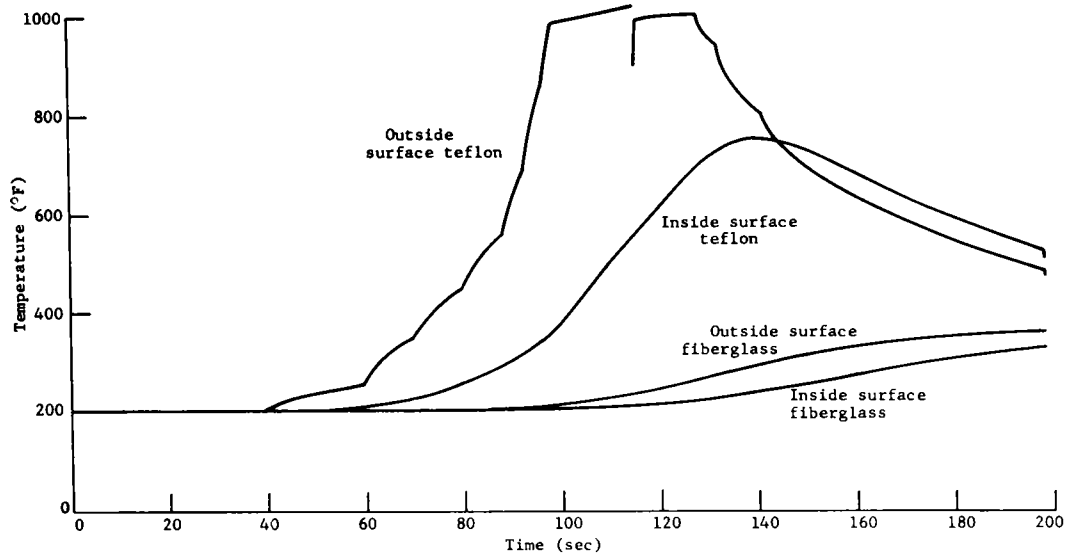
Figure 69. Temperature response of fiberglass at Station H
(0.030 inch teflon ablated)
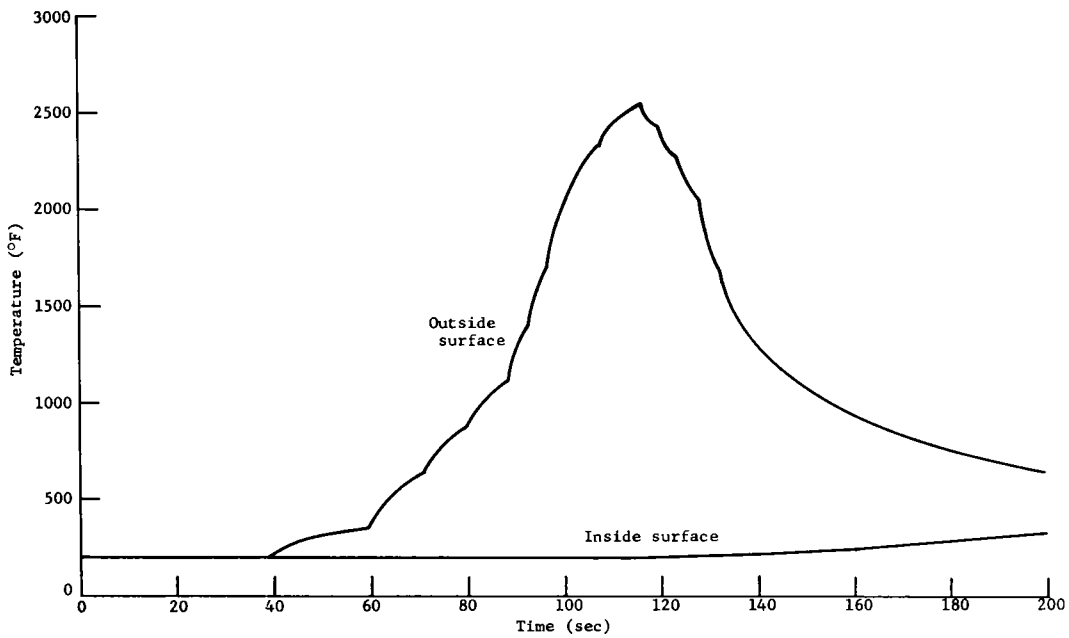
Figure 70. Temperature response of fiberglass at Station I

80
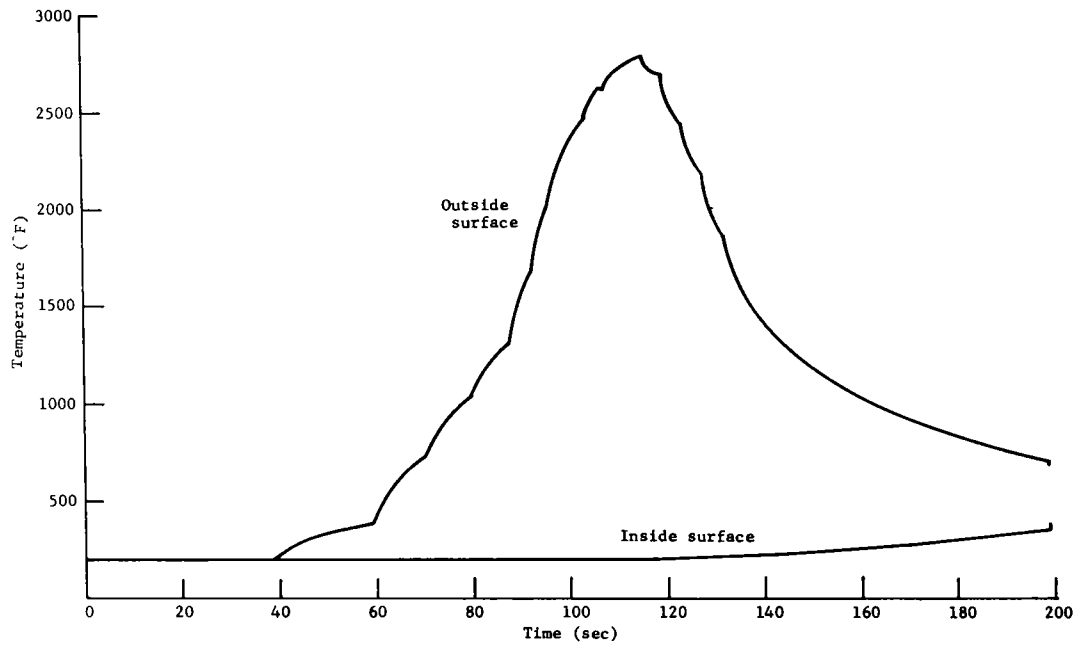
Figure 71. Temperature response of fiberglass at Station J

SECTION IX -- EXTERNAL FUEL ROD EXPERIMENT

General

The safety of SNAP-10A depends ultimately on the complete ablation and dispersion of its UZrHx fuel rods. However, knowledge of how UZrHx will behave when it is exposed to the environment of re-entry into the atmosphere is very limited. Calculations indicate that the aerodynamic heating associated with orbital decay re-entry is probably insufficient to ensure complete ablation of the SNAP-10A fuel elements. In any case, aerodynamic heating may be substantially augmented by the heat from exothermic chemical reactions of zirconium with the atmosphere.

Since the re-entry environment cannot be exactly simulated by laboratory experiments, it was decided to include a fuel rod ablation experiment on the RFD-1 flight test.

The objectives of this experiment were threefold:

1. To gain information on the ablation rate of, and the volume consumed by burnup of, fuel elements in general and SNAP-10A fuel rods in particular

2. To confirm theoretical calculations and predictions about re-entry burnup

3. To evaluate the optical instrumentation and techniques used.

The plan for the experiment was to eject simultaneously four groups of three rods early during the re-entry of the re-entry vehicle, and then record their burnup with spectral, plate, and motion picture cameras. Since all the rods followed the same trajectory and experienced essentially the same heating, it was expected that those in the group with the least wall thickness would first ablate away their outer UZrH to expose the tracer material contained inside them. The tracer would then burn and emit a characteristic flare. Each fuel element, because of varying wall thicknesses, would flare at a different time and altitude. Comparison of the volume consumed with the calculated heating for the flight trajectory would provide indications of the rate and volume of ablation versus re-entry heating.

During the design and fabrication of the flight-test elements, a number of simulated rods were tested in a plasma jet facility in order to observe the effects on ablation rate and structural integrity of the included tracers. This test also allowed a preflight test of the optical instrumentation. The results obtained established the adequacy of the fuel rod design and also yielded insights into the probable ablation sequence. (Details are available in Reference 13.)

Description of the Fuel Rods

Calculations performed before the flight test indicated that the reactor core can lid would not melt to allow the fuel rods to separate until relatively late in the trajectory. Consequently, it was decided to mount the fuel rods on the outside of the re-entry vehicle so as to be able to predetermine the time of their release into the atmosphere independently of events affecting the reactor. Their mounting and location are shown in Figure 6, p. 19. Explosive bolts actuated by the time decoder released the rods from their mounting.

To achieve the test objectives, it was necessary to measure the rate and volume of fuel rod ablation during re-entry burnup. This necessity dictated the design of the experimental rods. Their final configuration is shown in Figure 72. All the rods had the same external dimensions, but they were provided in four different groups of three, differentiated by internal dimensions and by the tracer element contained, as follows:

	Wall Thickness (inches)	Tracer
Group 1	0.106	Strontium
Group 2	0.184	Barium
Group 3	0.306	Silver
Group 4	0.406	Gold
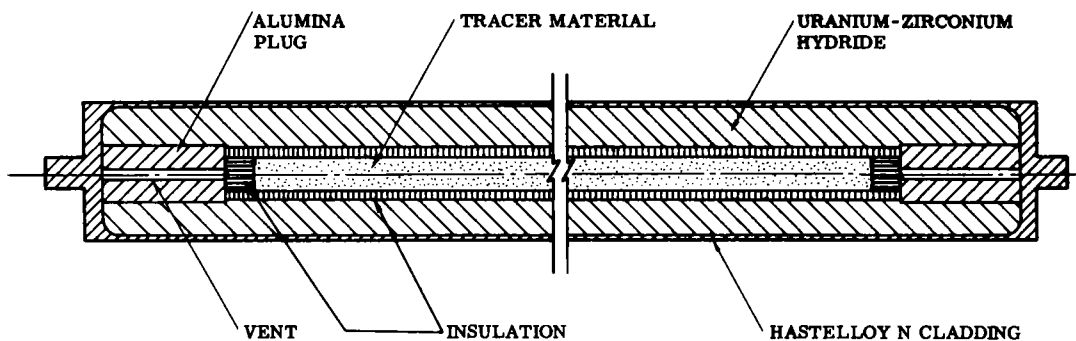
Figure 72. Sectional view of fuel element with tracer

These tracer materials were selected because their spectral lines are strong and easily identified. To maintain them below their boiling points until the UZrH cylinder ablated, it was necessary to provide a 0.100-inch layer of fiberfrax insulation. Vent holes were provided to prevent pressure build-up within the fuel elements. Because UZrH is extremely difficult to match, alumina plugs were sprayed in the ends to seal the elements. The Hastelloy N cladding and the external dimensions were exactly like those of the actual SNAP-10A fuel elements. In order to keep the ballistic coefficient (W/C_DA) of the four rod groups similar (so that they would follow the same re-entry trajectory), it was necessary to add lead ballast in the strontium and barium. A more detailed description and analysis of the external fuel rod experiment is given in Sandia Corporation report SC-RR-64-516.

SECTION X -- RELIABILITY PROGRAM

The reliability program was designed to provide to the re-entry vehicle, its subsystems, and components the maximum degree of reliability commensurate with the time available. The program for RFD-1 as a whole was begun with limited manpower in March 1962. By December of the same year the details of the design had become well enough established to permit reliability analysis to begin. The first re-entry vehicle was subsequently shipped to Wallops Island in March 1963.

The reliability studies involved (1) analytical work on the circuitry and its components, (2) analytical and test work on the subsystems, and (3) a component test program. These activities were planned and integrated with a view to gathering as much information as possible within the time allotted.

Some circuit and component changes were dictated by results obtained early in the reliability program. Later in the program, while the material was being assembled for qualification testing, analytical investigations were made of all the subsystems, components, and associated circuitry listed below:

1. Pyrotechnic Circuitry

2. Fourth-Stage Separation

> Explosive bolts
> Electronic delay timer
> MC1192 thermal battery
> Retro-rockets
> Ni-Cad battery

3. Flotation System

> Gas bottle
> Squib

4. Parachute System, Including Deployment Gear

> Drogue gun
> Squib
> Reefing cutter initiator
> Baroswitches

5. Recovery System

> Impact switch
> Salt-water switch
> SARAH beacon system
> Batteries

6. The following items related to the above were also analyzed:

> a. Connectors
> b. Diodes
> c. Relays
> d. Wire cutter.

Analytical investigations of these items exposed problems in some areas and dictated changeover to other components in some cases. Changes made to the pyrotechnic circuitry resulted in a rise in calculated reliability from 70 to 88 percent. Chart I in Appendix B shows the program in detail. In view of the newness of the Aerospace

Nuclear Safety work and the variety, complexity, and quantity of the units involved in RFD-1, the reliability program as described above may be regarded as having been effective.

Areas not included in the reliability analysis were:

1. The telemetry system and its battery
2. The timing control for sequencing the re-entry vehicle
3. Aerodynamics studies, analyses, and tests
4. Thermal aspects (ablation, insulation, and the temperature of the re-entry vehicle)
5. Selection of materials, including materials studies
6. Mechanical and structural design.

The analytical prediction of 88 percent reliability on the items covered by the analysis appears to have been reasonable. (Obviously, the action taken to attain this reliability figure rather than the original 70 percent was especially valuable.) Since some of the components tested revealed difficulties or failures that could not have been revealed by means other than test and evaluation, it may be concluded that the reliability program contributed materially to the flight test.

SECTION XI -- ENVIRONMENTAL CONDITIONS

The environmental conditions which would be encountered by the re-entry system were divided into three parts as follows:

1. Shipping, storage, and handling environments

2. Preflight testing environments

3. Flight environments.

Shipping, Storage, and Handling Environments

Mechanical -- The re-entry system was packaged in materials calculated to reduce the severity of various handling environments, and was shipped to the launch site by chartered aircraft. Since these handling environments were assumed to be less severe than those which would be encountered in flight, no specific tests were conducted for them.

Thermal -- The temperature extremes expected during shipping, storage, and at the launch site were from a -5° to 160°F. For the shipping containers and insulation used, the rise and decay time between the temperature extremes was estimated to be 30 minutes. The temperature cycle used in testing is discussed in the text section of this report.

Preflight Testing Environments

Environmental tests of the RFD-1 re-entry system were divided into two types: qualification tests and acceptance tests. The qualification tests were designed to certify the re-entry system as adequate for the flight environment. However, the environments used in these tests were more extreme than those expected during the flight. The acceptance tests, on the other hand, were designed to show that the two flight systems were properly fabricated to specifications. The environments used in them were less severe than expected flight environments.

Mechanical -- The mechanical environmental conditions were obtained from the following three sources:

1. A Scout Project Group specification titled "Recommended Mechanical Environmental Test Levels for Design Qualification and Flight Acceptance Testing of Scout-Launched Spacecraft" (NASA, LRC).

2. A NASA document titled "Environmental Test Specification and General Test Procedures for Design Qualification and Flight Acceptance Testing of Scout-Launched Satellites" (NASA-Q-15).

3. Test data derived from previously launched Scout payloads and from laboratory tests on the X-248 Scout fourth-stage motor.

Details of the test conditions are tabulated below:

Qualification Tests

Sine vibration	Amplitude: constant force of 500 lb
	Frequency: 10-2000-10 cps at a rate of two octaves/minute
Random vibration	Frequency: 20-2000 cps for 4 minutes with a PSD of 0.033 g^2/cps
Linear acceleration	15 g for a period of 3 minutes
Shock	**Three tests to a half-sine pulse of 30-g peak amplitude and 10 to 15 milliseconds duration**
Acoustical noise	The following acoustical noise for 4 minutes:

Octave Band	Sound Pressure Level
20-75	138.5 db*
75-150	142.5 db
150-300	141.2 db
300-600	139.6 db
600-1200	138.5 db
1200-2400	138.8 db
2400-4800	136.3 db
4800-9600	135.6 db

Overall SPL = 148.5 db

*Rev 0.0002 dyne/cm^2

Spin	Spun up to angular velocity of 200 rpm

Acceptance Tests

Sine vibration	Amplitude: constant force of 350 lb
	Frequency: 10-2000-10 cps at a rate of two octaves/minute
Random vibration	Frequency: 10-2000 cps for 4 minutes with a constant RMS force of 350 lb overall
Spin	Spun up to angular velocity of 180 rpm

Thermal --

Qualification Tests

Temperature cycling	The re-entry system was subjected to three temperature cycles from -50° to 160°F (see Figure 73)
Temperature shock	The re-entry system less telemetry was subjected to two temperature cycles from -5° to 270°F (see Figure 74)

Acceptance Tests

The flight systems were subjected to three temperature cycles from -5° to 160°F as shown in Figure 73.
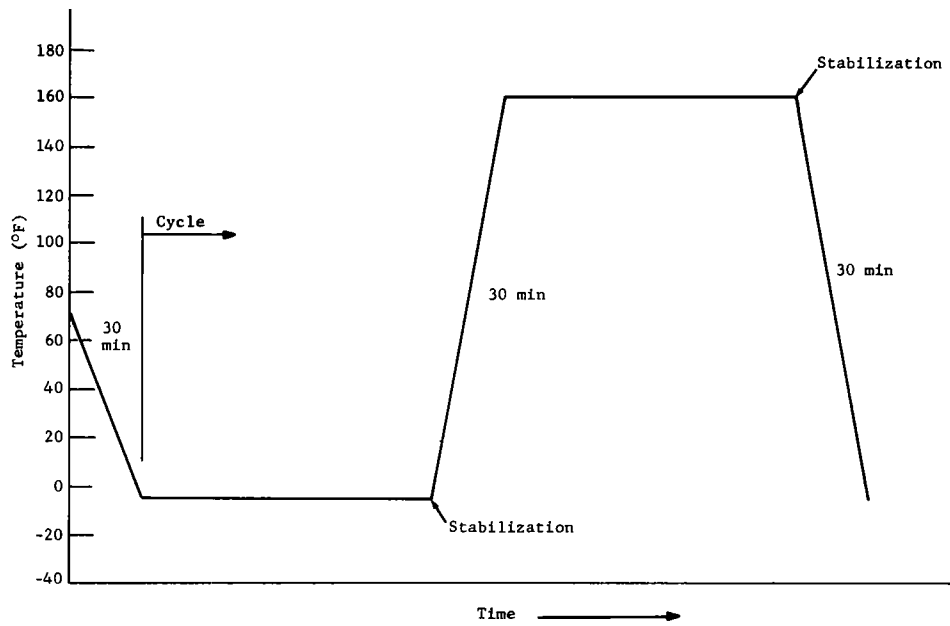
Figure 73. Qualification and acceptance test
temperature cycles
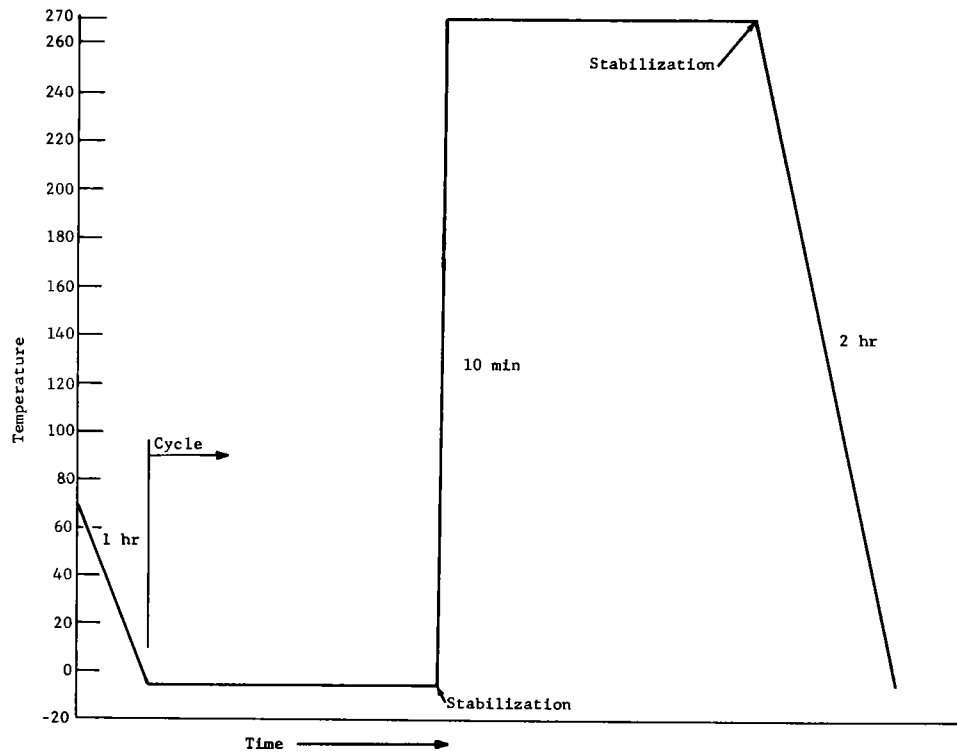
Figure 74. Qualification temperature shock-test cycles

Flight Environments

Mechanical -- Acceleration environments experienced during flight are caused by the four stages of the Scout vehicle during ascent, and by re-entry deceleration during descent. The maximum accelerations experienced during various parts of the trajectory are tabulated below:

Trajectory Phase	Acceleration (g's)
Algol 2A (Scout first stage)	4.75
Castor (Scout second stage)	7.70
X-259 (Scout third stage)	10.7
X-248 (Scout fourth stage)	5.0
Re-entry deceleration	22.0

The primary source of in-flight vibration is the X-248 fourth-stage motor. The vibration produced by this motor is characterized during the first part of burning by mixed high-frequency quasi-sinusoidal vibrations with high amplitude, and during the later part of burning by vibrations with a fundamental frequency of approximately 570 cps and high amplitude. These vibrations are created by the resonant burning or unstable combustion of the propellant. The peak amplitude, as measured on various static firings and full-scale launches, is in a range between ±20 and ±50 g for a 200-pound payload. In addition, there is evidence of some low-frequency, relatively low-amplitude vibration during the later part of first-stage burning. Random vibration, as recorded during fourth-stage burning on previous Scout flights, was about 0.001 g^2/cps in the frequency range between 200 and 700 cps.

In-flight shock environments are associated with ignition transients at the time the motor is ignited and with impact into the water at the end of the flight. However, the payload experiences ignition "spikes" only at ignition of the second-, third-, and fourth-stage motors. Because these "spikes" are difficult to measure, the general practice has been to use an arbitrary shock pulse definition based on the maximum amplitude of acceleration of the four Scout stages. The water-impact environment, on the other hand, was measured in early development tests.

In flight, the re-entry system and the fourth-stage motor are spun up to approximately 150 rpm by four 1KS40 Atlantic Research Corporation rockets. The burn time of these rockets is approximately 1 second.

The in-flight acoustic environment is a result of aerodynamic and power plant noise. Details relating to this environment are tabulated below:

Octave Band (cps)		Power Plant Noise (indicated time after 1st stage ignition)			Aerodynamic Noise
Lower	Upper	t=0 sec	t=1 sec	t=2 sec	Max. at t=2 sec
20	75	138.5	126.6	123.6	-
75	150	142.5	127.4	124.4	-
150	300	141.2	129.9	126.9	-
300	600	139.6	128.7	125.7	-
600	1200	138.5	122.2	119.2	137.1
1200	2400	138.5	123.3	120.3	136.1
2400	4800	136.3	123.4	120.4	138.1
4800	10000	135.6	123.0	120.0	141.1
20	10000	148.5	135.5	132.5	146.1
(overall)					

89

Sound pressure levels are for the frequency ranges indicated. All levels are in decibels (db), using a reference pressure of 0.0002 dyne per square centimeter. All levels are estimated at the exterior of the payload compartment (i.e., exterior to the heat shield).

Thermal -- All external surfaces of the RV were exposed to aerodynamic heating caused by the conversion of kinetic energy to heat during re-entry through the atmosphere. Laminar stagnation-point-heating rates to a 1-foot radius sphere re-entering on the same trajectory as the RFD-1 RS are shown in Figure 44, p. 65, as a function of time from 400,000 feet. Local heating rates over the surface of the vehicle were expected to vary from 0.2 to 0.01 times the rates shown in Figure 53, p. 70, depending on location and type of flow over the surface.

SECTION XII -- TEST PROGRAM

The test program for RFD-1 consisted of development, qualification, and reliability tests of individual components; and development, qualification, and acceptance tests of the re-entry vehicle and the re-entry system as a whole to qualify them for the RFD-1 flight. The major events during development are tabulated in Appendix C.

The development tests included both tests to prove that various individual components would comply with design criteria and tests to check whether the functioning of individual components and/or systems would meet the functional requirements placed on the RFD-1 flight vehicle. The development tests on components covered the salt-water switches, the pressure-sensing switches, the flashing light systems, and the SARAH transmitting system, as well as structural parts, ablation material, and separation hardware. Tests on the re-entry vehicle and the re-entry system included parachute deployment tests, water-tank drop tests, airdrop tests at Tonopah Test Range and Wallops Island, and tests in various mechanical and thermal environments. (The re-entry system, as was explained earlier, consists of the SNAP-10A STR, the external fuel rod experiment, and the re-entry vehicle.)

Development, Qualification, and Reliability
Tests of Components

Functional Shock Tests of the MC1441 Inertial Switch

Tests performed on this component, which was to be used to turn on the SARAH beacon system, showed that it met the water-entry requirements for that application. After the MC1441 was set to a linear acceleration of 30 to 34 g, it actuated within limits during shock tests. The test results showing typical functional characteristics are reproduced in Figures 75 and 76. (The requirements were not to actuate at less than 30 g, and to actuate at above 75 g, since actual water entry had been calculated as likely to be above 90 g.)

In addition, some MC1441 units were vibrated to determine their tendency to premature. In these tests, the units were modified by changing their 30-g actuating springs to 10-g springs (to simulate 20-g deceleration during re-entry). Random vibration of from 20 to 2000 cps was applied, and the PSD level was varied from 0.01 to 0.05 g^2/cps during a test of 1-minute duration. After this vibration test, the 30-g springs were reinstalled and the units were again shocked. The shock activation level of the switches before and after vibration compared favorably.

In order to determine the effect of angle impact, some other units were tested with the actuation axis of the switch 30 degrees off from the vertical axis. No significant increase in level of actuation was observed to be associated with angle impact as compared with vertical impact.
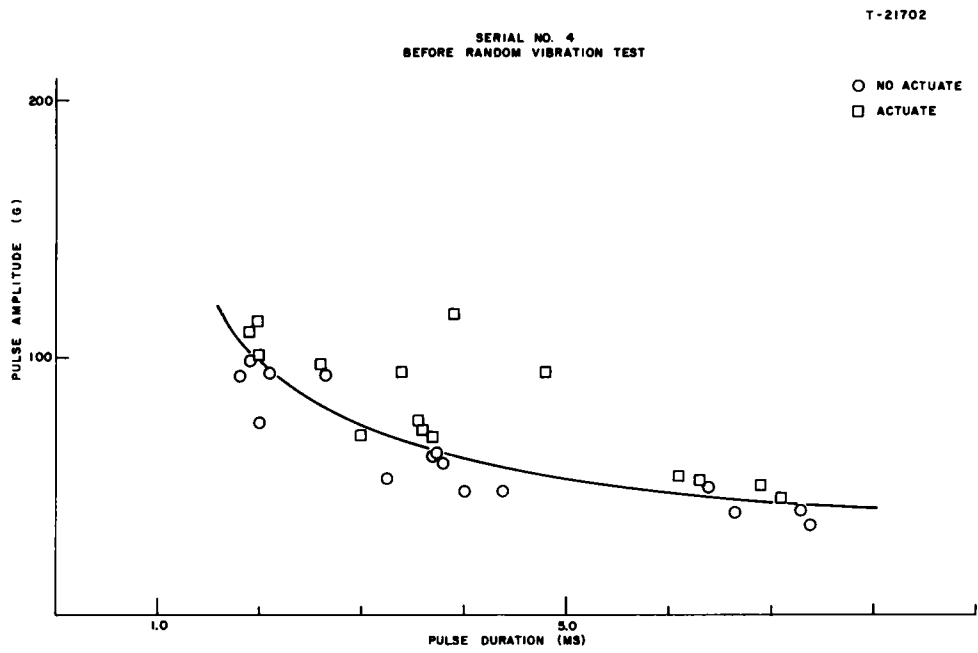
Figure 75. MC1441 functional shock test
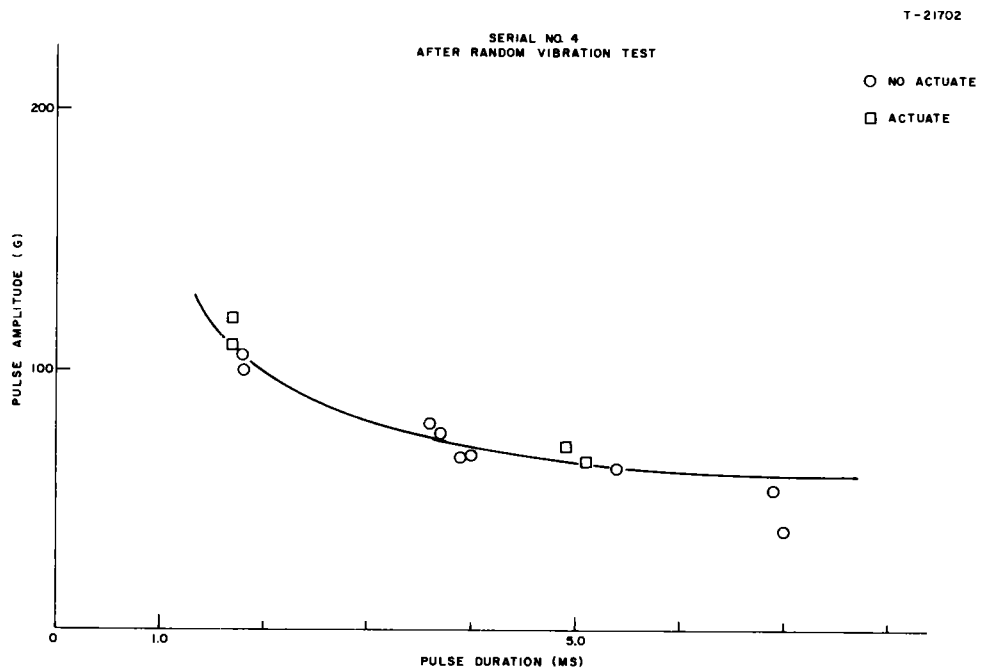
Figure 76. MC1441 functional shock test

92

Spin Test of the Fourth-Stage-Motor-Separation System

This test checked the functioning of the separation system under spin of 180 rpm. The test setup, using dummy weights, is shown in Figure 77. The results obtained showed that firing of either one of the two separation nuts installed on a marmon clamp would be adequate to effect separation. In addition, this test proved the efficiency of the clamp shield designed to protect the cables from outward movement of the marmon clamp after that clamp was released by the separation nuts. The clamp shield successfully contained the marmon clamp and did not obstruct separation of the adapter and the fourth-stage motor from the vehicle.
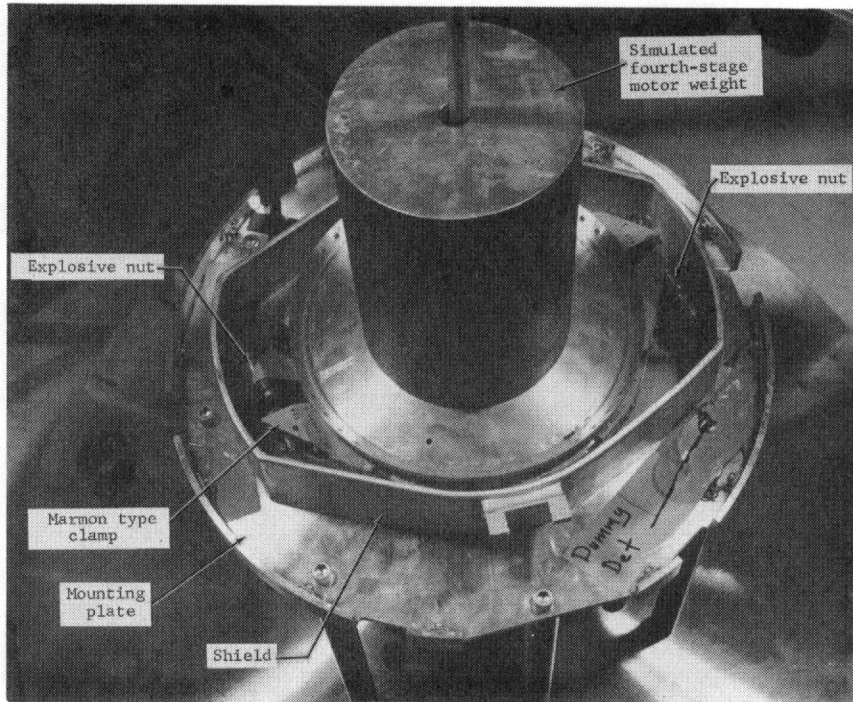
Figure 77. Test setup for spin test of fourth-stage-motor-separation system

Static Tests of the Drogue Gun

These tests were performed in order to: (1) obtain a reaction load figure to be used in design of the mount, and (2) establish the cartridge pressure that would be required to remove the bonded-in-place parachute cover, deploy the parachute, and extend the flotation bag. The cartridge finally selected for RFD-1 was one that ejected a 1-pound projectile at 250 feet per second. The reaction load obtained was between 25,000 and 27,000 pounds for a pulse duration of 0.5 msec.

Sled Tests of Structural Parts

Preliminary sled tests were performed on an aluminum simulated version of the structure of the parachute compartment of the re-entry vehicle. This test setup is shown on Figure 78. These tests demonstrated that the parachute compartment was structurally adequate. They also showed that, with a pressure cartridge able to eject a 1-pound projectile at 250 fps, the drogue gun would deploy the parachute

93

after releasing the bonded-in-place parachute cover. Four tests were conducted in velocities ranging from 398 to 453 fps (corresponding to dynamic pressures of from 158 to 206 lb/ft^2).

Figure 78. Test setup for sled tests of
an aluminum simulated version
of the parachute compartment

Sled tests were also performed on a simulated re-entry vehicle structure made of aluminum and fiberglass. A fiberglass vehicle mounted on the sled is shown in Figure 79. These tests gave further indication that the drogue gun was adequate and that the parachute compartment was structurally sound. The flotation bag was pulled into position by the drogue gun and parachute, and the SARAH beacon antenna extended as it was intended to do. Four tests were conducted at velocities of from 530 to 575 fps (corresponding to dynamic pressures of from 281 to 330 lb/ft^2). These last two tests were made with a ribbon parachute, which at that time was being considered for use in RFD-1.

The parachute finally selected for use in RFD-1 was a panel chute 7-feet in diameter. This parachute, reefed to 0.65-foot diameter with three mechanically activated explosive-driven reefing line cutters, was tested in three sled tests at sled velocities of 400, 510 and 530 fps. All three tests were successful, the reefed parachute deploying properly in each case; however, the reefing line, though cut during the 510 foot run, was not cut during the 400 and 530 fps test runs. A more positive activation mounting of the reefing line cutter was adopted for RFD-1.
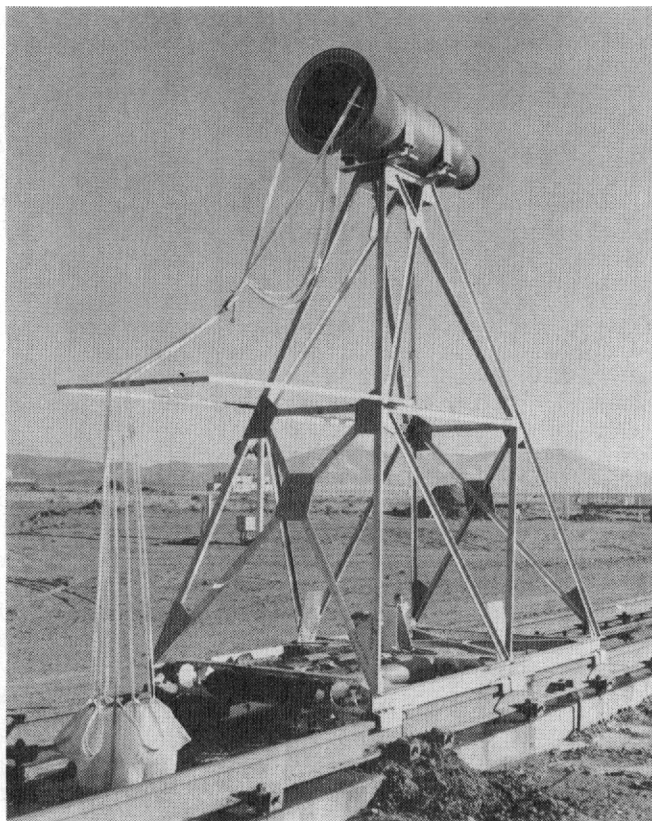
Figure 79. Test setup for sled tests of
a simulated re-entry vehicle
structure made of aluminum
and fiberglass

Salt-Water Immersion Test of Operating SARAH Beacon System

This test determined the ability of the SARAH system to function when sub-
merged in salt water of ocean density; it also determined the duration of operating
time. The potted SARAH system, complete with salt-water switch, was immersed in a
20-percent salt-water solution, and the unit operated satisfactorily until 26.25
hours later, when the batteries failed, indicating the duration of their operating
time.

Vibration Response Test of the Vibration-Isolation System Proposed for the Telemetry Package

This test determined the vibration-mitigating properties of various flexible
foams being considered for use to isolate the telemetry package from the vibration
induced by the Scout fourth-stage motor. The material best suited for the system
was ALPCO 292-77-B2, a flexible polyester urethane foam with a density of 14.5 lb/ft^3,
compressed to 90 percent of its normal thickness. The normal thickness of the foam
used was 1.0 inch on the sides and forward end of the telemetry package, and 1.25-
inch on the aft end. The natural frequency of this flexible foam system was 70 cps.

Plasma Jet Tests of Materials and Components

Several qualitative development tests were run in the Sandia Plasma Jet Facility during the RFD-1 program. Some of these tests compared various materials; others were configuration tests on such components as pins, doors, antenna windows, and the like.

At the time, it was not possible to determine the exact heating rates to which the samples were subjected, because the tunnel was not calibrated. It was estimated, however, that a heat input of approximately 40 to 50 $BTU/ft^2/sec$ was applied to the samples for the duration of each run. For this and other reasons, no attempt was made to simulate precise flight conditions. Rather, comparisons were made between one material or configuration and another.

There was some concern that jetting might occur along the edges of the door and cause a break in the seal. A series of tests was run to investigate this problem and also to study the behavior of the gasket material. The tests showed that a tight-fitting door backed up with a Cohrlastic gasket would not leak. The results of one such series is shown in Figure 80.

The teflon inserts for the C-band antenna windows also caused some concern because of the possible effects of differential expansion and because of the expected variation in ablation rates. As was expected, the teflon ablated faster than the surrounding fiberglass, but as the surface receded below the surroundings it received less heat. According to the results of this test, teflon antenna windows are satisfactory. Figure 81 shows the results of a test on a simulated window.

On RFD-1 it was necessary to fill countersunk bolt holes. Plasma jet tests showed that it was much better to use E-300 than fiberglass plugs bonded in place with Epon 931 (Figures 82 and 83).

Further tests showed that it is possible to extend electrical wires through the ablation material if the holes are small and the wires bonded in place with Epon 931.

Other significant materials tests showed that E-300 will survive about as well as fiberglass. D-65, RTV-102, and 301 form a nonconductive char layer (Figure 84).

Development, Qualification, and Acceptance Tests of
the Re-entry Vehicle and Re-entry System

Simulated re-entry vehicle shapes were made of aluminum for airdrop tests at Tonopah Test Range and of fiberglass for water-tank and airdrop tests at Wallops Island.

Tower Drop Tests Into a Water Tank

These tests simulated RFD-1 water entry conditions in order to determine shock forces in critical areas of the vehicle and to check the functioning of the flotation system. Two drops were made into salt water and one drop into plain water. The typical rigging of the vehicle for such a drop test is shown in Figure 85.

The first drop was made from a height of 133 feet with release occurring at an angle of 40 degrees from the vertical (measured from the longitudinal axis of vehicle) and impact at an angle of 8 degrees from the vertical. Impact velocity was 93 fps. The recorded decelerations ranged from 110 to 135 g, with the higher deceleration occurring in the aft flare section.

\
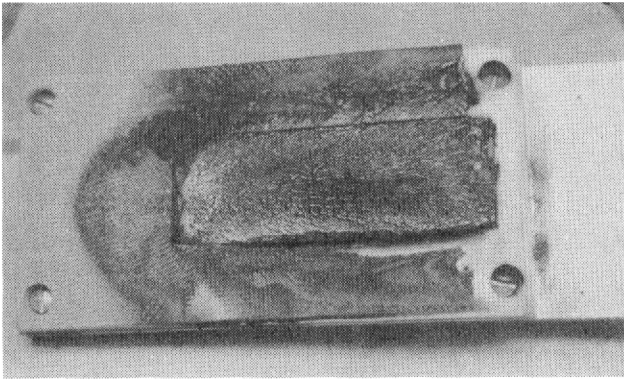
a. Door after test
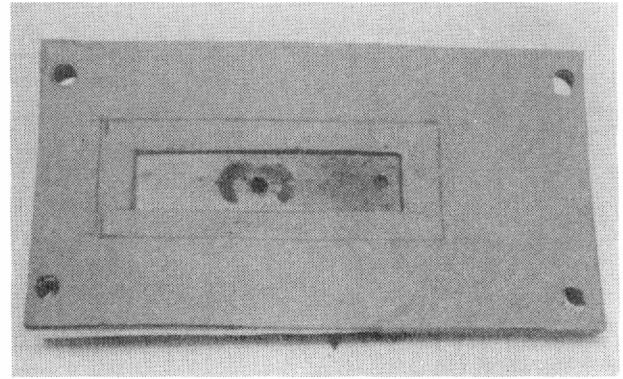
b. Back face of gasket
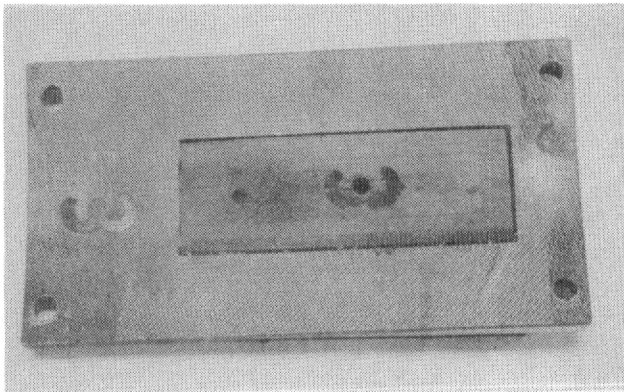
c. Back face of door
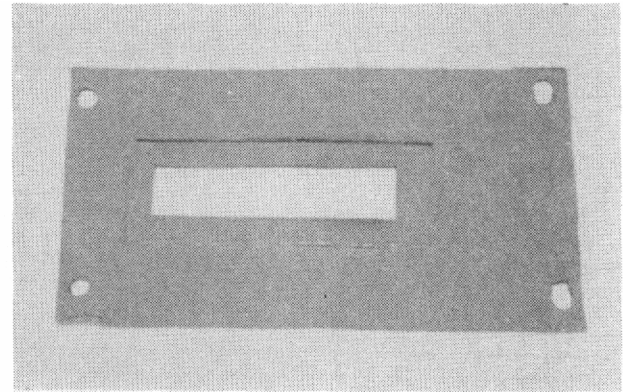
d. Char along open crack
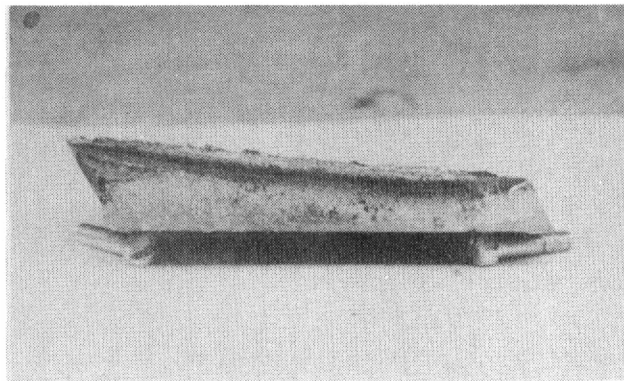
e. Sealed side of door
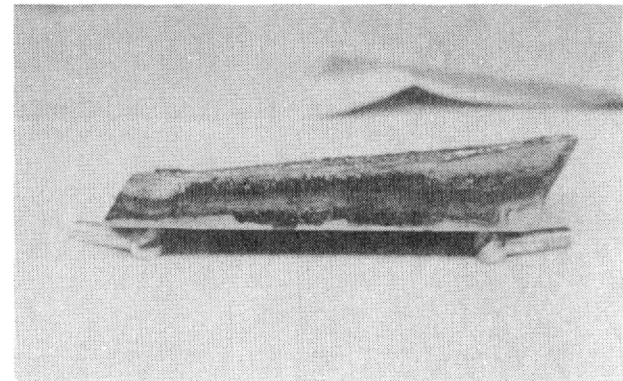
f. Open side of door

Figure 80. Results of plasma jet tests of door
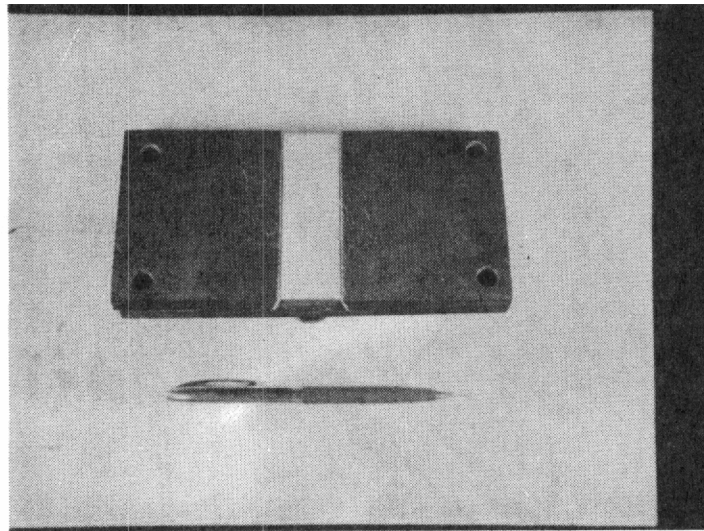
a. Before test
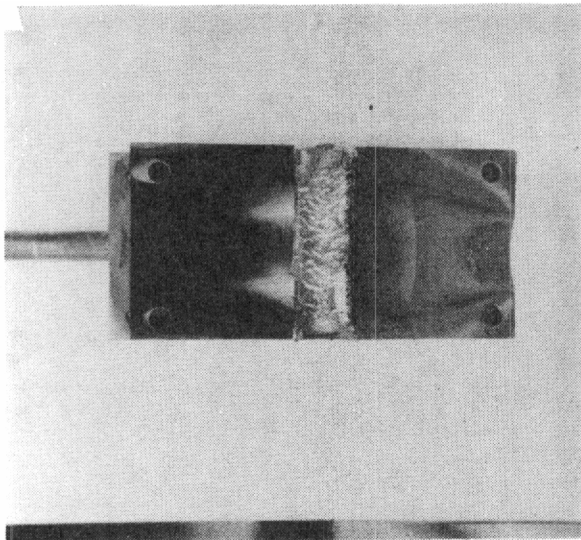
b. Top view
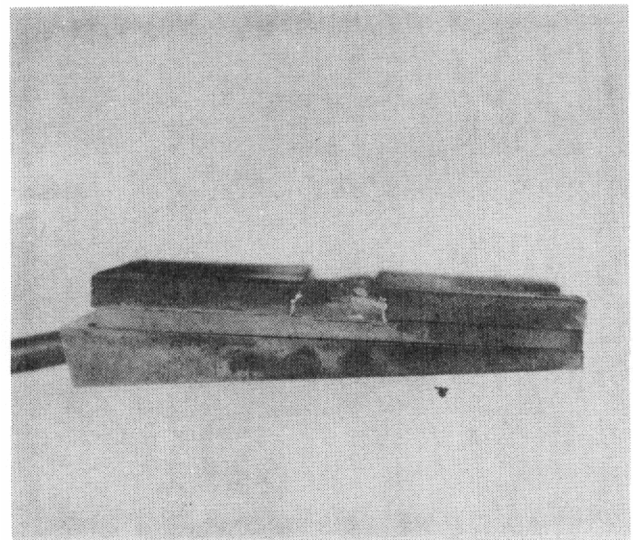
c. Side view

Eroded teflon insert for C-band window after test

Figure 81. Results of plasma jet tests of teflon
            inserts in simulated C-band antenna
            windows
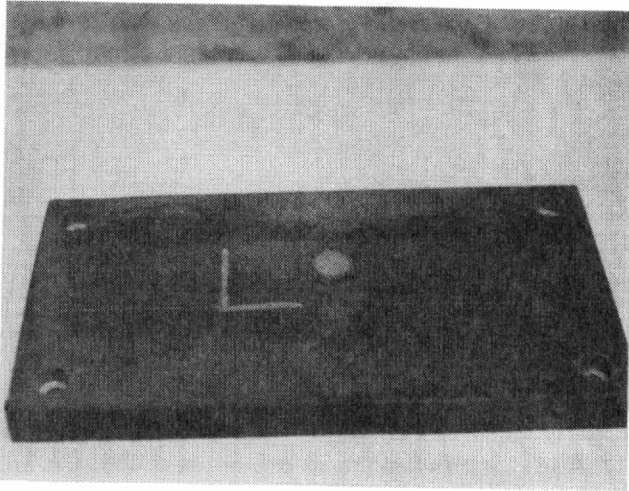
a. Before test
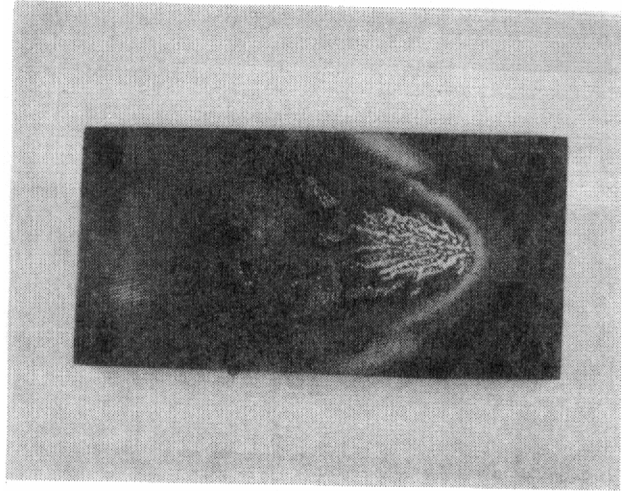
b. After test
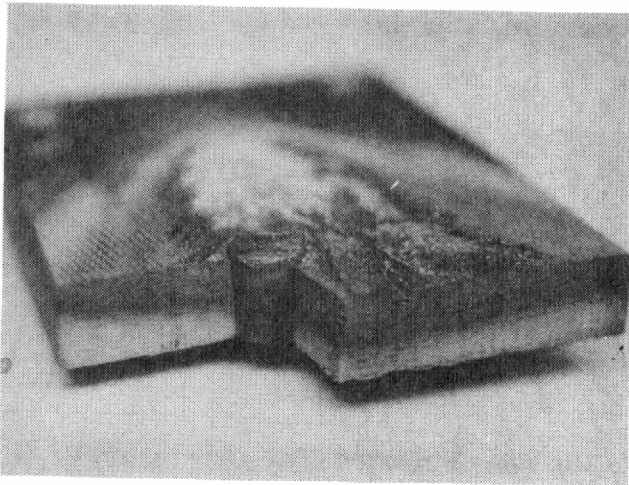
c. Loosened fiberglass pin
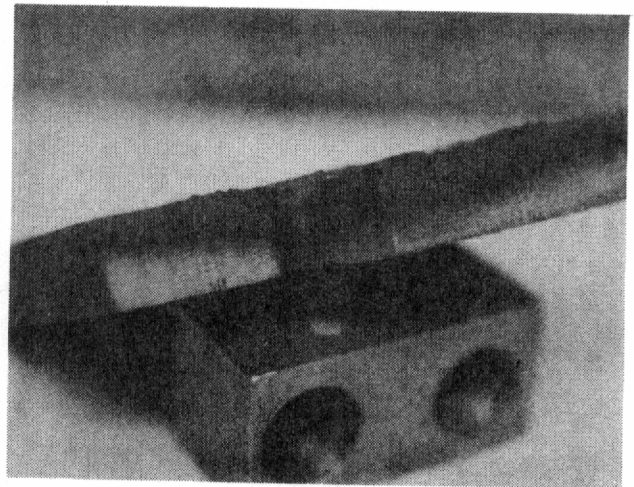
d. Cross section of sample

Figure 82. Results of plasma jet tests of fiberglass
plugs for countersunk bore holes
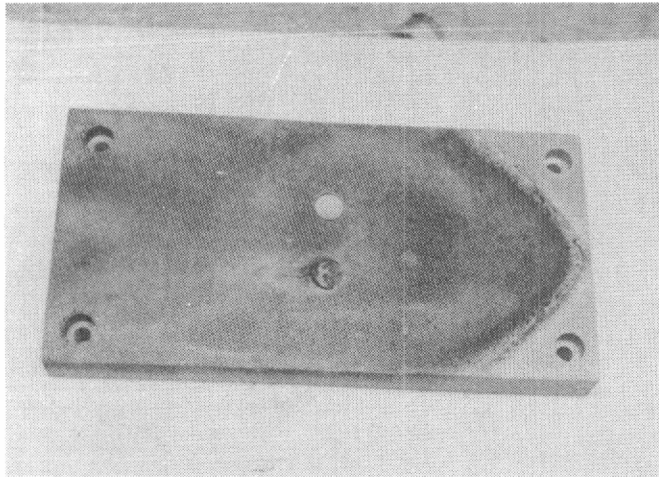
a. E-300 filler and fiberglass pin

b. Cross section of sample
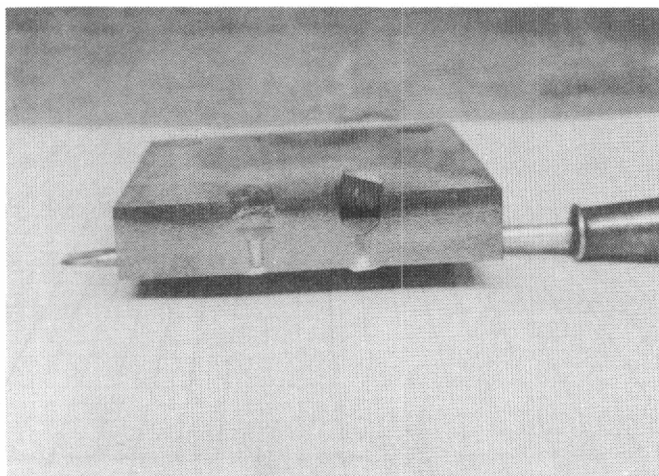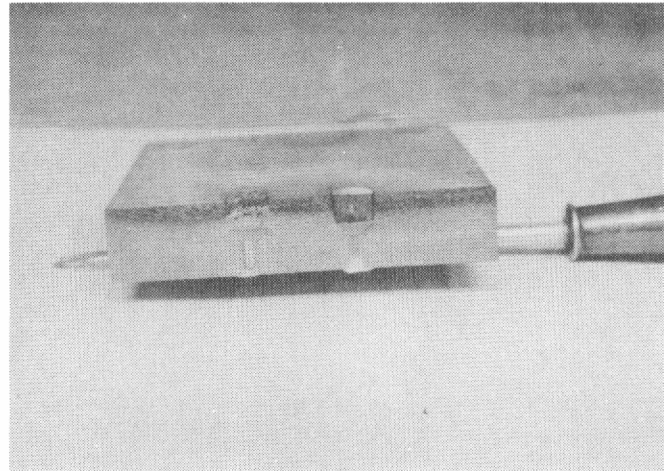
c. Loosened fiberglass pin

Figure 83. Results of plasma jet test of fiberglass plugs for countersunk bolt holes
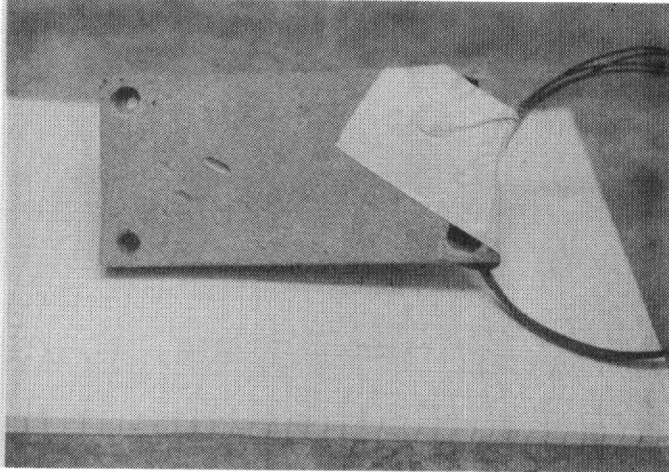
a. Before test

b. Top view
   (after test)
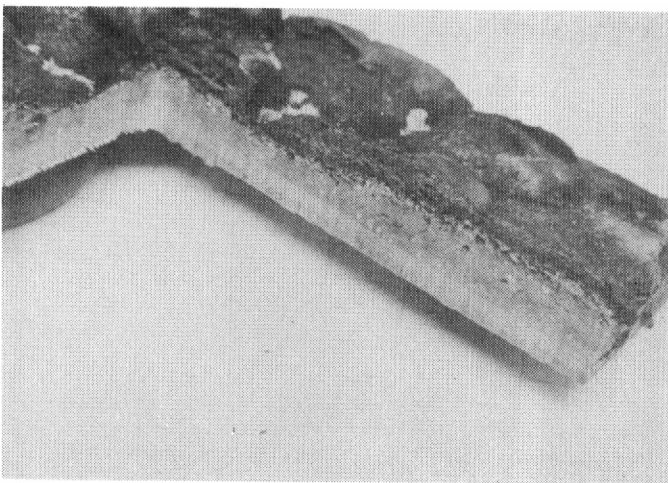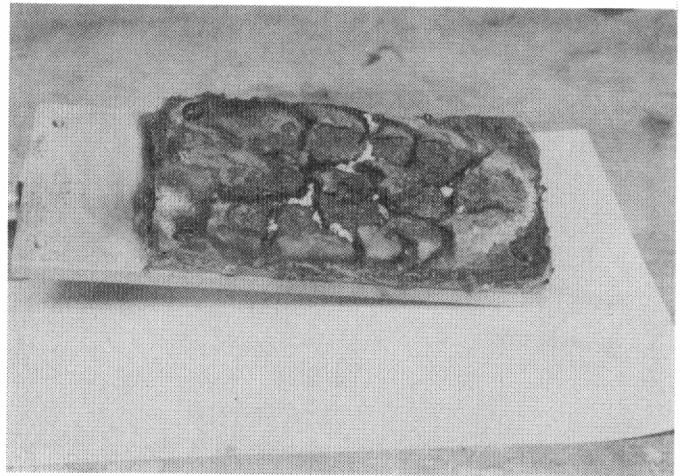
c. Cross section
   (after test)

Figure 84. Results of plasma jet tests
of Dyna-Therm E-300
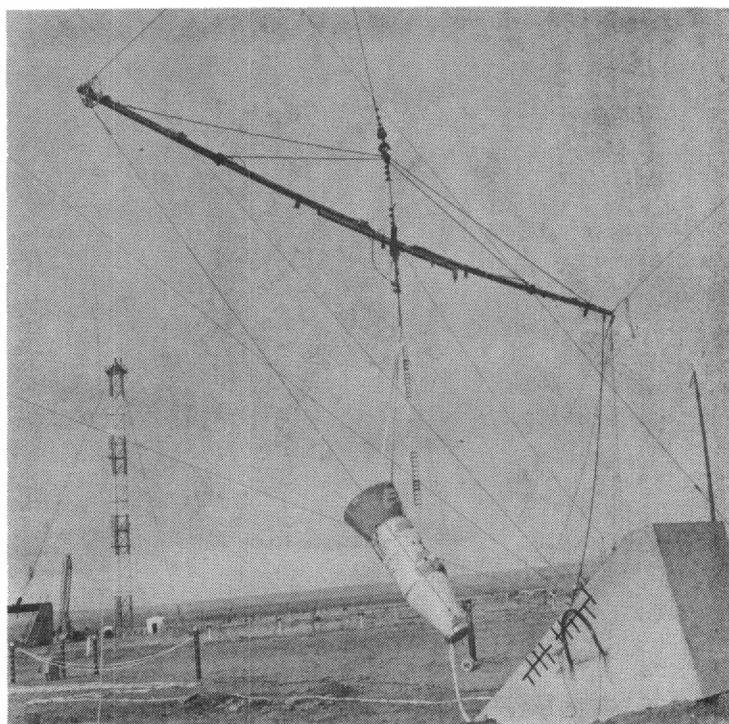
Figure 85. Rigging of the flight vehicle for
drop test into a tank of water

The second drop was made from a height of 139 feet with release occurring at an angle of 80 degrees from the vertical and impact occurring at an angle of 46 degrees from the vertical. Impact velocity was again 93 fps. The recorded deceleration in this case ranged from 30 to 135 g, with the higher g figure again recorded in the aft flare.

Structurally, the vehicle passed both these tests, and the flotation bag remained in position during both. However, two inertial switches installed for these tests (modified MC1441's) failed to activate during the second test, although they had functioned during the first. Two salt-water switches (intended as backups to the inertial switches for energizing the SARAH beacon system) functioned well in both tests, but the flashing light itself did not work in the second test despite having worked well in the first. After the test in which the flashing light failed, its energizing switch was changed to an MC824, operated by the signal to the drogue gun. This change meant that the flashing light would be activated at parachute deployment.

The drop into plain water was made from a height of 155 feet. Impact velocity was 100 fps. The recorded decelerations were 244 g on the nose, 168 g on the telemetry plate, and 143 g on the bulkhead in the flotation bag compartment. This test showed that more than friction would be required to hold the flotation bag in place during water entry; therefore, in later tests, the bag was anchored with fiberglass lines.

Static Load Tests

To check the structural integrity of the RFD-1 flight vehicle under the mechanical load environments associated with the Scout rocket, the vehicle was subjected to three different static load conditions with the test setup shown in Figure 86. The components checked were the 7075 T6 aluminum mounting plate, the 6061 T6 aluminum spacer, the magnesium adapter assembly, and the fiberglass re-entry vehicle shell. The limit load conditions for the three tests performed are tabulated below:

Test No.	P_1 Lateral Load at Center of Gravity of Re-entry Vehicle (pounds)	P_2 Lateral Load at Center of Gravity of Simulated Reactor (pounds)	P_3 Axial Load (pounds)
1	1440	140	1060
2	530	580	1380
3	530	580	3940
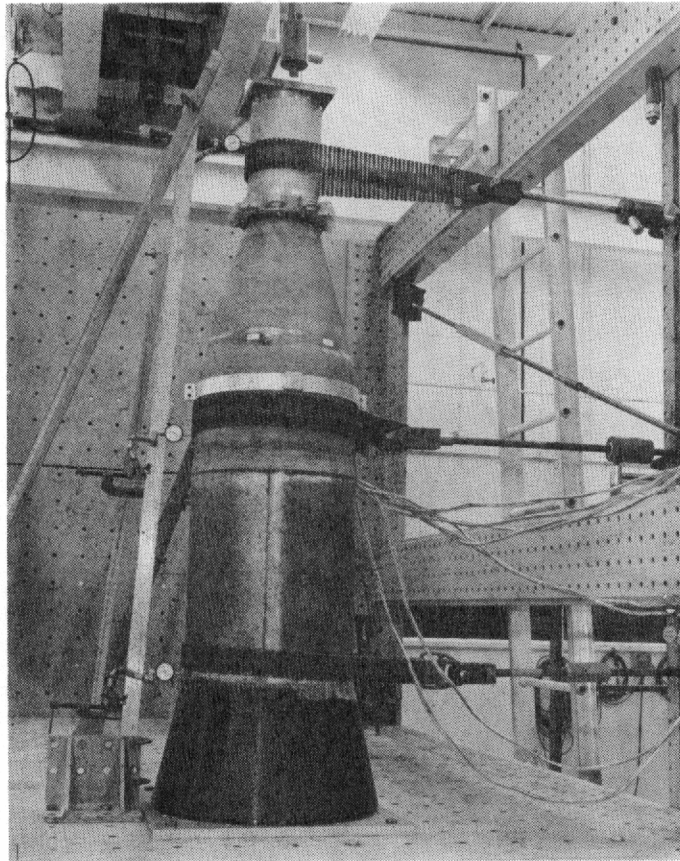
Figure 86. Test setup for mechanical load
tests of the flight vehicle

In Test No. 1, the loads were taken up to 170 percent of the limit load. The maximum stresses were 16,620 psi in the magnesium adapter, 3250 psi in the 6061 T6 aluminum spacer, and 10,371 psi in the 7075 T6 aluminum mounting plate.

In Test No. 2, the loads were taken up to 200 percent of the limit load. The lateral loads were applied so that the door cutout was on the tension side of the magnesium adapter. The maximum stresses were 15,480 psi in the magnesium adapter, 2110 psi in the 6061 T6 aluminum spacer, and 14,180 psi in the 7075 T6 aluminum mounting plate.

In Test No. 3, the loads were taken to 160 percent of the limit load, with the loading arrangement the same as during Test No. 1. The maximum stress in the magnesium adapter was 23,860 psi at 80 percent of limit load, but this went down to 19,820 psi at 160 percent of the limit load as the greater increment of axial load was applied. Maximum stress in the 6061 T6 aluminum spacer was 3750 psi, and in the 7075 T6 aluminum mounting plate, 25,690 psi.

No indications of failure appeared in the adapter, spacer, mounting plate, or fiberglass re-entry vehicle. No cracking or delamination resulted from any of the three tests.

Linear Acceleration Tests

Performed as follow ups to the static tests, these further checked the structural integrity of the re-entry vehicle and its response when subjected to linear acceleration simulating the loading condition during launch and flight of the Scout vehicle. The test setup is shown on Figure 87.
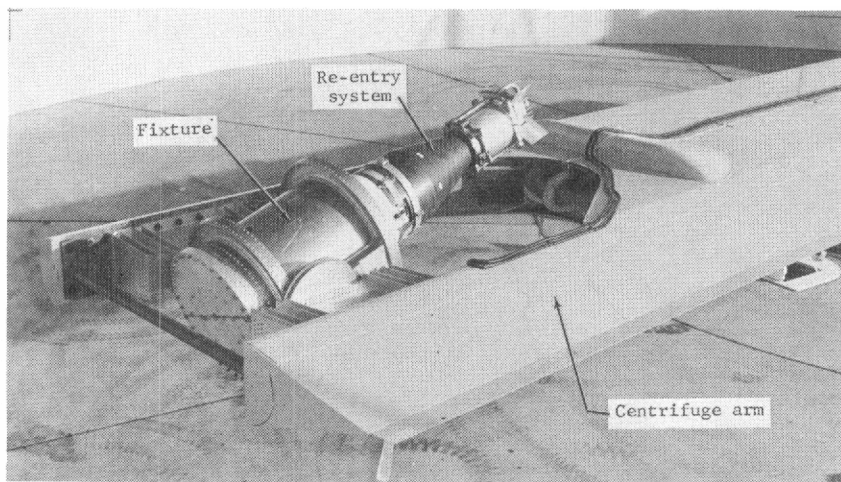
Figure 87. Test setup for linear acceleration
test of the re-entry vehicle

Three vehicles were tested, at acceleration of 16.9 (with longitudinal axis 18.75 degrees off the horizontal), and at acceleration of 11.25 g (with longitudinal axis 36.8 inches off the horizontal). Of the three vehicles tested, Unit 1 was a development vehicle and Units 2 and 3 were qualification vehicles.

The development unit was subjected to linear acceleration on the centrifuge tester for 2 minutes. Maximum stress in the 7075 T6 aluminum mounting plate was 26,950 psi during the 16.9-g load, and 15,290 psi during the 11.25-g load. No data were recorded during the testing of the qualification units, but each vehicle was tested for 3 minutes at each of the test conditions, and the telemetry system of each vehicle was operated before the test and after each test condition.

All three vehicles and the telemetry system passed this linear acceleration centrifuge test.

Acoustic Tests

These tests checked the ability of the flight vehicle to function under acoustic environments simulating noise from the burning Scout rocket motors and wind noise during launch. Suspended in the Progressive Wave Chamber as shown in Figure 88 the test vehicles were subjected to a random noise sound level for 4 minutes. The telemetry was operated during the test, and it and the test vehicles passed the test successfully. The sound levels applied were as follows:

Octave Band	Mean Sound Pressure Qual. Unit No. 1 (decibels)	Mean Sound Pressure Qual. Unit No. 2 (decibels)
0-75	129	130
75-150	141	138
150-300	138	144
300-600	140	143
600-1200	139	141
1200-2400	134	140
2400-4800	132	138
4800-9600	128	132
Overall	146	149

Reference Pressure = 0.0002 dyne/cm^2
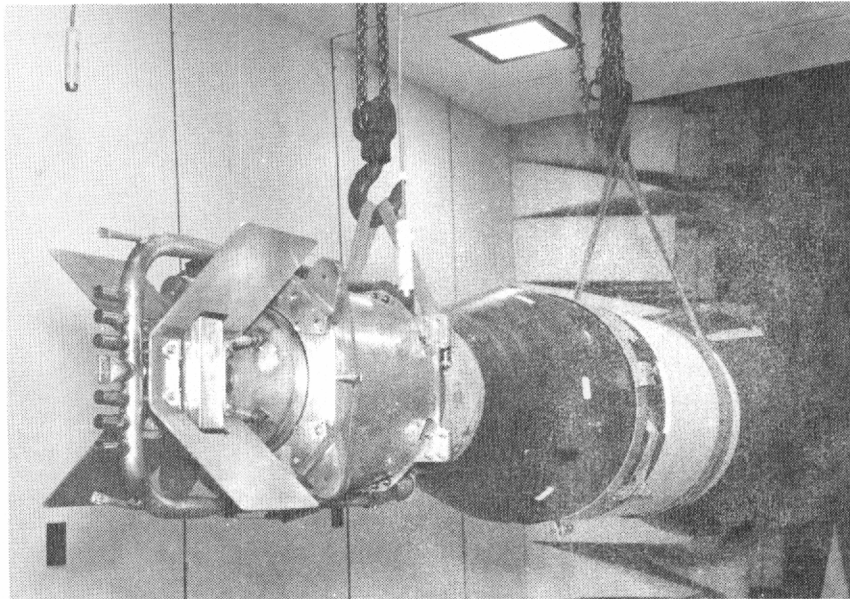
Figure 88. Test setup for acoustic tests
of the flight vehicle

Sinusoidal and Random Vibration Tests

These tests checked the structural integrity of the re-entry system under a vibration environment approaching a constant force of 1/10 the nominal rocket thrust. Since the X-258 motor was being considered for use on RFD-1, 5000 pounds was chosen as the figure for nominal thrust. The test setup is shown in Figure 89. Three vehicles were tested to this type of vibration: one development unit and two qualification units. The telemetry package of the development unit contained simulated components only, but operating telemetry systems were contained in the two qualification units.
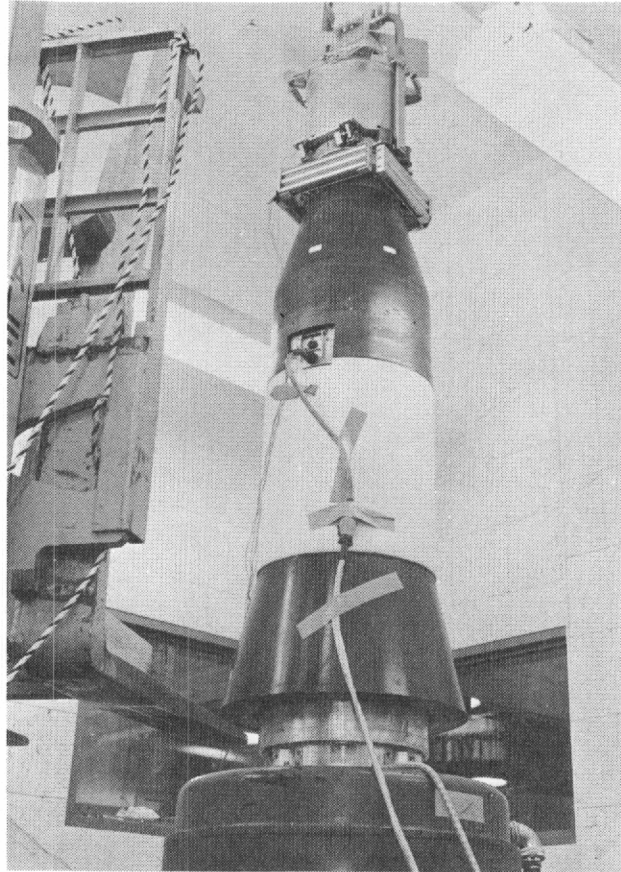
Figure 89. Test setup for sinusoidal and
random vibration tests of the
re-entry system

The telemetry system in Qualification Unit 2 operated satisfactorily during two complete vibration tests. The gyro in Qualification Unit 1 malfunctioned at the start of the first vibration test, so the telemetry was not operated during that test. The gyro was later repaired and the vibration test rerun, and the telemetry system operated satisfactorily in this test. No structural damage to any of the three units was noted during the vibration testing.

For the sinusoidal test, the units were vibrated for a 30-minute logarithmic cycle from 20 to 2000 to 20 cps at a nominal 500-pound force input. During this test, the telemetry package was preloaded to simulate the thrust force from the action of the Scout motors on it.

106

The random vibration test was run with a maximum input of 10 g²/cps at 40 cycles. The vibration was cycled from 10 to 2000 to 10 cycles in 4 minutes.

Shock Tests

These tests checked the vehicle and the telemetry package in a series of three shock tests simulating the shock load caused by ignition of the Scout rocket motors. The test setup is shown on Figure 90.

A development unit and two qualification units were mounted on a simulated fourth-stage motor fixture. The vehicle with motor fixture was then dropped on its aft end onto wedge-topped honeycomb prisms. Development Unit 1 and Qualification Unit 2 were dropped from a height of 16.75 inches onto a 72.25 in.² honeycomb pad, and Qualification Unit 1 was dropped 16.75 inches onto a 31.875 in.² honeycomb pad. The simulated fourth-stage motor on Qualification Unit 1 weighed about 400 pounds less than the one used for the other two drops.

Development Unit 1 was dropped three times at 27.5, 28.5, and 28.5 g, with rise times of 5, 5.5, and 5.5 msec, and durations of 17.8, 17, and 18 msec, respectively. On the third drop, three of the No. 8 screws radially inserted through the re-entry vehicle shell to the mounting plate failed in shear.

Qualification Unit 1 was dropped with the lighter Scout motor fixture, the shocks were 41, 38, and 37 g, with rise times of 3, 2.7, and 3.1 msec, and durations of 7.7, 5, and 5.2 msec, respectively. There were no failures with this drop unit.

Qualification Unit 2 was dropped once. The shock was 32 g with a rise time of 6.5 msec and a duration of 12 msec. The No. 8 screws installed radially through the re-entry shell to the mounting plate again failed in shear. These No. 8 screws were changed in the design to No. 10 high-strength screws.

Spin Test

This test checked the performance of the flight vehicle and the telemetry system under spinning of the re-entry vehicle to simulate spin of the fourth-stage motor and payload on the Scout rocket.

For this test, one development and two qualification vehicles were to have been spun at 200 rpm. However, as a result of an error in the speed indicator, Development Unit 1 was spun up to 280 rpm in 2 minutes and maintained at that speed for 5 minutes. Its telemetry functioned only intermittently at speeds over 180 rpm because one connector was not properly mated. After this connector was mated properly, the telemetry package met the established spin-test criteria.
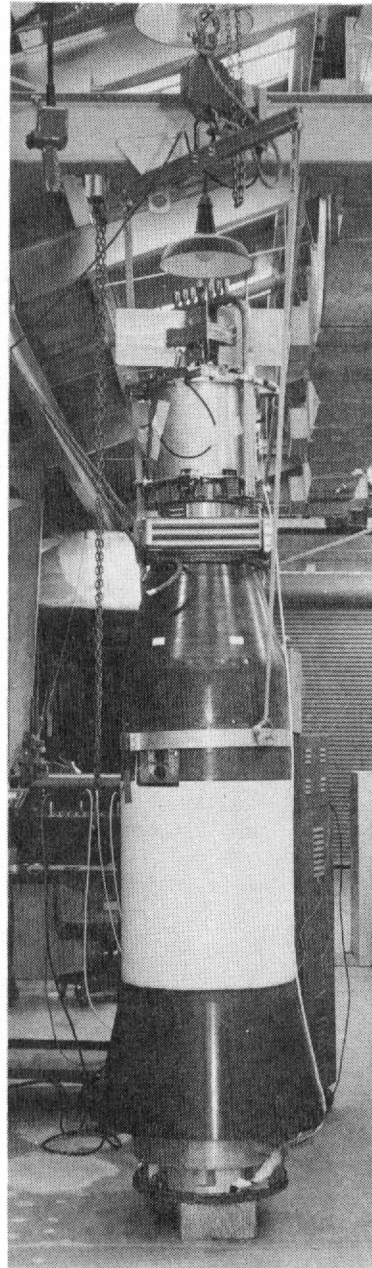
Figure 90.

Test setup for shock test of the re-entry vehicle and the telemetry package

The two qualification units were spun to 200 rpm without incident and passed the test. Their telemetry systems functioned normally and no failure in the re-entry system developed.

Radiant Heat Tests

Four major radiant heat tests (T18914) of the re-entry vehicle were performed under simulated re-entry heating conditions. On three of the tests, parachute deployment loads were simulated as well. These four tests included two full-scale tests of the complete re-entry vehicle, a test of the nose section, and a test of the flare section.

In the first full-scale test, the vehicle received the heating pulse shown in Figure 91. When a simulated parachute load was applied to the lugs after the heating phase, the inner frame separated from the vehicle. As a result of this failure, fiberglass pins were added to the structure to augment the bond joint.

Array No.	Factor (ft$^{-\frac{1}{2}}$)
①	0.225
②	0.120
③	0.055
④	0.045
⑤	0.086

To find local heating multiply $\dot{q} \sqrt{T}$ by factor
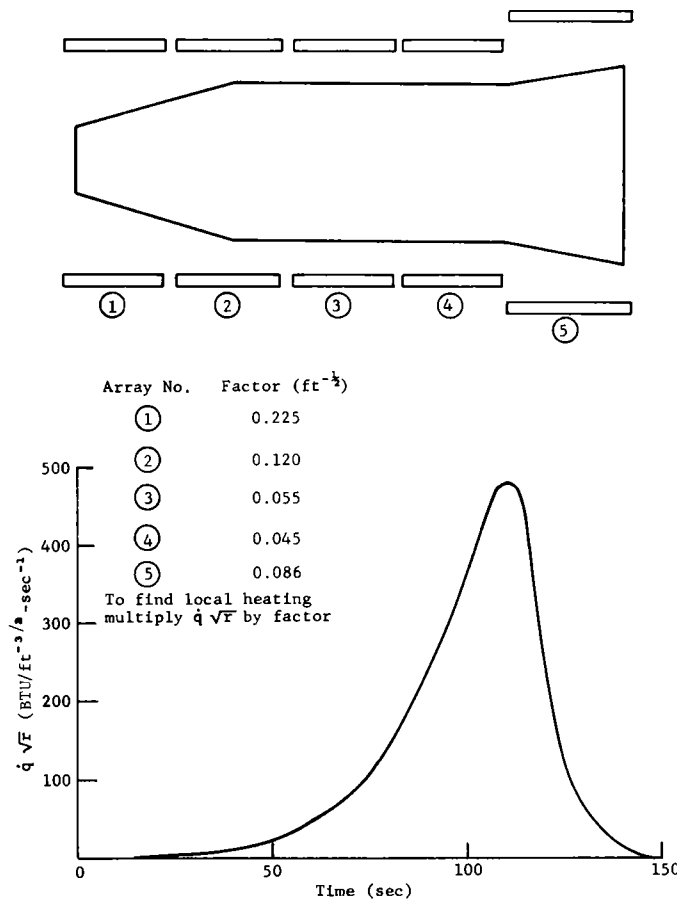
Figure 91. Radiant heat inputs used in first full-scale simulated re-entry heating test of the re-entry vehicle

In the second full-scale test, the heating equipment was programmed to provide the heating pulse shown in Figure 92; however, because of faulty calibration procedures, the vehicle received approximately twice the heating indicated. As a

108

result, the vehicle was very badly charred, the teflon sleeve ablated completely, and the antennas melted. In addition, the inner frame broke loose under an applied load of 3340 pounds. After the heating phase and the pull test, the hot vehicle was dropped into a tank of water. No thermal problems were revealed during this phase of the test.
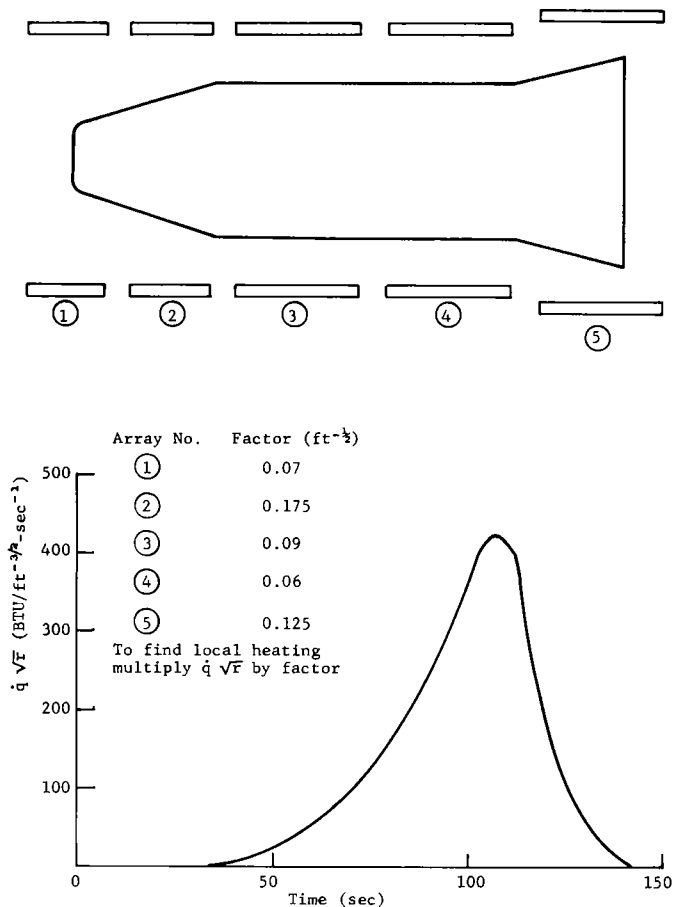
Figure 92. Radiant heat inputs requested for the second full-scale simulated re-entry heating test of the re-entry vehicle

Because this second full-scale test was apparently an overtest, it was decided to run a test on the flare only. The flare received the heat pulse shown in Figure 93. Only slight damage was incurred in this test, and the frame withstood the anticipated parachute load of 4375 pounds.

The fourth major radiant heat test was performed on a portion of the nose. The primary objective of this test was to observe the operation of the heat meter and the ablation sensor. However, ablation did not reach the threshold of the ablation sensor, and the output of the heat meter was erratic.
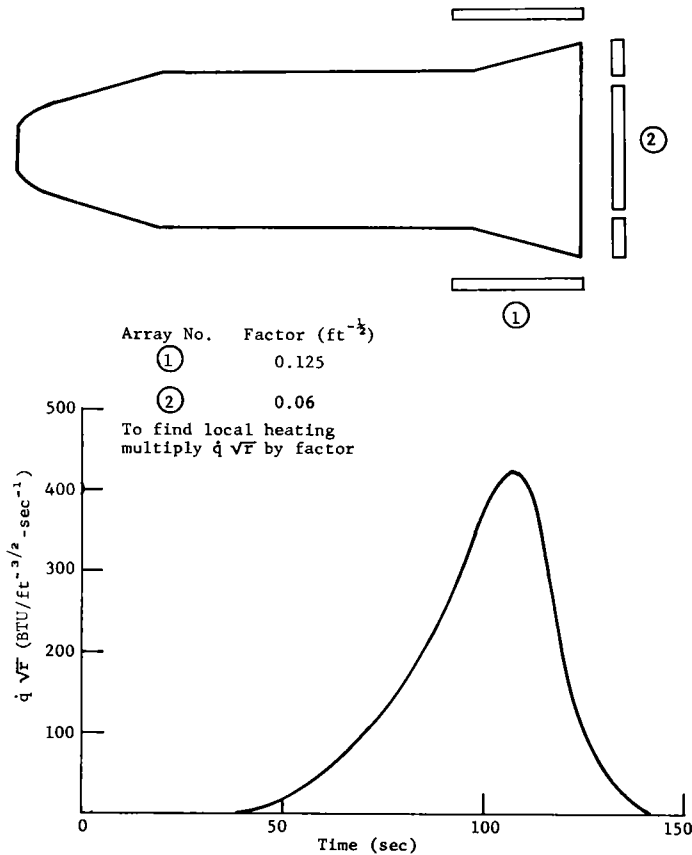
Figure 93. Radiant heat inputs used in simulated
re-entry heating test of the flare

A radiant heat test was also run on a SNAP-10A reactor core vessel (T18915) in order to determine the time and mode of the failure of the lip weld, and also in order to observe the temperature history of the vessel. Re-entry heating conditions were simulated as nearly as the capabilities of the radiant heat facility would permit. Heating inputs were as shown in Figure 94. Although the lip weld melted, the top head did not separate from the can of the weld, but rather melted through and separated inside the weld.

Development Temperature Shock Test

The RV with the telemetry system removed was subjected to five cycles from -10° to 250°F as shown in Figure 95. Thermal stresses encountered in the re-entry shell during re-entry cannot be duplicated by thermal shock without ablating the surface of the vehicle at the same rate as during re-entry, which was not possible with existing test facilities. However, thermal stresses in the structure can be simulated by increasing the temperature gradually to a point where differences in the coefficients of thermal expansion of the materials used in the RV give the desired thermal stresses and relative motion. Although thermal stresses were checked on the entire RV, the primary objective of this test was to determine if the Cohrlastic-TRV flexible bond could withstand the relative motion between the teflon antenna window and the phenolic-fiberglass body. Instrumentation included displacement gages and thermocouples.

In the original design, the cylindrical teflon antenna window was split longitudinally to facilitate fabrication. During the test of this design, the bond broke loose at the longitudinal seam and left a discontinuity. The assembly procedure was therefore changed to one of thermally expanding the complete teflon cylinder (without longitudinal split) and then shrinking it in place over the re-entry vehicle.

110
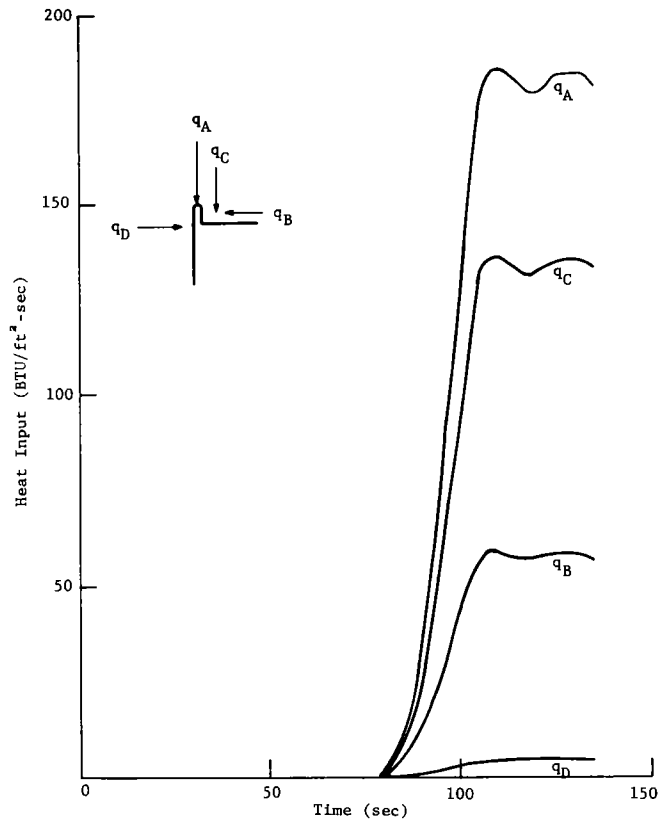
Figure 94. Radiant heat inputs used in simulated re-entry heating test of the SNAP-10A reactor core vessel
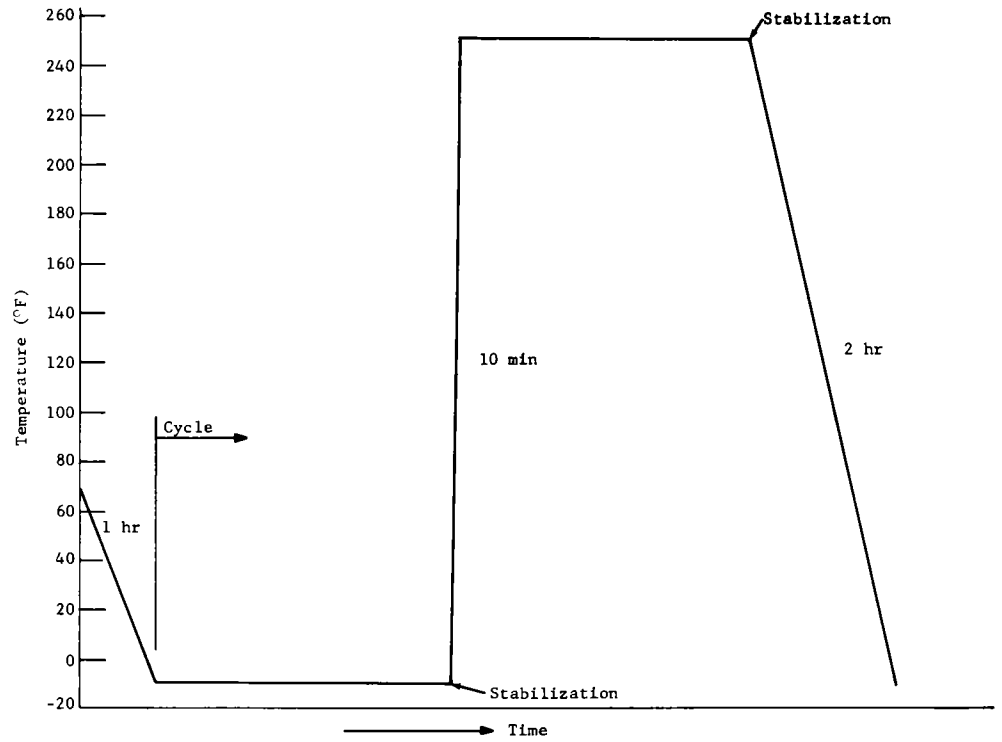
Figure 95. Development temperature shock test cycles

111

A phenolic fiberglass retainer ring intended to hold in the leading edge of the teflon was found to be inadequate, and this requirement was satisfied on later vehicles by extending the nose cap over the teflon. This final design successfully passed all further temperature shock tests.

Qualification Temperature Shock Tests

Qualification Units 1 and 2, less telemetry, were subjected to two of the temperature cycles shown in Figure 74, p. 88. These tests served the same purpose as the development temperature shock test. The change in cycle was caused by slight changes in the design of the vehicle.

During the first qualification test, the leading edge of the teflon behind the door expanded locally to form an air scoop during the high temperature portion of the cycles. This was corrected by assuring intimate contact between the aft side of the beveled door and the leading edge of the teflon.

During the second qualification test, the flexible bond between the case and the teflon failed locally, allowing the teflon to bulge slightly in these areas. However, no leading edges were exposed and the antenna window remained firmly attached to the case. No other damage due to thermal stresses was observed.

Qualification Temperature Cycling Tests

These tests simulated the temperature extremes expected during storage and transportation and at the launch site. The entire RS was subjected to three temperature cycles from $-5°$ to $160°F$ as shown in Figure 73, p. 88. The telemetry was operated intermittently to check its performance at temperature extremes and during temperature change, and to check the functioning of the reactor thermocouples through the telemetry. Thermocouples placed strategically throughout the RV showed that no excessive thermal stresses resulted from these tests. Visual inspection following the test revealed no structural damage.

Airdrop Tests

Airdrop tests were performed at Tonopah and Wallops Island Test Ranges as part of the development of the recovery system and the fourth-stage separation system. These drop tests were conducted at the conclusion of each phase of laboratory testing. The tests at Tonopah, which used simulated metal re-entry vehicles, were conducted to demonstrate the design adequacy of the parachute deployment system (including disreefing of the parachute and deployment of the flotation bag), but they also incorporated the preliminary design of the fourth-stage separation system. (This design, which included delayed ignition of retro-rockets, was difficult to test satisfactorily in the laboratory.)

The Wallops Island tests were conducted as part of the development of the recovery system. Prototype re-entry vehicles simulating the predicted water-entry configuration of the RFD-1 vehicle were used. Fourth-stage separation was also attempted in all the Wallops tests, again because of the difficulties associated with laboratory testing of this system.

A Navy A-1G aircraft was used in all the airdrop tests. Navy torpedo bands were used to suspend the vehicle below the aircraft until it was released (see Figure 96). They were designed to separate from the vehicle immediately after release from the aircraft. In order for the A-1G (or any aircraft) to be compatible with the RFD-1 electrical system, it was necessary to modify the aircraft wiring and to install a special RFD-1 control panel. Although it was possible to use the existing Sandia programmer during the early drop tests which did not use the RFD-1 electrical system, some minor modifications had to be made to allow for monitoring of the flotation gas bottle temperature and to incorporate the desired on-board photographic coverage.
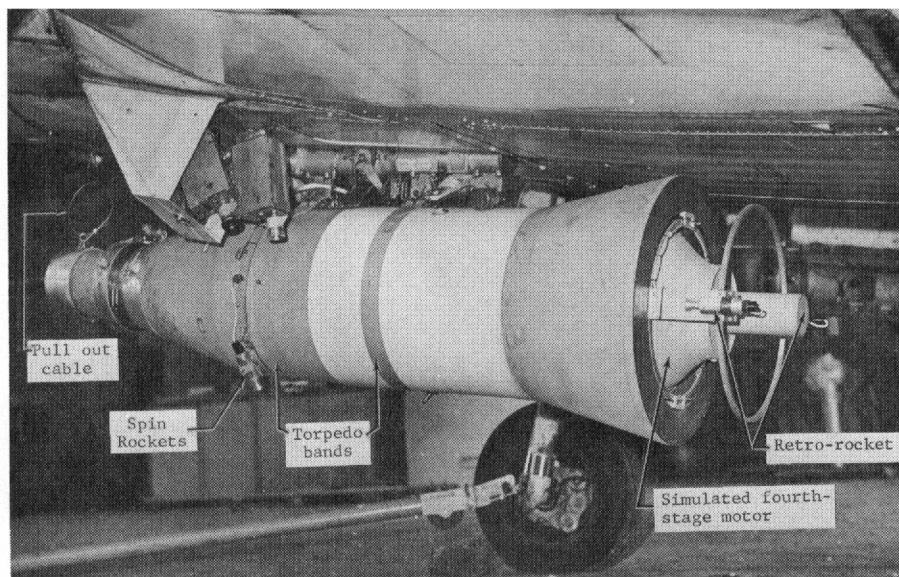
Figure 96. Prototype fiberglass re-entry vehicle
suspended by torpedo bands from Navy
A-1G aircraft before airdrop test

The fourth-stage-separation system used on all the drop tests, including the ignition system shown in Figure 8, p. 26, was identical to the system planned (at the time of each test) for use on the RFD-1 flight. With the exception of the last drop test (S10-8), an XMC1273 mechanical timer was used to deliver the signals for the sequenced functions. In the S10-8 test, a Logitek solid-state time code generator and time decoder (identical to components used in RFD-1) were used.

In the following sections a brief description of each drop test is given. A summary of the drop-test event data is given in Table I.

Tonopah Test Range

S10-2 -- This test was conducted on December 12, 1962. Since the test unit contained no telemetry, the event data were reduced from optical coverage. The vehicle performed as desired with the following events observed: (1) the spin rockets fired and resulted in the desired angular velocity, (2) the fourth-stage motor separated, and (3) the parachute deployed properly. However, inspection of the vehicle after impact showed that the internal flotation bag filled only partially, because the CO_2 gas froze as it was expanded through the gas-bottle orifice.

S10-3 -- This test vehicle was dropped on December 20, 1962, and like S10-2 it was provided with optical coverage only. Vehicle "spin-up" was observed and the vehicle functioned as designed. The fourth stage failed to separate, however, resulting in failure of the parachute at parachute deployment. The shroud lines of the parachute were severed by the retro-rocket-supporting hardware attached to the fourth stage.

S10-4 -- This test vehicle was dropped on January 14, 1963, after one dummy run. It was the first of the S10 series to carry RF telemetry. Data covered by the telemetry included functioning of the pyrotechnic circuitry, roll rate of the test unit, and movement and release of the fourth-stage motor.

TABLE I

Summary of Drop-Test Event Data

Event	Drop Test Number					
	S10-2 (sec)	S10-3 (sec)	S10-4 (sec)	S10-6 (sec)	S10-7 (sec)	S10-8 (sec)
Release	0	0	0	0	0	0
Reset monitor	-	-	0.068	0.137	0.131	0.164
Spin rocket fire	1.08	1.13	1.282	1.314	1.307	1.21
Marmon clamp fire	-	-	2.929	2.975	2.857	
Actual marmon squib CKT 1 and 2	-	-	2.933	2.977	2.859	
4th stage connection			2.949		2.873	
Physical 4th stage movement			3.066		3.851	
4th stage motor separation	3.79					4.20
Spin rocket hardware release(signal)			4.190	5.617	5.625	6.03
Spin hardware release	6.96	7.02	5.851	6.018	6.142	7.36
First chute action				10.67	10.73	6.73
Nose weight release (signal)			15.015		11.102	Malfunction 7.5
Physical nose weight release	15.25		15.776		11.833	
Chute and flotation deployment time		16.78	17.085	12.103	12.031	
Chute tears off		17.15				
Tail plate (smoke)	17.87					
Line stretch	18.27					
Chute filled	18.63					

The CO_2 gas problem in the S10-2 drop was attributed to exposure of the vehicle to low temperature while it was being transported to the test site on the A-1G aircraft. Consequently, heater strips were added to the gas bottles before S10-4 to keep the temperature of the gas at the desired level. A temperature-monitoring system was built in as well, and the Weaponeer in the aircraft for S10-4 reported no difficulty in maintaining the proper temperature. Heater power was turned off at release and the flotation bag filled at the proper time. (This temperature problem was confined to the airdrops. A study indicated that there would be no gas-bottle temperature problem in the actual RFD-1 flight.) The range reported that the telemetry in S10-4 remained on after impact. The pyrotechnic circuitry in this unit, which used a mechanical timer, ran properly and delivered all timer functions as programmed.

The only rate gyro available for S10-4 was one with a maximum rate of 900°/min. Since the rates predicted for S10-4 were below this figure, it was installed. However, the actual maximum roll rate of S10-4 exceeded 900°/min and consequently the 900°/min gyro was on its stops during that part of the trajectory when the roll rate was of greatest interest. On subsequent drop test units, the roll rate was determined by roll-rate sensors which utilized the earth's magnetic field. These roll-rate sensors gave the roll rate on the test unit as desired.

Vehicle spin-up, fourth-stage separation, and parachute deployment were observed and functioned properly.

Wallops Island Test Range

S10-6 -- This test was conducted at Wallops Island on February 4, 1963. Except for minor modifications, instrumentation was identical to that used in S10-4. The vehicle spun up to the required velocity, the fourth stage separated, and the parachute deployed properly. The flotation bag was deployed and the vehicle floated (see Figure 97). However, the impact switches designed to turn on the SARAH beacon system upon water impact failed to actuate. This failure was attributed to an adverse impact angle (more than 30 degrees from vertical) caused by coning of the vehicle after parachute deployment.
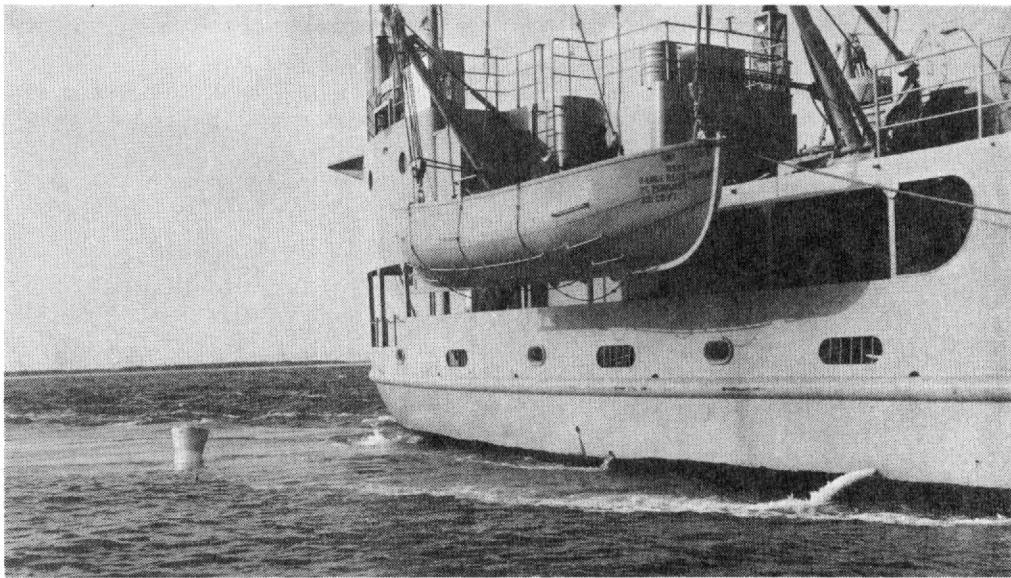
Figure 97. Floating of the re-entry vehicle after Airdrop
Test S10-6 (Wallops Island Test Range)

S10-7 -- The test vehicle for this test, identical to S10-6, was dropped on February 5, 1963. The vehicle spun up, the fourth stage separated, and the parachute deployed properly, but the impact switches again failed.

S10-8 -- This test, the last of the airdrops, was conducted on March 3, 1963. The test unit incorporated pyrotechnic circuitry as much like that planned for the RFD-1 as possible, with only some minor parts and circuits of the system changed because of the different launch method employed. (In all previous drop tests, a specially designed pyrotechnic circuit had been employed which did not simulate the RFD-1 circuit, but did deliver the proper time signals and voltages to the systems being tested.)

The vehicle spun up and the fourth stage separated properly. The ribbon parachute deployed, but it failed to open completely, with the result that the impact velocity was unusually high (approximately four times that expected). The flotation bag was found inflated on recovery, but all the other recovery aids (SARAH beacon, flashing light, etc.) were inoperable. However, the salt-water switch used to turn on the SARAH system was found intact and had functioned properly.

Flight Acceptance Tests

To verify that all the re-entry systems were adequate for the flight, Flight Unit 1 and Flight Unit 2 (backup) were subjected to spin, sine and random vibration, and temperature cycling tests as follows:

Spin Test -- The two units were spun up to 150 rpm for 5 minutes, after which the telemetry system operated satisfactorily. The two units were therefore considered to have passed the spin test.

Sine and Random Vibration Test -- This test checked the functioning of the telemetry system and the structural integrity of the flight vehicle under sinusoidal and random vibration sweeps along the thrust axis at room temperature. Each unit was vibrated for one 30-minute sine sweep from 10 to 2000 to 10 cps with a constant 350-pound peak force input. This was followed by 4 minutes of random vibration, with an overall 350-pound rms force input between 10 and 2000 cps. During this test, the telemetry pack was not preloaded. The vehicles passed the test structurally and their telemetry systems functioned satisfactorily.

Temperature Cycling Test -- The purpose of these tests was to check thermal instrumentation through the telemetry and to discover any material flaws or poor bond joints. The two flight units were subjected to two of the temperature cycles shown in Figure 73, p. 88, and both units successfully passed.

116

SECTION XIII -- PERFORMANCE

This section contains a brief discussion and analysis of the performance of the re-entry vehicle during the RFD-1 flight. Each major function of the vehicle is discussed. Where the preflight theoretical analysis does not agree with the flight-test data, a discussion of the differences is given. The postulated causes of failure are discussed in those cases where predicted test data were not obtained from the flight. A complete tabulation of the flight data is given in "Re-entry Flight Demonstration Number One (RFD-1): Data Book," Sandia Corporation report SC-RR-64-502.

Ablation and Insulation

A trajectory based on optical coverage through the heat pulse, on the radar tracking records, and on the times of reported SARAH signals indicated that there was no catastrophic failure of the RFD-1 RV. There is no positive indication of what caused the failure to receive postblackout TM signals and the inability to re-cover the vehicle. However, postflight studies using the actual observed flight trajectory and more accurate heat inputs and ablation data indicate that there is a possibility that some parts of the RV may have become too hot to function properly.

Ratios of local RV heating to stagnation heating on a 1-foot-radius hemisphere were calculated for various locations along the body of the RV using postflight hot shot tunnel tests at Rhodes and Bloxsom in the laminar region[14] and turbulent data from the similarly shaped RVX3 vehicle. These postflight values were considerably higher than those found in preflight tunnel tests. An analysis of the phenolic fiberglass ablation system, using this new data and the actual stagnation heating shown in Figures 98 and 99, showed higher than predicted inside temperatures, but not temperatures high enough to cause structural failure of the vehicle. An analysis of the TM antenna, using the earliest possible transition from laminar to turbulent flow assuming a boundary layer trip, indicated that the teflon window could have burned through during re-entry and allowed the substructure to char. The following heating ratios and material properties were used for this study.

Time (sec)	$\dot{q}_L/\dot{q}_{ss}$ $\sqrt{R}$	
	Station G	Station H
250-371	0.24	0.16
371-430	0.70	0.50

Property	Teflon	Cohrlastic	Phenolic Fiberglass
E	0.80	--	--
Tab ($^\circ$R)	1600	--	--
ρ (lb/ft^3)	134	20	117
Cp (BTU/lb $^\circ$F)	0.26	0.35	0.23
K (BTU/ft hr $^\circ$F)	0.22	0.032	0.125
Q*lam (BTU/lb)	$Cp\Delta T + 500 + 0.45\Delta h$	--	--
Q*turb (BTU/lb)	$Cp\Delta T + 500 + 0.14\Delta h$	--	--

Δt = rise of material temperature from ambient
Δh = boundary layer enthalpy minus air enthalpy at wall temperature

Results through the ablation of the teflon are shown in Figures 99 and 100. They show that the teflon could have burned through at approximately 380 seconds, which is when the last short burst of TM was received. The substructure was sufficiently thick to survive the rest of re-entry even without the reduced heating which would have occurred due to separated flow in this area.

$$\dot{q}_{ss} \sqrt{R} = 16{,}425 \text{ BTU/ft}^{3/2}$$
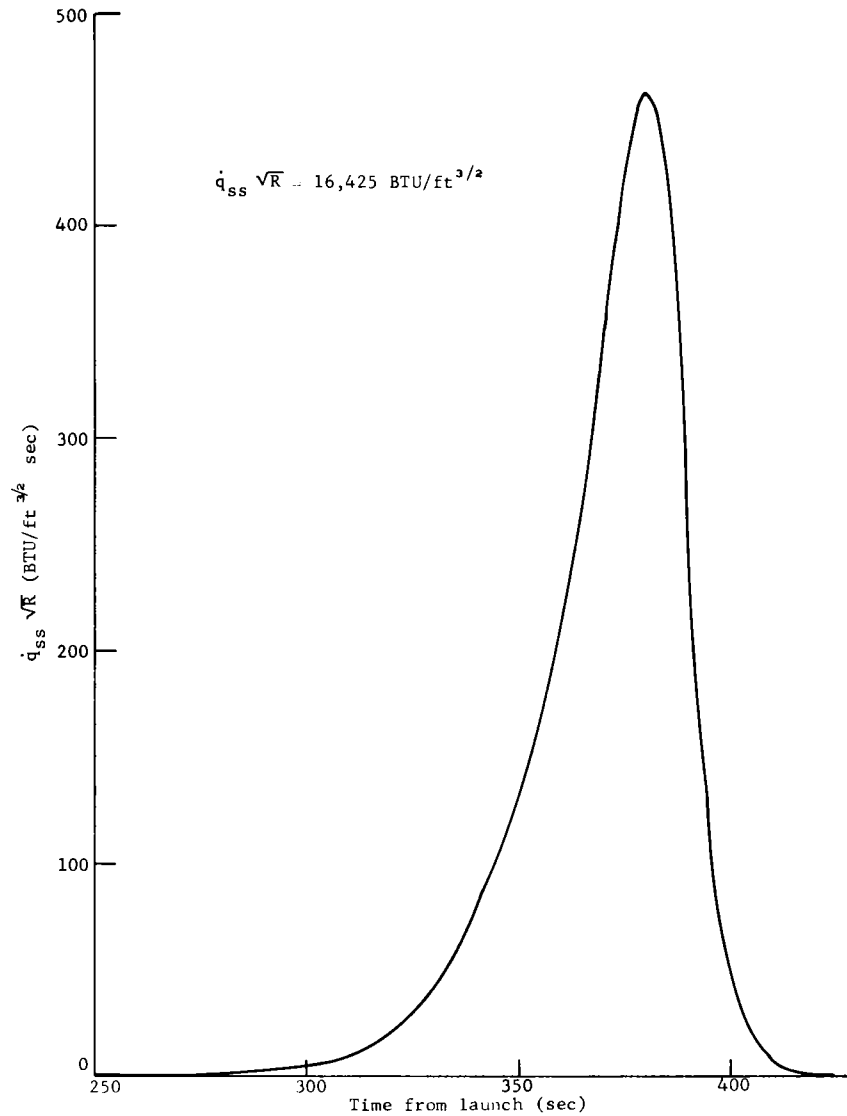
Figure 98. Actual RFD-1 stagnation heating
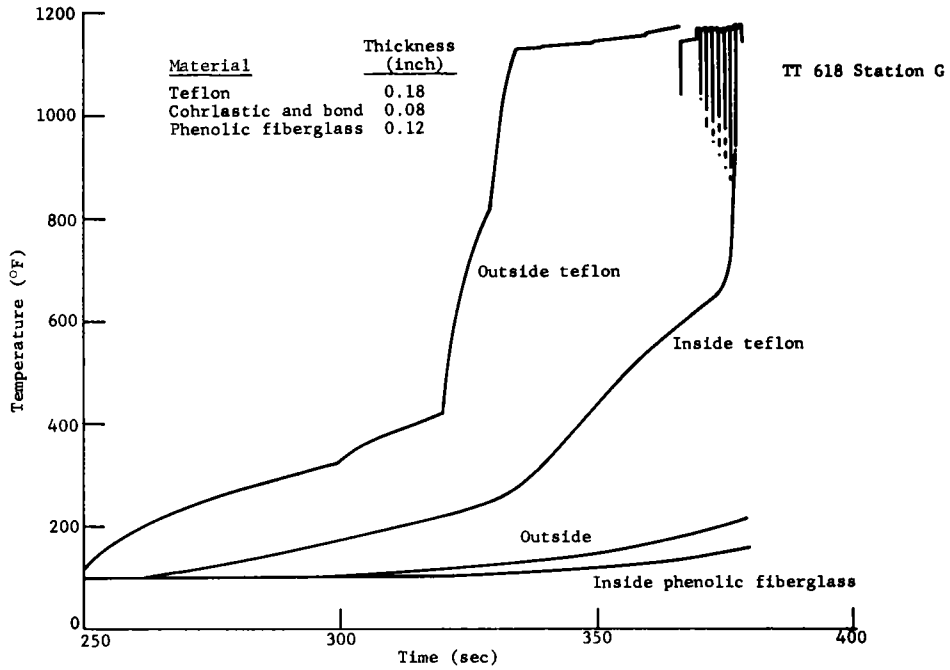
Figure 99. Results of analysis of teflon
ablation system (Station G)
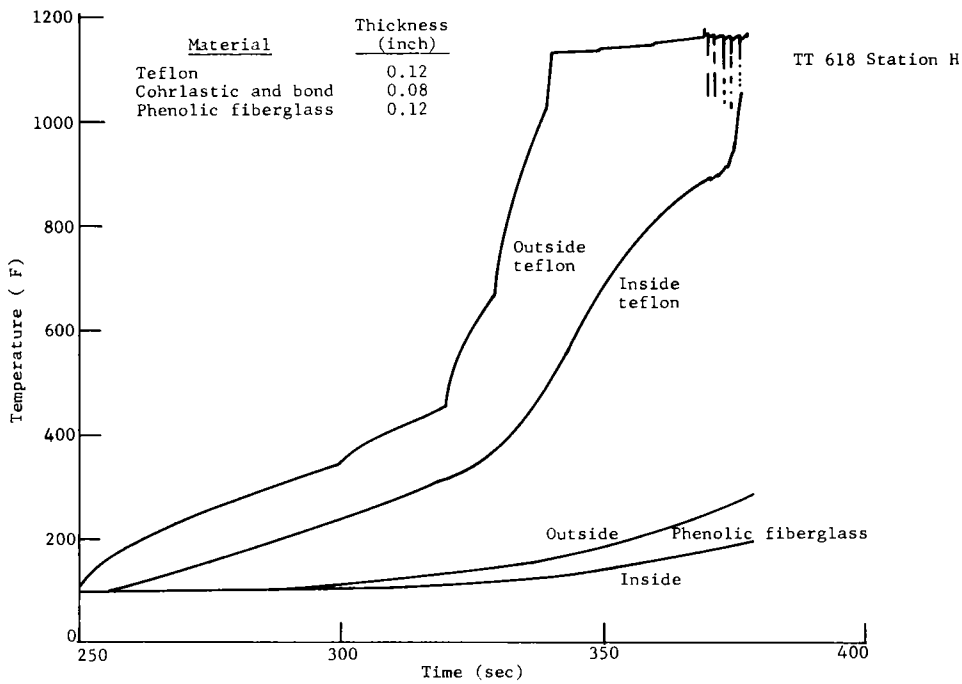
Figure 100. Results of analysis of teflon
ablation system (Station H)

119

Parachute Door

The parachute door should have had an adequate amount of thermal protection. This door was designed and tested to a peak heat pulse of 50 BTU/ft^{2}sec. Recent data indicate that the actual heat pulse was as high as 75 BTU/ft^{2}sec, but there was sufficient safety factor in the thermal design to enable the door to withstand a 75 BTU/ft^{2}sec heat pulse and probably even a heat pulse as high as 100 BTU/ft^{2}sec.

Flare Liner

The flare liner was designed to withstand a heat pulse of 9 BTU/ft^{2}sec and was tested to as high as 27 BTU/ft^{2}sec. Recent data indicate that the actual heat pulse was no greater than 45 BTU/ft^{2}sec and probably was lower. Test data from a sample of the liner indicated that the maximum heat pulse which the liner could have withstood was about 30 BTU/ft^{2}sec. If the actual heating was in the region between 30 and 45 BTU/ft^{2}sec (estimated from postflight "Hot Shot" tunnel tests), it is possible that the liner might have warped or cracked, allowing the foam to ignite and thereby to destroy the parachute and SARAH system in the flare.

Dipole Antenna

The dipole antenna was designed to withstand a heat pulse of 9 BTU/ft^{2}sec. Recent data indicates that the heat pulse was no greater than 45 BTU/ft^{2}sec and probably was lower. Tests on a sample of the antenna indicated that the antenna could survive a heat pulse of 30 BTU/ft^{2}sec but none higher. If the actual heat pulse was in the region between 30 and 45 BTU/ft^{2}sec the antenna would have warped and partially melted. Also, at this heat pulse, the D-65 coating would have charred and shorted out the antenna.

CO_2 Bottles

The CO_2 bottles were designed to withstand a heat pulse of 9 BTU/ft^{2}sec. It is possible that the actual heat pulse in this region was as high as 45 BTU/ft^{2}sec. The CO_2 bottles had enough thermal protection to have easily survived 30 BTU/ft^{2}sec although at 45 BTU/ft^{2}sec there is a possibility that the squib in the valve assembly could have fired prematurely.

Flotation Bag Cover

The flotation bag cover was designed to withstand a heat pulse of 9 BTU/ft^{2}sec and it could probably have survived a heat pulse as high as 18 BTU/ft^{2}sec. However, the actual heat pulse may have gone as high as 45 BTU/ft^{2}sec; if it went over 18 BTU/ft^{2}sec, it is not likely that the flotation bag would have survived.

Baroswitches

The baroswitches had the same thermal protection as the CO_2 bottles and should have survived the heat pulse even if it reached 45 BTU/ft^{2}sec. However, increased temperature would have changed the mean altitude at which the switches were set.

Parachute Cord

The parachute cord was designed to withstand a heat pulse of 9 BTU/ft^{2}sec. According to recent data, some parts of the cord could have been subjected to heat pulses as high as 45 BTU/ft^{2}sec. Although a sizable safety factor was used in the thermal protection system, the cord could have failed if the heat pulse reached as high as 45 BTU/ft^{2}sec.

Connectors and Wire Protection in the Cavity

The connectors and wiring were designed to withstand a heat pulse of 9 BTU/ft^2 sec and probably could have survived a heat pulse as high as 30 BTU/ft^{2}sec. In some regions, however, the wiring could have received a heat pulse as high as 45 BTU/ft^3 sec. The wiring to the drogue gun in the flare was in one such region, and it is questionable whether this wiring would have survived at 45 BTU/ft^2 sec.

Observed Aerodynamic Stability of the Re-entry System

The observed epicyclic attitude motion of the RFD-1 re-entry system, a motion typical of spinning re-entry systems, is presented in Figures 101 through 104.* The initial high angles of attack were caused by impinging of the ejected fourth-stage motor's retro-rocket exhausts on the re-entry system base. Section VII of this report, "Aerodynamic Design," explained that the re-entry system is almost neutrally stable aerodynamically and that it depends on gyroscopic stability until the reactor disassembly process starts. This is verified by the attitude data from the stable platform which shows very little damping over the time interval from 288 seconds to about 315 seconds after launch.

The following reactor disassembly events occurred during and slightly after the time during which attitude data was available from the stable platform:

Time (seconds from launch)	Event
323	Reflectors ejected
340	Fins came off
354	Pump, NaK pipe, and core can lid came off

Sandia Corporation report SC-RR-64-515 presents a detailed description of the reactor disassembly.

It should be noted that even with the above events defined, the re-entry system configuration cannot be precisely defined. For example, there is no way of knowing how much the fins may have ablated before they separated from the re-entry system.

Detailed comments on the aerodynamic stability of the re-entry system will have to wait until the complete stability analysis referred to below is completed, but the following general comments based on a rough preliminary analysis can be made:

1. The convergence of the angle of attack between 330 and 350 seconds, when attitude data was lost, was approximately what would be expected.

2. The nutational frequency of the epicyclic motion compares reasonably well with the frequency that would be expected. This implies that the static stability of the re-entry system was approximately what it was predicted to be before the flight.

3. Nothing can be said concerning the dynamic stability of the re-entry system, since attitude data was lost comparatively early in its trajectory. However, as a result of the rapidly increasing dynamic pressure, the static stability of the re-entry system was contributing far more to damping at the time when attitude data was lost than the dynamic stability was. Thus, any effects of the dynamic stability of the re-entry system on damping would be very small compared with the damping from static stability, and thus could not be separated very accurately.

---

*Coning angle is defined as the angle between the flight path vector and the longitudinal axis of the RS. The angle is plotted as viewed from the rear of the re-entry system.
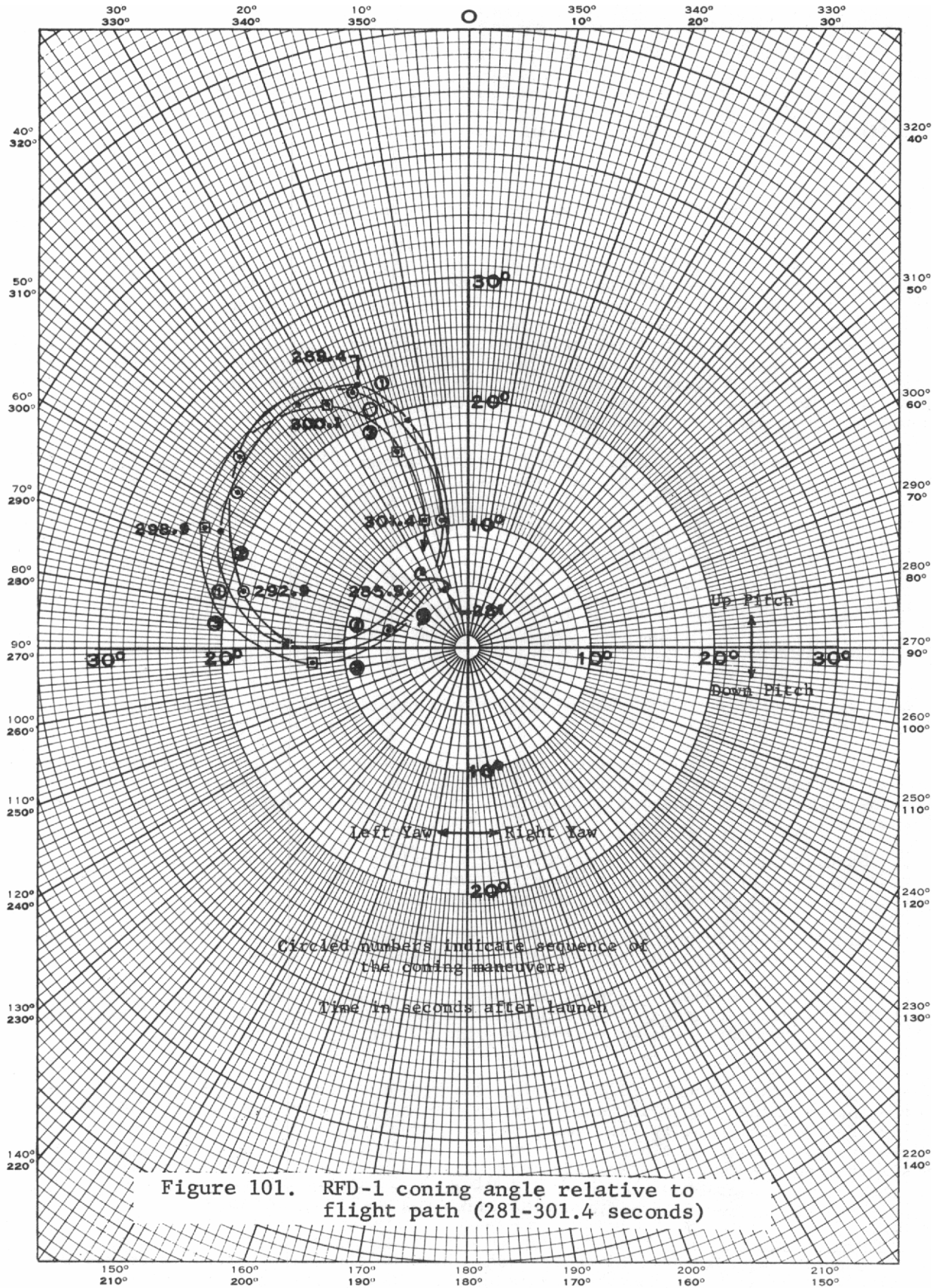
Figure 101. RFD-1 coning angle relative to flight path (281-301.4 seconds)
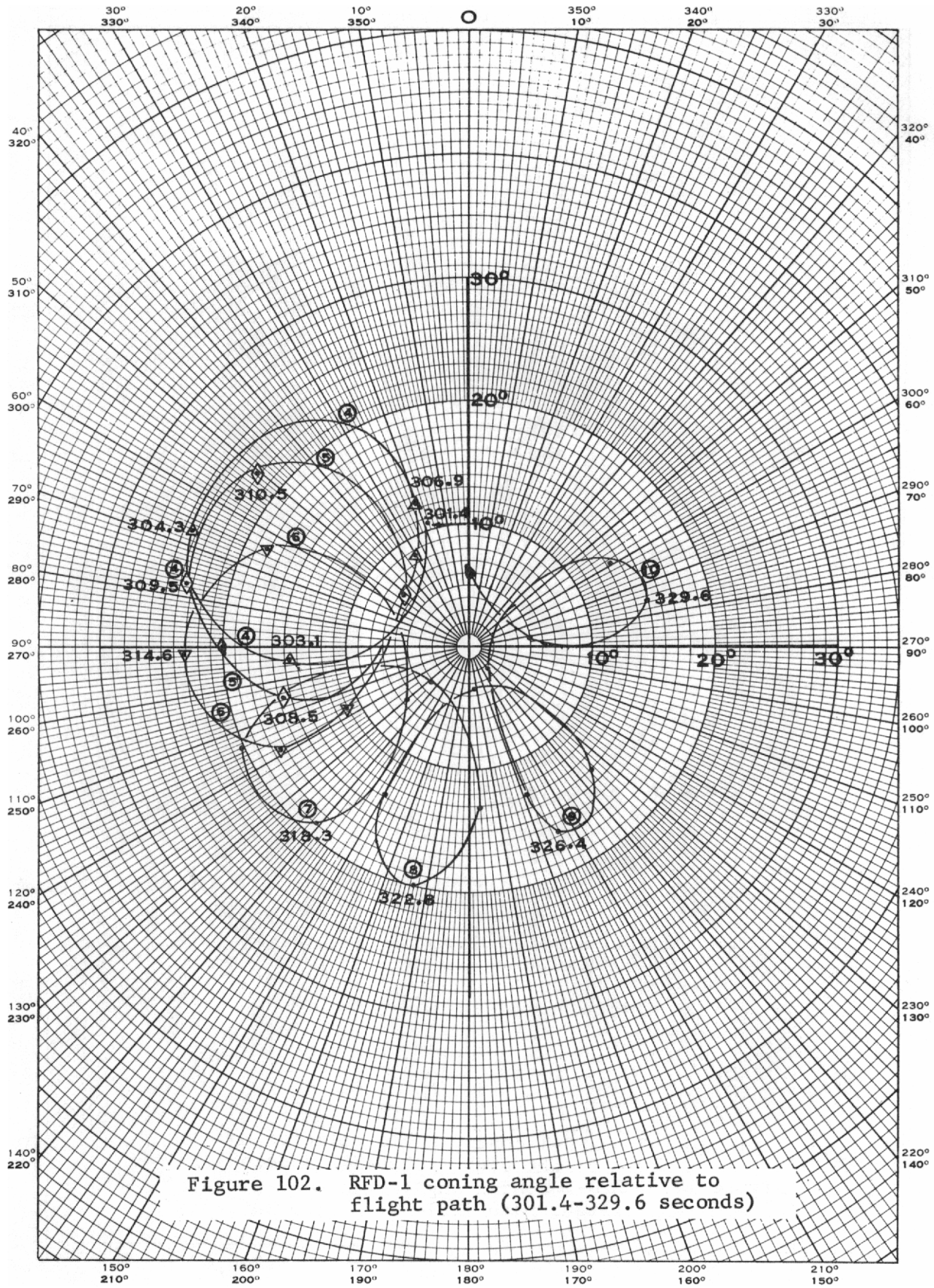
Figure 102.   RFD-1 coning angle relative to flight path (301.4-329.6 seconds)

123
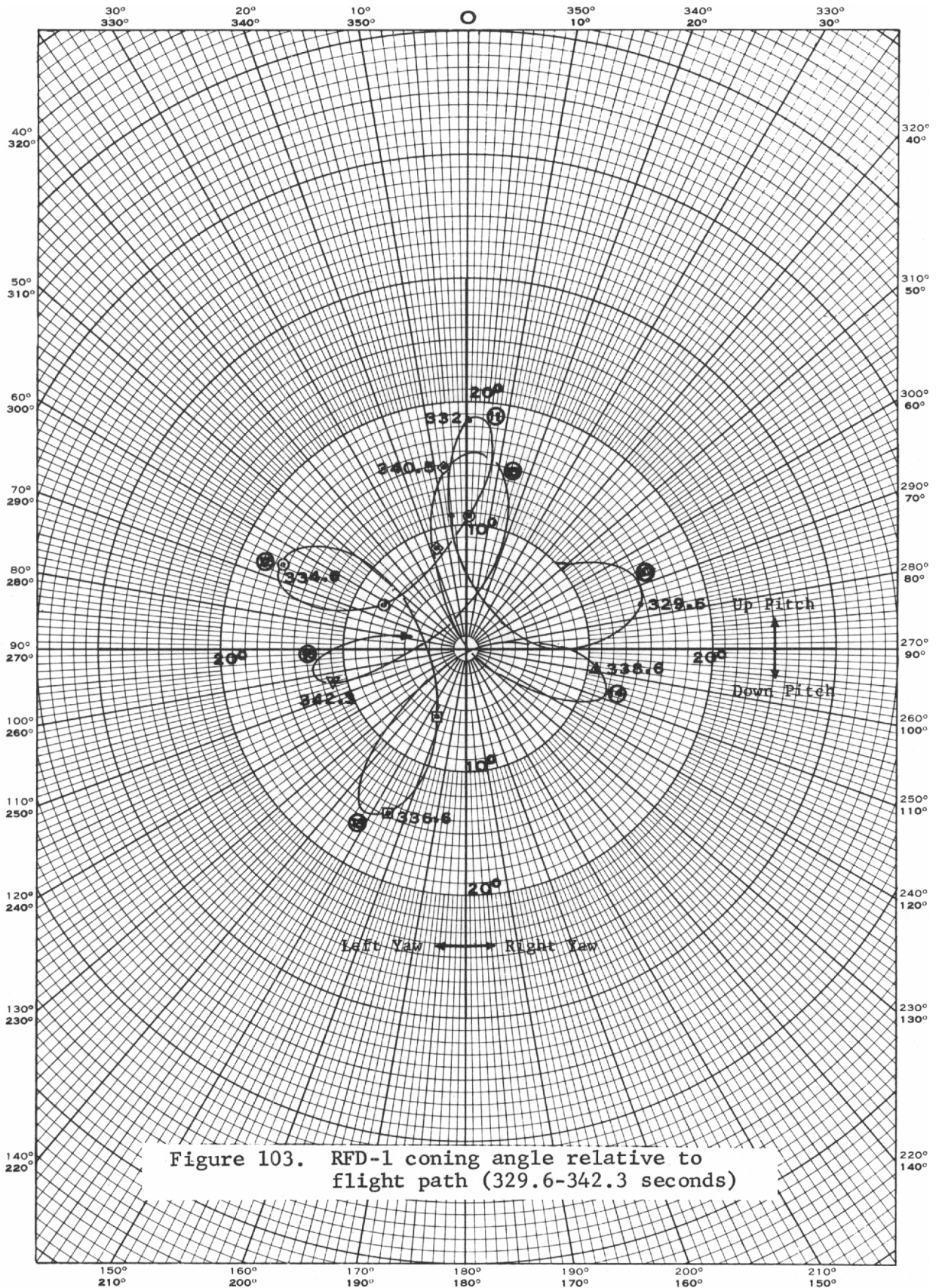
Figure 103. RFD-1 coning angle relative to
flight path (329.6-342.3 seconds)

124
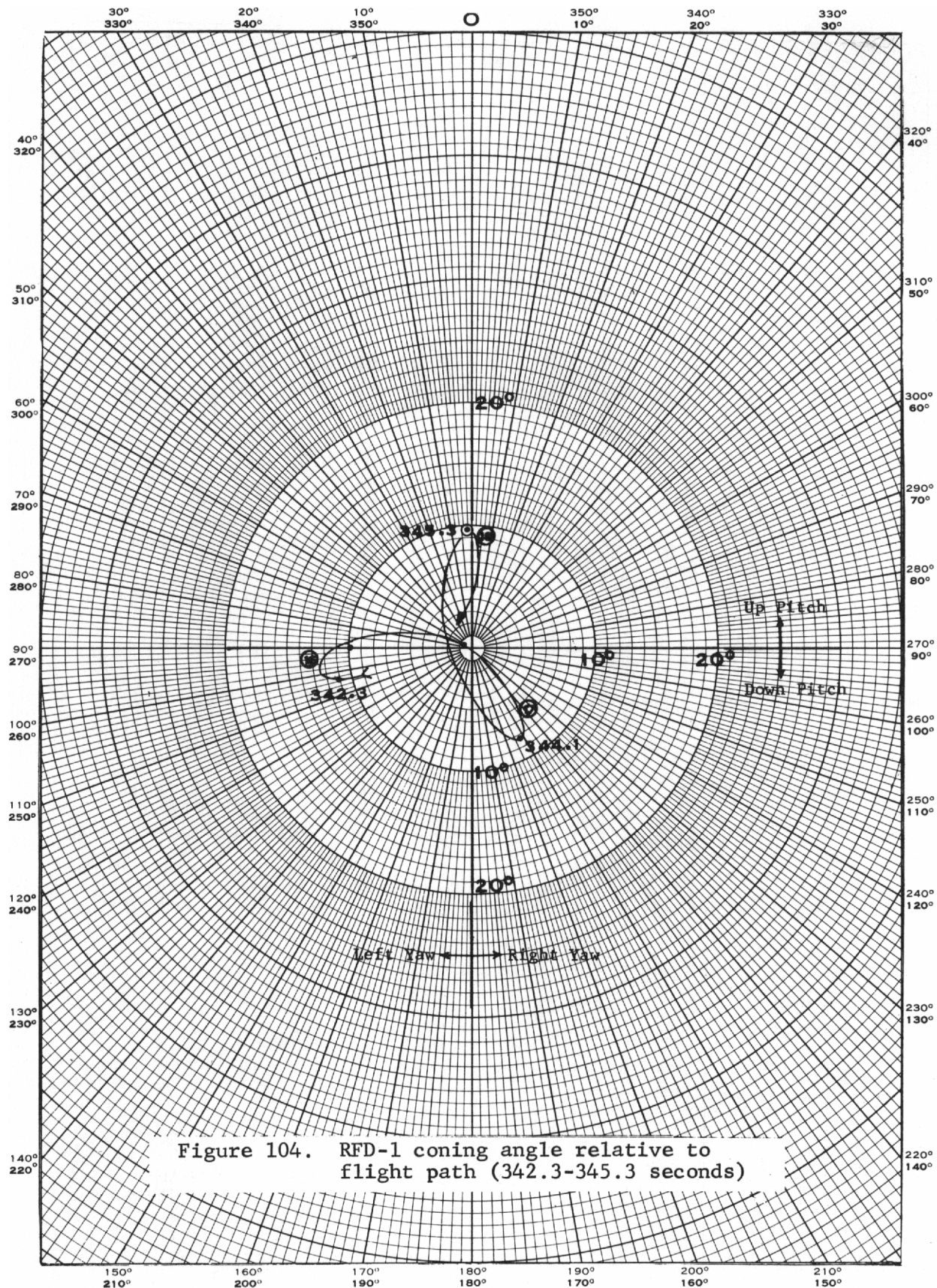
Figure 104. RFD-1 coning angle relative to flight path (342.3-345.3 seconds)

A detailed analysis of the observed data on RFD-1 re-entry system attitude will be completed, using a six-degree-of-freedom trajectory program, in the future. It will be issued in the form of an Appendix to this report and will have the same distribution list.

In summary, the epicyclic attitude motion of the RFD-1 re-entry system compares satisfactorily with a rough preliminary stability analysis. The re-entry system had damped from an initial angle of attack of approximately 25 degrees, caused by the exhausts of the retro-rockets on the ejected fourth-stage motor, to about a 10-degree angle of attack and was damping rapidly when attitude data was lost at 350 seconds after launch.

Fourth-Stage-Motor Separation

Although the fourth-stage motor separated satisfactorily, the vehicle had pitched over approximately 25 degrees at separation. Analysis of the flight data showed that the pitching motion began with ignition of the fourth-stage retro-rockets and reached a maximum angular displacement at burnout of the retro-rockets. Tests to explore these data further were conducted in an altitude chamber (90,000-foot equivalent altitude), with 6 feet separating the retro-rocket from the re-entry vehicle. (Six feet was the separation distance expected during the actual flight.) In the test, the vehicle was provided with instrumentation to measure the unbalanced forces caused by impingement of the retro-rocket exhaust on the back of the re-entry vehicle. These measurements showed that the magnitude of the forces was enough to cause the motion observed during the RFD-1 flight. The effects of exhaust plumes are discussed in References 15 and 16.

Recovery System

The RFD-1 vehicle was not recovered. A SARAH signal was the only data, associated with the recovery system, derived from the flight. The signal was received for less than 30 seconds by various downrange recovery elements at approximately 504 seconds after lift-off. This time in the trajectory corresponds approximately to the time at which an unretarded vehicle would have impacted the water. The impact time was taken from a trajectory based on the TM and optical data from the RFD-1 flight. Wind-tunnel tests conducted after the flight indicated that the temperature of the recovery system was appreciably higher than the calculated temperatures used in design. The postulated actual in-flight temperature would have resulted in failure of the recovery system package in the flare of the vehicle. However, since no post-blackout data were recorded, the exact modes of failure can only be postulated.

Instrumentation

Telemetry System

While the Scout vehicle and its payload were still on the launch stand, two instances of malfunctioning were detected in the telemetry system: the transmitter could not be modulated, and the C-band beacon failed to respond to interrogation. In both instances, different units were substituted and no further trouble was encountered.

A strong, clean signal was received at Mainbase Telemetry (Wallops Island) before and during the launch. This signal continued to be serviceable until approximately 331 seconds after launch, and then no further signals were received at Wallops Island. Up until that time, the monitored battery voltage had not changed and all channels had functioned normally. It had been predicted that blackout would

begin at about 302 seconds, corresponding to 300,000 feet in altitude, but complete loss of TM signal did not actually occur until an altitude of about 180,000 feet was reached; usable data were obtained until an altitude of approximately 200,000 feet. Although a serviceable signal was never received again after blackout, a 0.05-second burst of discernible signal was received at 383.5 seconds (approximately 100,000 feet altitude) by one of the AFMTC aircraft. The few commutator segments obtained during this interval indicate no degradation either in system behavior or battery voltage. This performance is analyzed more fully later in this chapter.

The telemetry records show that all functions occurred in the correct order and at the times programmed on the time decoder. The indication of fourth-stage separation occurred as had been anticipated and at the time desired. At the times that the second-, third-, and fourth-stage motors were ignited, RF signal losses of 30, 60, and 80 milliseconds, respectively, were noted. Figures 105 and 106 provide a comparison between the signals received at Wallops and those received at Bermuda at the time of retro-rocket firing.

All the thermocouples showed temperature rises occurring before loss of signal. Within the time resolution of the commutated data, the fusible link band of the reactor broke, immediately after the temperature of the fusible link had risen to its melting point.

The Mathematical Services Department of Sandia fitted a curve through the known points of the trajectory, and using the equations for this curve, extrapolated it to the point of impact. With this trajectory as a basis, computer runs were then made for acceleration, heating rate, and velocity, and the three resulting curves were also extrapolated to the point of impact. Figure 107 gives these curves as functions of time from launch. The figure shows that complete loss of telemetry signal (LOS) occurred about 120,000 feet lower and 45 seconds later than had been anticipated. It is possible that the delay of signal loss was the result of a disturbance of airflow, caused by the "nonsmooth" structure of the reactor at the front of the re-entry vehicle. (All preflight predictions had been based, because of limited experimental information, on smooth nose cones.)

The time when one of the aircraft received the very short burst of telemetry signal is marked on Figure 107. This time corresponds closely with the peak of the heat-rate curve. It has been conjectured that the burst signal was received either because the plasma sheath was disturbed by parts streaming by from the melting and disassembling reactor or because part of the antenna system integral with the re-entry vehicle ceased functioning at about the time that blackout was ending.

Gyro Data

The data obtained from the roll-stable gyro platform follow the programmed pitch maneuvers. Gradual pitchdown occurred from launch until 128 seconds. At that point, pitchdown changed from 60 to 119 degrees in the course of 32 seconds. The 119-degree pitchdown was maintained for 26 seconds, and then decreased to approximately 100 degrees at 285.5 seconds. The gyro records indicate that the vehicle then began a coning motion about the flight path, with a maximum excursion from the flight path of approximately 25 degrees. This coning action was complex, in that the center line of the coning angle was itself coning about the flight path. The gyro records indicate that the amplitude of the coning was decreasing up to loss of usable signal at 350 seconds, with a maximum angle of attack of less than 10 degrees when the telemetry signal was lost.
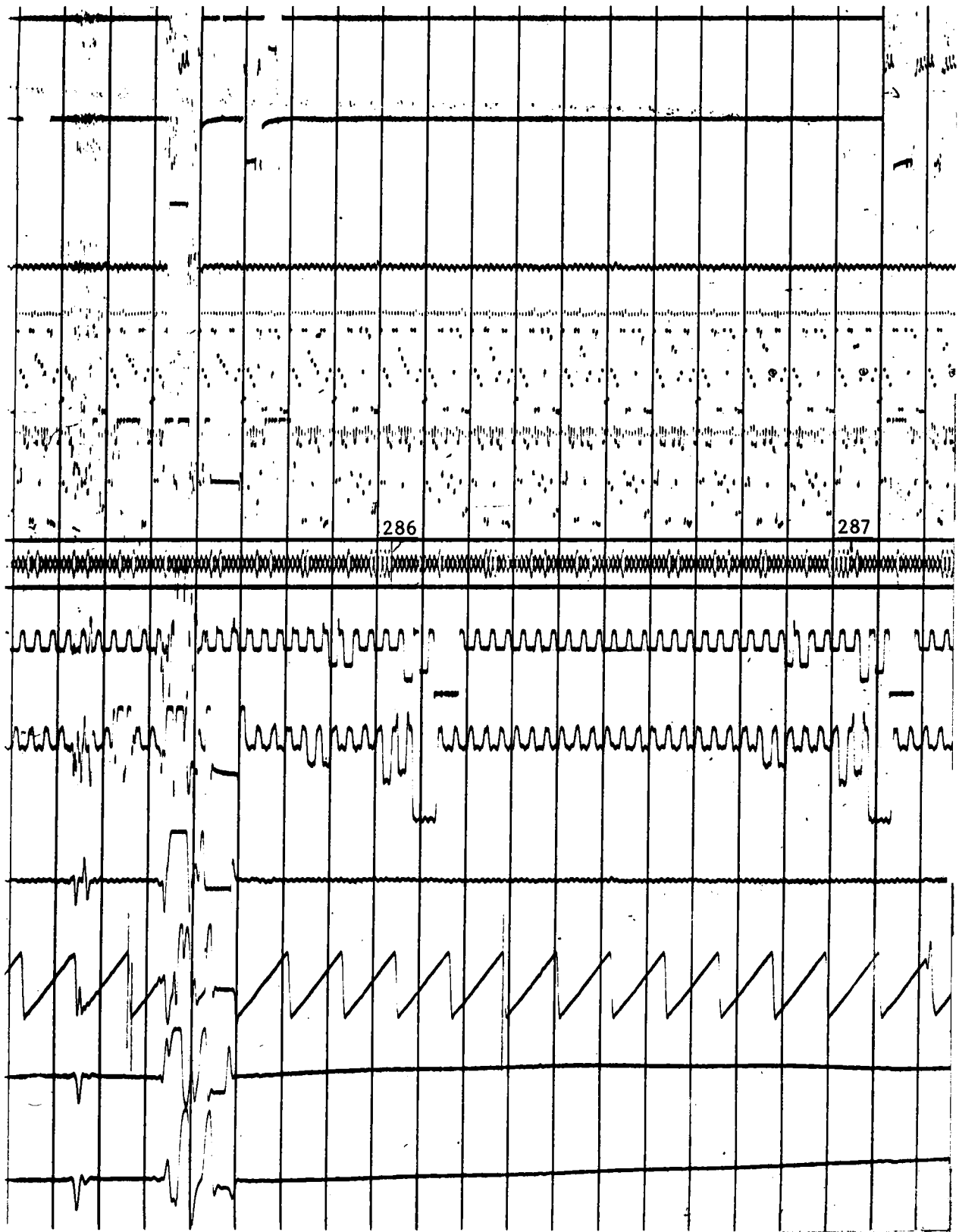
Figure 105. Wallops Island telemetry record
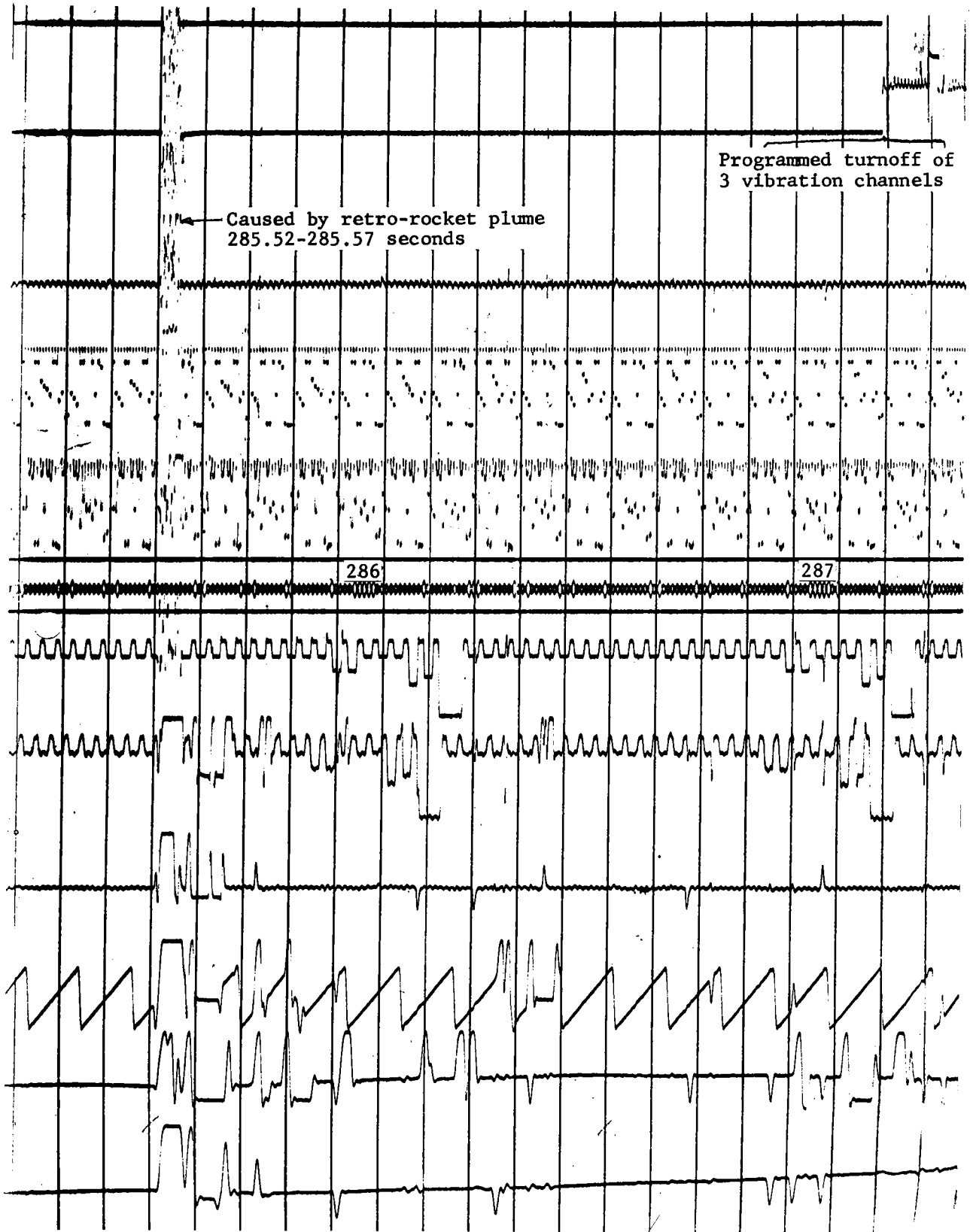
Figure 106. Bermuda Island telemetry record

129
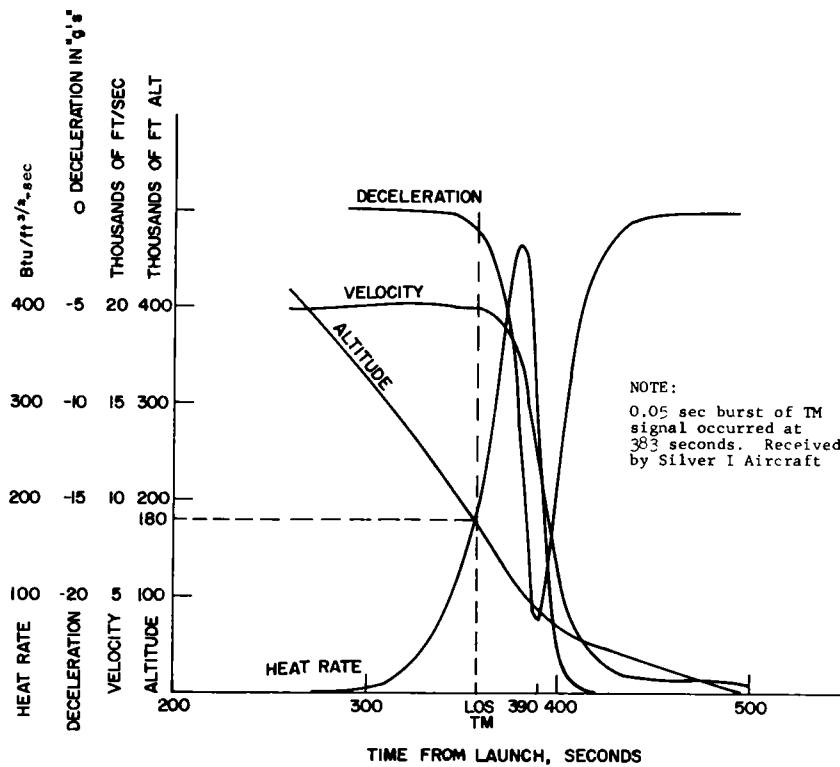
Figure 107. Acceleration, heating rate, and velocity
as functions of time from launch

Heat Meter Results

The results from the heat meters appear to lag the expected heating $(Q \sqrt{R})$ by about 10 to 15 seconds as shown in Figure 108. Possible causes for this are as follows:

1. **Error in Time Base** -- Possible errors involved in correlating the data would be less than 1 second and could not account for the 10- to 15-second error which is present.

2. **Time Response of the Heat Meter** -- The time response of the heat meter is about 0.6 second and would not account for the observed error.

3. **Heat Losses in the Heat Meter** -- Heat losses in the heat meter might possibly account for an error of the observed magnitude much later during the heating pulse when there were large temperature gradients present. However, the data shown in Figure 108 occurred early in the heating pulse, before any sizable temperature gradients were built up; and past testing and analysis indicate that heat losses could not account for the observed error.

4. **Error in q_L/q_s Ratio** -- An error in q_L/q_s could account for the observed heating, if this ratio were reduced by a factor of 3. However, the q_L/q_s ratio used was based on AEDC results, which were lower than Rhodes and Bloxsom results and other results obtained from flights. This means that the probable error in q_L/q_s would tend to make the 10- to 15-second heating error larger, rather than reducing it.

130

5. <u>Pitching and Shock-Wave Interaction</u> -- Since the RV had an epicyclic motion during the early part of the re-entry trajectory, it is possible either that this could have caused shielding of the heat meters or that various shock-wave interactions could have influenced the local heating rates in some unpredictable manner. This source of error is extremely difficult to analyze but probably offers the only reasonable explanation for the observed heating error.
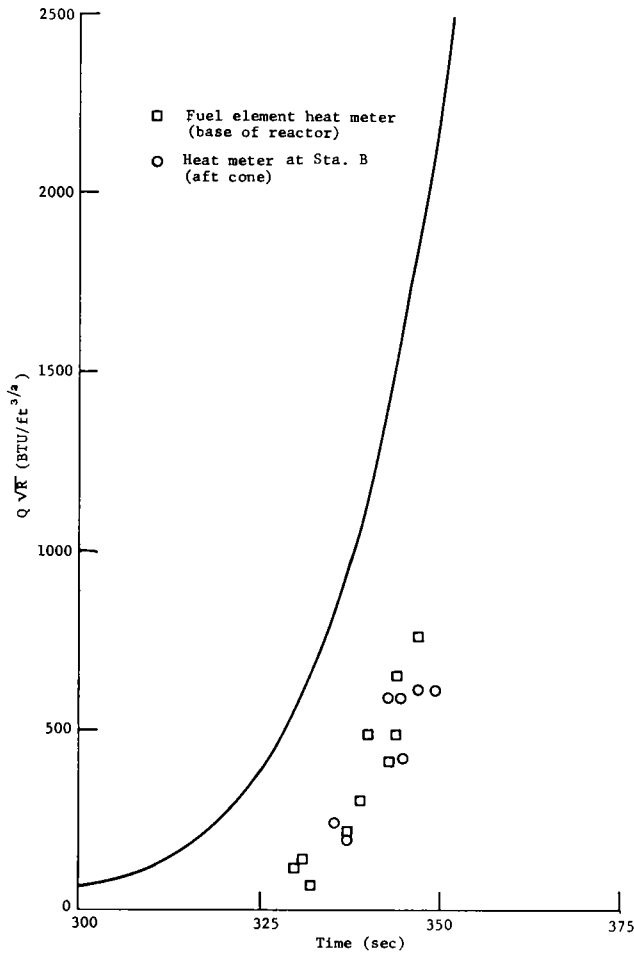
Figure 108.

RFD-1 heat meter results compared to expected stagnation integrated heating

NASA Pressure Data

In order that the motor thrust chamber pressure of the X-248 motor (Scout fourth stage) might be measured, a pressure transducer supplied by NASA was included in the flight. A curve of the data reduced from the transducer is shown in Figure 109. In addition, this figure shows a comparison between flight-test data and data taken from a previous static firing (ground test) of an X-248 motor. As seen in the figure, the flight data compare well with the ground test data. Unfortunately, even though data were recorded after burnout of the fourth stage, it was not possible to determine residual thrust because the data were of the same order of magnitude as the reading accuracy.
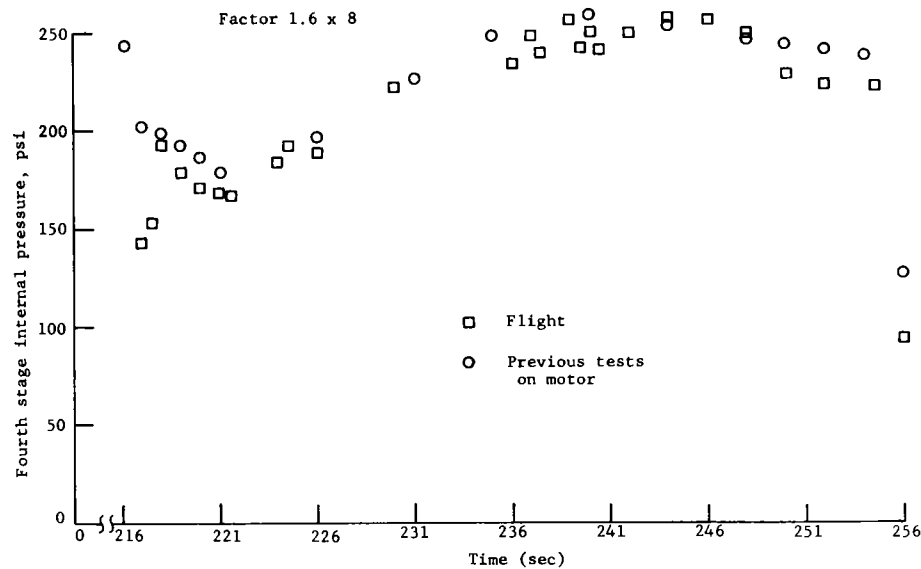
Figure 109. Data reduced from NASA pressure
transducer included in RFD-1

Accelerometers

Three accelerometers were installed in the telemetry package to record acceleration data during the flight. These accelerometers were aligned with three mutually orthogonal axes, one of which was the longitudinal axis of the re-entry vehicle. The maximum accelerations measured during the burning of the four Scout stages are tabulated below:

Scout Stage	Acceleration (g)
First	4.4
Second	7.7
Third	10.7
Fourth	4.8

Although data were recorded from lift off until RF blackout, the only significant acceleration data recorded (other than those tabulated above) were obtained during fourth-stage separation when the accelerometers verified the perturbation measured by the gyro.

Solar Cell

The purpose of the solar cell was to determine (1) whether the illumination from the ion sheath could be detected with a solar cell, and (2) whether the light intensity of this illumination was high enough to be measured when this device was mounted in the cavity vacated by the fourth-stage motor. (Aerodynamic heating in this cavity was relatively much less severe than that on the external periphery of the vehicle. However, since no postblackout data were recorded during the RFD-1 flight, the performance of the solar cell could not be evaluated.)

Vibration Transducers

Vibration transducers were mounted on the adapter section (Figure 6, p. 19) to measure the vibration input from the Scout booster. Vibration data were recorded from lift off to fourth-stage separation (the transducers separated with the fourth stage). The vibration data recorded during resonant burning of the fourth stage are shown in Figure 110. Except for this short period of high-amplitude vibration, no discernible vibration was recorded during the boost phase of the trajectory. During the boost phase, the noise level was equivalent to 1/2 g.

Between the actual flight data and the expected flight environment tabulated in Section XII, the only major difference in vibration data was in the longitudinal direction. The double amplitude of 75 g recorded in the 80 to 120 cps frequency range during the flight was not predicted on the basis of the development vibration test. During postflight analysis, it was found that the 75 g peak was actually at 110 cps. In addition, the 110 cps frequency was found to be the natural frequency of the separation adapter upon which the transducers were mounted.

Ablation Depth Sensors

No ablation depth sensor signals were recorded during flight. This is not surprising, because the first sensor should have triggered in the neighborhood of peak heating and complete loss of TM signal occurred approximately 45 percent of the way to peak heating.
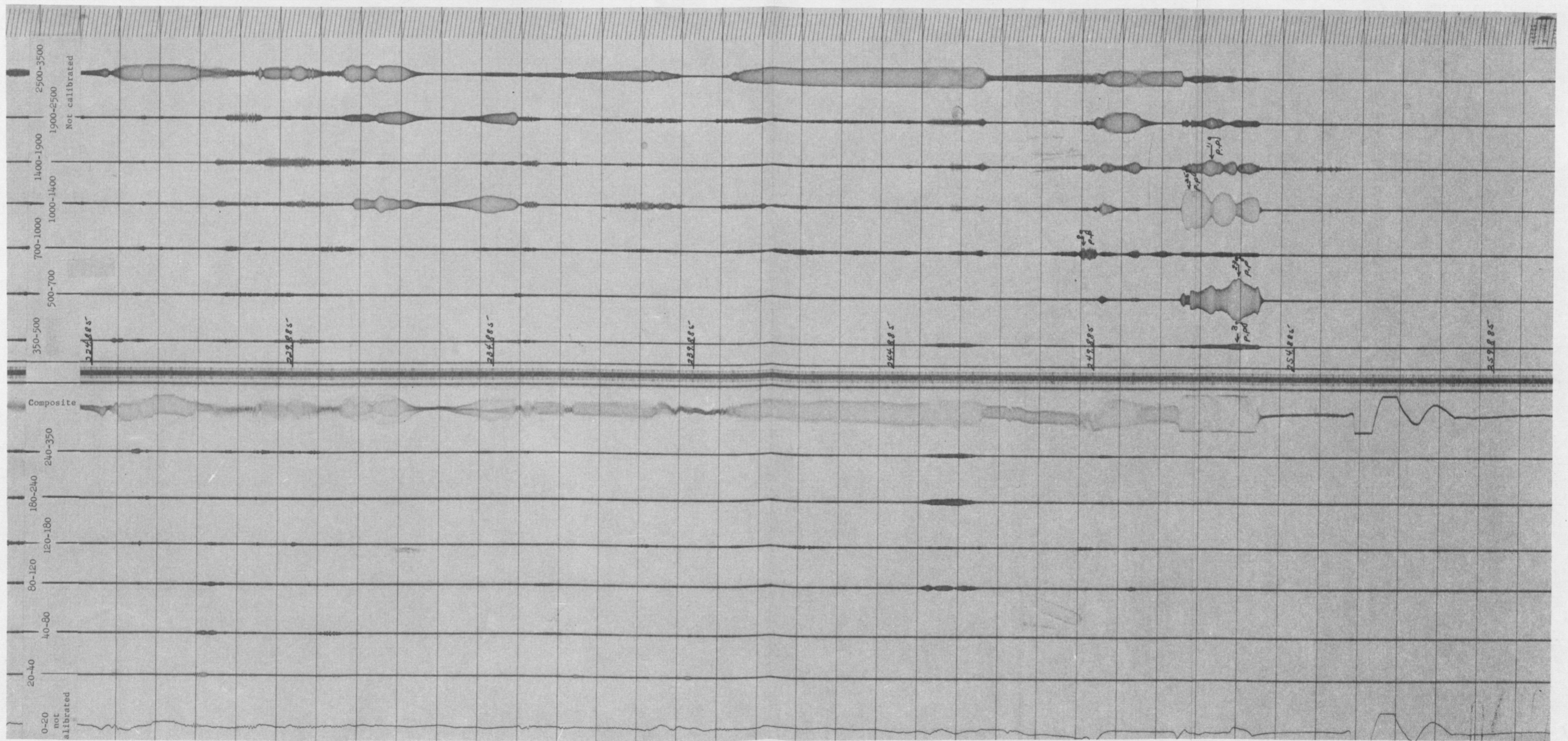
a. Pitch vibration

Figure 110. RFD-1 vibration data
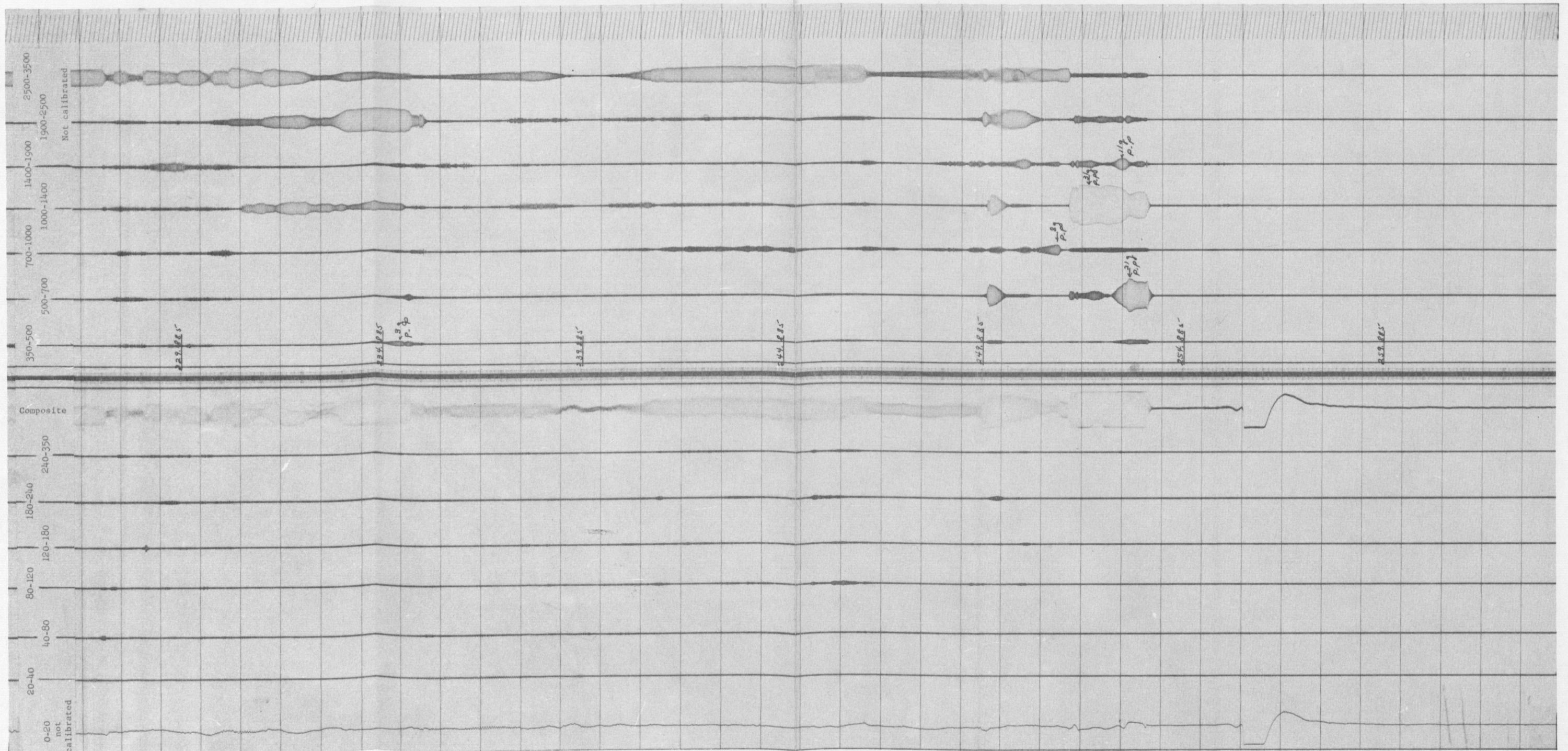
b. Yaw vibration

Figure 110. RFD-1 vibration data (continued)
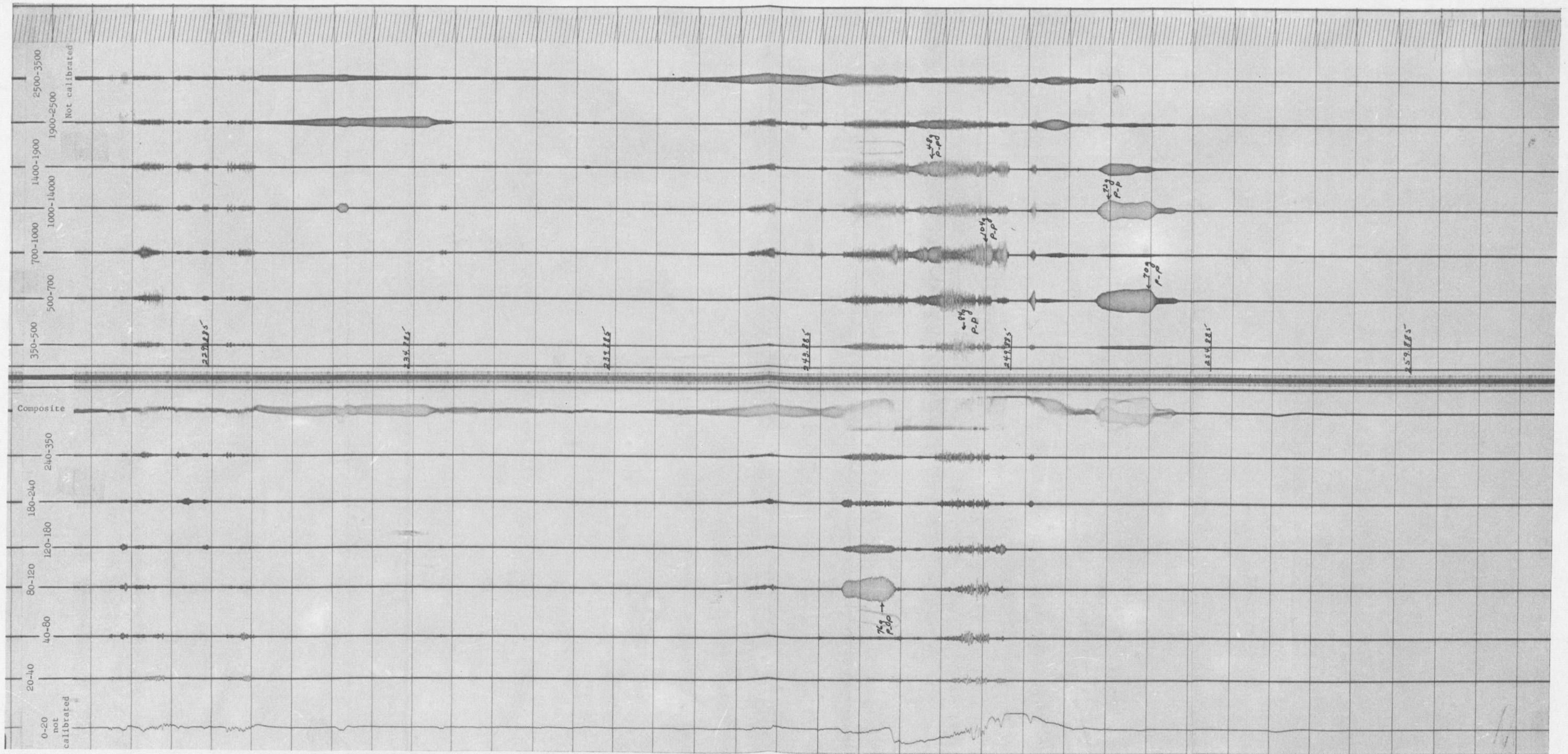
c. Longitudinal vibration

Figure 110.   RFD-1 vibration data (continued)

LIST OF REFERENCES

1. Kane, M. T., and Widdows, H. E., Development and Testing of a Recovery System for the SNAP-10A Re-entry Vehicle, Sandia Corporation Technical Memorandum SC-TM-64-518.

2. Bustamante, A. C., Aerodynamic Analysis and Characteristics of the SNAP-10A Re-entry Test Vehicle for the RFD-1 Re-entry Flight Test, Sandia Corporation Research Report SC-4927(RR), October 1963. (Official Use Only)

3. Everett, R. N., Force Test of SNAP-10A Re-entry Vehicle - Program III-108, Sandia Corporation Technical Memorandum SCTM 98-63(71), May 1963. (Official Use Only)

4. Mitchell, R. A., Stability and Drag Tests of SNAP-10A Re-entry Vehicle at M = 7.5, Sandia Corporation Technical Memorandum SCTM 188-63(71), July 1963. (Official Use Only)

5. Wilkinson, D. B., Hypersonic Force Test of Six Sandia SNAP Configurations, Cornell Aeronautical Laboratory, Inc., Report No. I02 - 010, Suborder 10, January 1963.

6. Hauser, R. J., Transonic Wind Tunnel Tests of Scale Models of the Sandia TX-53 and SNAP-10A, Cornell Aeronautical Laboratory, Inc., Report No. I08-303 (Volumes 1 and 2), March 1963.

7. Chapman, Dean R., An Approximate Analytical Method for Studying Entry into Planetary Atmospheres, NASA TR R-11 (1959).

8. Lovelace, Uriel M., Charts Depicting Kinematic and Heating Parameters for a Ballistic Re-entry at Speeds of 26,000 to 45,000 Feet per Second, NASA TN D-968 (1961).

9. Allensworth, J. A. F., The TTA Generalized Rigid Body Theoretical Trajectory Program for Digital Computer, SC-TM-64-526 (1964).

10. Larson, H. T., Heat Transfer in Separated Flows, IAS-59-37 (1959).

11. Wolney, William, Heat-Transfer and Pressure Measurements on the Full-Scale SNAP-2/10A at M = 19, AEDC-TDR-63-84 (1963).

12. Class, P. L., Thermalog, A Passive Network Analog Computer for the Solution of Transient Heating Problems, SCTM 264-62(71) (1963).

13. RFD-1 Fuel Rod Qualification Tests - Phase I, SCDR 124-63.

14. Bloxsom, D., Heat Transfer Testing on Sandia Model RFD-1, SNAP-10A System, August 23, 1963.

15. Study of Exhaust Plume Effects on the Athena Payload From the 1.0KS40 Control Rocket and the Spherical Retros, Atlantic Research Corporation ARCAS-02-720-001, January 17, 1963.

16. Latvala, E. K., Spreading of Rocket Exhaust Jets at High Altitudes, Arnold Engineering Development Center, ARO, Inc., AEDC-TR-59-11, June 1959.

APPENDIX A

STRUCTURAL DESIGN CRITERIA
FOR THE
SNAP-10A SCOUT RE-ENTRY VEHICLE
RELEASE NO. 2

(Supersedes Structural Design Criteria,
Release No. 1)

Structural Analysis Division 7182

Prepared by: W. L. Craver

October 1962

APPENDIX A

Structural Design Criteria For The
SNAP-10A/Scout Re-entry Vehicle

1. General

This document defines the criteria which are currently being used in the
structural evaluation of the SNAP-10A/Scout Re-entry Vehicle. These criteria
will be revised and supplemented as needed by means of additional releases in
this series. The configuration of the re-entry vehicle/reactor combination
inside the heat shield is shown in Figure A-1.
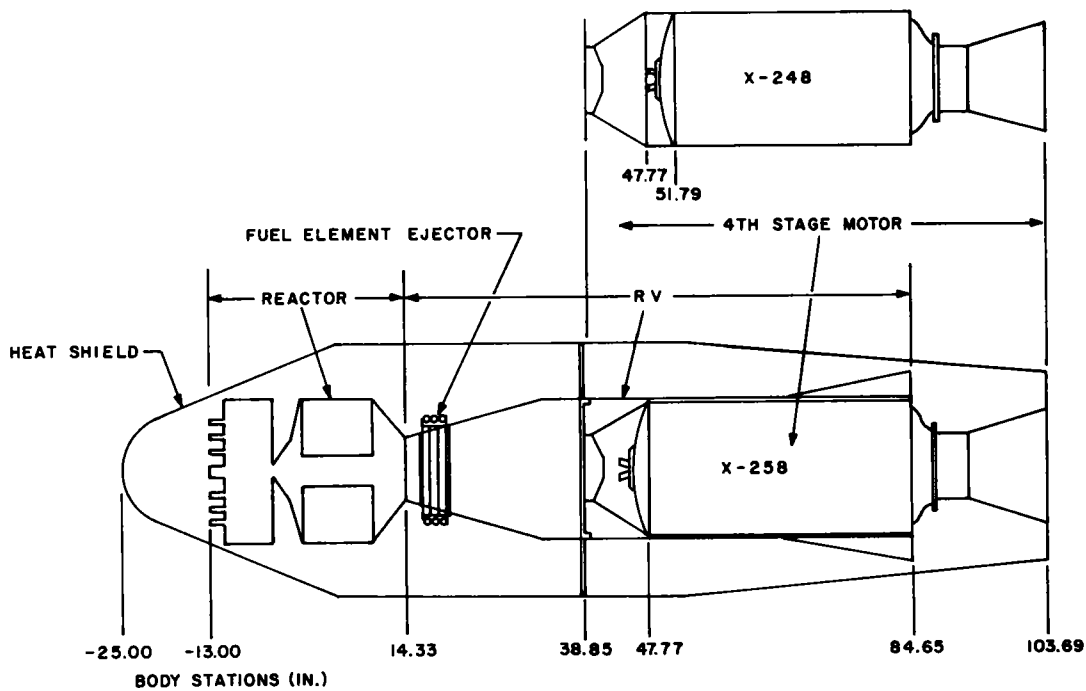
Figure A-1. Configuration of RV/reactor combination in
heat shield, SNAP-10A/Scout with X-258 and
X-248 fourth-stage motors

1.1 Limit Loads - Unless otherwise specified, all loads resulting from the
loading conditions given herein are design limit loads.

1.2 Factors of Safety - The factors of safety to be applied to the loading
conditions are as follows:

Yield FS = 1.15, Ultimate FS = 1.50, for all loading conditions.

In addition to the factors of safety given above, a fitting factor of 1.15 shall be used for all fittings which constitute the only major load path or whose failure would interfere with the proper functioning or integrity of any component. The fitting factor applies to all portions of the fitting, the means of attachment, and the bearing on the members joined.

1.3 Determination of Structural Adequacy - Wherever feasible, determination of structural adequacy shall be made by stress analysis and demonstrated by test. For any conditions where determination of structural adequacy by stress analysis is not feasible, testing shall be utilized to determine structural adequacy.

    1.3.1 Stress Analysis - Whenever possible, structural analysis shall be based on conventional methods of stress analysis. Unconventional methods of analysis shall be substantiated and the derivation of supporting formulas shown. The allowable material stresses shall be in accordance with MIL-HDBK-5 and/or the Sandia Materials Manual. For contemporary materials not covered by MIL-HDBK-5 or the Sandia Materials Manual, the allowable stresses shall be based on acceptable test data.

    1.3.2 Structural Testing - Structural tests shall be coordinated with the Structural Analysis Division and shall be in accordance with the structural test criteria given in the Appendix.

1.4 Load Environment - (Loading conditions are tabulated in Table A-1.

TABLE A-1

SNAP-10A RV Loads

Condition	Axial Load Factor	Transverse Load Factor	Transverse Applied Load	Angular Acceleration (ωx)	Angular Velocity (ωx)	Factor of Safety
Handling	0.0	4.0	0.0	0.0	0.0	Yield FS=1.15 Ult. FS=1.50
Ascent	0.0 to 11.0	1.0	0.0	0.0	0.0	Yield FS=1.15 Ult. FS=1.50
Ascent	4.2	1.0*	1240 lb at* Sta. 38.85	0.0	0.0	Yield FS=1.15 Ult. FS=1.50
Ascent	5.0 to 11.0	See Fig. A-4	0.0	0.0	0.0	Yield FS=1.15 Ult. FS=1.50
Ascent	11.0	0.0	0.0	0.0	0.0	Yield FS=1.15 Ult. FS=1.50
Ascent	0.0	1.0	0.0	2.34 rev/sec²	0.0	Yield FS=1.15 Ult. FS=1.50
Ascent	11.0	1.0	0.0	0.0	3.0 rev/sec	Yield FS=1.15 Ult. FS=1.50
Re-entry	20.0 (cos 15°)	20.0 (sin 15°)	0.0	0.0	3.0 rev/sec	Yield FS=1.15 Ult. FS=1.50
Parachute Deployment	See Section 1.4.4					

*Transverse load and applied load are additive.

    1.4.1 Handling and Transportation - The RV ballistic case, the telemetry package, and the reactor will be shipped separately. It is expected that the RV ballistic case and the telemetry package will be supported in such a way that no critical loads will occur.

    During handling, the RV/reactor combination is supported by a chock at Stations 67.65 and 21.65. A limit load factor of 4.0-g transverse shall be assumed to be applied.

144

During mating of the RV to the Scout, the RV/reactor combination
will be connected to the heat shield. The loads incurred are
expected to be less than during ascent.

1.4.2 Missile Ascent - The axial load factor versus time during missile
powered flight is shown in Figure A-2. This plot of axial load
factor of the fourth stage is for the X-248 motor. Since it has
not been determined whether the X-248 or the X-258 motor will be
used for fourth stage, an axial load factor of 11.0 is assumed
for the X-258 motor. This 11.0-g is the design limit axial load
for the fourth stage. In addition to the axial load factor, the
following transverse loads are considered for either motor:

a. 1.0-g transverse at any time during the ascent trajectory,
    including coast phase between stages (Reference 1, p. 149).

b. 1240-pounds transverse load from the ascent heat shield,
    applied to Station 38.58. This load occurs at 35 seconds
    after launch (Reference 3a).

c. (See Figure A-3.) Transverse load factor varying linearly
    with body station such that the g-level is 3.0-g at the center
    of gravity of the RV/reactor combination and 0.0 g at the aft
    end of the fourth stage, Station 103.69. This loading occurs
    at any time during third-stage burning (Reference 3a).
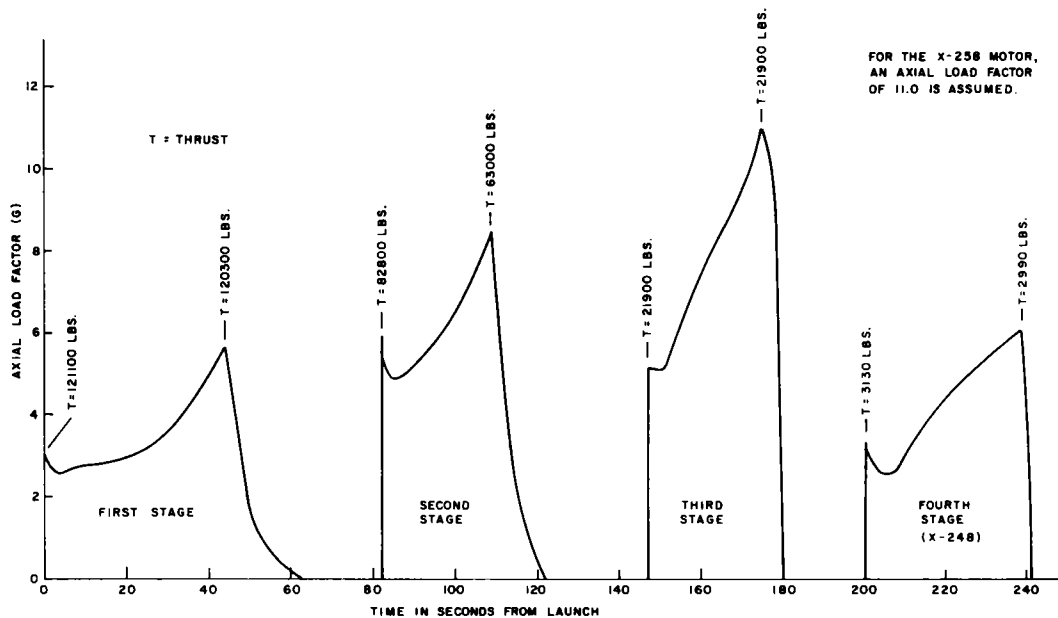
Figure A-2. Axial load factor versus time Scout missile
             with 400-lb payload
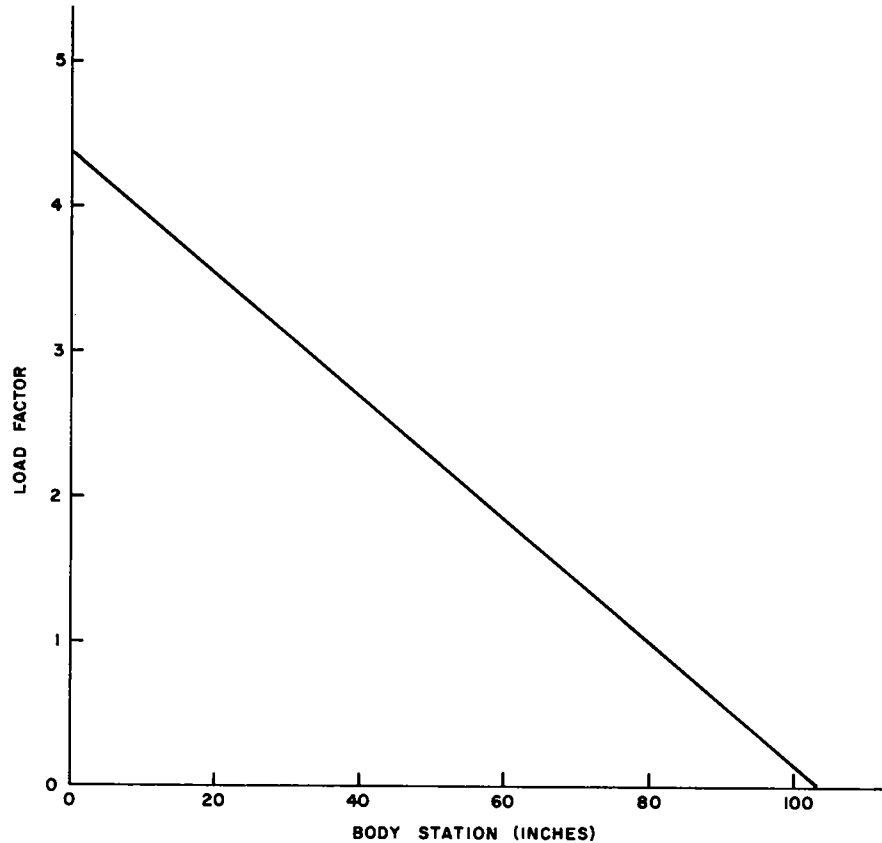
Figure A-3. Transverse load factor versus body station
during third stage burning

The transverse loads given above are assumed to occur in any
transverse plane. In addition to the axial and transverse
loads, the following rolling acceleration and rolling velocity
are considered:

(1) Rolling acceleration of 2.343 rev/sec^2 which occurs
    during fourth-stage spin-up

(2) Rolling velocity of 3 rev/sec which is obtained before
    fourth-stage firing and maintained throughout remainder
    of flight

Combinations of the transverse loads, axial loads, rolling
acceleration, and rolling velocity are tabulated on page 144.

In Reference 2, the vibration environment table listed a
vibration level of ±30.0 g at frequencies from 2000 to 20
cps. This load has been neglected since it is not applicable
(Reference 3b).

1.4.3 Re-entry - Loads have been calculated assuming a peak re-entry
       load of 20.0 g at an angle of attack of 15 degrees. Figure A-4
       shows the axial load factor versus time for re-entry with zero
       angle of attack from variable W/C_DA trajectory No. 257 (Reference
       5). These loads do not exceed the assumed loads used in the
       calculations.
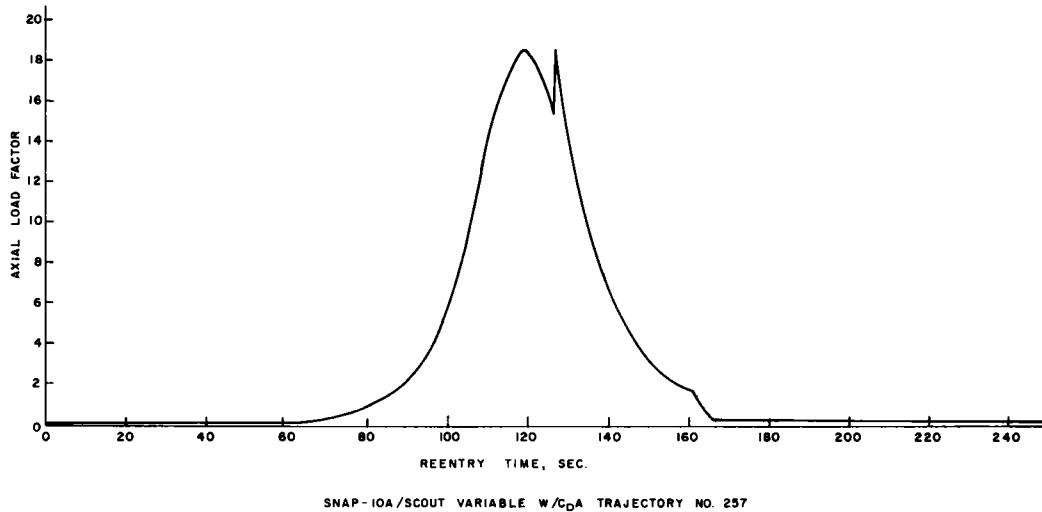
Figure A-4. Re-entry of SNAP-10A/Scout RV axial load factor versus
time (zero angle of attack)

1.4.4 Parachute Deployment - A parachute with solid nylon canopy and
nominal diameter of 7.0 feet is being used. The drag coefficient
is assumed to be 0.75 and XK* factor 1.0. The parachute will be
reefed with a reefed area-to-open area ratio of 0.2. With present
information, an assumed deployment at 20,000 feet, velocity of 765
ft/sec, and q of 260 psf would lead to a parachute load of 1500
pounds. In the actual case, reefed deployment will be made between
10,000 and 30,000 feet, and a maximum q of 320 psf is expected.
The final weight of the RV without parachute is expected to be
about 280 pounds. Due to the preliminary nature of these data,
however, a parachute load of 2500 pounds has been used for design
purposes (H. R. Spahr, 7112). A variance in line tension of ±15
percent will be assumed to cover possibility of an angle of attack
and actual line tension variance. (See Note below.)

1.4.5 Water Entry - After preliminary tests with impact velocity of 100
fps, impact angle of 90 degrees, and a flat plate nose of 9 inches
diameter, the loads are as follows:

Max. g level	- 235
Rise time	- 0.2 msec
Duration 1st phase	- 0.9 msec
Drag phase ave. g	- 10-15
Duration	- 0.1 sec

(Reference 6)

---

*XK factor defined in USAF Parachute Handbook

NOTE: A final parachute load of 3750 lb at any angle of attack
from 0 to 60 degrees was the design condition - W.L.C.,
2-28-64

1.5 Temperature Environment

1.5.1 Handling and Transport - Undefined.

1.5.2 Missile Ascent - Undefined. For structural analysis purposes, material properties at room temperature will be used.

1.5.3 Re-entry - Re-entry temperature of fiberglass structure of flare versus time is shown in Figure A-5. This was obtained from P. L. Class, 7183-3. The flare-inner cylinder temperatures are shown in Figure A-6. The gradient between the temperature points given is assumed to be linear.

1.5.4 Parachute Deployment - Undefined.

1.5.5 Water Entry - Undefined.
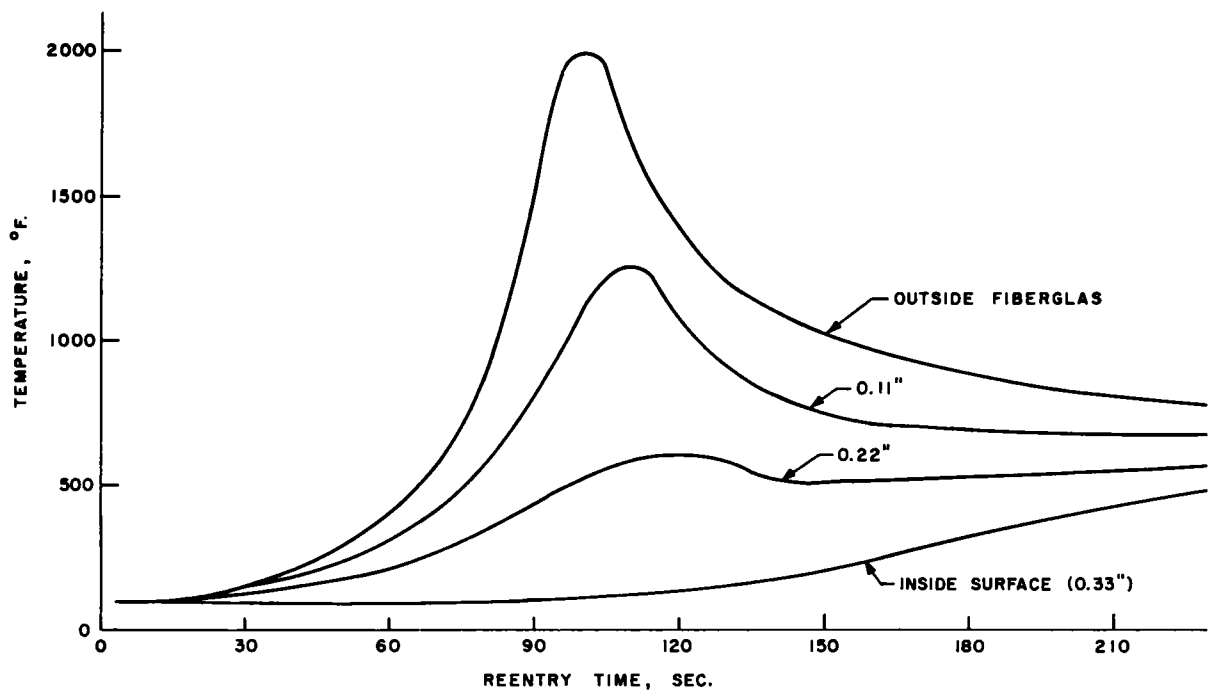
Figure A-5.   Temperature versus time for fiberglass structure of flare during re-entry

148

TEMPERATURES OF FLARE - INNER CYLINDER CONNECTION

$T_{\text{A}} = 525°\text{F}$

$T_{\text{B}} = 330°\text{F}$

$T_{\text{C}} = 1100°\text{F}$
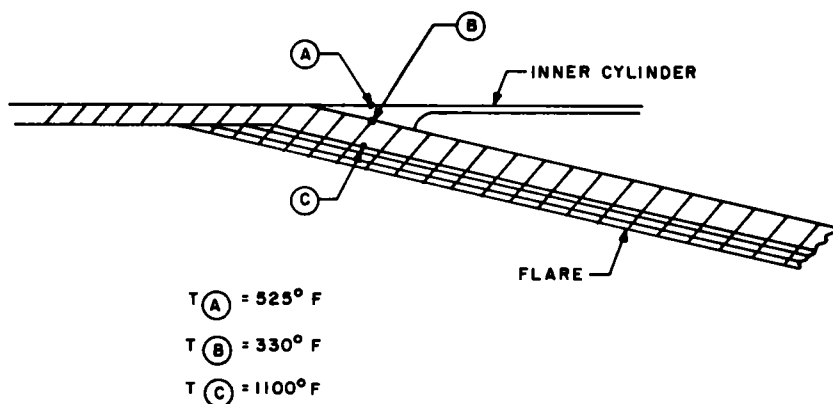
THE TEMPERATURE GRADIENTS BETWEEN THESE POINTS
ARE ASSUMED TO BE LINEAR.

Figure A-6. Temperatures of flare-inner cylinder connection

APPENDIX A REFERENCES

1.   U. S. Air Force Blue Scout User's Guide, publication No. U-1345, Aeronutronic
      Division, Ford Motor Company, August 15, 1961.

2.   The Scout, publication by Astronautics Division, Chance-Vought Corporation,
      June 1962.

3a.   Information obtained by J. Jacobs, 7112, during trip to Ling-Temco-Vought,
      Ft. Worth, Texas, June 11 and 12, 1962.

3b.   J. Jacobs and H. Togami, 7112.

4.   Enclosure (4) to Chance-Vought Corporation Letter No. 13000/2L-1132, Theoreti-
      cal Trajectory Data, Sandia B, Wallops to Bermuda, Routine No. 55-29-01,
      Problem No. 47. (Available from Division 7112.)

5.   "SNAP-10A/Scout Variable $W/C_D A$ Trajectory No. 257," H. R. Spahr, 7112.

6.   D. W. Doak, 7181-1.

APPENDIX B

RELIABILITY TESTING OF RFD-1 COMPONENTS

APPENDIX B

Reliability Testing of RFD-1 Components (Notes 1, 2)

Item No.	Component or Subsystem	Quantity Tested in Program (Note 1)	One-Shot Device Capability or Test Repeatedly	Criticalities	Use of Components in System	Conclusions or Recommendations
1*	Impact switch (MC1441 type) (Sandia Corporation)	8	Repeatable device	Functions satisfactorily up to water entry of 30 degrees between the component piston travel axis and the velocity vector of the vehicle.	Activate flashing light and SARAH beacon. Redundant with salt-water switch.	Use modified MC1441; continue to provide future work to obtain even better components.
2*	Squib for activating carbon dioxide container in flotation system (Walter Kidde)	30	One-shot	Testing showed that the pyrotechnic material did not always cover both bridgewires.	To break a frangible diaphragm in the CO_2 container allowing CO_2 to expand into flotation bag.	Both bridgewires should be covered. It was recommended that all units be X-rayed in at least 2 planes.
3*	Ni-Cad batteries (Goddard)	32	Repeatable device	One cell of the 32 tested tended to become depleted excessively and too soon.	To supply power for initiating functions in flight.	These batteries appeared adequate. Their function may have been improved by screening.
4*	Separation nuts, their shrouds or structures, and the PC24 power cartridge used with them (Hi-Shear)	48	One-shot	Function critical to operation and separation of the fourth stage.	Firing of power cartridge separated clamp and allowed spring to eject fourth-stage motor.	Generally satisfactory, although slow pulses of slightly lower voltages than specified would not fire the cartridge bolts.
5*	Baros (Custom Components)	24	Repeated operating capability	These were part of a redundant circuit, but they did have poor temperature compensation.	Initiation of parachute deployment (in parallel with timer initiation).	Considerable temperature variation and sensitivity required insulation.
6	CO_2 bottle (Walter Kidde)	2 units	Reusable	Needed for flotation.	Inflated flotation bags.	Insulation was required. This commercial product operated satisfactorily when refilled with CO_2.
7	Retro-rockets (Atlantic Research)	12	One-shot	Required for stage separation.	Fired to pull fourth stage away from v vehicle.	Satisfactory.
8	Reefing cutter (Ord. Assoc.)	40 units	One-shot	Parachute operation dependent on these units.	Used to cut rope on parachute to unreef.	Satisfactory.
9	Relays (Sandia Corporation)	30 units	Repeatedly testable	Operated in redundant circuit, generally.	Upon signal, armed and operated the RV squib circuitry.	Satisfactory.
10	Drogue squib (Ord. Assoc.)	40 units tested, including 12 16-fps type, and 12 of the 125, 175, and 250 fps type.	One-shot	Necessary to provide rear cover removal and parachute deployment.	Initiated deployment of chute after removing cover.	The 250-fps variety was satisfactory.
11	Salt-water switch (Sandia Corporation)	5	Repeatable	Possibility of inadvertent operation by shorting probes.	Activated circuitry for SARAH beacon and flashing light. Redundant impact switch.	Satisfactory, if care is taken not to short contacts during assembly.

Note 1: This information applies mostly to the component tests of Division 7412 on Aerospace Nuclear Safing, Mechanical, but as aided by the Reliability, Test, and other groups.

Note 2: These components were tested to be compatible with the requirements specified in Section XI of this report, "Environmental Conditions."

* The more critical components.

APPENDIX C

SNAP-10A (RFD-1) ACTIVITIES

SNAP-10A (RFD-1) Activities

ITEM	ACTIVITY	DATE 1962	OBJECTIVE	DESCRIPTION	RESULTS/REMARKS	EST DAYS FROM START*
1	RFD-1 Design started	Mar 1	To design a re-entry system to test atmosphere burnup of the Snap 10 APU	A system capable of withstanding and functioning from launch through flight out of atmosphere and back. Recovery was not part of the design.	RFD-1 R/V is now at Wallops Island awaiting launch (two separate vehicles, as of Items 66 and 70, below)	0
2	Publication of responsibilities S.C./A.I.	Apr	To define the manner and areas in which Sandia would operate	Described by document	Understanding provided of functions of the companies; also R/V reactor interface presumably agreed upon	36
3	Preliminary Snap 10 Drawings prepared	May 14	Design definition	Drawings adequate to allow fabrication to begin		63
4	Four R/V Units ordered	May 21	For development and qualification work	Two development R/V's and two qualification units	Enabled model building to start	69
5a)	Publication of Sandia Safety Test Plan	Jul 20	a) To provide detailed advice, internal and external to Sandia Corp. on details of our proposed action	a) Report "SCDR 230-62, Tentative Snap 10A Safety Flight Test Plan" was published	a) Self-explanatory	119
5b)	Design for recovery		b) R/V Recovery from water	b) Ocean recovery after impact	b) First documented change found showing recovery-New requirement (Item No 1)	119
6	Plasma Jet first tests	Aug 8	To determine optimum bonding material and re-entry heat and other effects on structural parts	Materials for structures, bonding, filling cracks, and performing functions like pins were investigated	Enabled choices of various R/V materials	135
7	Two more R/V's ordered (for total of six)	Aug 9	For drop testing	To provide drop test preliminary and, later, advanced information	See below	136
8	Fuel Rod Ejection System Design began	Aug 28	Evaluate effect of high altitude release on the rods	Rod-shaped structure to be used to demonstrate adequate fuel burnup and dispersion	A design was made available for RFD-1 flight	152
9	Heat Meter Test	Sept-Nov	To find a reliable method of measuring incident heat flux	Several heat meters were exposed to various heat sources and results evaluated	Design of the on-board heat meters was aided by these tests	159
10	CPM Planning Action - eight units	Sep 15	To provide a CPM Plan - Critical Path Method		A CPM Plan was achieved	167

* Six day week used throughout; if five day week data is desired, it can be obtained closely by dividing by 0.80; estimates made to the nearest day or two.

ITEM	ACTIVITY	DATE 1962	OBJECTIVE	DESCRIPTION	RESULTS/REMARKS	EST DAYS FROM START
11	Nose Cone Thermal Shock	Sep 20	To check the effects of severe thermal shock on phenolic fiberglass	A section of the nose cone was heated to 600°F and immersed in a tub of water		171
12	Plasma Jet Tests	Oct 1	To test ablation materials used in the R/V design and evaluate new materials			180
13	Aerodynamic drag and static stability tests of RS models	Oct 4-Oct 12	To measure aerodynamic forces and cavity pressure on six 1/10-scale models of the RS at various stages of reactor burnup	Models were tested over a Mach number range of 13 to 22 at angles of attack from -6° to 20° at Cornell Aeronautical Laboratory's 40-inch shock tube	The RS will be aerodynamically stable throughout the hypersonic portion of the re-entry	190
14	Delivery of the first Wallops Island drop R/V (W-1) - to 7112	Oct 12	To prepare for drop test at Wallops Island - see Nov. 6, 1962	Shell had no ablation material; it was used for water tank drops and later at Wallops to check aerodynamics		190
15	Order 1 R/V (additional)	Oct 16	To provide for seven R/V's, total	First development model; assembled with Refrasil and Teflon. For assembly, Teflon was split as in a sleeve	Revealed need for development type changes	193
16	Delivery of first development model R/V (D-1)	Oct 18	To provide a unit for environmental testing, including radiant heat tests	Units that were assembled were Refrasil and Teflon; a split was made in the Teflon sleeve for installation	Various tests were run including radiant heat, unit was destroyed; need revealed for development changes	195
17	Aerodynamic drag and static stability tests of Snap 10A RS models	Oct 20, 1962 to Jan 1963	To measure aerodynamic forces and cavity pressure on four 1/15 scale and two 1/10 scale models of the Snap 10A RS at various stages of reactor burnup	Models were tested over a Mach number range of 0.5 to 3.0 and at M = 9 at angles of attack from -6° to 14° in the Sandia Corp. 12-inch transonic and 18-inch hypersonic wind tunnels	The RS will be aerodynamically stable through the supersonic and subsonic portions of the re-entry. The RS will be aerodynamically statically stable through the transonic portion of the re-entry	
18	CPM Planning revised	Oct 22	Seven units provided for	CPM-type plan as before	Planning was updated	198
19	Temperature Shock on D-1	Oct 28	To determine the effect of extreme temperature changes	Evaluation of thermal expansion	Ablation sleeve and retainer ring were redesigned	203
20	CPM Planning action	Nov 2-Nov 7	Six units were provided for			208
21	Vibration on (D-1)	Nov 2	To perform sine and random vibration tests	The 248 vibration environment was utilized	Indicated TM package was attenuated from 3 g input down to 2-1/2 g	208
22	Fuzing sequence tests began	Nov 5 and later	Check fuzing circuitry	Various circuits were checked	Generally successful in ground tests	210

23	First drop test	Nov 6	W-1,Wallops I was dropped from an aircraft at W.1. to check aerodynamics and function	Unit was lost--nose weight and fourth stage failed to come off	Parachute ripped off; recovery not possible	211
24	Ordering of aluminum test shells	Nov 8	To procure two test shells for Tonopah drops	See Item Nos, 35 and 39		213
25	Ordering of aluminum test shells	Nov 15	To procure two more shells for Tonopah drop tests	See Item No 42		218
26	Static and centrifugal	Nov 29	To determine if structural capacity is adequate for X-258		It is structurally satisfactory to replace X-248 motor with X-258	229
27	Delivery of Qualification unit No. 1	Nov 30	Qualif cation tests	Solid Teflon sleeve expanded by heat. Slipped over nose section	Considerable improvement over D-1	230
28	Lip-weld tests	Nov 30	To determine the heat required to cause failure and mode of failure	Front of reactor core can was heated with graphite resistors	A new philosophy as to the mode of failure was established	230
29	A reliability study	Nov 30	A study and test program was organized to determine the circuit and component reliability and to propose changes needed	Analytical work was performed on the circuit and quantities of various components for evaluation were ordered; test planning began	An approximate 18 percent improvement in the circuit was ultimately obtained based on analytical studies and partly on results of the component test program. Test program results have been utilized as they became available. This is continuing.	230
30	Access (umbilical) door design**	Nov 30	To obtain a design improvement	A door held in place by screws was evolved	Heat resistance improved	230
31	Temperature shock on (Q-1)	Dec 2	Temperature shock tests to evaluate effects of thermal expansion on redesigned Teflon sleeve and retainer ring		Successfully passed tests	231
32	AEDC 100 inch hot shot tunnel tests	Dec 3	To determine local re-entry heating on the reactor and the R/V.	Data to be utilized in design and development work	Satisfactory; R/V design information was obtained	232
33	Qual tests on (Q-1)	Dec 7	Completion of tests. Start Dec. 7	Tests per "Tentative Snap 10A Safety Flight Test Plan"	Tests completed Jan. 5	236
34	Ordering of BX R/V shells	Dec 8	To obtain faster delivery	Three R/V shells ordered	Delivery began on Jan. 21 1963, about 6 weeks from order	237
35	Tonopah aluminum shell No. 1 drop test - (S10-2)	Dec 12	To perform functional drop tests especially on parachute system, on a simulated R/V - aircraft drop	A solid canopy chute and a Wallops-type circuit were used	Apparently good, except chute had no reef	240
36	Ordering of one R/V	Dec 14	To provide eight fiberglass R/V's, total	Designated (D-2) for development	See below	242

** Some development activities, or work, such as this item are included to give added perspective to the reader regarding the finding and solving of development problems, while yet meeting the RFD-1 schedule.

159

ITEM	ACTIVITY	DATE 1962	OBJECTIVE	DESCRIPTION	RESULTS/REMARKS	EST DAYS FROM START
37	CIRCUIT SYSTEM-TYPE ANALYSIS	DEC 17	REVIEW OF THE R/V CIRCUIT BY THE SYSTEMS ENGINEERING GROUP, 7160, AT OUR REQUEST; THIS WAS TO EVALUATE THE OVER-ALL CIRCUIT CAPABILITIES	THE SINGLE CHANNEL CIRCUIT OF THE R/V, AND THE COMPONENTS WERE EXAMINED AND SOME CHANGES RECOMMENDED	A CHANGE FROM THE SINGLE CHANNEL CIRCUIT TO A REDUNDANT DUAL CHANNEL WAS RECOMMENDED, AND CERTAIN COMPONENT CHANGES WERE RECOMMENDED ALSO	244
38	FULL SCALE RADIANT HEAT TEST	DEC 19	TO DETERMINE THE THERMAL ADEQUACY OF THE R/V DESIGN	THE ENTIRE R/V WAS GIVEN A RE-ENTRY HEAT PULSE AND THEN THE PARACHUTE SUPPORT WAS PULL-TESTED	FIBERGLASS PINS WERE INSTALLED TO AUGMENT THE ADHESIVES	246
39	TONOPAH ALUMINUM SHELL	DEC 20	TO PERFORM FUNCTIONAL AIRCRAFT DROP TESTS, ESPECIALLY ON THE PARACHUTE SYSTEM, BY AIRCRAFT DROP TESTS OF A SIMULATED R/V	SOLID CANOPY CHUTE AND "MODIFIED WALLOPS-TYPE CIRCUIT" WERE USED	FOURTH STAGE AND NOSE WEIGHT FAILED TO SEPARATE; THUS CHUTE FAILED ALSO	247
40	QUAL NO. 2 DELIVERED	DEC 26	TO CONDUCT HEAT TESTS INCLUDING TESTS OF HEAT METERS AND DEPTH SENSORS	UNIT MADE WITH THICKENED ABLATION SYSTEM AS A RESULT OF HEAT CALCULATION CHANGES	TESTS COMPLETED AND UNIT WAS LATER CONVERTED TO DEVELOPMENT MODEL (D-2) FOR "F AND F" DROP AT WALLOPS--SEE FEB. 28, 1963, ITEM BELOW	251
41	R/V CIRCUIT REDUNDANCY AND CERTAIN DESIRABLE COMPONENT CHANGES ACHIEVED (SUBSTANTIALLY)	DEC 26	TO INITIATE CHANGES IN RFD-1 R/V CIRCUIT AFTER SUFFICIENT REVIEW	DUAL CHANNELING OF R/V WIRING AND REPLACEMENT OF ATLAS SQUIBS BY RC TIMER AND THERMAL MC-TYPE BATTERY, MAINLY	AN ESTIMATED 18 PERCENT IMPROVEMENT IN RELIABILITY	251

ITEM	ACTIVITY	DATE 1963	OBJECTIVE	DESCRIPTION	RESULTS/REMARKS	EST DAYS FROM START*
42	TONAPAH ALUMINUM SHELL NO. 3 DROP TEST (S10-4)	JAN 15	TO PERFORM FUNCTIONAL DROP TESTS (SEE NOS. 39 AND 35)	SEE ITEM NO. 39	ALL FUNCTIONS WERE SATISFACTORY	263
43	HEAT PULL TEST	JAN 16	TO CHECK PARACHUTE SUPPORT STRUCTURE AT ELEVATED TEMPERATURES	THE R/V WAS SOAKED AT 400°F AND THEN THE PARACHUTE SUPPORT WAS PULL-TESTED	THE TEST SETUP WAS REDESIGNED. IT WAS NOTED THAT ALL BOLTS SHOULD HAVE NUTS	264
44	SLED TESTING WITH TONOPAH-TYPE ALUMINUM SHELL NO. 4 UNIT	JAN	TO EVALUATE DROGUE GUN PARACHUTE AND OVER-ALL PARACHUTE SYSTEMS, INCLUDING RIBBON-TYPE CHUTES	PRELIMINARY TESTING ON THE GROUND WITH SLED	NUMEROUS TESTS WERE RUN; SATISFACTORY DROGUE GUN AND RIBBON-TYPE PARACHUTE FUNCTIONS WERE ACHIEVED	
45	DELIVERY OF WALLOPS NO. 2 (W-2) R/V UNIT	JAN 17	TO BE PREPARED FOR FEB 5TH DROP AT WALLOPS ISLAND	THE UNIT HAD NO ABLATIVE NOSE OR TEFLON SLEEVE	SEE NOTES FOR FEB 5, BELOW (ITEM NO. 53)	265
46	DELIVERY OF QUAL TEST UNIT R/V NO. 2	JAN 21	TO OBTAIN A Q-2 REPLACEMENT	THIS UNIT INCLUDED ONE OF THE BENDIX R/V SHELLS. IT HAD A TEFLON SLEEVE WITH THE SAME THICKNESS AS THAT WHICH WILL BE ON THE TWO FLIGHT UNITS	SEE NOTES FOR MAR. 11, BELOW	268
47	ROPE TEST - THERMAL	JAN 24	TO DEVELOP ROPE CAPABLE OF WITHSTANDING HIGH TEMPERATURES AND TO PROVIDE ADEQUATE THERMAL PROTECTION FOR FLOATATION BAG PULL-OUT ROPE	RADIANT HEAT TESTING WAS CONDUCTED	THERMAL PROTECTION WAS IMPROVED BY USE OF ABOUT 0.040 INCH OF D-65 "DYNATHERM" MATERIAL	271

48	QUAL TESTS ON QUAL TEST UNIT NO. 2 TO	JAN 25 FEB 5	QUAL TESTS PER "SNAP 10A SAFETY FLIGHT TEST PLAN"	ALL TESTS RUN EXCEPT TEMPERATURE SHOCK, SCHEDULED FOR FEB. 26 AND RADIANT HEAT, SCHEDULED FOR MAR. 6 (THIS WAS RUN ON MAR. 11)	TESTS COMPLETED SATISFACTORY EXCEPT AS NOTED BELOW	272
49	COMPLETION OF "MECHANICAL" CHECKSHEETS	JAN 26	TO PROVIDE CHECKSHEETS FOR THE ASSEMBLY OF THE UNIT	CHECKSHEETS WERE ENTITLED "ASSEMBLY OF THE TM PACKAGE, REACTOR, AND R/V"; DOUBLE SIGNOFF WAS SPECIFIED	THESE CHECKSHEETS PROVIDED FOR A MORE SAFE AND RELIABLE ASSEMBLY PROCEDURE IN THE AREAS OF DIV. 7112 RESPONSIBILITIES	273
50	COMPLETION OF "ELECTRICAL" TONOPAH CHECKSHEETS	JAN 31	TO PROVIDE CHECKSHEETS FOR THE ASSEMBLY OF THE TONOPAH DROP UNIT	THE TITLE OF THE SHEETS WAS "S-10 DROP TEST UNIT ASSEMBLY"	THESE CHECKSHEETS ENABLED A MORE RELIABLE AND SAFER ASSEMBLY OF THE S10 UNIT IN AREAS OF DIV. 7113 RESPONSIBILITIES	277
51	WALLOPS ISLAND DROP OF Q-1	FEB 4	TO CHECK THE OPERATION OF THE RECOVERY SYSTEM	UNIT WAS DROPPED IN THE WATER OFF WALLOPS ISLAND FROM AN AIRCRAFT	UNIT WAS RECOVERED AFTER SYSTEM FUNCTIONED SATISFACTORILY EXCEPT THAT IMPACT SWITCH DID NOT FUNCTION; THUS SARAH BEACON A D FLASHING LIGHT WERE NOT TURNED ON	280
52	M5TV IMPACT SWITCH	FEB 5	TO INVESTIGATE TYPES OF IMPACT SWITCHES OTHER THAN THE M5TV USED SO FAR	VARIOUS DEVICES WERE DISCUSSED WITH ORG. 1332 FOR MODIFICATION	THE MC1441 INTEGRATOR APPEARED TO BE THE BEST CHOICE	281
53	WALLOPS ISLAND DROP TEST	FEB 5	TO CHECK THE OPERATION OF THE FOURTH STAGE SEPARATION, AND ALSO THE RECOVERY SYSTEM	SAME AS DROP OF FEB 4	SAME AS DROP OF FEB. 4; UNIT WAS RECOVERED BUT M5TV IMPACT SWITCH FAILED	281
54	IMPROVED THERMAL PROTECTION FOR FLOATATION SYSTEM PARTS	FEB 5 TO FEB 11	TO PROVIDE ADEQUATE THERMAL PROTECTION FOR (1) THE FLOATATION BAG AND (2) THE GAS BOTTLE			281
55	FUEL SAMPLE TEST	FEB 7	TO DETERMINE THE EFFECT OF VIBRATION ON FUEL MATERIAL AND SUPPORT STRUCTURE	VIBRATION TESTS WERE RUN	NO DAMAGE WAS CAUSED BY THE TEST	283
56	PLASMA JET TESTS	FEB 7 TO FEB 12	TO DETERMINE THE MATERIAL AND STRUCTURAL PROPERTIES OF SEVERAL SAMPLES OF TEMPERATURE RESISTANT MATERIALS	SEVERAL MATERIAL SAMPLES WERE EXPOSED TO PLASMA JET	DOOR BONDING MATERIAL WAS REINVESTIGATED	283
57	CIRCUITRY REVIEW OF R/V AND TM	FEB 7	TO CONDUCT AN OVER-ALL STUDY OR REVIEW OF THE ELECTRICAL CIRCUITRY OF BOTH THE R/V AND THE TM GEAR	VARIOUS POSSIBLE CHANGES WERE CONSIDERED	FINAL CONCLUSIONS RESULTED IN INSTALLING A BAROSWITCH IN THE CIRCUITRY; IT ACTUATES THE DROGUE GUN; IT STILL ALLOWS FOR TIMER ACTUATION. THUS, EITHER BAROSWITCH OR TIMER DROGUE GUN OPERATION FOR PARACHUTE DEPLOYMENT WERE PROVIDED	283

ITEM	ACTIVITY	DATE 1963	OBJECTIVE	DESCRIPTION	RESULTS/REMARKS	EST DAYS FROM START
58	VARIOUS MODIFICATIONS OF THE MC1441 ACCELERATION SENSING DEVICE	FEB 8	TO REVIEW THE SEVERAL MODIFICATIONS POSSIBLE REGARDING THE MC1441 AND DECIDE ON THE BEST—IN TIME SCALES AVAILABLE	MODEL BUILDING OF THE "MC1441 MODIFIED" WAS AGREED UPON AND PUT ON AN EXPEDITED BASIS; A GROSSLY LIGHTENED PISTON WAS UTILIZED BY REDUCING THE SIZE AND CHANGING TO ALUMINUM; A STRONGER SPRING WAS DESIGNED AND BUILT; THE SILICON OIL WAS REMOVED FROM THE UNIT, AND OVER 95 PERCENT OF THE INTEGRATING CAPABILITY OF THE UNIT WAS THUS REMOVED	THE UNIT FUNCTIONS ON R/V IMPACT WHEN THE ANGLE IS LESS THAN 30 DEGREES FROM THE VERTICAL	284
59	DELIVERY OF R/V FOR RFD-1 FROM THE SHOP	FEB 11	TO ALLOW FOR ADDITIONAL ASSEMBLY, ADJUSTMENT, CHECKOUT AND TEST BY ORG. 7110 PERSONNEL	LATEST FEATURES WERE INCLUDED EXCEPT THAT THE NEW IMPACT SWITCH WAS UNAVAILABLE (SEE ITEM OF FEB. 15 BELOW ITEM No. 61).	THE UNIT SUCCESSFULLY PASSED THE MEASUREMENTS AND TESTS REQUIRED FOR ACCEPTANCE PER THE "TENTATIVE SNAP S10A SAFETY FLIGHT TEST PLAN"	286
60	FIT AND EJECTION TESTS	FEB 15	TO PERFORM FIT AND EJECTION TESTS ON Q-2 AT CVC WITH RFD-1 HEAT SHIELD	TESTING PERFORMED	FIT WAS GENERALLY SATISFACTORY. THE TEST WAS SUCCESSFUL; ONLY MINOR CHANGES WERE INDICATED AND THEY WERE MADE SATISFACTORILY	290
61	DELIVERY OF NEW IMPACT SWITCHES	FEB 15	TO OBTAIN DELIVERY OF THESE COMPONENTS	FIRST "MC1441 MODIFIED" IMPACT SWITCHES	TWO UNITS WERE SUPPLIED TO DIV. 7112 BY DIV. 1332 FOR RFD-1 AND OTHER USES	290
62	DELIVERY OF R/V FOR RFD-1 UNIT No. 2	FEB 21	TO BE USED FOR ANTENNA CHECKS, SPECIAL MEASUREMENTS, AND ACCEPTANCE TEST; THEN IT WILL BE A BACKUP FOR UNIT No. 1 OF RFD-1	LATEST RFD-1 CONFIGURATION	SATISFACTORY—SEE MARCH 22; THIS UNIT WAS SHIPPED	295
63	WATER TANK DROP OF R/V	FEB 21	PRIMARILY TO TEST NEW SALT WATER SWITCHES AND "MODIFIED MC1441" IMPACT SWITCHES	R/V AXIS WAS 8 DEGREES FROM VERTICAL AT WATER ENTRY; SPEED WAS ABOUT 92 FEET PER SECOND	SALT WATER SWITCHES AND "MC1441 MODIFIED" ALL WORKED SATISFACTORILY	295
64	F-AND-F DROP TEST OF UNIT (D-2) TO DEMONSTRATE SYSTEM AND COMPONENT FUNCTION	FEB 28		THIS TEST WAS SIMILAR TO THE F-AND-F TYPE TESTS ON OUR SANDIA WEAPONS. THE UNIT WAS MADE WITH THE EXTRA THICK ABLATION MATERIAL. ALSO, IT CONTAINED RFD-1 TYPE CIRCUITRY TO THE EXTENT OF UTILIZING THE LOGITEK TIMER AND ENCODER THAT BECAME AVAILABLE	DROP TEST WAS SATISFACTORY EXCEPT THAT THE RIBBON PARACHUTE DID NOT FULLY DEPLOY ALLOWING VERY HIGH IMPACT VELOCITY AT TERMINATION (DESIGN REVERTS TO USE OF SOLID CANOPY CHUTE)	301
65	RFD-1 CIRCUIT	FEB 28	ESTABLISHMENT OF FINAL RFD-1 CIRCUIT	THE CIRCUIT, GENERALLY AGREED UPON ON FEB. 27, WAS INCORPORATED IN RFD-1 WITH THE BARO-SWITCH NOW IS PARALLEL WITH THE TIMER FOR PARACHUTE DEPLOYMENT	PROVIDES FOR ADDED CHUTE DEPLOYMENT CAPABILITY BY PRESSURE-ALTITUDE, IF TIME-ACTUATION BECOMES INCOMPATIBLE WITH TRAJECTORY	301

66	RFD-1 Shipment	Mar 11	Shipment of RFD-1	Unit No. 1 of RFD-1	Shipped on time	310
67	Radiant heat test on Qual. No. 2	Mar 11	Radiant heat test of R/V	Test to simulate re-entry heating was found to be an overtest	"Vehicle caught fire," see Mar. 18, 1962 Report, Jeffers to Clark	310
68	Water tank drop of R/V	Mar 13	To test salt water and new "MC1441 Modified" Impact Switches	Similar to water tank drop described above on Feb. 21 except that R/V entered the water with its axis 44 degrees from the vertical	Salt water switches worked satisfactorily; "MC1441 Modified" did not function since it was designed to work at no more than 30 degrees from vertical	312
69	RFD-1 Unit No. 1 Preparation	Mar 22	Prepare Unit No. 1 for launch	Completion of Sandia preparation work on Unit No. 1, RFD-1 at Wallops. This involved (1) doubling the amount of Thermo-lag on rear cylinder, (2) adding D-65 to the TM, (3) installing a thicker parachute cover and T-500 coating, (4) more T-500 insulation applied to inner cylinder, and (5) change from copper to "Heavymet" ballast ring	Activities completed on time	320
70	RFD-1 Unit No. 2	Mar 22	To ship to Wallops	To meet Sandia's schedule	Shipment on time	320
71	Aerodynamic dynamic stability test of a Snap 10A RS Model	Mar 25	To measure the aerodynamic dynamic and static stability of one 1/3 scale model of the Snap 10A RS	A model was tested over a mach number range of 0.7 to 1.25 at angles of attack from -9 to +9 degrees in the Cornell Aeronautical Laboratory 9-foot transonic wind tunnel	The RS will be aerodynamically stable through the transonic portion of the re-entry	322
72	Radiant heat test on (W-2)	Mar 29	Radiant heat test on R/V rear flare	Test of Item No. 67, above, was an overtest; rear flare was only part receiving excess damage. Re-test was proper heating run	Satisfactory, the flare. Apparently the most critical part, withstood the proper test	326
73	RFD-1 Unit No. 1	Apr 15	Vehicle preparation completed by NASA	Ready for launch		340
74	Reliability Program		Completion of work in reporting	Last testing scheduled to begin near the end of April; analysis and reporting of the results in progressing. Test results have been utilized as they become available. The final summation should prove useful for future programs		397

DISTRIBUTION:
TID-4500 (27th Ed.) UC-36 (467)
J. A. Lieberman, Assistant Director for Nuclear Safety, Division of Reactor
    Development, USAEC, Washington 25, D. C.
F. K. Pittman, Director, Division of Reactor Development, USAEC, Washington 25, D.C.
H. G. Hembree, Safety Engineering & Test Branch, Division of Reactor Development,
    USAEC, Washington 25, D.C.
Lt. Col. W. K. Kern, Aerospace Safety Section, Engineering & Test Branch,
    Division of Reactor Development, USAEC, Washington 25, D.C. (6)
R. L. Kirk, SNAP Program Director, Division of Reactor Development, USAEC,
    Washington 25, D.C.
Robert Lowenstein, Director, Division of Licensing & Regulation, USAEC,
    Washington 25, D.C.
Brig. Gen. D. L. Crowson, USAEC, Division of Military Applications,
    Washington 25, D.C.
L. Otoski, Area Manager, AEC Albuquerque Operations Office, P.O. Box 5400,
    Albuquerque, New Mexico (2)
S. A. Upson, Director, Reactor Operations Division, AEC Albuquerque Operations
    Office, P.O. Box 5400, Albuquerque, New Mexico (3)
J. V. Levy, Area Manager, USAEC, Canoga Park Area Office, P.O. Box 591,
    Canoga Park, California, Attn: C. A. Malmstrom (2)
I. A. Peltier, Idaho Operations Office, Idaho Falls, Idaho
C. A. Keller, USAEC, Oak Ridge Operations Office, P.O. Box E, Oak Ridge, Tenn.
T. R. Wilson, Phillips Petroleum Company, Idaho Falls, Idaho
Col. I. J. Russell, AFWL (WLRB)
Col. R. A. Gilbert, AFWL (WLG)
Lt. Col. J. W. Talley, AFWL (WLDN)
Col. D. C. Jameson, AFINS-R, KAFB
A. Glassner, Argonne National Laboratory, P.O. Box 299, Lemont, Illinois
R. L. Detterman, Atomics International, P.O. Box 309, Canoga Park, California (4)
NASA Langley Research Center, Langley Station, Hampton, Virginia,
    Attn: E. D. Schult (5)
T. B. Kerr, RNS, NASA Headquarters, Washington 25, D.C.
R. D. Ginter, NASA Headquarters, Washington 25, D.C.
W. A. Guild, NASA Headquarters, Washington 25, D.C.
J. Whitfield, Asst. Br. Mgr., Hypervelocity Br., Von Karman Gas Dynamics
    Facility, Arnold Engr., Div. Center, Arnold AFB, Tenn.
S. P. Schwartz, 1
R. W. Henderson, 100
E. H. Draper, 1000
C. F. Bild, 1100, Attn: E. R. Frye, 1112
W. M. O'Neill, 1120
L. D. Hopkins, 1300, Attn: J. P. Cody, 1320
G. I. Hildebrandt, 1330
J. H. Findlay, 1400, Attn: J. P. Shoup, 1430
G. W. Rodgers, 1420
J. M. Wiesen, 1440
L. D. Smith, 1500, Attn: H. H. Patterson, 1530
S. A. Moore, 1540
R. A. Bice, 2000
H. E. Lenander, 2500
L. J. Heilman, 2600
J. R. Meikle, 2640
R. B. Powell, 3000
K. A. Smith, 3100
D. S. Tarbox, 3200
S. P. Bliss, 3300
M. K. Linn, 3400
C. W. Campbell, 4000
R. J. Hansen, 4200
K. S. Spoon, 4300
T. T. Robertson, 4400, Attn: F. F. Eichert, 4410
R. E. Hopper, 4500
R. C. Fletcher, 5000
R. S. Claassen, 5100
J. W. Easley, 5300
T. B. Cook, 5400, Attn: B. F. Murphey, 5410

DISTRIBUTION (cont):
J. D. Shreve, 5414
F. C. Cheston, 6000
G. A. Fowler, 7000
L. E. Hollingsworth, 7200, Attn: H. E. Viney, 7210
W. T. Moffat, 7220, Attn: R. N. Browne, 7224
D. Beatson, 7223-5
G. E. Hansche, 7240
J. C. Eckhart, 7250
W. A. Gardner, 7300/7310
R. H. Schultz, 7320
J. W. Pearce, 7330
D. B. Shuster, 7400
V. E. Blake, 7410
H. E. Hansen, 7411   (6)
I. B. White, 7411
A. J. Clark, Jr., 7412   (6)
J. Jacobs, 7412-2
J. I. Hegge, 7412-2
R. D. Klett, 7412-2
H. R. Spahr, 7412-2
H. K. Togami, 7412-2
A. E. Bentz, 7413   (6)
C. E. Erickson, 7413-1
A. Y. Pope, 7420   (3)
J. H. Scott, 7430
W. C. Scrivner, 7600, Attn: J. L. Tischhauser, 7620
B. S. Biggs, 8000
L. Gutierrez, 8100
D. R. Cotter, 9100
E. A. Paxton, 8232-1
B. R. Allen, 3421
M. G. Randle, 3428-1, Bldg. 836
M. G. Randle, 3428-1, Bldg. 880
J. M. Zanetti, 3412 (2)
R. C. Smelich, 3427-3   (50)
L. D. Patterson, 3411-1 (2)